Synthesis and Mechanistic Studies into the Cytotoxic Activity of Garlic-Related Trisulfides in Cancer Cells

Thesis submitted for the degree of

DOCTOR OF PHILOSOPHY

Department of Chemistry
Faculty of Science
University of Cape Town

DOAA ALI

SUPERVISORS
Professor Roger Hunter and Doctor Catherine H. Kaschula

October 2024

Declaration

I, **Doaa Ali**, affirm that the thesis entitled "**Synthesis and Mechanistic Studies into the Cytotoxic Activity of Garlic-Related Trisulfides in Cancer Cells**" is my own work and was completed under the guidance of my supervisors. I make the following declarations:

1. The research presented in this thesis is my own, with all guidance and contributions from supervisors appropriately acknowledged.
2. Proper citation and acknowledgment have been made for all sources and prior work referenced in this thesis.

3. Two publications have been produced from the research presented in this thesis and are appropriately cited within the text.

4. No part of this thesis has been, or will be, submitted for any other degree or qualification at this or any other institution.

5. I grant the University of Cape Town permission to reproduce this thesis, in whole or in part, for research and educational purposes.

This submission fulfills the requirements for the degree of **Doctor of Philosophy** in the Department of Chemistry at the University of Cape Town.

Doaa Ali
30th October 2024

Abstract

Garlic has long been recognized for its medicinal properties and is well-documented to produce organosulfur compounds (OSCs) with significant chemopreventive and therapeutic potential. Among these, trisulfides are notable phytochemicals that exhibit a broad range of biological activities, including anticancer effects both in *vitro* and in *vivo*, as well as antimicrobial, antioxidant, and antithrombotic properties. Recent methodologies have enabled the development of novel synthetic methodologies for synthesizing unsymmetrical organotrisulfides. This thesis explores our contributions to the synthesis of these compounds, their cytotoxicity and their mechanisms of action against cancer cells. Building on our group's previous research on the cytotoxicity of ajoene, which demonstrated its ability to modify proteins by *S*-thioallylation of cysteine residues through a thiol-disulfide exchange reaction, we extend these findings to trisulfides, providing new insights into their potential as anticancer agents.

Chapter One offers an overview of naturally occurring trisulfides, highlighting their significant biological activities. It emphasizes trisulfides from natural sources, particularly diallyl trisulfide (DATS), a garlic-derived compound with notable anticancer potential. This chapter sets the stage for exploring trisulfides therapeutic potential in cancer treatment, a central theme of this dissertation.

Chapter Two reviews existing synthetic methods for trisulfide formation, highlighting the need for greener and more sustainable approaches. It discusses current challenges, including the difficulty of synthesizing unsymmetrical trisulfides, and introduces our novel method for achieving these compounds with high yield, purity, and selectivity. This chapter lays the groundwork for the synthetic developments detailed in chapter 4.

Chapter Three shifts the focus to the cancer biology of organosulfur compounds (OSCs), with a detailed examination of trisulfides. It provides an in-depth analysis of their extraction, biosynthesis, metabolism, and bioavailability, particularly in relation to cancer chemoprevention**.** The chapter investigates the role of reactive species, including hydrogen sulfide (H_2S) and perthiols (RSSH), generated through thiolysis exchange of trisulfides with protein thiols.

The role of H_2S as a crucial gaseous signaling molecule is examined, highlighting its involvement in various physiological processes. The chapter also explores perthiols,

characterized by their unique chemical properties, which enable them to participate in redox reactions and radical processes.

Chapter Four presents our novel methodology for synthesizing unsymmetrical trisulfides, including details of the optimization conditions and the stability of the products. The methodology yields aliphatic trisulfides in high yield and purity, while aromatic trisulfides are more labile. The trisulfide's distinct chemical shifts in ^{1}H NMR allow for their identification and differentiation from other sulfur species. The applicability of this method extends to a range of functional groups, including those derived from cysteine and sugar moieties.

Chapter Five investigates the cytotoxic effects of trisulfides in cancer cells, focusing on a refined library of trisulfides to identify structure-activity relationships, particularly in benzyl derivatives. The chapter examines the impact of various substituents on perthiol stability, demonstrating that electron-donating groups prolong perthiol lifetime and enhance cytotoxicity. This by raising their p*K*a and reducing their disproportionation to homotrisulfides. The *p*-OMe derivative, in particular, displayed higher extracellular perthiol concentrations, as measured by Ellman's assay, corroborating initial stability studies. The chapter further extends to monitoring H_2S production in WHCO1 cancer cells using a fluorescent probe, establishing that fluorescence intensity, indicative of H_2S concentration, increases with greater electron release from *para*-substituents. This relationship between enhanced perthiol stability and increased H_2S production reinforces the thiolysis-based mechanism of trisulfide cytotoxicity and suggests a pathway for designing more effective anticancer agents. Additionally, studies using a dansyl-propyl trisulfide probe indicated localisation in the endoplasmic reticulum (ER), suggesting a role for the unfolded protein response (UPR) in conjunction with H_2S signaling in promoting apoptosis.

Publications and Conferences

Publications

1. **Ali, D**.; Amer, Y.; Petersen, W. F.; Kaschula, C. H.; Hunter, R. "A Review of Heterolytic Synthesis Methodologies for Organotri- and Organotetrasulfane Synthesis". *SynOpen.* **2021**, 05, 49-64.
2. **Ali, D**.; Hunter, R.; Kaschula, C. H.; De Doncker, S.; Rees-Jones, S. C. M. "Unsymmetrical Organotrisulfide Formation via Low-Temperature Disulfanyl Anion Transfer to an Organothiosulfonate. *J. Org. Chem.* **2019**, 84, 2862-2869.

Conferences

- **Online Oral Presentation: ‘’** Synthesis and Mechanistic Studies into the Anti-cancer Activity of Garlic-Related Trisulfides’’ at ***the 2nd SU-UF-US-NU AC21 PG/postdoc Symposium,*** February 2022, **Germany**.

- **Online Poster Presentation**: "Investigating the Cytotoxic Effects of Trisulfide Analogues on Cancer Cells" at the *4th Annual International Conference on* ***Cancer Health Disparities***, August 2021, UTRGV School of Medicine, **USA**.

- **Poster Presentation**: "Synthesis of Trisulfide Libraries for Drug Discovery" at the ***L'ORÉAL-UNESCO FOR WOMEN IN SCIENCE*** *Award Ceremony*, November 2021, Kigali, **Rwanda**.

- **Oral Presentation**: "New Synthetic Methodologies for Unsymmetrical Trisulfides" at the ***Frank Warren Conference***, July 2019, Northern Drakensberg, **South Africa**.

Acknowledgements

In the name of Allah, the Most Gracious, the Most Merciful. Without His blessings, this achievement would not have been possible

This thesis is dedicated to my beloved brother, Mustafa Ali, and my dear friend, Razan Ahmed

First, my deepest gratitude goes to my family. To my extraordinary mother, Howida Mustafa, for her boundless love and constant encouragement. I am forever grateful for your sacrifices and for always being there to lift me up. To my great father, Mohamed Alamin, for his constant encouragement, wisdom and guidance. To my sister, Dania, for our long and comforting chats, and to my brothers, Thamir and Abdalla, for their steadfast support. Your love and encouragement have been my pillars of strength.

This PhD was conducted across two universities: the University of Cape Town (UCT) and Stellenbosch University. During my years at UCT, I focused on the development of our methodology. The following years at Stellenbosch University allowed me to focus on biological investigations involving cancer cells.

‘’*To my doctoral supervisors, thank you for shaping the scientist I have become. I am honoured to be part of your academic family*’’

Dear Prof. Hunter, your mentorship has been truly exceptional. It has been both an incredible adventure and great opportunity to be part of your research lab as a postgraduate student. Your passion for organic synthesis has instilled in me a profound appreciation and love for the field. You believed in me when I doubted myself, guiding my transformation from a novice into a confident scientist, ready to tackle the complexities of the molecular world. Your insightful feedback and support have not only enhanced my technical skills but also fostered my critical thinking and problem-solving abilities. You encouraged me to explore new ideas and challenged me to push beyond my limits. I am deeply grateful for the invaluable lessons and experiences you have provided.

Dear Dr., Kaschula, your guidance throughout my PhD studies at Stellenbosch University has been instrumental. Our collaboration has expanded my scientific horizons beyond organic chemistry, encouraging me to embrace interdisciplinary research. I have developed a deep passion for working with cancer cells. The biological skills I have acquired through our work have opened up exciting opportunities to potentially shift my career towards this vital field. Your support and expertise have not only enriched my

academic experience but also inspired me to explore new avenues in my research. I am truly grateful for your mentorship you have provided along the way.

I also extend my gratitude to the people:

At the University of Cape Town
Prof. Anwar Jardine (HOD), for his unconditional support during the most challenging times of my PhD journey. Your mentorship and encouragement have been invaluable, showing me that true courage comes from within. I am also grateful to the past and present students in the Hunter and Jardine research labs for their camaraderie and the lifelong friendships we have formed. Special thanks go to the non-academic staff in the Chemistry Department at the UCT for their invaluable assistance. Your efforts behind the scenes have contributed significantly to the smooth completing my degree.

At Stellenbosch University
I would like to express my gratitude to Prof. Willem Otterlo for welcoming me and providing laboratory space in the De Beers building at the beginning of my journey. I also extend my thanks to both past and current students in Kaschula's and GOMOC group for their support and the shared experiences that have enriched my time here. Your collaboration and friendship have been invaluable to my growth as a researcher.
Beyond academia, I am deeply thankful to my aunts, cousins, friends, my G.P., and my physiotherapist, who stood by me through tough times.
I would also like to express my heartfelt gratitude to the **Organization for Women in Science for the Developing World (OWSD)** for supporting my PhD journey through their PhD Fellowship Program. Your generous support made it possible for me to pursue my research and education, and for that, I am immensely grateful. A special thank you to Prof. Jennifer Thomson, President of OWSD, and Tanja Bole, OWSD Programme Coordinator, for their leadership, encouragement, and support throughout this journey.
I am also incredibly grateful to **L'Oréal-UNESCO For Women in Science** for their award, which provided me with both recognition and financial support, allowing me to further my scientific endeavors and inspire me to push forward even in challenging times.
This PhD journey has been fraught with several challenges, but it has also been immensely rewarding. Each obstacle overcome has made this achievement all the more meaningful. Thank you all for being part of this amazing journey.

Table of Contents

List of Figures

List of Tables

List of Schemes

Abbreviations

^{1}H-NMR	Hydrogen-1 nuclear magnetic resonance
^{13}C-NMR	Carbon-13 nuclear magnetic resonance
AGE	Aged garlic extract
ABTS	Allyl benzyl trisulfides
AdSH	1, Adamantanethiol
$ArB(OH)_2$	Arylboronic acid
Boc	*Tert*-butyloxycarbonyl protecting group
C18	Octadecyl carbon chain
$CDCl_3$	Deuterated chloroform
ACN	Acetonitrile
Cys	Cysteine
DADS	Diallyl disulfide
DAS	Diallyl sulfide
DATS	Diallyl trisulfide
DATTS	Diallyl tetrasulfide
DBTS	Dibenzyl trisulfides
DBU	1,8-Diazabicyclo [5.4.0] undec-7-ene
DCM	Dichloromethane
DMAP	4-(Dimethylamino)pyridine
DMEM	Dulbecco's modified eagle's medium
DMF	*N, N*-Dimethylformamide
DMSO	Dimethyl sulfoxide
DPTS	Dansyl propyl-trisulfide
ER	Endoplasmic reticulum
EtOAc	Ethyl acetate
FBS	Foetal bovine serum
GE	Garlic extract
GSH	Glutathione
GSSG	Glutathione disulfide
HOMO	Highest occupied molecular orbital
HPLC	High-performance liquid chromatography

HRMS	High-resolution mass spectrometry
HSAB	Hard-soft acid-base theory
IC_{50}	Half maximal inhibitory concentration
I_2	Iodine
IR	Infrared spectroscopy
J	Coupling constant
LG	Leaving group
LUMO	Lowest unoccupied molecular orbital
M	Metal
M	Multiplet
m/z	Mass to charge ratio
MDA-MD-231	Breast cancer cells
Me	Methyl
MeCN	Acetonitrile
MeOH	Methanol
mg	Milligram
mL	Millilitres
mmol	Millimole
min	Minute
Mp	Melting point
MS	Mass spectrometry
MTT	3-(4,5-Dimethylthiazol-2-yl)-2,5-diphenyltetrazolium bromide
N_2	Nitrogen
n-BuLi	*n*-Butyl lithium
n-BuMgBr	*n*-Butylmagnesium bromide
NEt_3	Triethylamine
NH_4Cl	Ammonium chloride
OSC	Organosulfur compound
p	*Para*
p-$TolSO_2S$-	4-Methylbenzenethiosulfonate ion
PBS	Phosphate-buffered saline
Ph	Phenyl

$(PhthN)_2S_2$	Bis(1-phthalimidyl) disulfide
(PhthNSCl)	Phthalimidosulfenyl chloride
PMBCl	4-Methoxybenzyl chloride
Rf	Retention factor
ROS	Reactive oxygen species
RS-	Thiolate ion
RSS	Reactive sulfur species
RSS-	Perthiolate ion
Rt	Room temperature
SAC	*S*-Allylcysteine
SAMC	*S*-Ally lmercaptocysteine
SAR	Structure-activity relationship
SD	Standard deviation
S_NAc	Nucleophilic Acyl Substitution Reactions
SDS	Sodium dodecyl sulfate
S_N2	Bimolecular nucleophilic substitution
SO_2Cl_2	Sulfuryl chloride
SU	University of Stellenbosch
t-BuSSTs	*Tert*-butyl thiotosylate
TrSH	Tritylthiol
TsSK	Potassium thiotosylate
TMSCl	Trimethylsilyl chloride
THF	Tetrahydrofuran
TLC	Thin layer chromatography
UT	Untreated
UCT	University of Cape Town
Uv	Ultraviolet
WHCO1	Oesophageal cancer cell line

Literature Review

CHAPTER 1: The Occurrence of Trisulfides in Nature

1.1 Introduction

Based on its historical connection, in this thesis, we will use the term trisulfide rather than trisulfane as the IUPAC nomenclature.

Organotrisulfides, defined as organic molecules containing the polysulfide -S-S-S- linkage, are found in a variety of natural environments, including in plants, in the atmosphere, in the soil, and in living organisms. They are synthetically interesting molecules that find connections into a variety of fields including the life sciences, material science, and natural products chemistry.[1] Organotrisulfides elicit a range of biological activities that include antimicrobial,[2] antioxidant,[3] antithrombotic,[4] antiatherosclerotic[5] as well as antitumor[6-8] properties. Trisulfide natural products of the type R^1SSSR^2 have a broad variation of R^1/R^2 groups, which can be the same (homotrisulfide) or different (heterotrisulfide), covering both (hetero) aromatic and aliphatic groups (linear or branched). The following sections describe various classes of organotrisulfide natural products.

1.2 Trisulfide Natural Products

1.2.1 Epitrithiodioxopiperazines

This class of naturally occurring trisulfide based on biosynthesis from an amino acid dating back to 1966 and is categorized by the presence of a trisulfide bridge over a dioxopiperazine core, **Figure 1.1**.

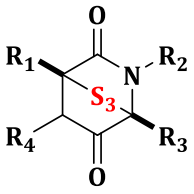

Figure 1.1: General structure of the epidithiodioxopiperazine natural products.

The class can be sub-divided based on biogenetic origin depending on the aromatic amino acid (tyrosine, phenylalanine, or tryptophan) precursor. Mass spectroscopy as well as NMR spectroscopy have proved to be powerful characterization tools for establishing

their structural integrity, particularly in assigning trisulfide over disulfide or tetrasulfide counterparts. Epitrithiodioxopiperazines secondary metabolites have been shown to possess potent antifungal, antibacterial and anticancer biological activities in which the R_1, R_2, R_3 and R_4 groups (**Figure 1.1**) are variable.[9-14] A range of natural products derived from tyrosine and phenylalanine are shown in **Figure 1.2** below together with their year of discovery and principal bioactivity.

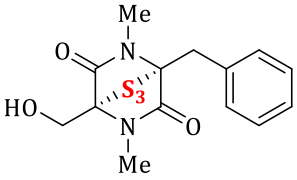

Hyalodendrin, 1
Antibacterial
1973, Devault *et al.*[9]

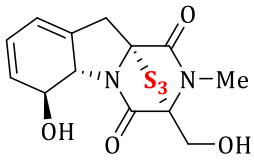

Gliotoxin, 2
Immunosuppressive activity
1987, Waring *et al.*[10]

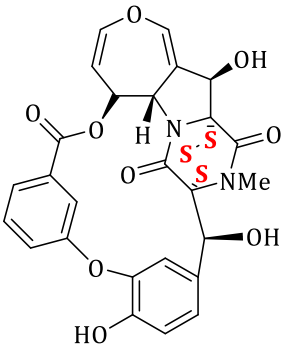

Emestrin B, 3
Antibacterial
1987, Kawai *et al.*[11]

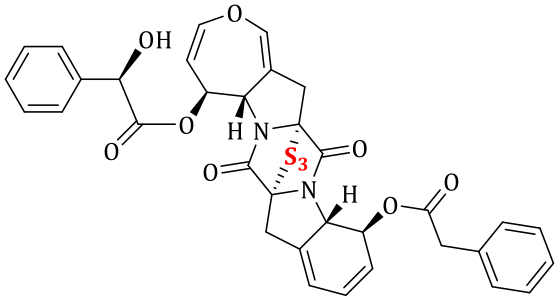

Emethallicins, 4
Histamine release
1990, Kawai *et al.*[12]

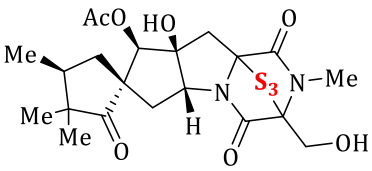

Sirodesmin C, 5
Phytotoxicity
2012, Mitrovac *et al.*[13]

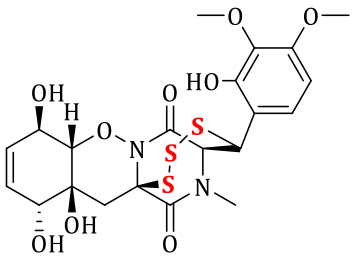

Outovirin C, 6
Antifungal
2014, Mattila *et al.*[14]

Figure 1.2: Tyrosine and/or phenylalanine - derived epidithiodioxopiperazines.

Members of another class of epidithiodioxopiperazines that are tryptophan-derived are shown in **Figure 1.3** from various fungi.[15-20] They exhibit a variety of potent biological activity ranging from antifungal to antinematodal as well as anticancer properties typical of indole-derived moieties. In contrast, Sporidesmin **C** does not yet have data on its biological activity.

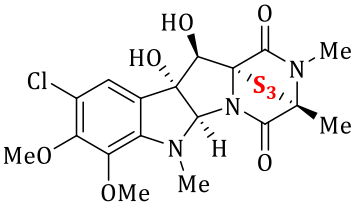

Sporidesmin C, 7
1966, Hodges *et al.*[15]

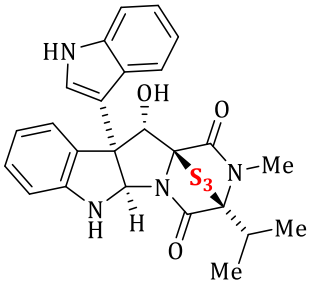

Leptosin E, 8
Anticancer
1994, Numata *et al.*[16]

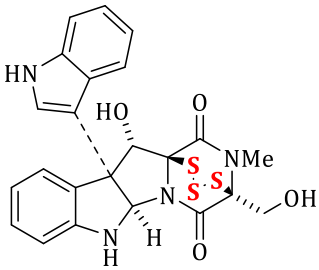

T988 A, 9
Anticancer
2004, Munro *et al.*[17]

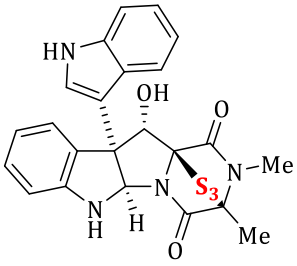

Gliocladine D, 10
Antinematodal activity
2005, Zhang *et al.*[18]

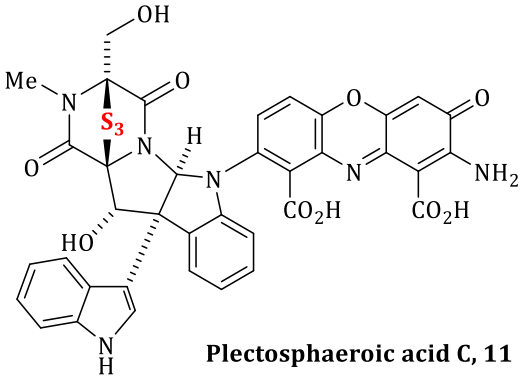

Plectosphaeroic acid C, 11
Anticancer
2009, Andersen *et al.*[19]

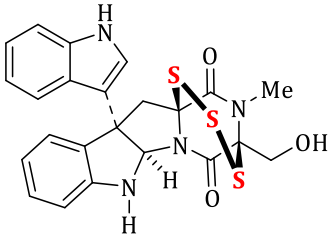

(+)-Luteoalbusin B, 12
Anticancer
2012, Wang *et al.*[20]

Figure 1.3: Tryptophan-derived epidithiodioxopiperazines.

More complex dimeric tryptophan-derived[16,18,21-24]Epitrithiodioxopiperazines are known as shown in **Figure 1.4**, building on the monomeric motifs displayed in **Figure 1.3**.

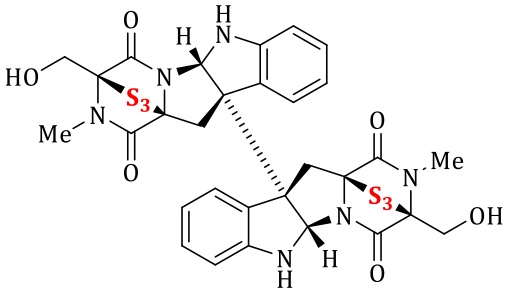

Chaetocin C, 13
Antimicrobial, Anticancer
1988, Natori *et al.*[21]

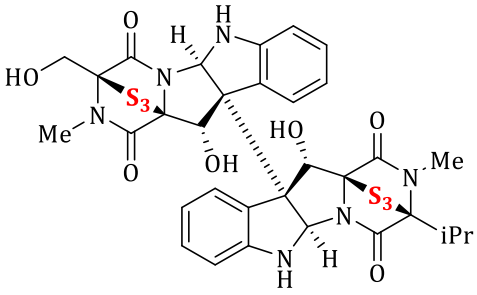

Leptosin G_1, 14
Anticancer
1994, Numata *et al.*[16]

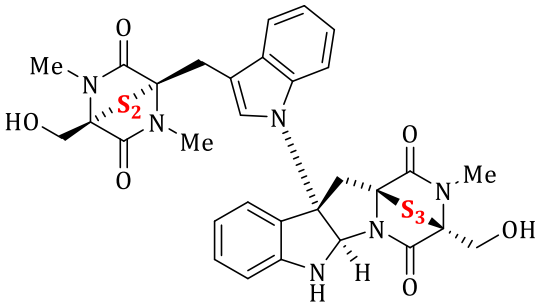

Chetoseminudin A, 15
Immunosuppressive activity
2004, Fujimoto *et al.*[23]

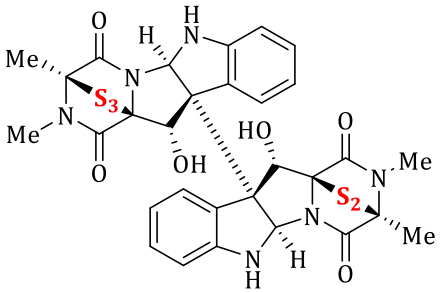

Gliocladine A, 16
Antinematodal
2005, Zhang *et al.*[18]

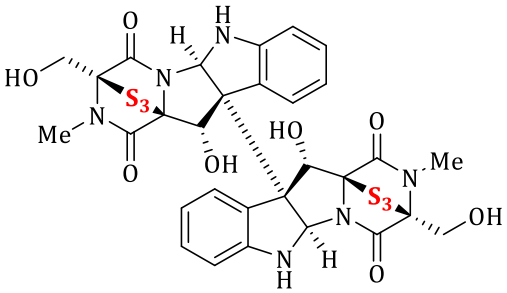

Chetracin C, 17
Anticancer
2012, Zhu *et al.*[24]

Figure 1.4: Dimeric epidithiodioxopiperazine trisulfide alkaloids.

1.2.2 Varacin Family

In the early 1995's, new trisulfides containing a cyclic trisulfide appended to an aromatic ring were reported by Makarieva and co-workers[25] as Varacin **18** and its derivatives **19**, **20**, **Figure 1.5**. These compounds were isolated from marine sources and shown to exhibit potent antibiotic, cytotoxic, and antiviral activities.[25] This was followed by the discovery of similar structures such as Lissoclmotoxin A **21** and the methylthio derivative

12 that were isolated from tunicates *lissbclihum perfuratum*[26] and *Lissoclinium* cf. *badium*, respectively.[27]

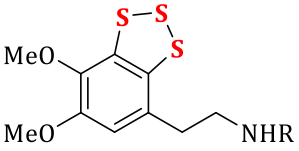

Varacin, 18
Antibiotic, cytotoxic, antiviral
1995, Makarieva *et al.*[25]

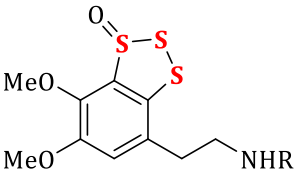

Varacin, 19
R=H,OMe
Antibiotic, cytotoxic, antiviral
1995, Makarieva *et al.*[25]

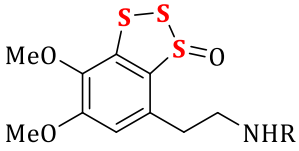

Varacin, 20
R=H,OMe
Antibiotic, cytotoxic, antiviral
1995, Makarieva *et al.*[25]

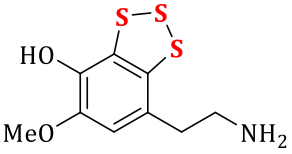

Lissoclinotoxin, 21
Antimicrobial and antifungal
1991, Guyot *et al.*[26]

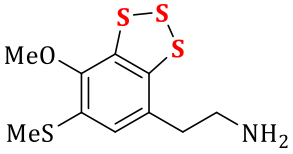

Methyl thio, 22
Antimicrobial
2005, Namikoshi *et al.*[27]

Figure 1.5: Varacin family and its derivatives.

1.2.3 Functionalised Cyclic Trisulfides

Another interesting class of organotrisulfide comprises having the motif as part of a medium-sized carbocyclic ring system, often with other sulfurs present. In 1966, Morita and Kobayashi[28,29] successfully extracted the first organic cyclic trisulfides pentathiepane **23** and its analogue[30] **24** from Shiitake mushrooms extract. These compounds have been reported to show antibacterial activity as well as platelet aggregation inhibition. This was followed by the discovery of the cyclooctane trisulfide analogue **25**, which was isolated from 'stink bean' Parkia speciose[31,32] as displayed in **Figure 1.6**. One year later in 2002, Řezanka and Dembitsky isolated substituted 1,2,3-trithiocane cycles **26** from the sea squirt *Perophora viridis*.[33] Thereafter, the last two decades of the 20th century experienced the emergence of a new natural product family of cyclic trisulfides containing the 1,2,3-trithiane ring.[34] Examples **27-30**[35-39] shown in **Figure 1.6** were isolated from various plants and shrubs (*asparagus,* alga *Chara globularis*, *Aplidium* and *Cassipourea guianensis*), and they showed a range of biological properties.

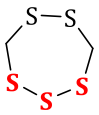

Pentathiepane, 23
1966, Morita *et al.*[28, 29]

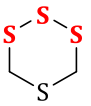

Tetrathiane, 24
1986, Chen *et al.*[30]

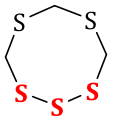

Pentathiocane, 25
2001, Miyazawa *et al.*[32]

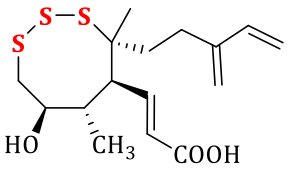

1,2,3-trithiocane derivative, 26
Antibacterial
2002, Řezanka and Dembitsky.[33]

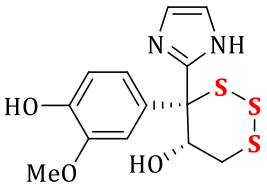

Imidazol-trithiane, 27
Anticancer
1989, Blunt *et al.*[36]

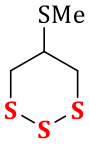

Methylthio trithiane, 28
Herbicides (Photosynthesis inhibitor)
1980, Anthoni *et al.*[35]

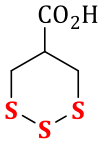

Trithiane-carboxylic acid, 29
antibacterial, nematicidal
1996, Wolf *et al.*[34]

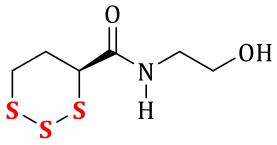

Trithiane-carboxamide, 30

2000, Ichimaru *et al.*[39]

Figure 1.6: Naturally occurring cyclic trisulfides.

1.2.4 Enediyne-Containing Trisulfides

The final and probably the most inspiring class of trisulfide natural products is to be found as the enediyne class of natural products, which have attracted significant attention from top synthetic organic chemists for total synthesis programmes because of both their complexity and their extraordinary antibiotic and antitumor activities. The first members isolated were Esperamicin **31**[40-41,42] and Calicheamicin **32**,[43] **Figure 1.7**, in 1985 and 1987 respectively from bacterial origin. Both compounds **31** and **32** were prepared by total synthesis a few years later by Nicolaou and his group in 1992[44] and 1993[45] respectively. Their biological mode of action has been extensively studied to involve binding to the minor groove in DNA, after which trisulfide cleavage initiates a cascade of reactions resulting in a Bergman-type cyclization to generate a diradical species. This abstracts a hydrogen atom from the deoxyribose (sugar) backbone of DNA leading to strand scission.[46] Other fascinating members of this family include Namenamicin **33**[47] and Shishijimicin A–C[48] **34**, **Figure 1.7**. These two compounds are very attractive

molecules for total synthesis, which have also been conquered by Nicolaou and coworkers in recent studies,[49-51] (Shishijimicin synthesis will be mentioned in Chapter Two).

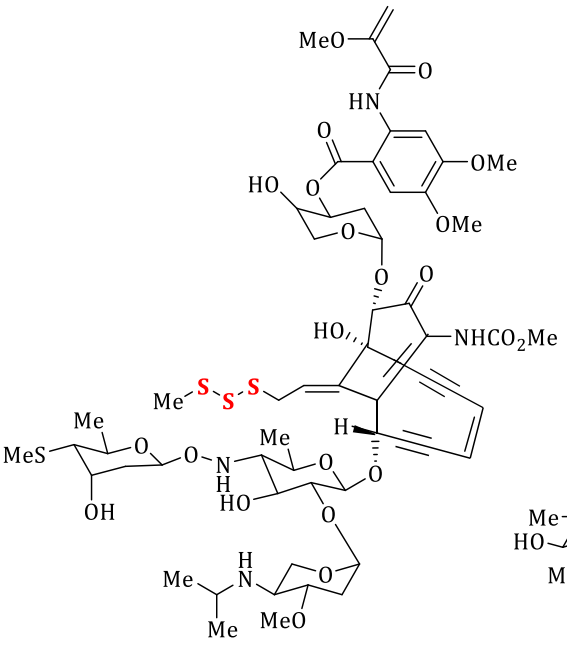

Esperamicin A1, 31
Antibiotics and antitumor
1985, Konishi *et al.*[40-42]

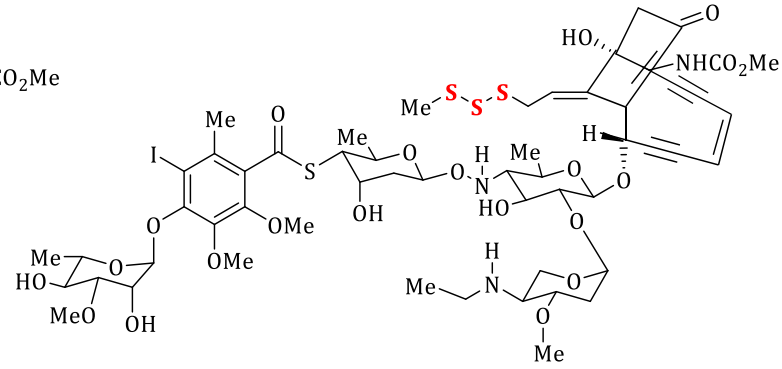

Calicheamicin, 32
Antitumor
1987, Lee *et al.*[43]

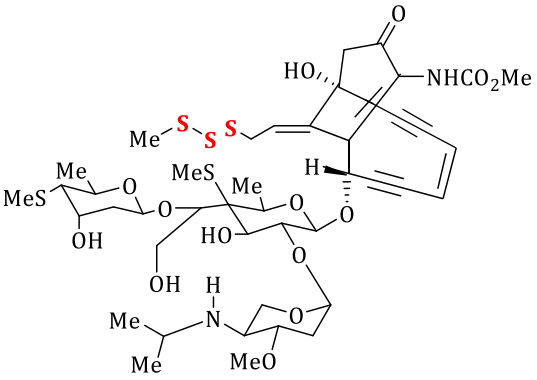

Namenamicin, 33
Anticancer, antimicrobial
1996, Ireland *et al.*[47]

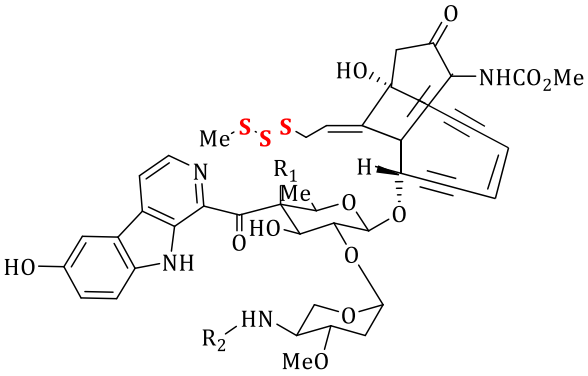

Shishijimicin, 34
Anticancer
2003, Fusetani *et al.*[48]
A: R_1 = SMe, R_2 = i-Pr
B: R_1 = H, R_2 = i-Pr
C: R_1 = SMe, R_2 = Et

Figure 1.7: Examples of naturally occurring enediynes trisulfide compounds.

1.2.5 Miscellaneous

A cyclic trisulfide recently discovered in 2023 by Shen *et al.*[52] is the bridged angucycline, Neogrisemycin **35**, from *Streptomyces albus* bacteria. However, this compound did not

exhibit antibacterial activity nor anticancer activity at low concentrations under the tested conditions, **Figure 1.8**.

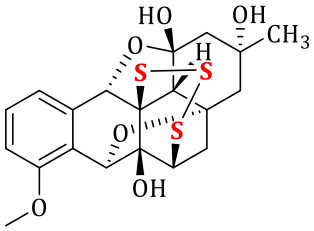

Neogrisemycin, 35

2023, Shen *et al.*[52]

Figure 1.8: Structures of Neogrisemycin.

1.3 Acyclic Trisulfides

1.3.1 The Alliaceae Family

In 1971, Boelens *et al*. reported on the first trisulfides from the *Alliaceae* family, which is the most famous family containing organosulfur compounds (OSCs). This family includes the genus *Allium*, which contains many species of flowering plants, including onions, garlic, shallots, leeks, and chives. The study analysed steam-distilled onion oil,[53] which was found to contain various homo- and hetero-trisulfides **36-47** depicted in **Figure 1.9**. The structure of these compounds was elucidated by a combination of gas chromatographic and mass spectrometric techniques.[53-55]

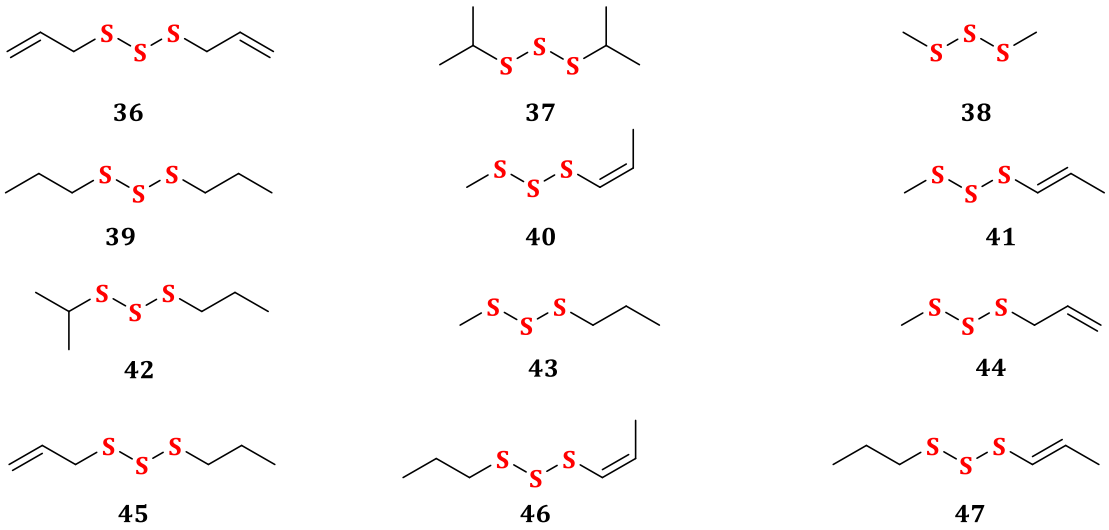

Figure 1.9: Naturally occurring organotrisulfides from steam-distilled onion oil.

Extensive studies over the last few years has been directed at diallyl trisulfide **36** (DATS) in view of its various biological activities such as anti-cancer, anti-bacterial, anti-thrombotic,[7,8] anti-inflammatory and immunomodulation.[6] DATS will be extensively discussed in Chapter three on the Biology Review. In 2006, Ariga *et al*. reported that allyl methyl trisulfide (AMT), **45**, is the most active of the garlic derivatives against platelet aggregation both *in vitro* and *in vivo*.[4]

1.3.2 Functionalised Linear Trisulfides

Further unsymmetrical trisulfide substructures have been discovered from a tropical plant named *Scorodophloeus zenkeri* with significant anti-bacterial and anti-fungal activity.[56] They are usually found as an inseparable mixture with their symmetrical derivatives. **Figure 1.10** shows **48**, **49** and **50** as examples, which all contain an extra sulfur-based functionality as either a thioacetal or a thioaldehyde beyond the trisulfide. Compounds **51** and **52** are also found along with **48** and **49** in extracts of the plant Tulbaghia,[57] which is known as wild garlic, and is native of South Africa, Tanzania and Mexico where it has been widely used in traditional medicine.

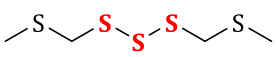

48
antibacterial and anti-fungal
2002, Kouokam *et al*.[56]

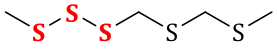

49
antibacterial and anti-fungal
2002, Kouokam *et al*.[56]

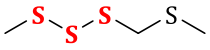

50
antibacterial and anti-fungal
2002, Kouokam *et al*.[56]

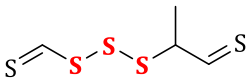

51
2008, Pino *et al*.[57]

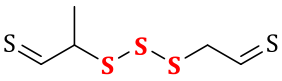

52
2008, Pino *et al*.[57]

Figure 1.10: Naturally occurring linear trisulfides.

Other functionalized natural product trisulfides bearing extra functionality isolated from a range of bacteria and sea sponges[58-64] are shown in **Figure 1.11**.

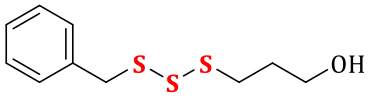

53
antimicrobial
1972, Hoyer *et al.*[58]

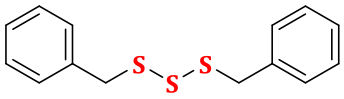

54
Anticancer
1990, De Sousa *et al.*[59]

55
Anticancer
1992, Kohama *et al.*[62]

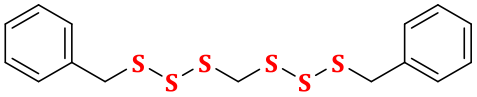

56
Antifungal
2001, Bolzani *et al.*[64]

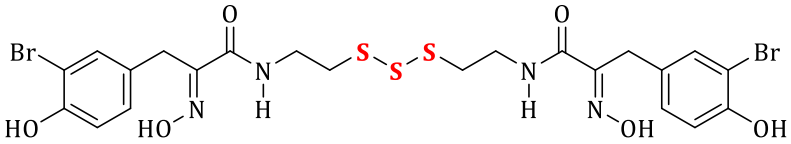

57
Antibacterial
2003, Jung *et al.*[63]

Figure 1.11: Examples of functionalized-trisulfide containing compounds.

The trisulfide analogues of cystine and glutathione disulfides **58** and **59** shown respectively in **Figure 1.12** have also been reported as natural products.[65] They have been shown to contribute to the control of 5-aminolaevulinate synthetase activity in *Rhodopseudomonas spheroids*, which plays a major role in the control of bacteriochlorophyll synthesis.[65]

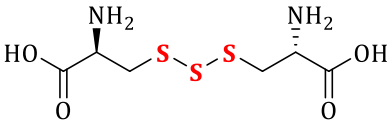

Cysteine trisulfide, 58
1976, Xifra *et al.*[65]

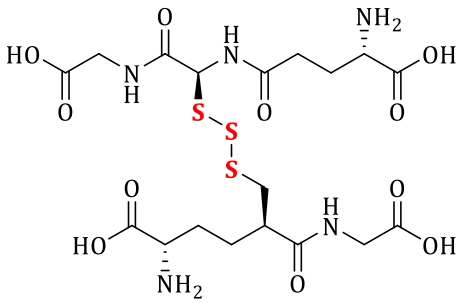

Glutathione trisulfide, 59
1976, Xifra *et al.*[65]

Figure 1.12: Cysteine and Glutathione trisulfide.

In summary, this Chapter has presented several classes of naturally occurring trisulfides occurring in Nature, with many of them demonstrating an impressive array of potent

biological activities. Taking modern biological studies on simplified synthetic organotrisulfides as a model, these beautiful trisulfide natural products presumably exert their biological activity through their ability to regulate hydrogen sulfide (H_2S), a crucial signalling molecule involved in cardiovascular health and inflammation. This is an important topic of this thesis and will be described in detail in Chapter five. The next Chapter will review synthesis methodologies available for organotrisulfide synthesis.

CHAPTER 2: Review of Methodologies for Organotrisulfide Synthesis

2.1 Introduction

This review Chapter is based on our Review on organotri-and tetrasulfides published in *SynOpen*[66] in 2021 building on previous reviews of the field.[67,68] The formation of the S-S-S triad through heterolytic approaches is the sole focus of this review, as predictive radical or concerted methodologies are unknown in the field. In this review, as with Chapter 1, we will adopt the popular and much used (particularly in the older literature) ''sulfide'' throughout rather than the IUPAC nomenclature of ''sulfane''. The terms symmetrical/unsymmetrical trisulfide and homo/heterotrisulfide will also be used interchangeably. The recent emergence of a range of organopolysulfide motifs in a range of expressions and applications including natural products,[51] as cytotoxic agents,[69] the design of substrates for H_2S production as a bio-gasotransmitter,[70] as linkers in antibody-drug conjugates,[71] and as high-capacity materials for cathodes in rechargeable lithium batteries[72] reflects the importance of the field of which trisulfides are an important sub-class. Key examples are shown in **Scheme 2.1**.

Natural Products

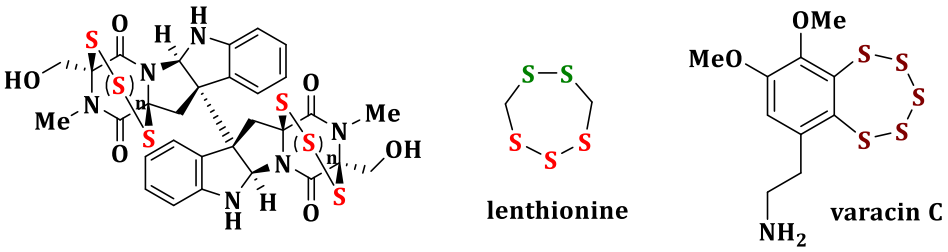

n = 1; (+)-chaetosin C

n = 2; (+)-12,12'-dideoxychetracin A

Trisulfides as cytotoxic agents

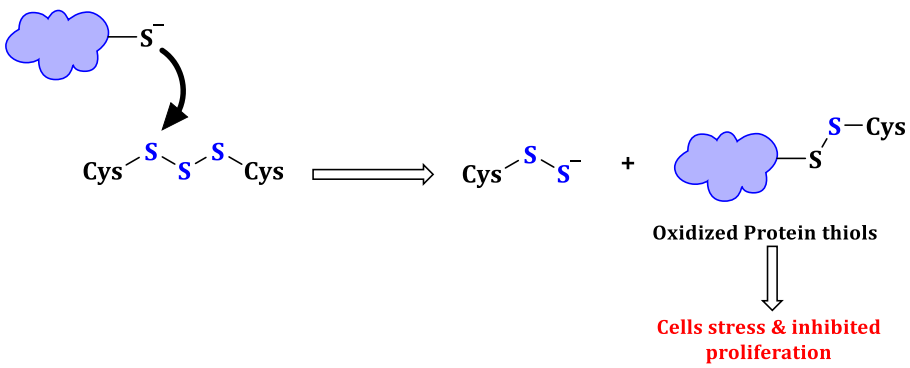

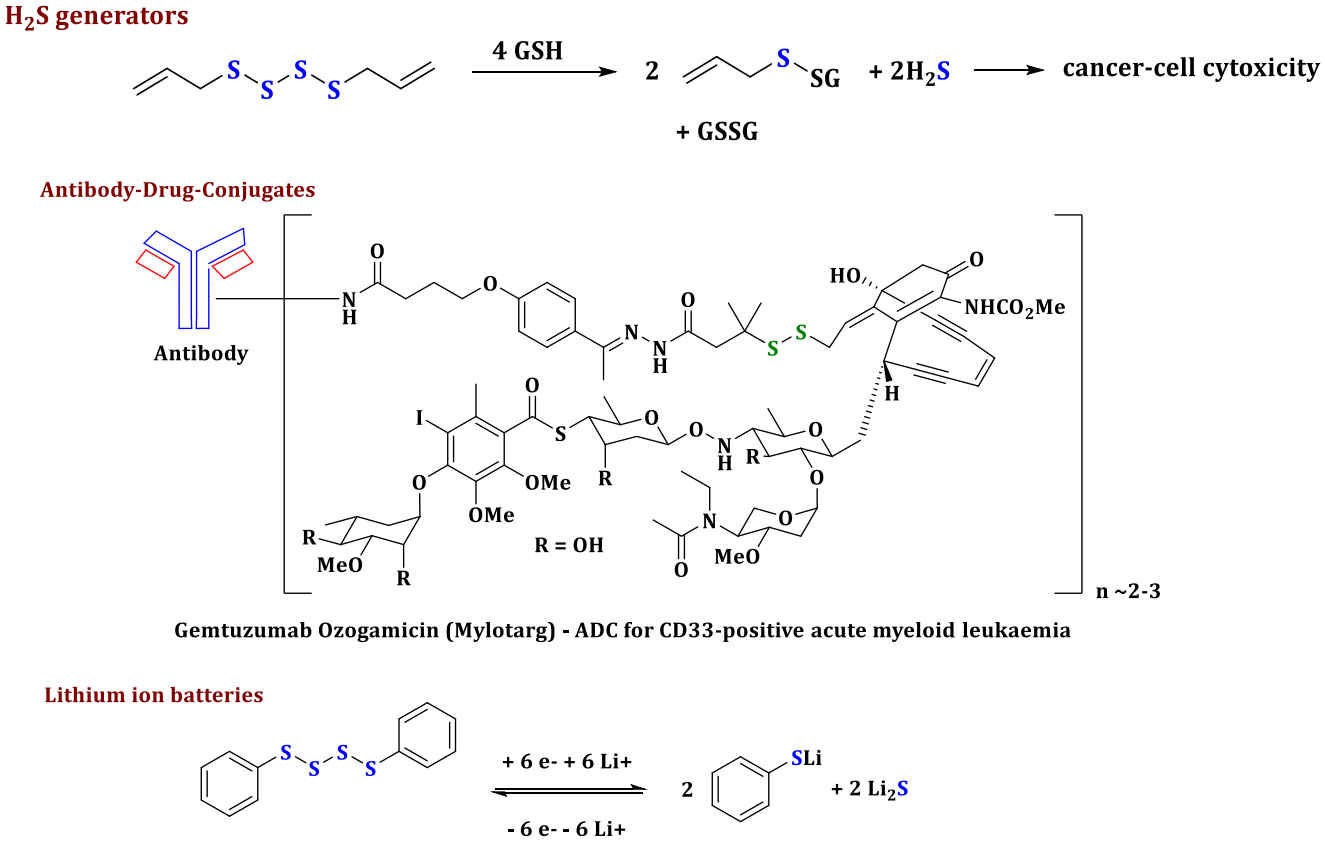

Scheme 2.1. An overview of the application of polysulfide motifs.

The remainder of this Review will focus exclusively on methodologies available for organotrisulfide synthesis.

2.2 Mechanistic Considerations for Organotrisulfide Synthesis

In the present era of rational synthesis (retrosynthesis), it is useful to start this review by rationally identifying the various heterolytic disconnection points on offer to the synthetic chemist for trisulfide synthesis. **Figure 2.1** identifies the two disconnection points for a symmetrical (homo) case, translating to a variety of heterolytic nucleophilic and electrophilic sulfur synthons ultimately.

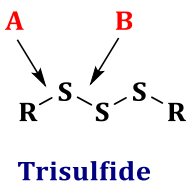

Figure 2.1: Disconnection points for a symmetrical trisulfide.

An examination of known literature methodologies for accessing the two disconnection points shown in **Figure 2.1** reveals that only two types of overall disconnection sequence have representation in the literature. These involve the coupling of either two synthons (from a one-bond disconnection involving either disconnection **A** or **B** in **Figure 2.1**) or three synthons (from a two-bond disconnection sequence). Each type assumes that a one-pot reaction can access the respective target. While one-bond disconnections can satisfactorily access unsymmetrical (hetero) trisulfides (and therefore also homotrisulfides), two-bond disconnections are realistically only suitable for homotrisulfide synthesis. The various methodological approaches known are illustrated in **Table 2.1**, in which the nucleophilic partner is always placed first in the combination description in brackets, and the numbers refer to the number of sulfurs in any synthon. The two-bond disconnections are placed first because they are the oldest known.

Table 2.1: Known methodologies for synthesizing trisulfides (R = organic group; M = H or metal; Lg = leaving group)

Designation in text	Number of disconnections	Combination	Synthon description
A	Two	[3 + 0 + 0]	MS_3M + RX + RX
B	Two	[1 + 1 + 1]	MSM+ RSLg + RSLg
C	Two	[1 + 1 + 1]	RSM + LgSLg + RSM
D	One	[1 + 2] [0 + 3]	RSM + RSSLg RM + RSSSLg
E	One	[2 + 1]	RSSM + RSLg

2.3 Methodology A – Double Alkylation of a Trisulfide Dianion

Methodology **A** involving the double alkylation of an inorganic trisulfide anion is the oldest known of all the methodologies in **Table 2.1**. Though there are reports on the reaction of polysulfide anions with alkyl halides dating back to the late nineteenth and early twentieth century, they suffer from low purity in the sulfide starting material. This methodology predates methodologies **B-E** in which sulfenylating agents are required **Table 2.2** summaries the various alkylating agents used for this option over more than a century.

Table 2.2: Homotrisulfides via methodology A

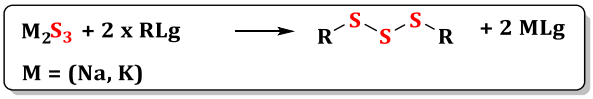

Entry	Year/ Author	M	R-Lg	RSSSR % yield
1	1908/ Strecker.[73]	Na	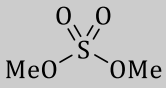	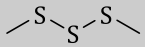 80%
2	1946/ Fuson et al.[74]	Na	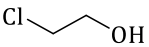	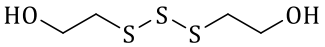 80%
3	1957/ Feher et al.[75]	K	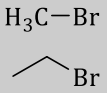	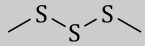 81% 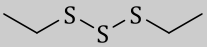 55%
4	1989 / Penczek et al.[76]	K	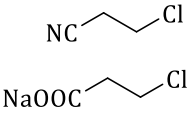	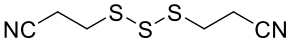 20% 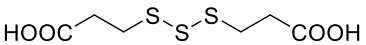 56%
5	2013 / Wirth *al.*[77]	Na	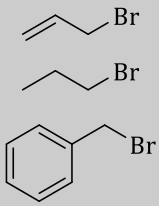	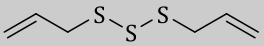 53% 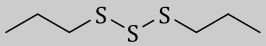 33% 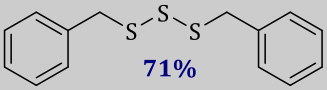 71%

The earliest report of dialkylation of a trisulfide dianion was more than a hundred years ago[73] when Strecker (that is Willem, not Adolph, the latter famous for the Strecker reaction) demonstrated that dimethyl trisulfide could be prepared by reaction of Na_2S_3 (prepared from Na_2S + 2S) with dimethyl sulfate in about 80% isolated yield. The trisulfide was purified by vacuum distillation ($bp_{14\ mmHg}$, 60-2°) out of the mixture of polysulfide products and analysed by combustion analysis since NMR was not available. In more recent times (e.g., the 2013 paper in entry **5**), the trisulfide dianion was accessed from reacting sulfur and anhydrous sodium sulfide in water, but this too results in an equilibrium mixture of polysulfide dianions.[74,77] Hence, the main limitation of this method is the formation of the corresponding di-, tetra- and pentasulfides. Understandably, separating compounds with non-polar R groups is problematic because of their similar Rf values on TLC, and is only possible using C18 reverse-phase silica chromatography.[77] This separation challenge also means that methodology **A** is only effective for

homotrisulfide synthesis in view of the added difficulty of separating the homo- and heterotrisulfides produced when using two different alkylating agents. Although the authors didn't explicitly comment on mechanism, one can safely assume that the reaction likely proceeds via a rapid S_N2 process.

A number of groups in the early period reported that higher polysulfide dianions such as tetrasulfide and pentasulfide could also be used to access homotrisulfides, albeit in an indirect way. **Table 2.3** shows some examples.

Table 2.3: Homotrisulfides prepared from tetra- and pentasulfides via methodology A

Entry	Year/ Author	M_2S_n	R-Lg	RSSSR % yield
1	1908/ Strecker.[73]	Na_2S_4 Na_2S_5	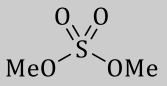	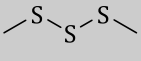 **20%**
2	1923/Riding and Thomas.[78]	K_2S_5		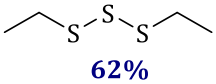 **62%**
3	1965/ Dannley and Zazaris.[79]	Na_2S_4	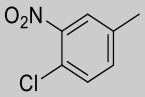	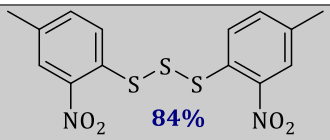 **84%**

In the publication in 1908 mentioned in **Table 2.3**,[73] Willem Strecker showed that trisulfide (MeSSSMe) could also be accessed from the pentasulfide (MeSSSSSMe) via distillation, in which sodium pentasulfide (Na_2S_5) was used as the first reported case of using a sulfur dianion source with high sulfur content in a trisulfide synthesis. Furthermore, trisulfide was also obtained from sodium tetrasulfide (Na_2S_4) via an unclear mechanism.[73] Entry **2** also shows another case from using pentasulfide as the starting material that was developed by Riding and Thomas between the Universities of Cape Town and Liverpool, which was reported in *J. Chem. Soc* in 1923.[78] In their work, diethyl pentasulfide could be obtained by treating ethyl iodide with pure potassium pentasulfide (the source of this wasn't given) in ether at room temperature. On heating the crude pentasulfide, disulfide and elemental sulfur were produced, which then reacted (recombined) to afford the trisulfide on distillation. Once again, a separation issue would

have been encountered, and mechanistic details, given that it was reported almost a hundred years ago, were absent. **Scheme 2.2** summarises these events:

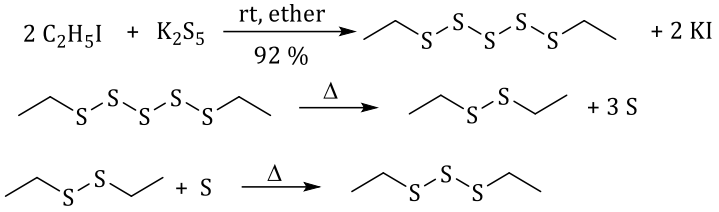

Scheme 2.2: Homotrisulfide synthesis via pentasulfide bisanion (S_5^{-2}).[78]

Similarly, tetrasulfide dianion (**Table 2.3**, entry **3**) could be accessed by dissolving 3 equivalents of elemental sulfur (S_8) into molten sodium sulfide (Na_2S). This was then reacted with 3-nitro-4-chlorotoluene in ethanol in an S_NAr reaction to yield the trisulfide ultimately.[79] No details were provided for the sulfur extrusion. In summary, one can start with Na_2S (this is stable) and add appropriate equivalents of sulfur to convert to the tri (Na_2S_3)[80] or tetrasulfide (Na_2S_4) dianions,[81] but these will always exist in an equilibrium of polysulfide anions.

A recent study reported that the interconversion and alkylation of polysulfides operate under Curtin–Hammett control, indicating that the rates of equilibration and interconversion of polysulfides are faster than the electrophilic labeling process.[82] Overall, the challenge of generating specific functionalized polysulfides is influenced not only by the reactivity of the nucleophilic sulfide species but also significantly depends on the characteristics and behaviour of the electrophiles employed in the labeling process.

No-one has found a solution to this problem as yet (possibly they never will), and hence the best that one can conclude for this methodological option is that although straightforward to carry out, it is limited in both the production of a questionable purity in the product and only being able to access mixtures of homopolysulfides.[79] Rather than start with the inorganic sulfide, reacting sulfur with an inorganic hydroxide together with an alkyl halide is also known[83] in which it is safe to assume that reaction proceeds via a polysulfide anion or dianion and hence suffers from the same limitations. Similarly, one may start from S_8 using a tin/copper promotor (**Scheme 2.3**),[84] but once again, reaction with RX yields a range of polysulfides.

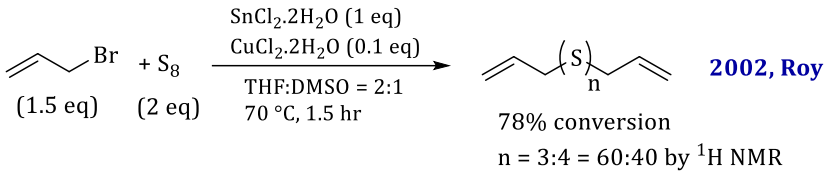

Scheme 2.3: Example of methodology A via elemental sulfur and alkyl halide.

Interestingly, reaction of sulfur in DMF and ammonia with acrylonitrile has also been reported to yield a moderate yield (49%) of the trisulfide, **Scheme 2.4**.[76]

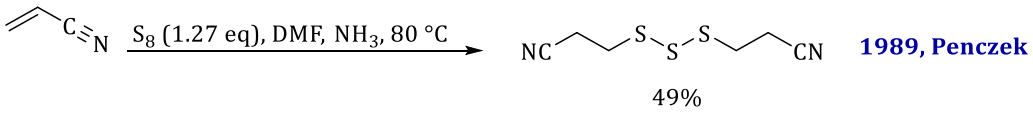

Scheme 2.4: Homotrisulfide synthesis via elemental sulfur and acrylonitrile.

Cyclic trisulfides are also known to be available using methodology **A** and have been fully reviewed,[67,85] but once again, mixtures of polysulfides are invariably produced. In the following section, we will examine the second of the two-bond disconnection methodologies as a [1+1+1] protocol.

2.4 Methodology B – Double Sulfenylation of a Mono Sulfide Dianion

The next sub-division as formulated in **Table 2.4** chronologically, methodology **B**, involves the central sulfur of the trisulfide acting as a nucleophilic source (S^{-2}), reacting twice with a suitable electrophilic partner, RSLg, and was developed from the 1960s once sulfenylating agents had become available. **Table 2.4** depicts various examples spanning an almost sixty-year timeframe to the present day.

Table 2.4: Homotrisulfides prepared from mono sulfide dianions via methodology B

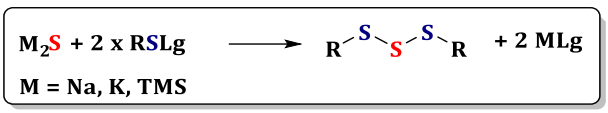

Entry	Year/ Author	M	RSLg	RSSSR % yield
1	1961/Swan et al.[86,87]	Na	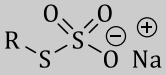 **Bunte salt** R = C_3H_5, C_2H_5, C_6H_{11} Bn, $PhCOCH_2$, *p*-Tol	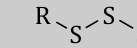 R = C_3H_5, C_2H_5, C_6H_{11} Bn, $PhCOCH_2$, *p*-Tol **65-70%**

2	1962/Pitombo.[88]	H	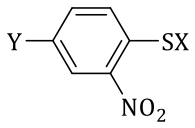 X = Br, Cl; Y = Br, Cl, CH_3, H, NO_2	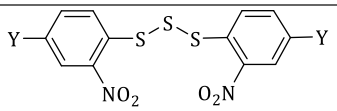 X = Br, Cl; Y = Br, Cl, CH_3, H, NO_2 **51-81%**
3	1967/Field et al.[89]	K,Na	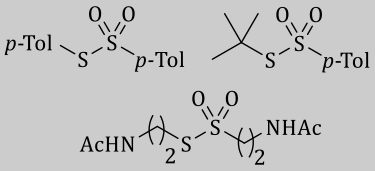	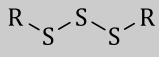 R = *p*-Tol; ^{t}Bu; AcNH $(CH_2)_2$ **82-94%**
4	1982,1986 / Field et al.[90,91]	Na	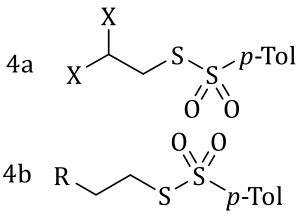	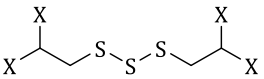 X = $(CH_2)_3Cl$, $(CH_2)_3SBn$, **52,59%** 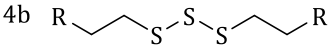 R = BnSO, **69%**
5	1989/Capozzi et al.[92]	TMS	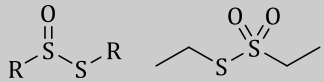 R= Me, Ph, *p*-Tol	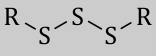 R =Me, C_2H_5,Et, *p*-Tol **73-95%**
6	2019/Bhabak et al.[93]	Na	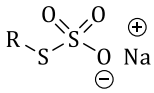 **Bunte salt** R = C_3H_5, C_3H_7, C_5H_9, C_4H_9 R = x Bn x = *p*-Me; *p*-^{i}Pr; *p*-^{t}Bu; *p*-F; *p*-Cl; *p*-Br *p*-CF_3; *o*-NO_2; *m*-NO_2; *o*-Me; *m*-Cl; *m*-Br,	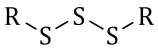 **24 - 97%**
7	2019/Tanini et al.[94]	TMS	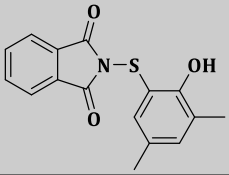	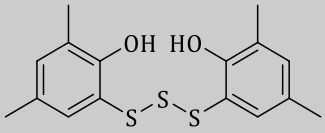 **53%**

One can see that most cases use a group 1 metal as counter-ion for the M_2S synthon, although silicon (entries **5** and **7**) has also been used. Seminal work by Brian Milligan and John Swan in the early 1960s[86,87] established the first examples of trisulfide synthesis using this methodology in which a Bunte salt (an *S*-alkyl or *S*-arylthiosulfate salt as $RSSO_3M$) was used as the sulfenylating agent for sodium sulfide (Na_2S), which is the most reliable of all the sulfide salts in regard to purity and constitution (**Table 2.4**, entry **1**). Bunte salts first appeared in the literature in 1874 when Hans Bunte reacted thiosulfate with ethyl bromide,[95] and Xuefeng Jiang's group have recently reviewed their usage in sulfur-carbon bond formation.[96] The Bunte salt can be obtained via a number of different routes as shown in **Scheme 2.5** as: (i) mono-*S*-alkylation of thiosulfate, (ii) *S*-sulfenylation

of sulfite with a disulfide, or (iii) by reaction of tetrathionate ion with a thiol, with expulsion of sulfur from the leaving group in the substitution:

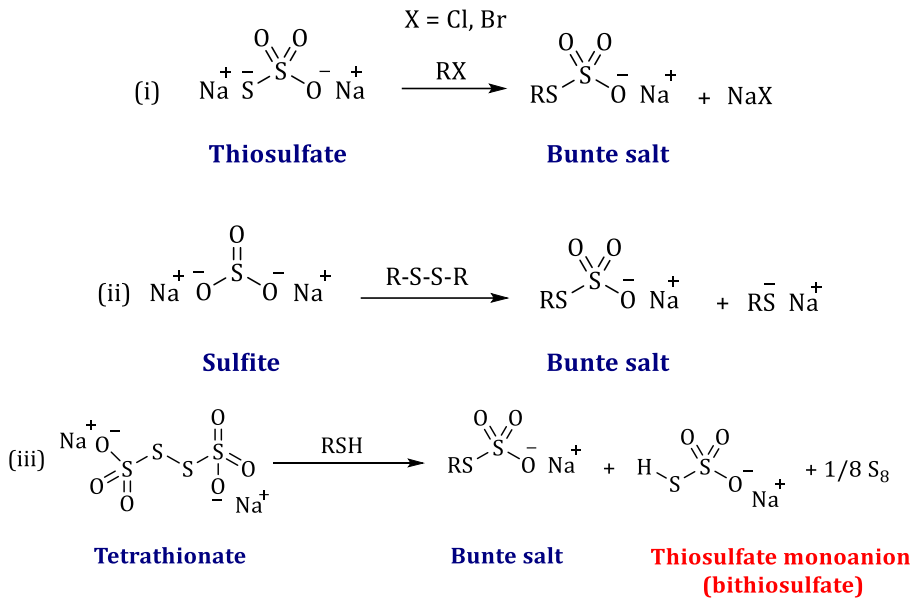

Scheme 2.5: Bunte salt formation via three methods.

Milligan and Swan et al.[86,87] utilized a large excess of the Bunte salt as the electrophile to access homotrisulfides, and the reaction proceeds via mixing the reactants in water or a water/ethanol mix (to dissolve the sulfide) at room temperature to give bis alkyl/phenyl trisulfides in moderate yields (65-70%), using a phosphate buffer to maintain a constant pH of 8. To enhance the purity, Milligan and Swan later on[87] improved the method by adding formaldehyde to prevent the sulfite by-product from attacking the trisulfide, resulting in the formation of a disulfide as an undesirable by-product.[87] The reaction was revisited by Bhabak et al. very recently in 2019 (**Table 2.4**, entry **6**). They optimized Milligan and Swan's method by lowering the reaction temperature to 0 ºC and limiting the equivalents of sodium sulfide nonahydrate to 0.5.[93] Overall, their optimization afforded aliphatic and substituted benzylic homotrisulfides in low to high yields (24–97%). **Scheme 2.6** illustrates the proposed mechanism of sulfenylation by a Bunte salt.

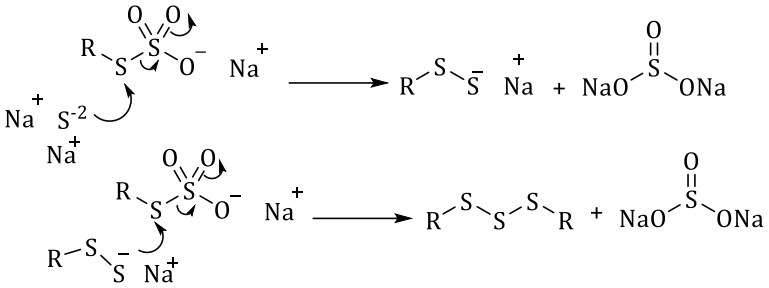

Scheme 2.6: Proposed mechanism for the formation of homotrisulfide using a Bunte salt.

Milligan and Swan also went on to use their method to prepare cyclic trisulfides from di-Bunte salts (see **Scheme 2.7**).[97] Indeed, cyclic polysulfides can only be realistically accessed using two-bond disconnections (three synthons) but where one of the substrates accommodates two of the synthons.

1965, Milligan and Swan

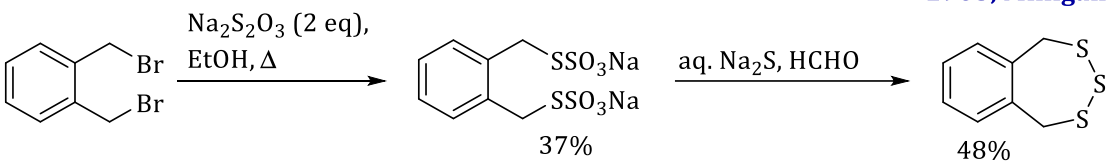

Scheme 2.7: Synthesis of a cyclic trisulfide using a di-Bunte salt.

Recent advancements in the chemistry of Bunte salts have achieved a novel methodology utilizing *S*-substituted sulphenylthiosulphates as a versatile and scalable reagent for the construction of unsymmetrical organotrisulfides.[98] This approach allows for the efficient coupling of various alkyl electrophiles, including bromides, chlorides, iodides, and tosylates, with thiourea as an additional sulfur source. The method demonstrates excellent functional group compatibility and has been successfully applied to the late-stage modification of drug-like molecules, thereby expanding its utility in medicinal chemistry. Notably, the in-*situ* generation of thiosulfenyl iodide is identified as a key intermediate in the reaction mechanism, facilitating the formation of trisulfide bonds under mild conditions.[98]

Several other mono-sulfur electrophiles have also been used for trisulfide synthesis via methodology **B** including a sulfenyl bromide or chloride (entry **2** in **Table 2.4**), an *N*-thiophthalimide (entry **7**) as well as various examples of an *S*-thiosulfonate (entries **3** and **4**) by Field et al. **Scheme 2.8** shows the sequence of mechanistic events for entry **4b** with an *S*-thiosulfonate, in which soft-soft S-S bond formation drives the process.

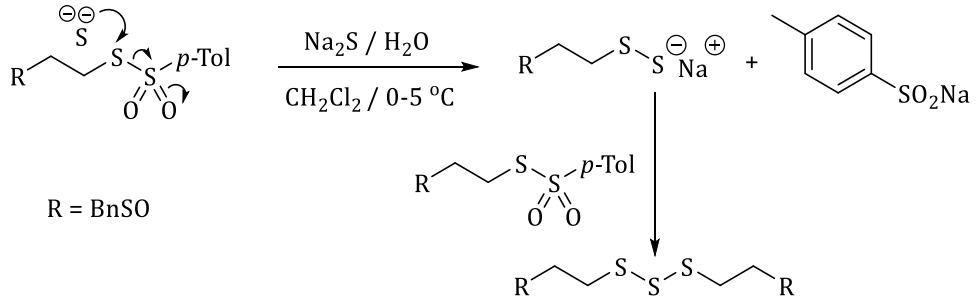

Scheme 2.8: Trisulfide synthesis via double alkylation with a thiosulfonate.

Entries **5** and **7** in **Table 2.4** use bis(trimethylsilyl)sulfide (hexamethyldisilathiane) as nucleophile and not the metal sulfide. For instance, Capozzi et al.[92] reacted $(TMS)_2S$ with the electrophile (either a thiosulfinate or a thiosulfonate) in anhydrous chloroform at 60 ˚C to afford the trisulfide in an excellent yield (73-95%), with hexamethyl disiloxane or silyl sulfinate ester as by-product respectively. The mechanisms are non-obvious. **Scheme 2.9** shows the steps involved, which reveals that the driving force, not unexpectedly, is formation of the strong silicon-oxygen bond.

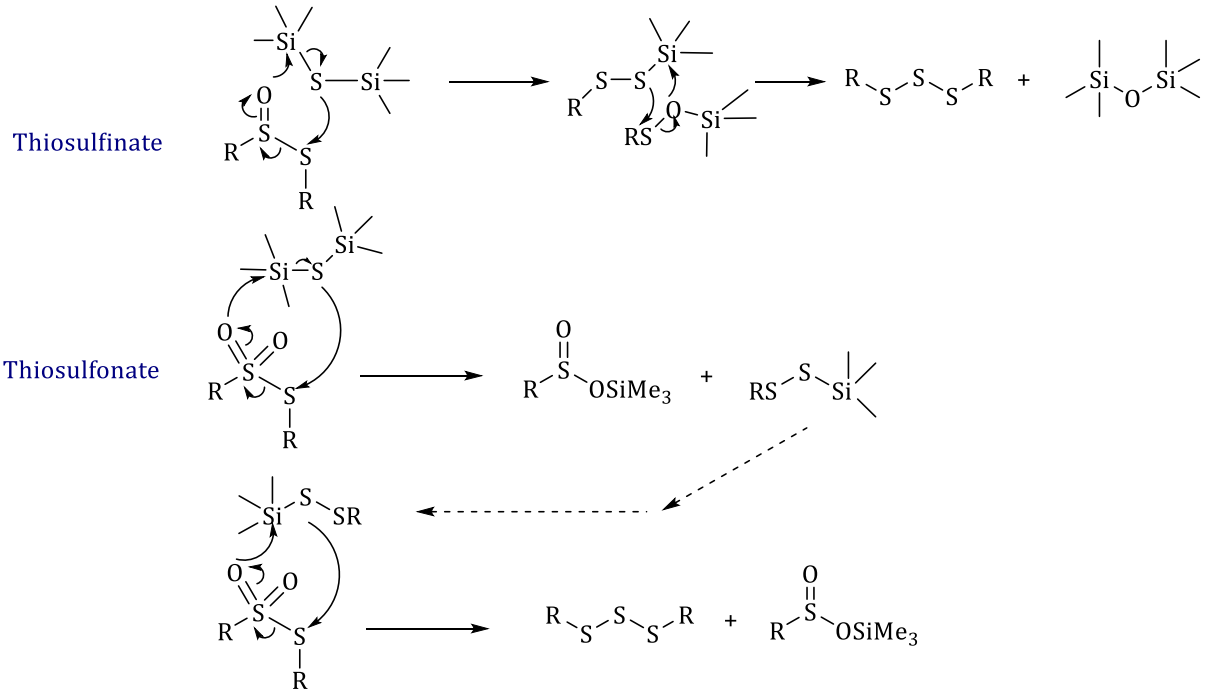

Scheme 2.9: Proposed mechanisms[92] of reactions in entry 5 in Table 2.4.

In summary, methodology **B** affords trisulfides in good yields and reasonable purity. However, as with methodology **A** using trisulfide anion, it can only access homotrisulfides in view of product separation issues in which Field's thiosulfonate methodology (entries **3** and **4**) is arguably the most efficient option. In the upcoming section, we will investigate

the final two-bond disconnection [1+1+1] protocol that utilizes an electrophilic source, $(Lg)_2S$, for the central trisulfide sulfur and which is applicable to the synthesis of unsymmetrical organotrisulfides.

2.5 Methodology C – Double Substitution of an Electrophilic Sulfur $(Lg)_2S$

There are a number of methods in the literature for synthesis of an alkyl/aryl trisulfide having the central sulfur as the electrophilic centre $(Lg)_2S$, here designated as methodology **C**. The reagent of choice in the early years was sulfur dichloride (SCl_2) as a bifunctional synthon for S^{+2}, which despite its ungreen character has survived to the present day. SCl_2 was and still is prepared by the reaction of excess chlorine with S_8, the conversion proceeding via S_2Cl_2 (disulfur dichloride). Early examples of methodology **C** used a variety of metal thiolates or surrogates in which no base was needed since MCl is produced. Some examples with SCl_2 as the electrophilic source covering an almost seventy-year span are shown in **Table 2.5**.

Table 2.5: Homotrisulfides prepared from sulfur dichloride (SCl_2) and RSM via methodology C

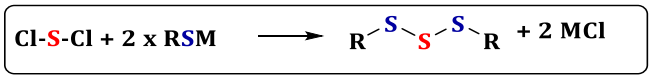

Entry	Year/ Author	RSM	RSSSR % yield
1	1920/ Bloch and Bergmann.[99]	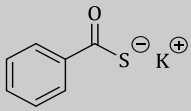	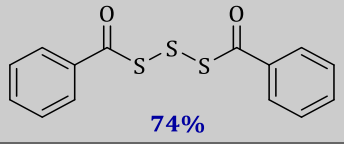 74%
2	1927/ D.Twiss.[100]	**2a** 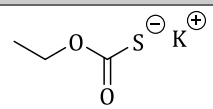 **2b** 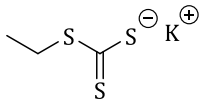	**2a** 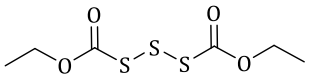 **2b** 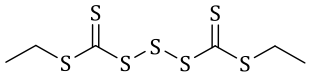
3	1958/ Feher et al.[101]	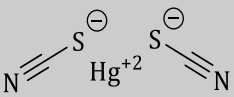	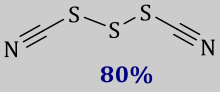 80%
4	1964/ Abel and Armitage.[85]	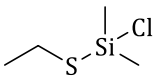	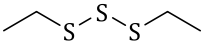 87%

5	1971/ Wardell and Clarke.[102]	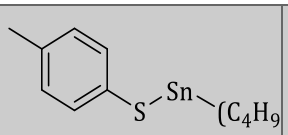	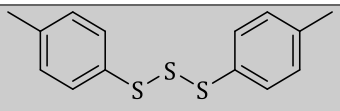 **25%**
6	1984 / Barany and Mott.[103]	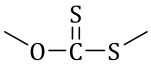	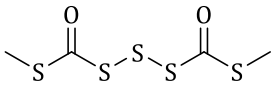 **68%**
7	1987/ Knoth and Gatto.[104]	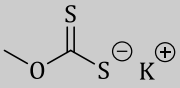	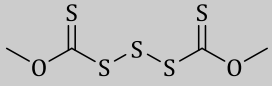 **93%**
8	1993/Munavalli et al.[105]	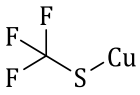	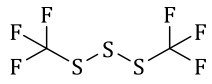 **61%**

The method requires distilling the sulfur dichloride fresh to achieve a high yield and purity of the final product. As seen in the table above, early cases involved a range of metals (M in RSM) involving various protected thiolates such as potassium thiobenzoate (entry **1**), potassium O-ethyl monothiocarbonate as a derivative of Bender's salt (entry **2a**), potassium ethyl trithiocarbonate (entry **2b**), and potassium methyl xanthate (entry **7**). However, other surrogates for M are also known such as the *S*-silyl compound (entry **4**) thiostannane (entry **5**) and thiocuprate (entry **8**), all of which deliver a nucleophilic sulfur. Entry **6**, involving a non-metallic sulfur source in the form of a xanthate, deserves mentioning. The paper[103] describes evolution of methyl chloride (a gas at room temperature), which fits with the mechanism shown in **Scheme 2.10**. Note the preference for loss of the methyl group from MeO rather than the MeS.

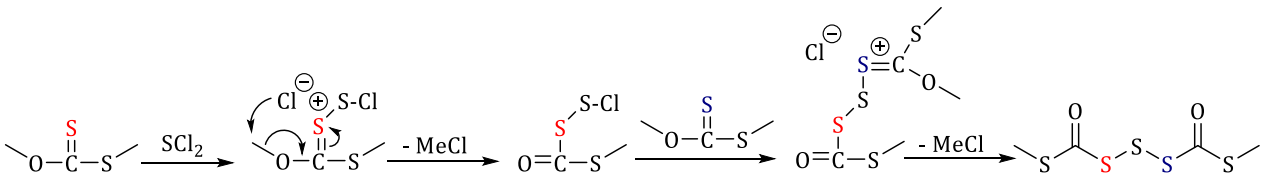

Scheme 2.10: The mechanism of entry 6.

However, despite these early examples, by far the most popular nucleophile used has been thiol. The earliest example of this dates back to 1947, and they have been routinely used ever since. A base is normally used to neutralize the HCl produced in which a variety of amine bases such as triethylamine[106] and pyridine[106,107] have been used for this purpose. **Table 2.6** summarises examples spanning a number of decades and once again involving SCl_2 as the electrophilic source.

Table 2.6: Homotrisulfides prepared from sulfur dichloride (SCl_2) and thiol via methodology C

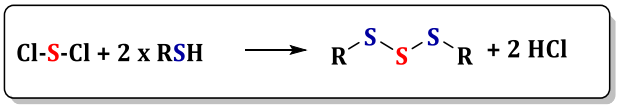

Entry	Year/ Author	R of RSH	Base	RSSSR % yield
1	1947/Clayton and Etzler.[108]	$C_{16}H_{33}$	No base added	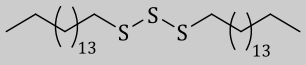 62%
2	1964/Nakabayashi et al.[109]	$(C_6H_5)_3C$	No base added	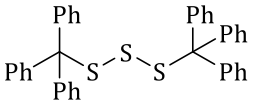 74%
3	1994/Derbesy and Harpp.[106]	R or R' = ^{t}Bu, ^{n}Bu, ^{i}Pr, ^{t}BuPh, Bz, *p*-Cl-Bz, allyl	NEt_3, 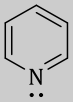 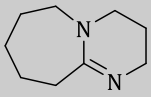 (DBU)	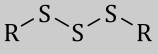 46 - 100% 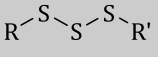 25 - 96%
4	2003/Harpp and Colman.[107]	Ph, *p*-Tol, $C_6H_5NO_2$		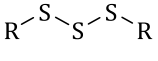 61 - 97%

Of note are the contributions by Professor David Harpp at McGill University in Canada shown in entries **3** and **4**.[106,107] His method utilizes a nitrogen base to neutralize the HCl produced and remains as one of the easiest and most efficient ways to prepare homotrisulfides. Using this method published in a seminal paper in *Tetrahedron Letters* in 1994, Harpp and Derbesy also successfully synthesised a few examples of heterotrisulfides in high yield and purity[106] by adding one equivalent each of two different thiols sequentially (entry **3**, **Table 2.6**). Harpp reported on the use of his method for optimizing the production of homotrisulfide in a paper in 2003[107] in which both R groups were aromatic. However, as with all the cases for this methodology type so far, the one drawback is the use of the relatively ungreen reagent, SCl_2. The mechanism for methodology **C** hasn't been studied, but an S_N2 process is likely, **Scheme 2.11**, although a single-electron transfer (SET) alternative can't be ruled out.

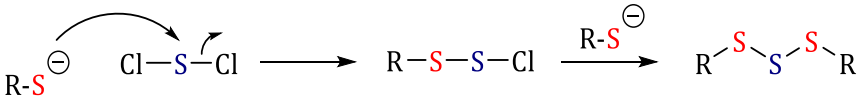

Scheme 2.11: Proposed mechanism of alkyl/aryl trisulfide synthesis prepared from SCl_2.

Several later methods involved replacing both chlorines of SCl_2 with nitrogen leaving groups (imide, imidazole or triazole-based; entries **3** and **4**) or one chlorine with a sulfur-based leaving group to afford a mixed, manageable reagent (entry **5**) as shown in **Table 2.7** below. *N*-thionylaniline has also been used (entry **1**). Importantly, both entries **1** and **5** can achieve heterotrisulfide synthesis.

Table 2.7: Homotrisulfides prepared from a Lg-S-Lg source and 2RSH/2RNu via methodology C

Entry	Year/ Author	Lg-SS-Lg	R of "RSH"	RSSSR % yield
1	1960/Kresze.[110]	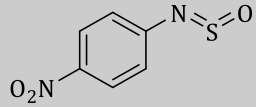	Ph, Et, ^{n}Pr, *p*-OMe-Ph	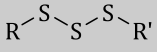 **3 - 64%**
2	1966/Vineyard.[111,112]	S_8	R = ^{n}Bu, Bu, ^{t}Bu, ^{i}Pr	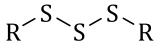 **10-95%**
3	1978/Harpp et al.[113]	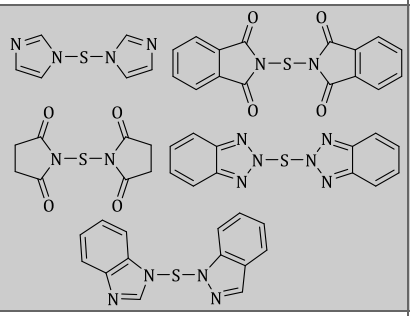	Benzyl	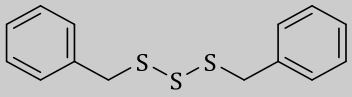 **27-100%**
4	1980/Banerji and Kalena.[114]	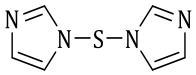	R = ^{t}Bu, ^{n}Bu, ^{i}Pr, ^{n}pr, allyl, Bn,Ph	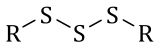 **66-90%**
5	1984/Barany andMott.[115,116]	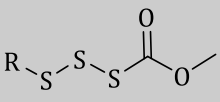 R = Me, ^{i}Pr, EtOH, $EtNH_2$.HCl	R of RSH = Me, ^{i}Pr, EtOH, $EtNH_2$.HCl R' = Tol, Bn, Bz	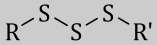 **25 - 71%**
6	2006/ An et al.[117]	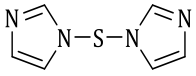	R = x Bn x = H; *p*-Me, ^{t}Bu, *p*-F, *p*-Cl, *p*-Br *m*-CF_3, *m*-Me, o-Cl, 2,4,6-tri-Me	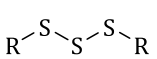 **68-100%**
7	2010/ An and Mo.[118]	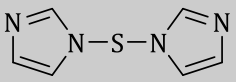	*p*-F-Bn	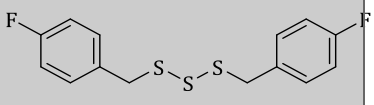 **63%**

Entry **2**, belongs to intriguing work by Billy Vineyard[111,112] of the Monsanto company in the 1960s, who showed that sulfur reacts with a thiol and an amine base as catalyst to afford homotrisulfides in decent yields and purity depending on the nature of the thiol R group and thiol to sulfur stoichiometry. Mechanistically, Vineyard rationalised this fascinating conversion as involving attack of the thiolate on the S_8 chain (as LgSLg) to generate a polysulfide anion that would undergo further S-S bond substitution by a second equivalent of thiolate. Further S-S exchanges would then be disproportionate to give the eventual dominant product according to the RSH/S stoichiometry. Given the nature of the starting electrophilic reactant S_8, the chemoselectivity is remarkable. Entry **3** involves nitrogen-based leaving groups developed by Harpp and published in a seminal *JACS* paper in 1978[113] in which the group leaves as the free amine base. Once again, a disadvantage of the method is that the electrophilic reagents are prepared from SCl_2 via double nucleophilic substitution. Mechanistically, it was first assumed that these reagents undergo facile direct substitution by the thiol. However, this was disproved by Harpp in favour of an acid-catalysed mechanism involving leaving group protonation followed by thiolate nucleophilic attack on the electrophilic sulfur atom as illustrated in **Scheme 2.12** below:

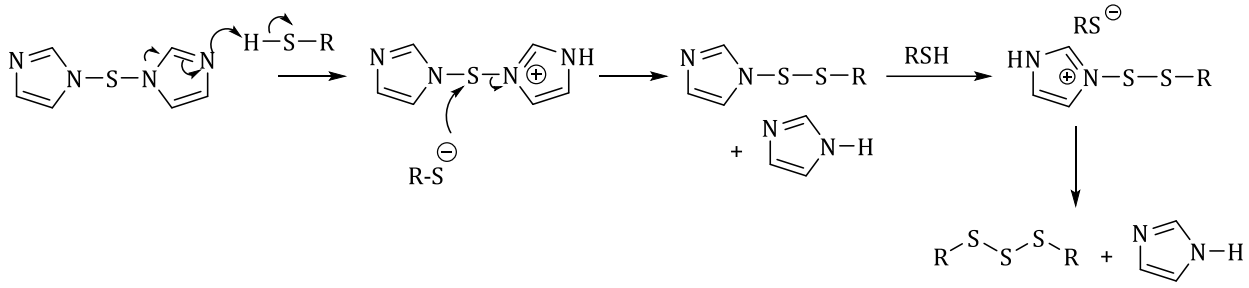

Scheme 2.12: Proposed mechanism of alkyl/aryl trisulfide synthesis from entry 3 in Table 2.7.[113]

Two years later in 1980, Banerji and Kalena[114] published a look-alike reagent to Harpp's as diimidazolyl sulfide, involving imidazole as the leaving group (entry **4**, **Table 2.7**). Once again, though, the reagent was prepared from SCl_2 but using *N*-(trimethylsilyl)imidazole in hexane (this generates the volatile TMSCl which is easily removed). Once formed, the dimidazolyl sulfide reacts with two equivalents of thiol at low temperature to form the organotrisulfide, producing imidazole as by-product, which precipitates out and can be filtered off. Yields using these types of reagents (entries **3** and

4) are decent but still only applicable to synthesizing homotrisulfides, again because of forming mixed products when using two different thiols. Recently, An et al. have used Banerji's method to synthesise a library of substituted dibenzyl trisulfides for cancer-cell cytotoxicity evaluation (entry **6**),[117] in which the parent dibenzyl trisulfide is a natural product that can be isolated from the roots of *Petiveria alliacea*.[59] A strong cytotoxic candidate shown in entry **7**, *bis*(4-fluorobenzyl) trisulfide (Fluorapacin), emerged from the study, which was patented by An in 2010.[118] Similarly, *S*-based leaving groups have been developed by Barany and Mott,[115] (entry **5**), who used MeO_2CSSCl (methoxycarbonyl disulfanyl chloride) as a mixed form of SCl_2 in which Cl and MeO_2CS (a carbonothioate) each act as leaving groups, with Cl the more reactive one. Mott and Barany's bifunctional reagent, MeO_2CSSCl, was prepared through multiple steps starting from commercially available methoxythiocarbonyl chloride, which was treated with SCl_2. This was followed by a demethoxylation process using a catalytic amount of ferric chloride,[116] and the resultant (chlorocarbonyl)disulfanyl chloride then reacted cleanly with methanol to give the final product as shown in **Scheme 2.13**.

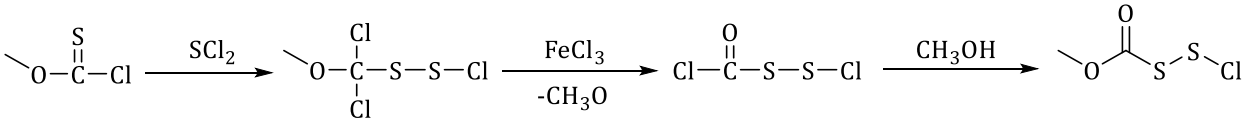

Scheme 2.13: Synthesis of MeO_2CSSCl.[116]

Although synthesis of the bifunctional reagent is challenging, the method allows the synthesis of heterotrisulfides using two different thiols based on the different leaving abilities of the two leaving groups (Cl as the more reactive). **Scheme 2.14** illustrates the sequence.

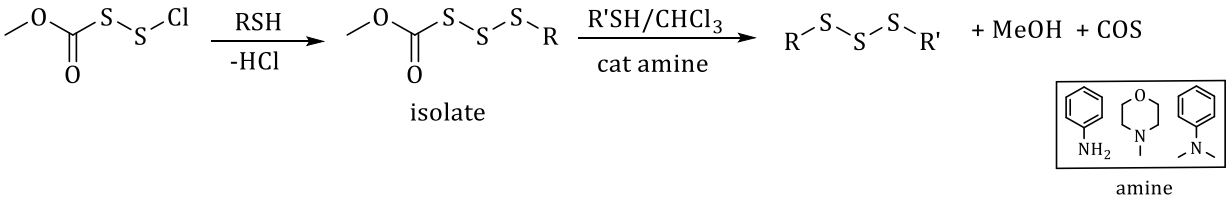

Scheme 2.14: Synthesis of heterotrisulfides via Barany's method.[115]

This method has certainly stood until the present time[119] as a popular way of preparing heterotrisulfides as illustrated in **Scheme 2.15**. However, more recent and improved methods (particularly given the long synthesis of the methoxycarbonyl disulfanyl chloride

using ungreen reagents) are now available for heterotrisulfides and are likely to find greater usage in the future.

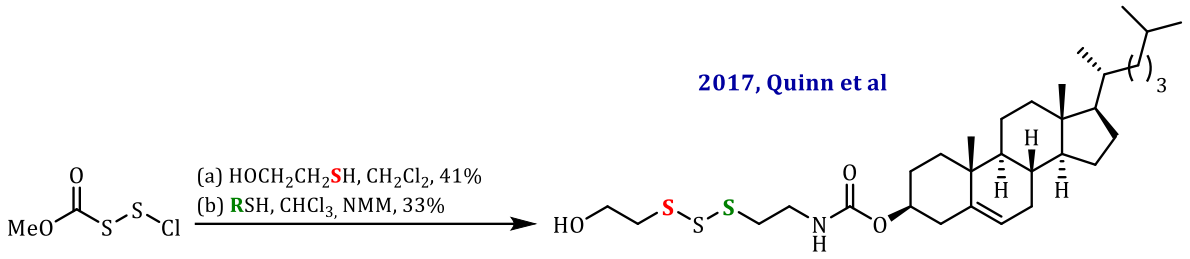

Scheme 2.15: Recent synthesis of a heterotrisulfide using MeO_2CSSCl.[119]

The final word on this variation of methodology **C** should be given to the intriguing chemistry in entry **1** from the German literature of 1960.[110] Here, *N*-thionylaniline is reacted with a thiol, which adds at sulfur to afford an *N*, *S*-mixed sulfite. A second thiol equivalent adds, with expulsion of aniline, to form an *S, S*-sulfite, which substitutes further at the divalent S to afford a disulfide and a thiosulfenic acid (RSSOH), which then undergoes further substitution to afford the trisulfide. As with other earlier methodologies, a mixture of di- and trisulfide products is obtained. Heterotrisulfides are formed by varying the R groups between the thiol and the *N*-thionylaniline, but this produces complex mixed systems. Alternatively, an *S, S*-sulfite (RSSO(SR)) can be used instead of the *N*-thionylaniline as the starting point. **Scheme 2.16** below presents the sequences of reaction steps for producing homotrisulfide.

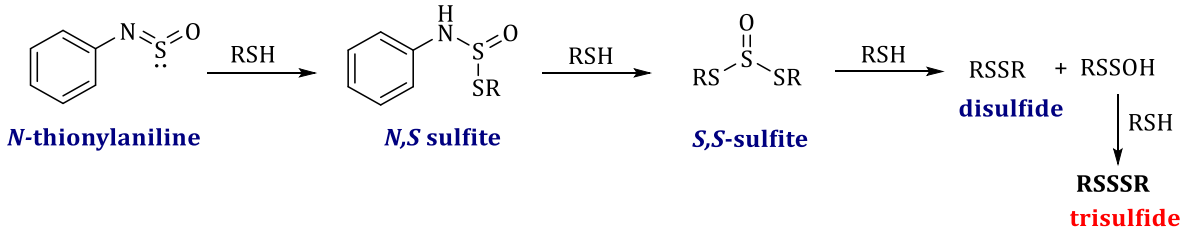

Scheme 2.16: Sequence of steps for entry 1 in Table 2.7.[110]

The next section investigates suitable approaches for efficiently producing unsymmetrical organotrisulfides that are free of symmetrical trisulfide byproducts. In this section, one can pick up on a number of rational design themes.

2.6 Methodology D: RSSLg + MSR

The first approach of the [1 + 2] hetero methodologies as methodology **D** involves the disulfur component as the electrophile and the S1 component as the nucleophile, which presents a thiol as an unambiguous choice. The earliest example of an electrophilic disulfanyl species RSSLg in context was with Lg as chloride,[120-122] which was first studied extensively by Böhme et al. in the 1950s. This outcome was followed by varying the leaving group of the disulfanyl species RSSLg. We will start this section by covering the popular case of using chlorine as the leaving group in which the methodology is suited for producing heterotrisulfides. **Table 2.8** depicts a range of examples of methodology **D** involving RSSCl over a forty-year period for preparing heterotrisulfides.

2.6.1 Using Lg = Cl

Table 2.8: Heterotrisulfides prepared from R-SS-Cl+ R'SH via methodology D

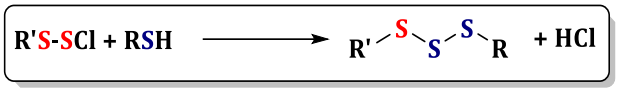

Entry	Year/ Author	RSH	R'SS-Cl	R" SSSR %yield
1	1952,1954/ Böhme et al.[120,122]	R = Me, Et, Bn, Ph 2-naphthyl	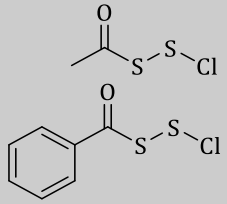	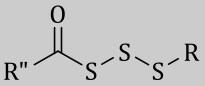 R" = Me, Ph **55-97%**
2	1964/Nakabayashi et al.[109]	TrSH	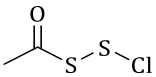	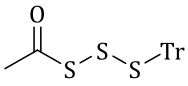 **85%**
3	1994, 2006/Harpp et al.[123-125]	RSH R = Bn, p-Cl-Bn *p*-OMe-Bn, *p*-Cl-Ph, *p*-OMe-Ph, *p*-NO_2-Ph, *p*-Br-Ph, 2-naphthyl *p*-phenyethylene	TrSSCl	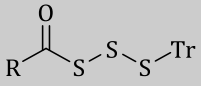 **86 – 96%**

Various methods, all using toxic chlorinating agents by modern-day standards, for accessing the disulfanyl chloride component have been reported, starting with seminal work by Böhme in the 1950s using the reaction of chlorine with diacetyl disulfide, which gave a separable mixture (by vacuum distillation) of acetyldisulfanyl chloride and acetyl

chloride.[120,122] Böhme went on to show that sulfuryl chloride (SO_2Cl_2) could also be used as the chlorinating agent starting with either a disulfanyl acetate (formed from AcSCl + RSH), or a trisulfide.[121] Another popular method for accessing RSSCl due to Feher is to react a thiol with sulfur dichloride.[126] Regarding the results in **Table 2.8**, the first example (entry **1**) of heterotrisulfide synthesis reported in the chemical literature via coupling of RSSCl with a thiol was reported by Böhme, who made AcSSSR in which R could be either an aliphatic or an aromatic group.[122] In a follow-up paper[120] in 1954, Böhme showed that the acetyl group of RSSSAc was a useful handle that could be deprotected by HCl in ethanol or methanol to give the trithiol RSSSH, which was then oxidised to the homo hexasulfide RSSSSSSR with iodine. This was the first mention of the synthesis of RSSSH in the chemical literature. A few years later, Nakabayashi et al.[109] followed up on his synthesis of unsymmetrical trisulfides from perthiols[127] (these will be discussed in methodology **E**) by demonstrating that thioacetic acid could be used as starting material in reaction with sulfuryl chloride for producing the pivotal AcSSCl, the reaction presumably proceeding via diacetyl disulfide as with Böhme's original method. Nakabayashi reacted the AcSSCl with TrSH (tritylthiol) to form TrSSSAc in 85% yield in which TrSSSAc can act as a precursor of TrSSSH via acid hydrolysis[109](entry **2**). On the subject of using a trityl group, Harpp used TrSSCl (prepared using Feher's method of TrSH with SCl_2) in this **D** methodology for the formation of trityl-protected heterotrisulfides (entry **3**).[123,124,128] Harpp's work on the synthesis and application[125]of $Tr(S)_nCl$ (n = 1-3) makes use of various aspects of the trityl group that include imparting crystallinity and stability to the compounds as well as interesting chemical properties based on the chemistry of the S-Tr bond. Importantly, such $Tr(S)_nCl$ reagents have been used for various expressions in this **D** category. For instance, Harpp reacted *n*-BuSH with TrSSCl to prepare the unsymmetrical trisulfide, TrSSSBu[125] in 72% yield. Similarly, as a little-known RSSSLg + RM variant equivalent to a [0 + 3] coupling, Harpp reacted TrSSSCl with *n*-BuLi (THF, -78 °C) or BuMgBr (ether, 0 °C) to prepare the trisulfide, TrSSSBu, in yields of around 50% after purification by chromatography.[125] Additionally, some intriguing heterolytic insertion reactions of TrSCl into polysulfides have been reported in a several papers.[124,129-132] For instance, TrSCl (as the electrophilic partner) reacts with a disulfide (as the nucleophilic partner) to generate a sulfonium salt, which undergoes a secondary fragmentation/recombination with expulsion of TrCl to afford a trisulfide as shown in **Scheme 2.17**.[131]

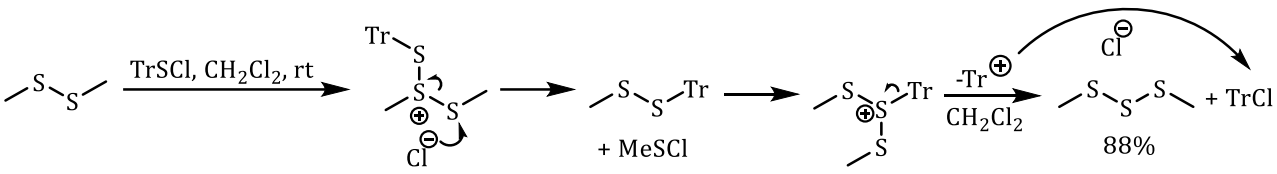

Scheme 2.17: Mechanism of homotrisulfide synthesis via heterolytic insertion reactions of TrSCl into a disulfide.[131]

This chemistry has recently been put to good use in natural product total synthesis by Mohammad Movassaghi's group for constructing the trisulfide bridges of the epipolythioketopiperazine alkaloids (see Chapter One in **1.2.1**), chaetocin **C** and dideoxychetracin A.[133] Here, the trityl group plays an important role in bridge closure, in which addition of the sulfur of the STr moiety onto an iminium ion to form an intermediate cyclic sulfonium ion is followed by loss of a trityl cation to form the trisulfide bridge. The sequence constitutes a [3 + 0] coupling overall in which the 3 corresponds to the RSSSTr moiety as nucleophile and the 0 as the iminium ion (a carbon electrophile). Importantly, the trityl group provides a synchronised stabilization of the incipient positive charge in addition to being lost as its cation to furnish the final neutral bridge trisulfide ultimately. **Scheme 2.18** depicts an example of this chemistry.[133]

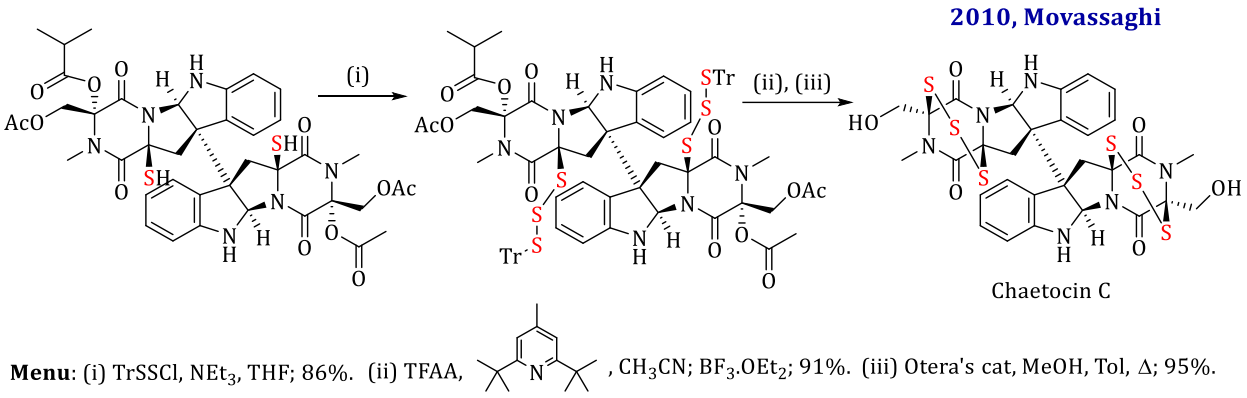

Scheme 2.18: Synthesis of trisulfide bridge in Chaetocin C via [3 + 0] approach.[133]

Despite their usefulness in context, chlorodisulfides present a number of challenges in their usage. These include their reactivity towards water as well as their thermal instability, making the separation of mixtures of RSSCl and RSCl formed in their preparation challenging. Additionally, they require the use (to date, at least) of harsh chlorinating agents in their preparation.

2.6.2 Using Other Lg Variants

RSSCl synthons have inspired the development of other more stable derivatives of the form RSSLg in which Lg covers phthalimide,[128] phosphorodithioate,[134] and *p*-tolylsulfinate,[135] as well as alkoxy.[1] Each of these important types are summarized in **Table 2.9**.

Table 2.9: Heterotrisulfides via methodology D using R-SS-Lg with Lg not as chlorine

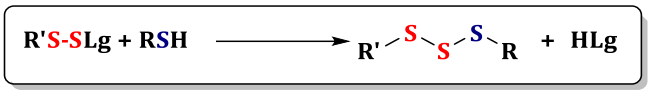

Entry	Year/Author	RSH	R'SS-Lg	RSSSR' %yield
1	1971/Harpp and Ash.[128]	R = Bn, *p*-Tol	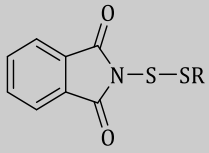 R' = ^{i}Pr, ^{n}Pr, *p*-Tol, Bn	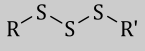 **33-67%** R = Bn, *p*-Tol R' = ^{i}Pr, *p*-Tol, Bn
2	2010/Witt et al.[134]	R' = $(CH_2)_{11}NHBoc$, $(CH_2)_{11}OH$, $(CH_2)_{10}CO_2H$, $(CH_2)_{10}CO_2Me$, ®-$CH_2CH(NH_2)$ CO_2Et ®$CH_2CH(NHAc)CO_2H$, Ph, 4 $MeOC_6H_4$, 2 naphthyl	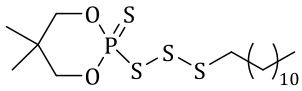	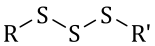 **55-99%**
3	2018/Jiang et al.[1]	R = ^{t}Bu, ^{i}Pr octyl, dodecyl, allyl	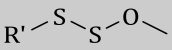 R' = Bn, ^{i}Pr, ^{t}Bu,^{n}Bu, ^{i}Bu octyl, dodecyl, allyl, Ad C_2H_4OH, C_2H_4OH, $C_2H_4OHC_2H_4(CF_2)_7CF_3$, $C_2H_4Si(OEt)_3$, *p*-^{t}Bu-Bn, *p*-OMe-Bn, *p*-OMe-Ph, *p*-Tol.	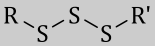 **50-99%**
4	2018/Xu et al.[135]	R = Ph, *p*-Br-Ph Bn, naphthyl	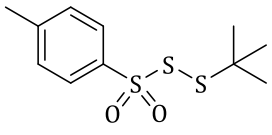	 **50-91%**
5	2020 / Jiang et al.[136]	R = Tol, *p*-Br-Ph Dodec, ad, *p*-OMe-Bn C_2H_4OH, $C_4H_4N_2$	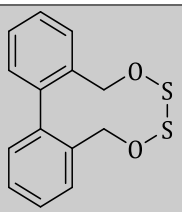	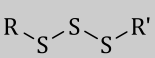 **52-80%**

6	2020 / Jiang et al.[137]	R = 1-ad, *p*-tol, cyclopentyl, 1-dodec,2-naphthyl, acetamido-3 methylbutanoate	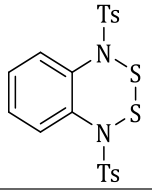	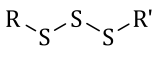 **73-90%**

Entry **1** shows one of the most popular non-chlorine leaving groups due to Harpp in the form of an imide (*S*-phthalimide) as a member of his transfer reagents in which the number of sulfurs can be varied. The disulfanyl imide, RSSPhth, shown in entry **1** was prepared by reacting phthalimide with sulfur dichloride with triethylamine as base for the HCl produced to furnish *N,N'*-thiobisphthalimide, which is exchanged with a thiol to produce the stable RSSPhth electrophilic sulfenylating agent.[128] Heterotrisulfides were reported in moderate yield (entry **1**) via substitution of RSSPhth with a thiol. Recently, MeSSPhth has gained recognition for its role in the synthesis of enediyne antibiotics, including the calicheamicins and shishijimicins.[119] These architecturally impressive natural products contain a methyltrithio (MeSSS) warhead and are potent antitumour agents (shishijimicin A has an IC_{50} = 0.48 pM against P388 leukaemia cells and is thus ideal for incorporation as the payload into an antibody-drug conjugate or ADC). Synthetically, Nicolaou, has improved on synthesis of this reagent in his shishijimicin A synthesis[119] using first reaction of sulfur monochloride (S_2Cl_2) with phthalimide to furnish bis(1-phthalimidyl) disulfide, $(PhthN)_2S_2$, which could be efficiently converted into phthalimidosulfenyl chloride, (PhthNSCl), with SO_2Cl_2 in 98% overall yield for the two steps. The sulfenyl chloride was found to be stable in a desiccator at room temperature for several months, making it a very useful Lg_1SLg_2 reagent for heterotrisulfide synthesis for the future (see methodology **C**). Thereafter, inspired by previous work by Harpp,[138] reaction of PhthNSCl with TMSiSMe led to the required transfer reagent, PhthNSSMe, in essentially quantitative yield after removal of the relatively volatile TMSCl. PhthSSMe reacted rapidly with a thiol group of the natural product at room temperature with loss of phthalimide, installing the required methyltrithio fragment. These innovations have greatly expanded the use of PhthNSSR as an important disulfanyl transfer agent. **Scheme 2.19** depicts these steps.

2018, Nicolaou

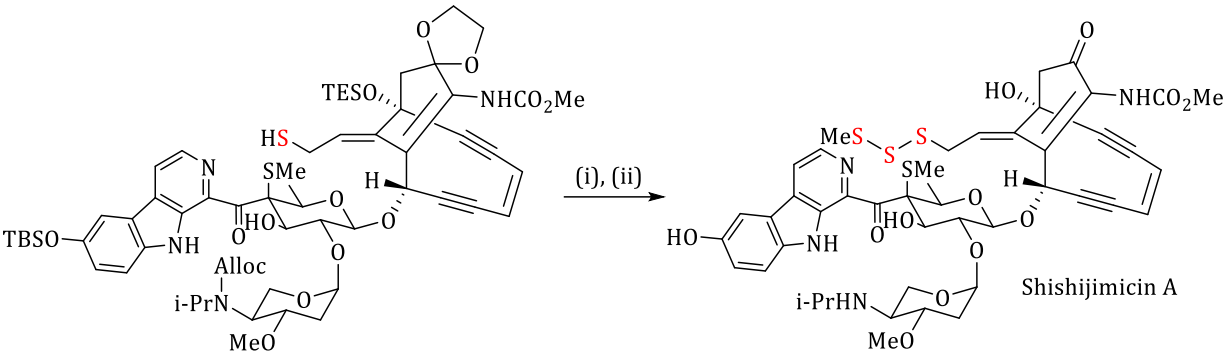

Menu: (i) PhthNSSMe (8 eq), MeOH; 60%. (ii) Remove the protecting groups

Scheme 2.19: Synthesis of Shishijimicin A using PhthNSSMe.[119]

The second variant of Lg in RSSLg to be discussed uses Dariusz Witt's cyclic phosphorodithioate,[134] which also comes up in methodology **E** in the next section as the RSLg partner in RSSH + R'SLg.[139] For accessing the RSSLg partner here, Witt used an intriguing synthesis in the style of methodology **C** involving a one-pot reaction of an equimolar mixture of the cyclic, diesterified phosphorodithioic acid and dodecane-1-thiol (as the two "thiols") with one equivalent of sulfur dichloride at -30 °C in DCM, using triethylamine as base as shown in **Scheme 2.20**.

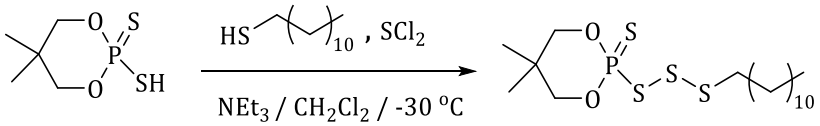

RSSLg = disulfanyl phosphorothioate

Scheme 2.20: Synthesis of cyclic phosphorodithioate according to Witt's method.[134]

Despite the homo-coupling possibilities, the mixed substitution product as R^1SSLg (Lg = cyclic phosphorodithioate fragment) was isolated in 68% yield after column chromatography. Substitution of the phosphorodithioate of R^1SSLg (note the sulfur leaving group here) with R^2SH proceeded cleanly and rapidly in DCM at rt, again using triethylamine as base, to afford unsymmetrical trisulfides containing a range of both aliphatic and aromatic R groups in > 75% isolated yield.[134] However, in order to avoid producing a complex mixture of symmetrical and unsymmetrical di- and trisulfides products from the final substitution, it was important to have the R^1SSLg component in slight excess so as to consume the thiolate of R^2SH.

The third example[135] of RSSLg to be covered is due to the group of Zhenghu Xu who demonstrated that Lg can be *p*-tolysulfonyl in R^1SSTs (entry **4**). The one limitation is that the only R^1 group covered was *t*-butyl, which was probably due to it being known from previous work by Harpp that sulfenyl thiotosylates (RSSTs), particularly with aromatic R groups, extrude sulfur in polar solvents to afford RSTs.[140] In Xu's case, the *t*-BuSSTs was readily accessed from reaction of the sulfenyl chloride, *t*-BuSCl, with TsSK, see **Scheme 2.21**.

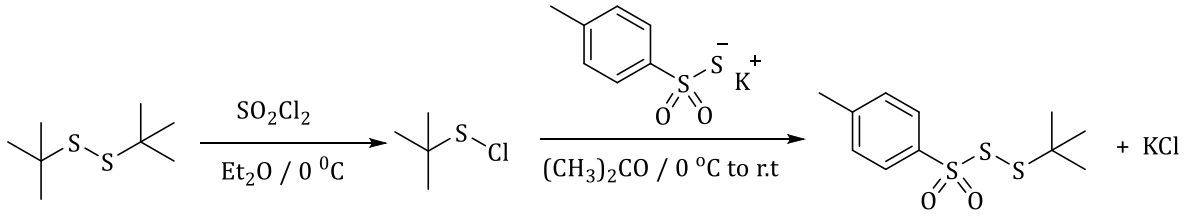

Scheme 2.21: Synthesis of *t*-BuSSTs according to Xu's method.

Reaction with a small library of aromatic and aliphatic thiols as R^2SH with *t*-BuSSTs (1.5 eq) in DCM at rt with loss of sulfinate ion gave the desired unsymmetrical trisulfide in moderate to excellent yields (50-91%) as shown in **Scheme 2.22**.

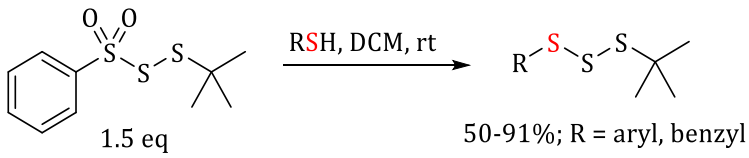

Scheme 2.22: Synthesis of heterotrisulfides via Xu's method.[135]

Not having to use a base for the final step is a clear advantage, but the method is limited by restrictions in the R^1 group (*t*-Bu only). As part of the work, Xu showed[135] that *t*-BuSSTs can be cross-coupled with a boronic acid, $R^2B(OH)_2$, using $CuSO_4/NaHCO_3$ to afford unsymmetrical disulfides, R^1SSR^2.

The final word on methodology **D** is left for describing Xuefeng Jiang's[1] recent innovative work on disulfanyl transfer agents. In this, he has significantly extended the usefulness of synthons of the type RSSLg and LgSSLg for preparing organopolysulfides using a variety of stepwise substitutions of S, N and, importantly, also C-based nucleophiles. Building on earlier work that demonstrated that a disulfanyl acetate (RSSAc) could be deprotected to its perthiol in situ and oxidatively coupled with a boronic acid, $RB(OH)_2$, to afford

unsymmetrical disulfides,[141] in later work,[1] Jiang used this protocol for converting RSSAc into the useful electrophilic synthon RSSOMe as depicted in **Scheme 2.23**.

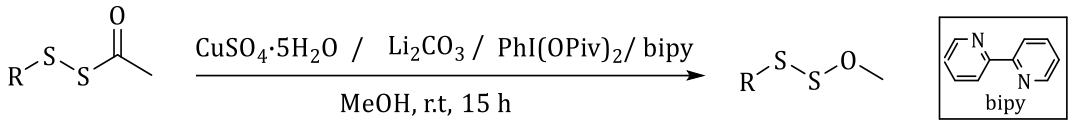

Scheme 2.23: Synthesis of electrophilic synthon RSSOMe via Jiang's method.[1]

The conditions for the cross-coupling involved using Li_2CO_3 for thioacetate deprotection in methanol, $PhI(OPiv)_2$ as S-H oxidant (to S-I) and a ligated Cu(II) catalyst for the cross-coupling with methanol. The RSSOMe products could be chromatographed without decomposition or rearrangement and then coupled with thiols in DCM at rt to afford a range of unsymmetrical trisulfides R^1SSSR^2 with excellent scope for the R groups in 50-99% yield as shown in entry **3**, **Table 2.9**.

However, Jiang clearly had his eye on a bilateral disulfanyl transfer reagent that would have greater versatility in producing a range of organopolysulfides through the sequential substitution by N or C-based nucleophiles. In 2020, he published[136] his first paper (entry **5**, Table **2.9**) on the design and development of such a construct, building on work from Shinichi Motoki[142] from 1977 who had demonstrated that homodialkoxy disulfides, ROSSOR (R = Me, Et), underwent stepwise substitution (the intermediate $R^1SSSOMe$ could be isolated via distillation) with thiols to afford unsymmetrical trisulfides in good yields. Jiang's design[136] rested on incorporating the dialkoxydisulfanyl moiety into a cyclic scaffold in which the chemoselectivity of substitution could take advantage of ring-strain release in the first step, making substitution much faster for the first substitution. After considerable trial and error, he established that a ten-membered scaffold built onto a 1,1-binaphthyl template provided the desired chemical outcome. Using this template, substitution with an arylboronic acid as a carbon nucleophile source using $Cu(MeCN)_4PF_6$ and 2,2'-bpy as ligand in DCM at rt smoothly generated a mono disulfanyl ether that could be purified. However, for trisulfide production, it was more convenient to carry out the second substitution in a one-pot fashion using a thiol with $B(C_6F_5)_3$ as promoter in DCM at rt, generating unsymmetrical trisulfides bearing an aryl group for R^1 and either an aryl or alkyl (including hindered R groups) group for R^2 in a 52-80% overall yield (entry **5**).[136] The substitution chemoselectivity (mono versus di-) was ensured by

virtue of a (calculated) 9.53 kcal/mol energy difference between the two S-O bond dissociation energies. **Scheme 2.24** depicts the sequence of these steps.

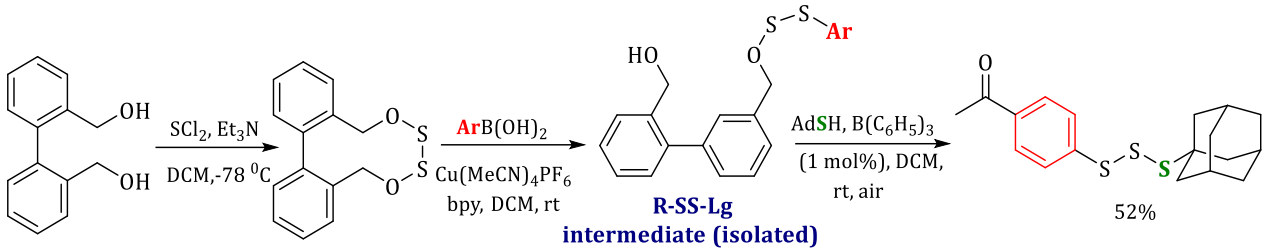

Scheme 2.24: Synthesis of heterotrisulfides via Jiang's method using O-S based Lg-SS-Lg.[136]

In a more recent publication,[137] Jiang has improved his concept further using a six-membered scaffold fused onto an aromatic ring, incorporating a disulfonamidosulfanyl motif (TsNSSNTs) for disulfanyl transfer as seen in entry **6**, **Table 2.9**. Unsymmetrical trisulfides could be accessed using first substitution with R^1SH at 0 °C in DCM followed by an acidic carbon nucleophile (e.g., a β-dicarbonyl type) using DMAP as promoter in DCM at rt as depicted in **Scheme 2.25**.

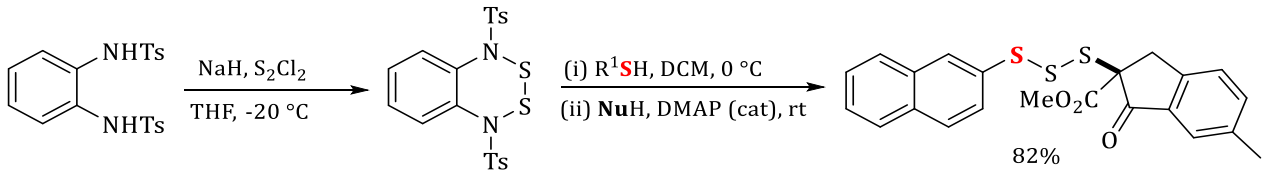

Scheme 2.25: Synthesis of heterotrisulfides via Jiang's method using N-S based Lg-SS-Lg.[137]

Fourteen diverse examples covering a yield range of 73-90% were reported.[137] These innovations serve to demonstrate that some considerable progress has been made in unsymmetrical trisulfide synthesis. However, it should be noted that all of Jiang's bilateral creations stem from using S_2Cl_2 to synthesise the scaffolds. The next subsection will examine the final case as a [2 + 1] approach in which the electrophile is now a mono-sulfur species (RSLg), while the disulfur moiety is the nucleophile in the form of RSSH.

2.7 Methodology E: RSSH + R'S-Lg

In this methodology **E**, coupling occurs via a [2 + 1] mode in which the disulfanyl nucleophilic component is a perthiol RSSH (also known in the literature as a hydrodisulfane, hydrodisulfide, or a persulfide) or its thiolate form. **Table 2.10** presents various examples of this approach from 1960 till the present day in which a range of chemotypes have been utilised as electrophilic sources, including sulfenyl chlorides

(entries **1** and **3**), and leaving groups based on sulfenyl imides (entries **2** and **5**), thiocyanates (entry **1**), 2-thiobenzothiazoles (entry **5**), thiosulfonates (entry **6**) and an interesting phosphorothioate from Witt's group in entry **4**. This methodology is eminently suited to preparing heterotrisulfides.

Table 2.10: Heterotrisulfides prepared from R-SSH + R'-SLg via methodology E

Entry	Year/ Author	RSSH source	R'SLg	RSSSR' % yield
1	1960/Nakabayashi and Tsurugi.[127]	RSSAc, EtOH, HCl, 30°C R = Bn, Bz	R'SCl, R'SSCN R' = *o*-NO_2Ph, *o, p*-NO_2Ph, *p*-Cl-*o*-NO_2Ph, 2--naphthyl,	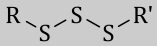 **70-98%**
2	1970/Harpp et al.[143]	BnSSAc, EtOH, HCl, 30 °C	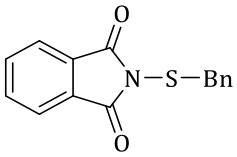	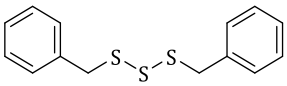 **98%**
3	(i)1992/Oberhammer et al.[144] (ii)1993/Munavalli et al.[105]	(i) CF_3SCl, $H_2S_{(g)}$, -78 °C (ii) CF_3SCl, $H_2S_{(g)}$, DMAP, DCM, -78 °C	CF_3SCl	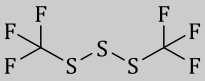 **35, 75%**
4	2013/Witt et al.[139]	RSSAc, NaOMe, 0 °C, MeOH R = $(CH_2)_{11}Me$, $(CH_2)_{11}OH$ $(CH_2)_{10}CO_2H$, $(CH_2)_{11}NHBoc$	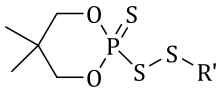 R' = $(CH_2)_{11}Me$, $(CH_2)_{11}OH$, NHBoc, $(CH_2)_{10}CO_2H$,$(CH_2)_{11}$ $(CH_2)_{10}CO_2Me$	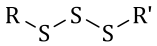 **63-99%**
5	2018/Xian et al.[145]	RSSFm, DBU, rt 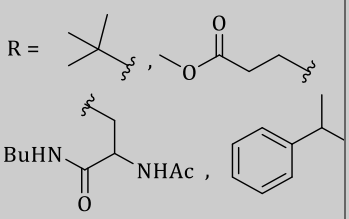	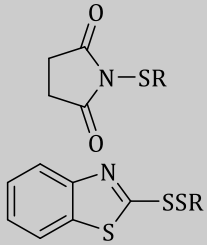 R' = Bn, ^{t}Bu, Cy, Ph, Et.	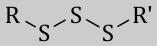 **32-95%**
6	2019/Hunter et al.[146]	RSSAc, NaOMe, -78 °C, THF R =^{n}Pr, ^{n}Hex, ^{n}propargyl, allyl, ^{n}dodec, *p*-tolyl, *p*-$MeOC_6H_4$	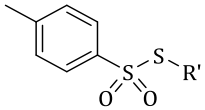 R' = allyl, Bn, Cy, Ph, $(CH_2)_3OH$, *n*- dodec, *p*-FC_5H_4, *p*-MeOPh,	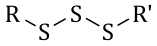 **52-96%**

Two aspects stand out for this methodology, which are the nature of the leaving group in RSLg and how the perthiol RSSH is accessed from a surrogate. Regarding the latter aspect first, perthiols are well known in the biological literature in conjunction with sulfur redox biochemistry and were first recognized synthetically in the 1950s by Böhme et al.[120] He demonstrated that the perthiol RSSH was reasonably stable in acidic medium (far less so in a basic one) and managed to prepare it via acid deprotection of a disulfanyl acetate RSSAc (formed by coupling of acetylsulfenyl chloride with a thiol) using methanolic HCl under mild conditions. Very recently, Ming Xian's group have generated a perthiol from a cyclic acyl disulfide using an amine as the unmasking agent.[147] **Scheme 2.26** shows Böhme's important synthesis methodology for producing a perthiol .

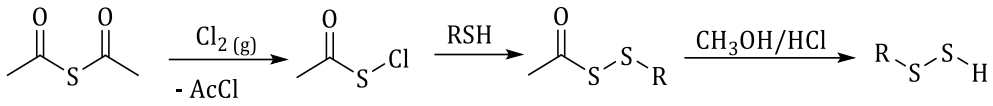

Scheme 2.26: Böhme's Synthesis of RSSH.[120]

In the early 1960s, a Japanese group headed by J. Tsurugi [148]extended Böhme's method to the synthesis of organotrisulfides as depicted in entry **1** of **Table 2.10**. Without purifying the perthiol RSSH (R as alkyl or benzyl/ benzoyl), they showed that heterotrisulfides could be prepared using a sulfenyl chloride or thiocyanate as electrophile.[127] The synthesis of the two electrophilic reagents had been reviewed previously by Norman Kharasch,[149] and generally involved oxidising either a disulfide or a thiol with chlorine or bromine to afford the sulfenyl halide, which could be substituted with thiocyanate ion for producing the sulfenyl thiocyanate. By the 1970s, Harpp made use of this accessibility of perthiols by reacting BnSSH with PhthNSBn (a Harpp transfer reagent) to form dibenzyl trisulfide (entry **2**) in excellent yield (98%).[143] Entry **3** in the Table shows an interesting way of accessing the perthiol from a sulfenyl chloride and H_2S,[144] in which the perthiol could be reacted with a second equivalent of sulfenyl chloride to afford the trisulfide. Although the paper only mentioned homotrisulfide synthesis, in principle this method could be used for accessing hetero cases. The same method was optimized one year later by Munavalli et al.[105] by adding 4-(dimethylamino)pyridine (DMAP) as a catalyst, which improved the yield to 75% with excellent purity of 96% as measured by GLC.

The first example of exploiting base deprotection of a disulfanyl acetate for heterotrisulfide synthesis appeared from Witt's group in 2013 when he used sodium

methoxide in dry methanol at 0 °C under N_2 to generate the corresponding perthiolate (RSS^-) without loss of sulfur (entry **4**).[139] However, importantly, the perthiolate was liberated insitu in the presence of a novel sulfanyl cyclic phosphorodithioate (the two oxygens diesterified in the form of a ring) as the electrophilic RSLg partner, which had the added advantage that it could also be used to source the disulfanyl acetate via its reaction with KSAc.[139] Undoubtedly, given the high instability of perthiolates, S-S bond formation ensued rapidly once the perthiolate was liberated to afford alkyl heterotrisulfides (no aromatic cases) in excellent yield and high purity, the chemistry of which is summarized in **Scheme 2.27**.

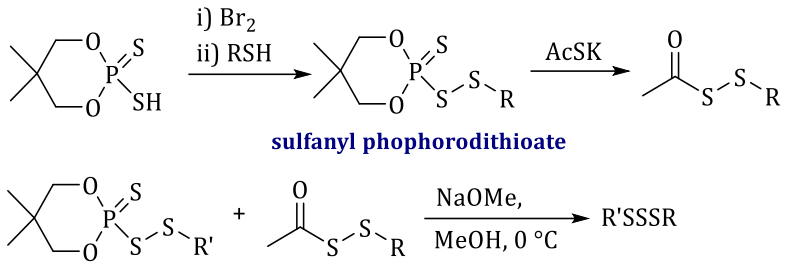

Scheme 2.27: Synthesis of heterotrisulfides via Witt's method.[139]

A few years later in 2018, Ming Xian's group[145] reported on a novel methodology for accessing the perthiol source via base deprotection of a 9-fluorenylmethyl disulfide (RSSFm) in which the focus was on R as a cysteinyl group (entry **5**, **Table 2.10**). The deprotection to the perthiol RSSH (or perthiolate, RSS^-) was achieved using DBU (2 eq.), taking advantage of the relatively acidic nature of the benzylic hydrogen of the Fm group (like the principle governing FMoc deprotection in peptide deprotection chemistry) as shown in **Scheme 2.28** below. The perthiolate coupled to SuccNSR, or 2-benzothiazole disulfide in low to excellent yield (32-95%). The targeted nature of these two recent methods ensures that homotrisulfides do not overly interfere as by-products.

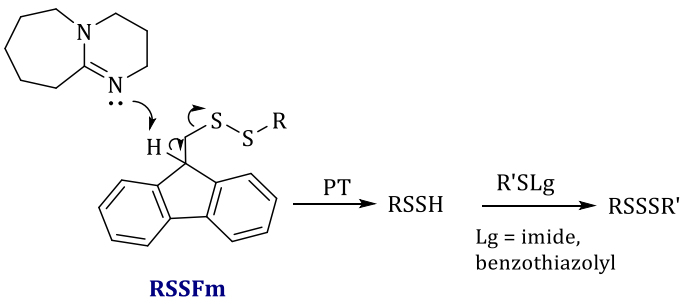

Scheme 2.28: Synthesis of heterotrisulfides via Xian's method.[145]

My own work at UCT (presented in Chapter Four in this PhD thesis) published in *JOC* in 2019 also used a [2 + 1] approach for developing a new method of synthesizing a wide range of heterotrisulfide in high yield and purity and relatively free of polysulfides.[146] The method involved the low temperature sulfenylation of a perthiolate generated using Witt's methoxide methodology by an organothiotosylate (entry **6**). This method will form the basis of Chapter Four on methodology and won't be discussed further here.

Finally, two groups have cleverly exploited certain disulfanyl reagents of the type RSSX that can generate *in situ* both the electrophilic (RSLg) and nucleophilic reagent (RSS^-) for methodology **E**. The reaction constitutes a homo-coupling with two prerequisites. Firstly, the X group of RSSX should be removeable via an S_NAc mechanism to liberate the perthiolate anion RSS^-. Secondly, the SX group should also act as a leaving group in another molecule as depicted by the **Scheme** in **Table 2.11**.

Table 2.11: Homotrisulfide prepared from R-SS-Lg base deprotection

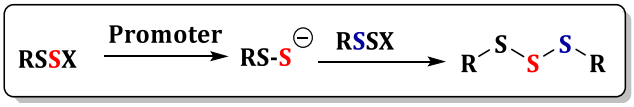

Entry	Year / Author	RSSLg	Promoter	RSSSR %yield
1	(i) 1976/Harpp et al.[44] (ii) 2019/ Pluth et al.[45]	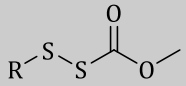 R = C_2H_5, C_3H_7, $(CH_3)_2CH$ $(CH_3)_3C$, Ph, Bn	(i)^{t}BuOK, MeOH (ii)^{t}BuOH, ^{t}BuOK, THF, H_2O	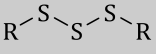 **36-98%**
2	2014 / Witt et al.[150]	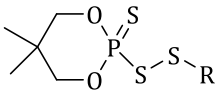 R = $(CH_2)_{11}Me$, $(CH_2)_{11}OH$, $(CH_2)_{10}CO_2H$, $(CH_2)_2OH$, 4-C_6H_4-CH_3 $(R)CH_2CH(NHBoc)CO_2Et$	TBAF	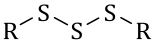 **85-97%**

Clearly, such a variant of methodology **E** is only applicable for synthesizing homotrisulfides, and the prototype reaction, as already mentioned, was discovered by Harpp in 1976.[151] It involved reacting a sulfenyl thiocarbonate (MeOCO(SSR)) with methoxide in methanol as solvent at 0 °C, which gave a mixture of the homotrisulfide and homodisulfide. However, as the steric bulk of the promotor increased, the percentage of

trisulfide dramatically improved, resulting in *t*-butoxide as the promoter of choice. Logically, the nucleophilic promotor stoichiometry must be less than half of the RSSX concentration. The sequence of events is illustrated in **Scheme 2.29**.

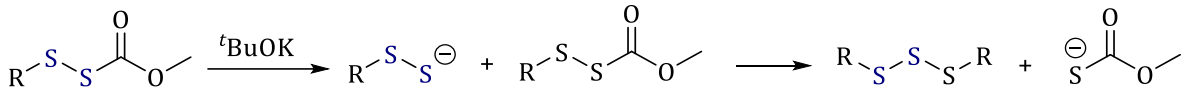

Scheme 2.29*:* Harpp's method for homocoupling.

Although perthiolates have the advantage of being considerably more (soft) nucleophilic than their thiolate counterparts due to a hyperconjugative a-effect, they suffer from the grave disadvantage of desulfurising to the thiolate,[152] explaining why so many procedures using perthiols result in a mixture of di- and trisulfide. Recently, Pluth used Harpp's method to prepare dibenzyl trisulfide (BnSSSBn) for studying its reaction with thiols to generate H_2S as a biotransmitter.[153] In their work, benzylsulfinyl thiocarbonate was treated with *t*-BuOK in methanol to afford an inseparable mixture of di- and trisulfides. The chemoselectivity problem was solved by switching to a mixture of tetrahydrofuran and water, which generated hydroxide ion as promoter, resulting in the formation of BnSSSBn cleanly, albeit in a low yield of 36% (**Table 2.11**, entry **1**).[153]

The other example of this intriguing methodology for homotrisulfide synthesis is due to Witt,[150] using a sulfanyl phosphorodithioate. In his case, TBAF acted as a hard, nucleophilic promoter, reacting at the harder phosphorus centre over the softer sulfur one (**Table 2.11**, entry **2**). Although elegant in principle, as already mentioned, the method can only access homotrisulfides and runs the risk of the disulfanyl anion intermediate losing sulfur to form a competing thiolate nucleophile leading to a disulfide by-product, **Scheme 2.30** shows the sequence of steps.

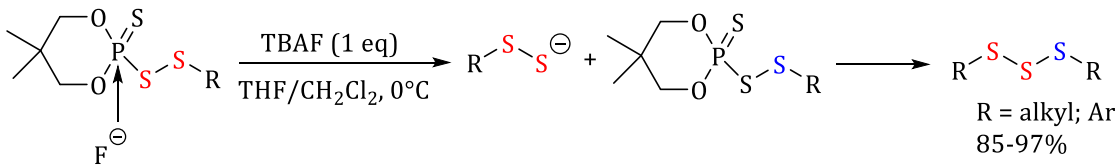

Scheme 2.30: Witt's method for homocoupling.[150]

Both methodology **D** and **E** are considered the most reliable way for accessing homo and hetero trisulfides with greater selectivity relatively free of polysulfides. Notably, both protocols provide a convenient and efficient method for accessing the trisulfides of

significant biomolecules such as amino acids, saccharides as well as heterocyclic derivatives.

In summary, this Chapter has reviewed the synthetic methodologies available for accessing trisulfides, which have become increasingly important in both biology and materials science. While current methods rely heavily on the use of starting materials such as SCl_2 and S_2Cl_2, the demand for green and sustainable, catalytic methods is growing. Recent innovations in disulfide synthesis offer potential avenues for trisulfide construction, but the unique challenges of creating unsymmetrical targets remain. The use of sulfur as a starting material and the development of aqueous systems represents promising areas for future research. The upcoming Chapter of this thesis will describe our novel and relatively green and innovative method for preparing unsymmetrical trisulfides in high yield, purity, and excellent selectivity.

CHAPTER 3: Organosulfur Compounds in Cancer Chemoprevention

3.1 The Burden of Cancer

Cancer is a broad term used for a set of diseases that may develop in any part of the body when abnormal cells proliferate out of control. This abnormal growth is invariably followed by the cancer, which may advance further by migrating or metastasising to the other organs,[154,155] this part of the disease is responsible for over 90% of cancer fatalities.[155] The descriptions of a neoplasm and "malignant tumour" are two terms commonly used to describe the early and advanced stages.[156] According to the World Health Organization, cancer represents the leading cause of mortality worldwide, with about 10 million deaths reported in 2020 accounting for nearly one in every six deaths.[157] In 2017, the yearly number of new cancer cases was predicted to rise from 14.1 million in 2012, to 21.6 million by 2030, according to the WHO's institutional repository for information system (IRIS).[158] Much evidence points towards a contemporary lifestyle and urbanization as key factors contributing to the increase in the number of cases, however, a nutritious diet which is tobacco-free, with regular exercise, avoiding UV radiation, maintaining a healthy body weight, and limiting exposure to pollutants. Therse actions can prevent 30–50% of all cancers. In South Africa, almost 110,000 new cancer cases were diagnosed with more than 56,000 fatalities in 2020 (**Figure 3.1**). However, this considerable burden is likely to grow in the following decades, with the number of new cancer cases expected to climb to 138,000 and 175,000 in 2030 and 2040, respectively.[159]

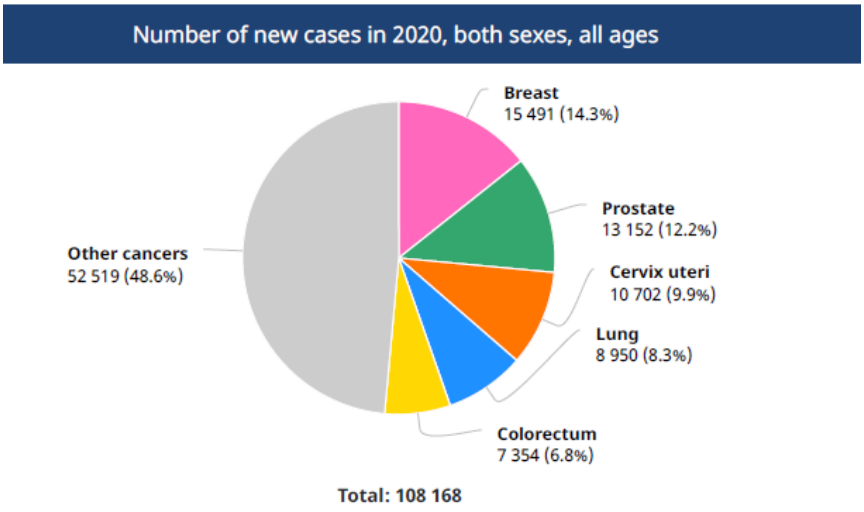

Figure 3.1: Summary cancer incidence in South Africa, 2020. Taken from WHO.[159]

On molecular level, cancer is defined as a genetic disorder resulting from DNA mutations that may arise either spontaneously, or as a result of environmental exposures. Chemicals, radiation, viruses, and germline variants all are examples of environmental factors which may cause a genetic mutation.[160] While non-genetic risk factors can be minimised, preventing genetic harm remains the most difficult challenge. There is a tight relationship between tumour development and the inhibition of apoptosis, which leads to cell immortality. As a result, genes that regulate apoptosis and DNA repair have the potential to function as proto-oncogenes or tumour suppressors.[160] There are two types of genes that prevent cancer development and these are often mutated and dysfunctional in carcinogenesis. These are tumour suppressor genes, which restrict cell growth and division, and proto-oncogenes, which promote cell growth and division (**Figure 3.2**). The latter type when upregulated or mutated, drive carcinogenesis.[161] Tumour-suppressor genes on the other hand inhibit cancer growth while also promoting normal cell development. Furthermore, genes involved in DNA repair are often mutated in cancer thus allowing dysfunctional genes to often persist.[160]

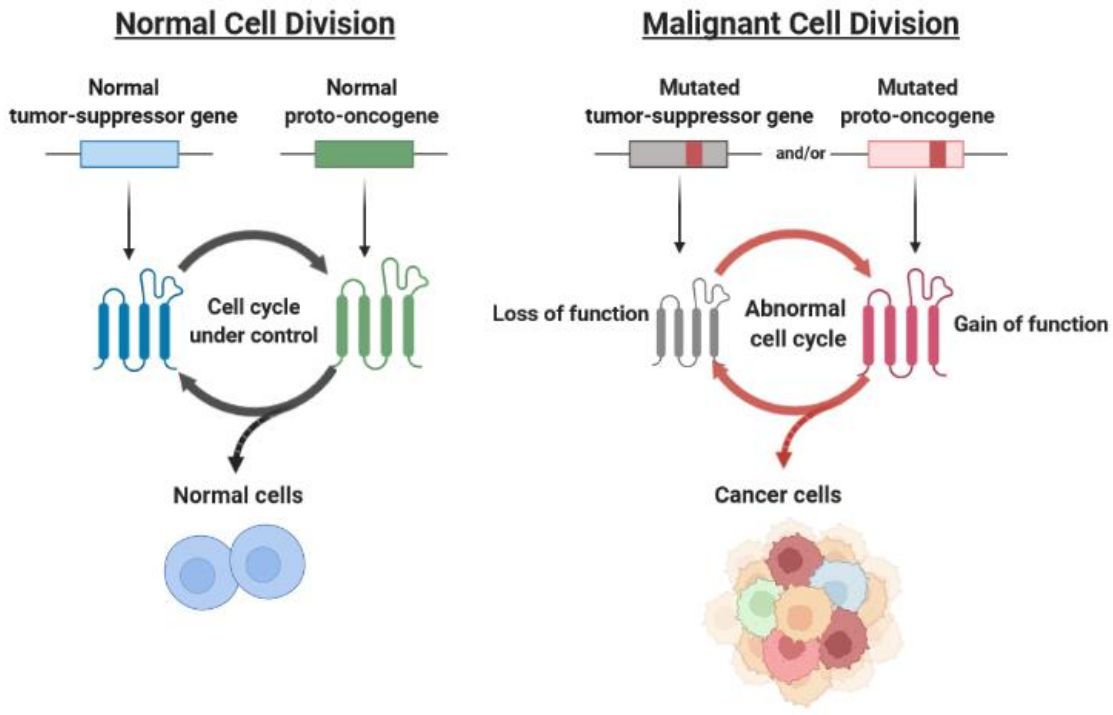

Figure 3.2: Cancer development showing the role of oncogenes and tumour suppressor genes. *Created using Biorender*.

3.1.1 Carcinogenesis: Stages of Cancer Development

Carcinogenesis is a multi-step process that starts with the accumulation of genetic changes ultimately leading to an altered phenotype in which normal cells are transformed into cancer cells. According to Pitot *et al.* (1989), carcinogenesis can broadly be divided into three stages as initiation, promotion and progression,[162] (**Figure 3.3**).

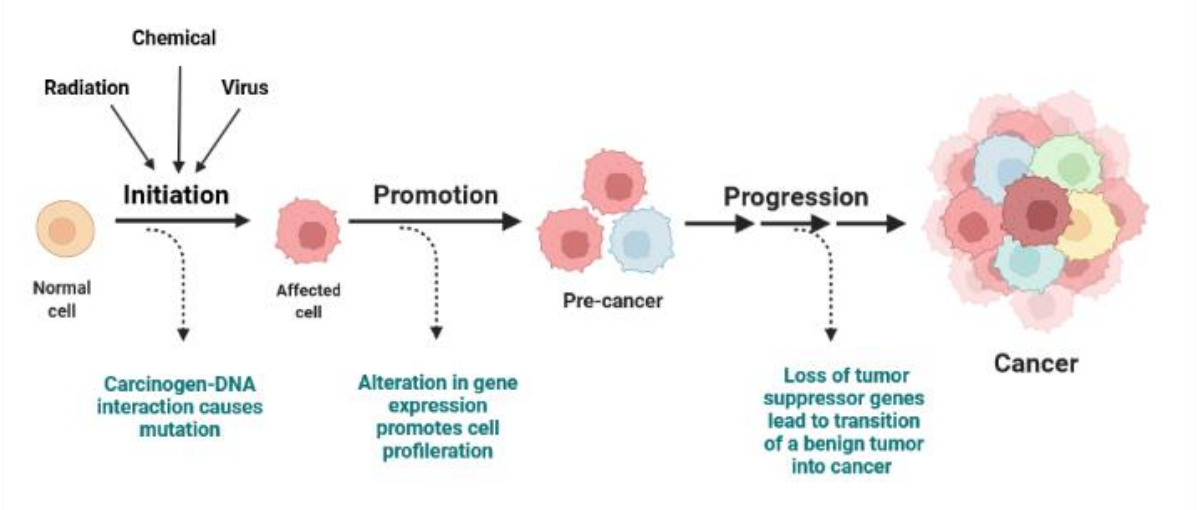

Figure 3.3: Carcinogenesis multistep process that turns a normal cell into a cancerous tumour*. Created using Biorender.*

The first stage, initiation, occurs when the carcinogen interacts with the cell DNA, triggering a mutation, which results in daughter cells produced from the mutant cell likewise containing the mutation.[163] Such modified cells become sensitive to promoter effects in which dietary and hormone factors play a significant role.[162] The last stage, progression, results from instabilities accumulated after the initial mutation, continued exposure to a carcinogen, and spontaneous further mutations. Altogether they eventually lead to a malignant neoplasm. Additionally, critical traits such as invasion, metastasis, anaplasia, and enhanced growth proceed to higher levels of malignancy.[164] For a more in-depth examination of the molecular pathogenesis of cancer, it is preferable to consider cancer-related genes as grouped within fundamental changes to the cell physiology. These are commonly referred to as ''cancer hallmarks'' which are described in the following section.

3.1.2 The Hallmarks of Cancer

Hanahan *et al.* have classified the "Hallmarks of Cancer" into 14 types, covered in three papers published in 2000,[165] 2011[166] and 2022.[167] These hallmarks are considered as a

classification for condensing the complexity of cancer phenotypes and genotypes into a collection of fundamental principles describing the mechanism of cancer development. (**Figure 3.4**)

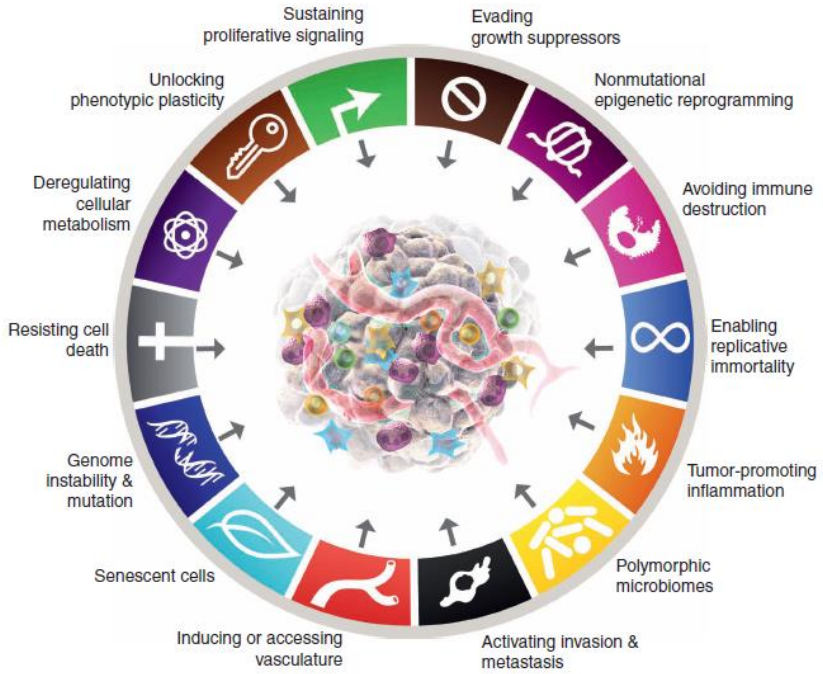

Figure 3.4: The Hallmarks of Cancer, taken directly from Hanahan *et al.*[167]

The "***Sustained proliferative signalling***'" covers a large proportion of the growth signals promoting carcinoma cell proliferation derived from the tumour's stromal cells. Proliferation of these cells is a tightly regulated process, triggered by growth signals that can originate either within or outside the cell.[166] Normal cell growth and division are controlled by the synthesis and release of growth-promoting signals which maintains homeostasis of cell numbers. In contrast, these signals are altered when cancer cells take control and generate their own proliferation signaling molecules.[166]

''Evading growth suppressors' is another hallmark that is strongly related to maintaining proliferative signaling, in which any signals that control cell proliferation programs are dependent on tumour suppressor gene activation. Many of these tumour suppressive mechanisms have lost function for the advantage of the cancer cell in malignancy.[166,168]

The concept of ***''Resisting cell death''*** is based on the idea that programmed cell death or apoptosis, acts as a natural barricade to cancer formation by clearing the damaged cells.[166] The apoptotic machinery is organized into two categories: sensors and

effectors.[165] Sensors are mainly responsible for monitoring the extracellular and intracellular environments and determining whether a cell should live or die based on the conditions of normality or abnormality. Through their response to pro-apoptotic signals as well as through the release of cytochrome C, mitochondria play an important part in programmed cell death.[160]

"***Inducing angiogenesis or vasculature***" may occur early in the multistage progression of invasive malignancies in both animal models and humans.[166] Tumour vascularization is required for growth and is governed by the balance of angiogenic and antiangiogenic substances produced by tumour and stromal cells. Even with all of the outlined growth advantages, tumours cannot grow larger than 1 - 2 mm in diameter unless they are vascularized.[160] Similar to normal tissues, tumours demand nutrition and oxygen as well as the ability to expel metabolic wastes and carbon dioxide.[166] As a result, cancer cells can drive neoangiogenesis, in which new vessels emerge from previously existing capillaries, or vasculogenesis.[169] Vascularization influences tumour development in two ways: perfusion provides the required nutrients and oxygen, and newly created endothelial cells encourage tumour cell growth through the secretion of growth factors.[160] Hypoxia can also promote angiogenesis by inhibiting the transcription of the pro-angiogenic factor, (vascular endothelial growth factor (VEGF) by Hypoxia-inducible factor 1 (HIF-1). Many genes involved in angiogenesis, glucose metabolism, cell proliferation/survival, and invasion/metastasis are activated by HIF-1.[170] In addition, another variable influence to angiogenesis is p53, which induces synthesis of the angiogenesis inhibitor TSP-1.[160] Overall, angiogenesis is necessary for tumour growth providing access to the vasculature and thus metastasis.

*''**Activating invasion & metastasis"*** is an additional critical and fundamental hallmark of cancer. Tumour spread is a complicated process requiring a series of processes known as the invasion–metastasis cascade. These processes include local invasion, followed by intravasation into the blood and lymph that transit through the vasculature. This step is followed by the migration of cancer cells from the lumina of these vessels into the parenchyma of distant tissues leading to micrometastases, and growth of micrometastases into macroscopic tumours. The last step is known as colonization[160,166] involving cell invasion and vascular dissemination and homing of the tumour cells. In some cancer types, the primary tumour's location can predict the metastatic site. Many cancers come to a halt in the first capillary bed that they encounter, often the lungs and

liver. Some cancers show organ tropism, which is thought to result from activation of adhesion or chemokine receptors whose ligands are expressed by endothelial cells at the metastatic location.[160] Normal cells, however, include adhesion mechanisms that allow them to adhere to neighbouring cells and the ECM. Cancer cells, in contrast, lose their adhesion structures, allowing them to break free from proto-growth and migrate to distant locations via the lymphatic and vascular systems.[171] Hence, invading cells can break through the surrounding tissue, to gain access to the blood vessel or lymph network, survive in the bloodstream, and find a foothold in a remote region.[172]

The ***''Reprogramming cellular metabolism***'' is a key aspect of cancer development. Cancer cells, despite sufficient oxygen, undergo a metabolic shift known as the Warburg effect.[160] They switch from using oxygen-dependent mitochondria to relying on glycolysis for energy production.[160] This metabolic switch occurs even in the presence of adequate oxygen levels, indicating the establishment of genetic alterations within tumour cells. The activation of oncogenes and mutation of tumour suppressor genes drive this change and provide advantages for cancer cells, such as enhanced proliferation, evasion of controls, and resistance to apoptosis.[166] Reprogrammed energy metabolism, particularly the reliance on glycolysis, is considered an important hallmark of cancer, highlighting its significance and independence from other core hallmarks.

"***Evading immune destruction***" The immune response is our body's ability to resist harmful diseases, which is activated when antigen-specific antibodies identify foreign molecules or cellular structures. The immune system however does not respond to antigens that are native to the body.[173] Immune surveillance is a long-standing idea that claims an ever-alert immune system and constantly monitors cells and tissues.[166] As a result, the immune surveillance is responsible for recognizing and killing the vast majority of incipient cancer cells and hence nascent tumours. According to this rationale, solid tumours that do grow have either escaped recognition by the immune system's numerous arms, or have been able to restrict the degree of immunological killing, allowing them to evade eradication.[166] Cancer cells may also express antigens that avoid immune detection, and produce immune suppressive factors.[174]

''***Replicative immortality***'' is another significant hallmark that is needed to create macroscopic tumours through limitless replicative potential immortality. In contrast, normal cells go through a limited number of cell division and growth cycles. This is controlled by two types of cell death: (1) senescence, which is an irreversible transition

to a non-proliferative but viable state, and (2) cell death which is at crisis.[166] Some cells may induce senescence during cell division, which is followed by a crisis period in which the vast majority of cells die. The cells that emerge from a population in crisis, usually do so with unlimited replication ability.[175] The characteristic of unlimited proliferation is regulated by telomeres, which are the protective caps on the ends of chromosomes.[176] The telomere sequence becomes shorter with each replication. The length of telomeres, however, can be increased by a DNA polymerase known as telomerase[176,177] which are abundant in cancer cells as a means of avoiding senescence and achieving immortality.[166] The final hallmark is "***unlocking phenotypic plasticity***". Phenotypic plasticity is generally restricted in order to avoid or escape terminal differentiation and this is a major component of cancer pathogenesis.[167] In most circumstances, the end effect of cellular differentiation is anti-proliferative, posing an obvious barrier to the continued proliferation required for neoplasia.[178] As a result, nascent cancer cells derived from a normal cell that has progressed down a pathway toward or adopting a fully differentiated state, may revert to progenitor-like cell states by dedifferentiating. On the contrary, neoplastic cells derived from a progenitor cell that is destined to follow a pathway leading to end-stage differentiation may short-circuit the process, keeping the cancer cells in a partially differentiated, progenitor-like state.[167]

In summary, normal cells often develop into a neoplastic state over time, and there are a series of hallmark alterations that occur along the way. This allows cancer cells to acquire characteristics that lead to tumour development and malignancy. Understanding the hallmarks of normal cells and unhealthy cells, relating them to the hallmarks of cancer, and trying to break the relationship may prove to be the key to cancer prevention.[167] The complexity and variability of treating cancer, at all levels of consideration, is to remain a big challenge. However, the impact of the hallmarks of cancer in conceptualizing new discoveries and helping to simplify this complexity into a science has been recognized with some success over the years. While the hallmarks model is a good description of what goes wrong in cancer cells, it does not address why those alterations are made in the first place. Hence, understanding cancer hallmarks has helped scientists acquire insights into therapeutic targets but not into disease prevention. In this regard, targeting cancer prevention by eating foods high in phytochemicals has been demonstrated in many studies to reduce the risk of cancer. There are several dietary bioactive compounds present in dietary plants which have strong anticancer and chemopreventative

capabilities, according to epidemiological and experimental studies. One of these plants, garlic, has been shown to reduce the risk of cancer, and has thus received considerable attention. This thesis will go into more details on this topic.

3.2 Garlic Organosulfur Compounds and their Anti-Cancer Activity

The anticancer properties of natural products and their derivatives have been extensively examined in cancer treatment and chemoprevention. These compounds are attractive because of their safety, low toxicity, antioxidant properties, and widespread use as dietary supplements.[179] One of the most well-known botanical natural products with chemopreventive activity is Garlic (*Allium sativum*), which is thought to have originated in central Asia, and is now grown around the world.[180] For over 5000 years, people have known and exploited the therapeutic properties of garlic. It's traditionally uses include the treatment of colds, infections, heart disease, diabetes, aches and pains, constipation, eye infections, snake bites, dandruff and tuberculosis.[181] In 1858, Louis Pasteur showed the antimicrobial effect of garlic.[182] Scientific studies have shown that garlic can lower blood pressure and cholesterol levels and protect against arteriosclerosis.[183] Some of the other important medicinal effects of garlic are antibacterial, antioxidant, antithrombotic, immunomodulatory, antidiabetic, drug metabolism modulation a well as anticarcinogenic properties.[181,183-186] One of the oldest medical texts, the Egyptian papyrus, Codex Ebers in 1550 BC describes garlic as a therapy for abnormal growths and abscesses.[185] In 1957, Weisberger and Pensky reported for the first time that anti-tumour effects of some organosulfur compounds from garlic.[187,188] Since then, much epidemiological research has shown that garlic consumption can protect against cancer. The relevant literature is summarized in the next sections.

3.3 Epidemiological Evidence for the Cancer-Preventive Effects of Dietary Garlic

The consumption of garlic has been shown to have beneficial medicinal effects and may aid in the prevention of cancer. This has been shown in epidemiological studies which have linked a lower cancer risk in people who eat allium vegetables (these include onions, garlic, leeks, scallions, chives, and shallots), in countries ranging from the Mediterranean to South and East Asia. **Table 3.1** summarises the research findings on this subject.

Table 3.1: The epidemiological evidence on garlic consumption and incidence of cancer

Entry	Authors	Study's conclusion	Cancer type	Country	Year/Ref
1	You *et al.*	A significant reduction in gastric cancer risk with increasing consumption of allium vegetables.	gastric cancer	China	1989[189]
2	Buiatti *et al*.	A reduction of risk factors for gastric cancer associated with consumption of garlic.	gastric cancer	Italy	1989[190]
3	Iscovich *et al*.	Consumption of garlic is associated with decreased risk of colon cancer.	colon cancer	Argentina	1992[191]
4	Hansson *et al.*	A high consumption of garlic was associated with reduced gastric-cancer risk.	gastric cancer	Sweden	1993[192]
5	Steinmetz *et al.*	Consumption of garlic was inversely associated with risk of colon Cancer.	colon cancer	USA	1994[193]
6	Witte *et al.*	This study supports the hypothesis that high intake of allium vegetables decreases the risk of colorectal adenomatous polyps.	Colorectal cancers	USA	1996[194]
7	Dorant *et al.*	The consumption of allium vegetables may considerably reduce the risk of stomach cancer.	Stomach cancer	The Netherlands	1996[195]
8	Franceschi *et al.*	Garlic intake inversely associated with cancer of the colon, rectum and breast.	colon, rectum and breast cancer	Italy	1998[196]
9	Gao *et al.*	Garlic frequency intake is associated with a reduction in the risk of esophageal and stomach cancer.	esophageal and stomach cancer	China	1999[197]
10	Levi *et al.*	This study suggested that a potentially broader favourable effect of garlic on digestive tract carcinogenesis.	digestive tract cancer	Switzerland	1999[198]
11	Fleischauer *et al.*	High intake of garlic may be associated with a protective effect against stomach and colorectal cancers	stomach and colorectal cancers	USA	2000[199], 2001[200]

12	Takezaki *et al*.	Frequent garlic consumption contributes to low mortality rates for esophageal and stomach cancers.	esophageal and stomach cancers	China	2001[201]
13	Muñoz *et al.*	Allium vegetables have been associated with a decreased risk of gastric cancer.	gastric cancer	Venezuela	2001[202]
14	De Stefani *et al.*	Allium vegetables have been shown to be effective in preventing stomach cancer.	stomach cancer	Uruguay	2001[203]
15	Setiawan *et al.*	The protective effect of allium vegetables (especially garlic and onions) against stomach cancer.	stomach cancer	China	2005[204]
16	Galeone *et al.*	These studies confirm the inverse association between the frequency of use of allium vegetables and the risk of several common cancers.	several common cancers	Italy	2006[205]
17	Ngo *et al*.	7 studies confirm the inverse association, with a 30% reduction in relative risk in colorectal cancer.	colorectal cancer	Australia	2007[206]
18	Shukla *et al*.	Several epidemiological studies link a lowered risk of stomach, oesophageal and colorectal cancer to a high dietary garlic consumption.	stomach, oesophageal and colorectal cancer	India	2007[207]
19	Pourfarzi *et al.*	People consuming allium vegetables more frequently, experienced a significantly lower risk of gastric cancer.	gastric cancer	Iran	2009[208]
20	Annema *et al.*	Garlic consumption has been linked to a reduced risk of colorectal cancer (CRC).	colorectal cancer	Australia	2011[175]
21	Zhou *et al*.	Consumption of high levels of Allium vegetables reduced the risk for gastric cancer risk.	gastric cancer	China	2011[209]
22	Zhu *et al.*	No evidence that higher intake of Allium	colorectal cancer	China	2014[210]

		vegetables reduced the risk for colorectal cancer.			
23	Nicastro *et al.*	The study indicated that associations of *Allium* vegetable consumption with decreased risk of gastrointestinal tract cancer.	gastrointestinal tract cancer	USA	2015[169]
24	Turati *et al*.	Frequent consumption of Allium vegetables was associated with reduced risk of several cancers	several cancers	Italy	2015[211]
25	Wang *et al.*	Consumption of garlic were correlated with reducing the related risk factors of colon cancer.	colon cancer	China	2018[212]
26	Kim *et al.*	The study does not support the hypothesis that high garlic intake reduces risk of gastric cancer.	gastric cancer	USA	2018[213]
27	Li *et al.*	Garlic intake was associated with a statistically significant reduced risk of death due to gastric cancer.	gastric cancer	China	2019[214]
28	Wu *et al.*	Consumption of allium vegetables is associated with a reduced risk of colorectal cancer.	colorectal cancer	China	2019[215]
29	Yuan *et al.*	Consumption of garlic may help to protect against gastric cancer.	gastric cancer	China	2020[216]
30	Wang *et al*.	An association between garlic intake and reduced risk of gastric and colorectal cancers was identified.	colorectal cancers	China	2022[217]

Thus, dietary changes suggest a cost-effective in reducing cancer risk since a multitude of epidemiological studies point towards garlic preparations and its components as likely preventative agents in cancer. The epidemiologic literature on garlic uses covers malignancies of the stomach, colon, lung, breast, oesophagus and prostate, as well as head and neck cancer.[200] Of the 30 publications reported in **Table 3.1**, twelve are reported on garlic and gastric cancer, with nine on colorectal cancer, which are thus the predominant cancer types covered in these studies. The first study was reported in 1989 by You *et al.* in China, where stomach cancer rates are high.[189] Here it was found that an increased

consumption of allium vegetables resulted in a considerable reduction in gastric cancer cases (**Entry 1**). The publications from specific case-control studies of stomach and colorectal cancer reveal a strong case in favour of the preventive benefit of raw and/or cooked garlic. Although a previous meta-analysis found that the protective effect of garlic on gastric and colorectal cancer may be exaggerated,[199] the results of comprehensive analysis published very recently by Wang *et al*.,[217] (**Entry 30**) have presented other data to indicate that garlic can help prevent gastrointestinal cancers. However, a small number of studies have found no link between garlic consumption and the incidence of colorectal and gastric cancer (**Entries 22 & 26**).[210,213]

Garlic is known to produce organosulfur compounds (OSCs) such as allicin, ajoene, *S*-allylmercaptocysteine (SAMC), *S*-allylcysteine (SAC), diallyl sulfide (DAS), diallyl disulfide (DADS), diallyl trisulfide (DATS) and diallyl tetrasulfide (DATTS), that have a strong anticancer property. There is convincing evidence to show that these compounds are anti-cancer agents. The organosulfur compounds in garlic will be discussed in the next section.

3.4 Phytochemical Overview of Garlic and its Organosulfur Compounds

Garlic (*Allium* sativum L.) belongs to the Lillaceae family of plants. The term "garlic" is thought to have come from the Anglo-Saxon word "gar leac," which means "spear plant".[218] The genus "*Allium*" is derived from the Celtic word "al" which means pungent or burning, whereas the species "sativum" indicates planted or cultivated.[185] Garlic has a strong and pungent flavour, as well as an aromatic and unique odour for which it is used as a spice. Garlic phytochemical analysis has shown the existence of both sulfur-containing and non-sulfur-containing chemical components which contribute to garlic's numerous pharmacological and therapeutic benefits. The non-sulfur compounds include polysaccharides, alkaloids, phenolic compounds, proteins, essential amino acids, flavonoids, saponins, sapogenins, glycosides, adenosine, allixin, steroidal glycosides, lectins, anthocyanins, prostaglandins, fructan, pectin, vitamins B1, B2, B6, C and E, biotin, nicotinic acid, fatty acids, glycolipids, and phospholipids and minerals.[219-225] Garlic is also a rich source of OSCs, with over 33 different types produced following crushing[226] Chemically, garlic OSCs are divided into two categories as water-soluble and oil-soluble, with both forms exhibiting anti-proliferative effects against cancer cells.[227,228] In 1985,

Block *et al.*[229] demonstrated how the garlic extraction procedure plays an important role in the type of OSC isolated, **Scheme 3.1**.

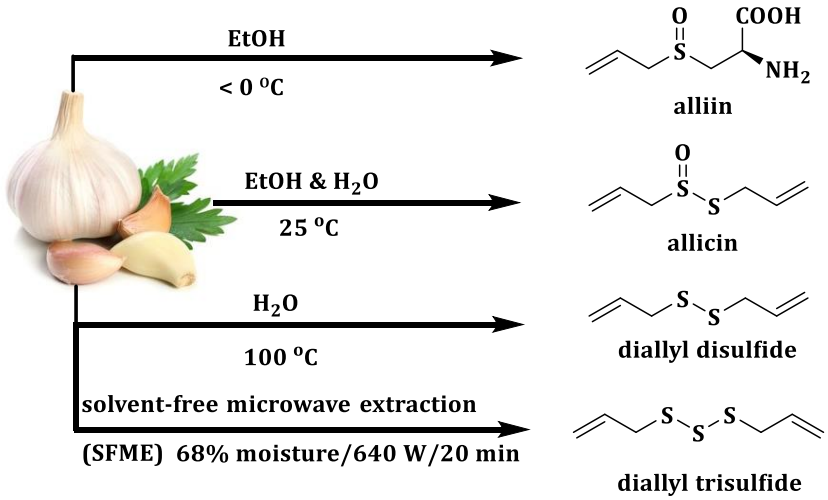

Scheme 3.1: Different methods of garlic extraction result in the isolation of different OSCs.[229,230]

It has been found that the OSCs extracted from garlic depend on the extraction solvent used for example water, alcohol or hexane.[229,231] While the high temperature of a steam distillation will prefer the formation of thermodynamically stable compounds such as DADS,[229] the isolation of important OSCs precursors such as allicin and alliin is achieved by nonpolar solvents with lower temperature extraction conditions. In 2006, Ichikawa *et al.* reported that a 90% methanolic solution containing 0.01 N hydrochloric acid at room temperature was suitable to isolate alliin, isoalliin, methiin, cycloalliin, and *γ*-L-glutamyl-*S*-methyl-L-cysteine.[232] Recently in 2022, Yingngam *et al.* discovered a novel method for extracting garlic oil rich in diallyl trisulfide using solvent-free microwave extraction (SFME) as an environmentally friendly technology, **Scheme 3.1**.[230] The two primary OSCs precursors found in whole garlic cloves are *S*-allyl-L-cysteine sulfoxide (alliin) and *γ*-glutamyl-*S*-allyl-L-cysteine (GSAC).[233] The starting point for the biosynthesis of OSCs is the conversion of GSAC into *S*-allyl-L-cysteine sulfoxide (alliin) by *γ*-glutamyl transpeptidase and oxidase in the cytoplasm of garlic clove cells,[226] (**Scheme 3.2**). Alliin is chemically stable and non-volatile, making it a main OSCs in both fresh and powdered garlic, with garlic cloves containing approximately 8 g/kg alliin.[234]

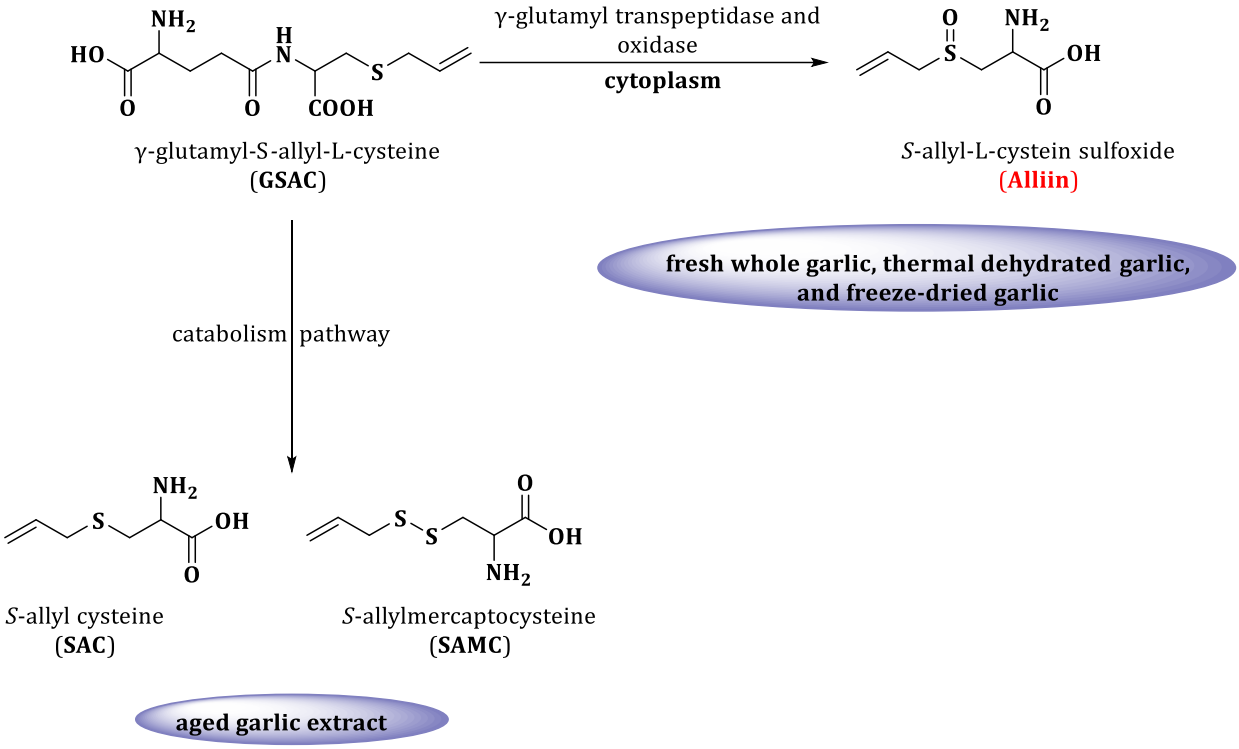

Scheme 3.2: Enzymatic transformation and biosynthetic origin of alliin.[226]

Notably, GSAC (*γ*-glutamyl-*S*-alk(en)yl-L-cysteine) is transformed to *S*-allylcysteine (SAC) and *S*-allylmercaptocysteine (SAMC) via a direct catabolism pathway. Both metabolites (SAC) and (SAMC) are water-soluble OSCs that are less odorous than the oil-soluble OSCs. When raw garlic is diced or crushed, the vacuolar enzyme alliinase is brought into contact with alliin. An elimination ensues to produce allylsulfenic acid, pyruvic acid, and ammonia. Following this, the allylsulfenic acid then rapidly condenses to generate allicin and water. Allicin, a chemically labile thioallyl ester of allylsulfinic acid, (**Scheme 3.3**), is responsible for crushed garlic's characteristic strong odour and also its antimicrobial properties. It readily decomposes into a wide range of products, including diallyl sulfide (DAS), diallyl disulfide (DADS), diallyl trisulfide (DATS), diallyl tetrasulfide (DATTS), dipropyl disulfide (DPDS), allyl methyl sulfide (AMS), allyl methyl disulfide (AMDS), allyl methyl trisulfide (AMTS) which are all found in steam-distilled garlic oil or cooked garlic. The other two sub-families of *E*-ajoene/*Z*-ajoene and 2-vinyl-4H-1, 3-dithiin/3-vinyl-4H-1, 2-dithiin are found in oil-extracted garlic. The rate of these transformations have been shown to be solvent-dependent, proceeding in a few hours at ambient temperature, and within minutes when heated.[226,235] The chemical structures and transformation pathways of the commonly investigated organosulfur compounds are depicted in **Scheme 3.3**.

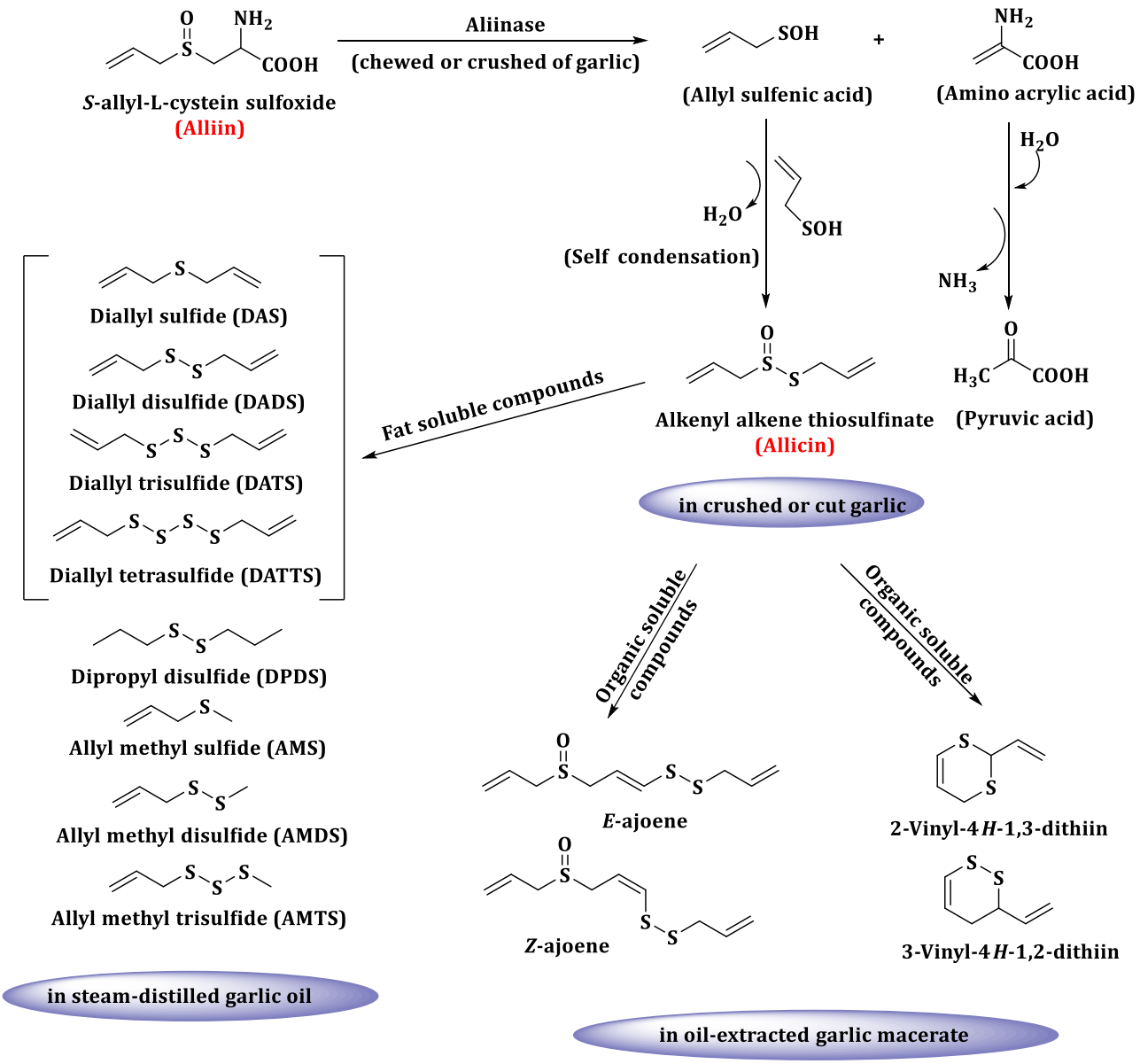

Scheme 3.3: Biosynthetic and enzymatic reactions of allicin to generate the oil soluble OSCs present in garlic.[226]

Allicin is a thiosulfinate whose chemical structure was identified by Stoll and Seebeck in 1948.[236] Mechanistically, there are four separate allicin decomposition pathways, which were elucidated by Block in the 1980s,[237] **Scheme 3.4** illustrates four different chemical pathways for the transformation of allicin to produce some of the key lipophilic allyl sulfur compounds.

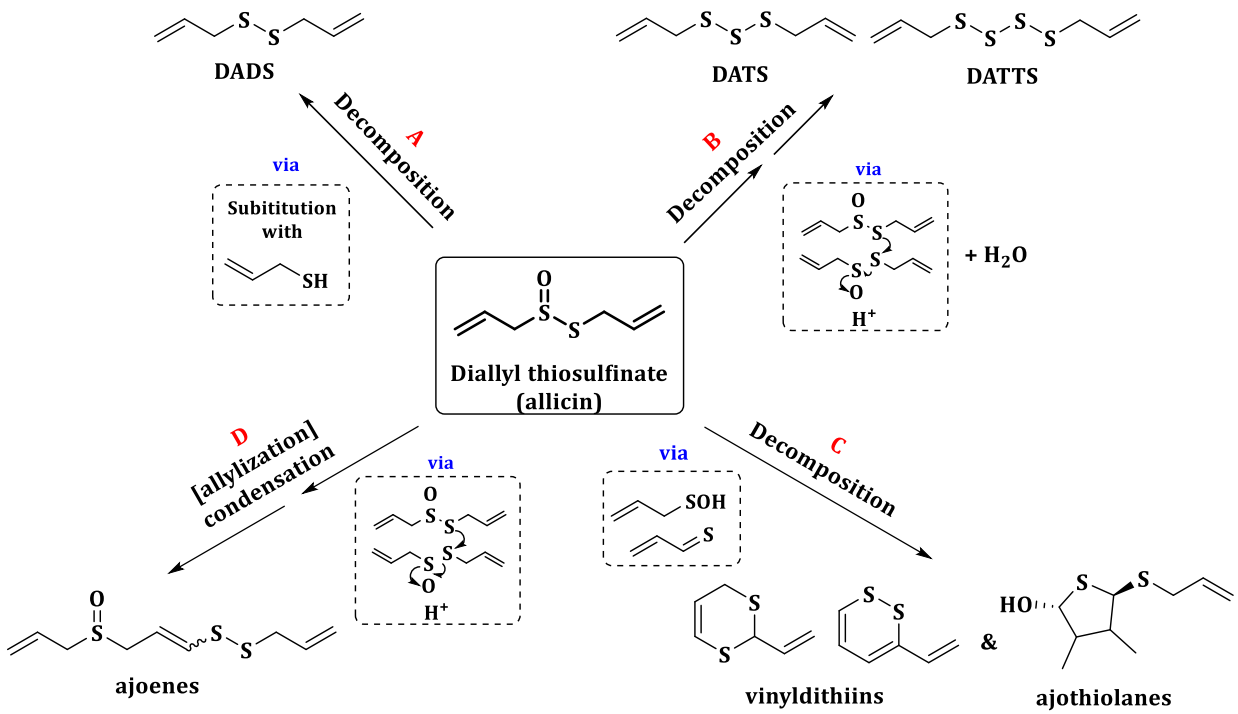

Scheme 3.4: Pathways for allicin transformation to produce oil-soluble second-generation OSCs.

Diallyl disulfide is produced by substituting allyl mercaptan at the sulfur of the thiosulfinate molecule via pathway **A**. Further substitutions with perthiol sulfinates in the presence of water will produce higher polysulfides as adducts such as DATS and DATTS through pathway **B**. Another possible allylization pathway **D** may occur when two allicin molecules undergo self-condensation via thioallylation to produce an intermediate sulfonium ion, which then undergoes elimination and Michael addition of 2-propenesulfenic acid to give ajoene. Lastly, pathway **C** utilizes a coordinated Cope-type elimination to produce 2-propenesulfenic acid and thioacrolein.[223] Diels-Alder cycloaddition of two molecules of thioacrolein produced by the elimination of allicin can produce vinyldithiins.[233] Recently in 2018, a multistep method was reported describing the condensation of two molecules of 2-propenesulfenic acid followed by a [3, 3]-shift and [2+3]-cycloaddition to produce a family of ajothiolanes according to Block et al.[238] In-depth discussion of the diallyl polysulfides, the family of interest, which do not exist in fresh cloves, but are produced during high temperature thermal processing of fried or baked garlic, will be the subject of the next section.

3.5 Diallyl Polysulfides Compounds from Garlic

The largest family of garlic OSCs are the diallyl polysulfides (R_1-$(S)_n$-R_2 (n = 1-6), which have bioactivity due to sulfur's ability to form S-S bonds through redox reactions.[239] The various bioactivities, especially anticancer activity, raise some fundamental chemical and physiological questions about the mode of action of polysulfides in biological systems, particularly di, tri and tetrasulfides.[240] **Scheme 3.5** depicts the range of secondary metabolite polysulfides produced from allicin as the primary garlic product.[184,226]

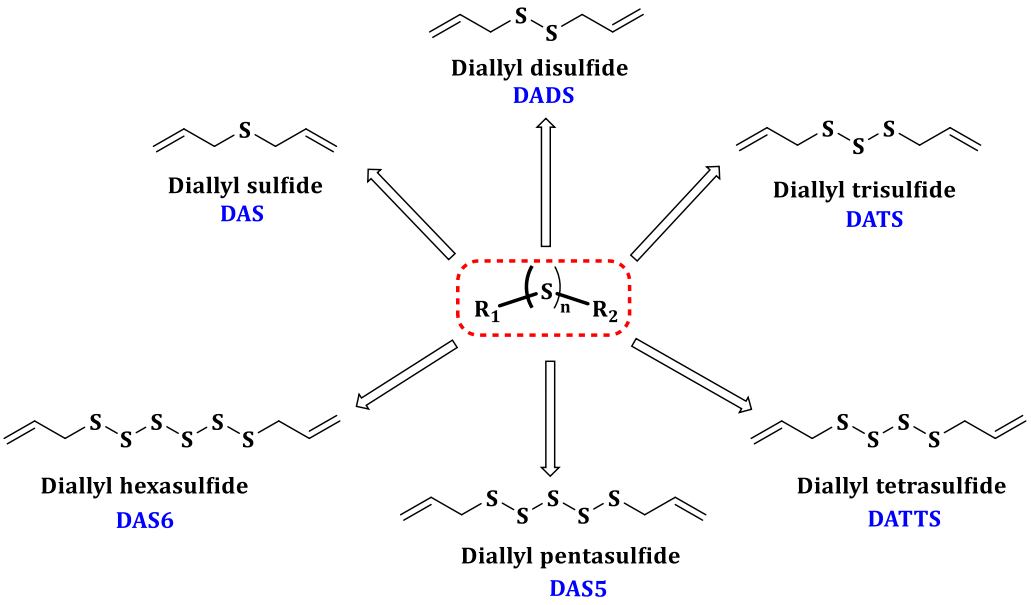

Scheme 3.5: The range of diallyl polysulfides found in garlic. Produced from allicin.

Because of their increased stability, functionality and target specificity, diallyl polysulfides have a bioactivity that is comparable to or better than allicin.[239] DADS is the primary diallyl disulfide compound identified in crushed garlic[241] (> 50%) and is generated as a direct result of allicin degradation via substitution pathway **A (Scheme 3.4**). In 2000, Maslin et al. reported that garlic oil, produced from a particularly potent British garlic variety, contained 530 mg/g of DADS, followed by DATS (115 mg/g), DAS (106 mg/g), DATTS (43 mg/g), diallylpentasulfide (DAS5) (1.5 mg/g), and diallylhexasulfide (DAS6) (0.14 mg/g).[242] In addition to methyl allyl and dimethyl sulfides, Maslin's analysis revealed that higher polysulfides were only present in very low concentrations. DAS, DADS, DATS, and DATTS have recently attracted sufficient interest, and in vitro evidence on tumour growth and toxicity points towards the tri and tetrasulfides being particularly potent. Indeed, several biological experiments have shown that, as the number of sulfur

atoms in a polysulfide increases, so does its anticancer activity, leading to assumption that *"the more sulfur atoms in the polysulfide, the more active it is*''.[239] In general, the ability of OSCs to inhibit tumour cell proliferation is ranked as follows, from most active to least active: ajoene, DATS > DADS, allicin > DAS > SAMC > SAC, with the presence of an allyl disulfide or allyl trisulfide backbone in the molecule being an essential structural features.[243,244] Munday et al. in 2003 reported that the anticancer activity increased in the order of tetra- > tri > disulfide, with the allyl moiety being more potent than the propyl.[245] In 2009, Cerella et al. discovered that DATTS was the most active at inducing apoptosis in U937 lymphoma cells, followed by DATS. DAS and DADS, however, were rather inactive.[246] The general trend shows that DAS is poorly active, DADS has modest activity, and polysulfides with three or four sulfur atoms exhibit enhanced activity. According to Munchberg et al., the increased activity is due to their oxidizing ability and thiol production. DATS and DATTS are significantly more active, possibly due to the production of perthiols (RSSH). However, the decreased stability of penta- and hexasulfides prevents further enhancement of activity, despite higher perthiol production.[239] The bioavailability and pharmacokinetics of each OSC should be investigated first in order to fully support the considerable evidence for the chemotherapeutic and chemopreventive effects of garlic OSCs, which will be discussed briefly in the following section.

3.6 Metabolism and Bioavailability of OSCs Derived from Garlic

Pharmacokinetic properties are highly dependent on water solubility.[247] SAC being a water-soluble, and allicin as an oil-soluble OSC, have received the most attention.[226] The bioavailability of garlic phytochemicals has been shown to be affected by whether they are taken together with other food components.[248] When fresh garlic is crushed or blended, allicin is formed well before intake[249] and the majority of the OSCs in garlic come from allicin. Allicin is not detected in blood or urine following consumption of substantial quantities of garlic, indicating that it is rapidly metabolised.[235,250,251] Allicin reacts with components of the plasma membrane and is trapped before absorption, and cannot circulate in the blood.[251] **Figure 3.5** illustrates the metabolism and bioavailability of the main garlic OSCs.

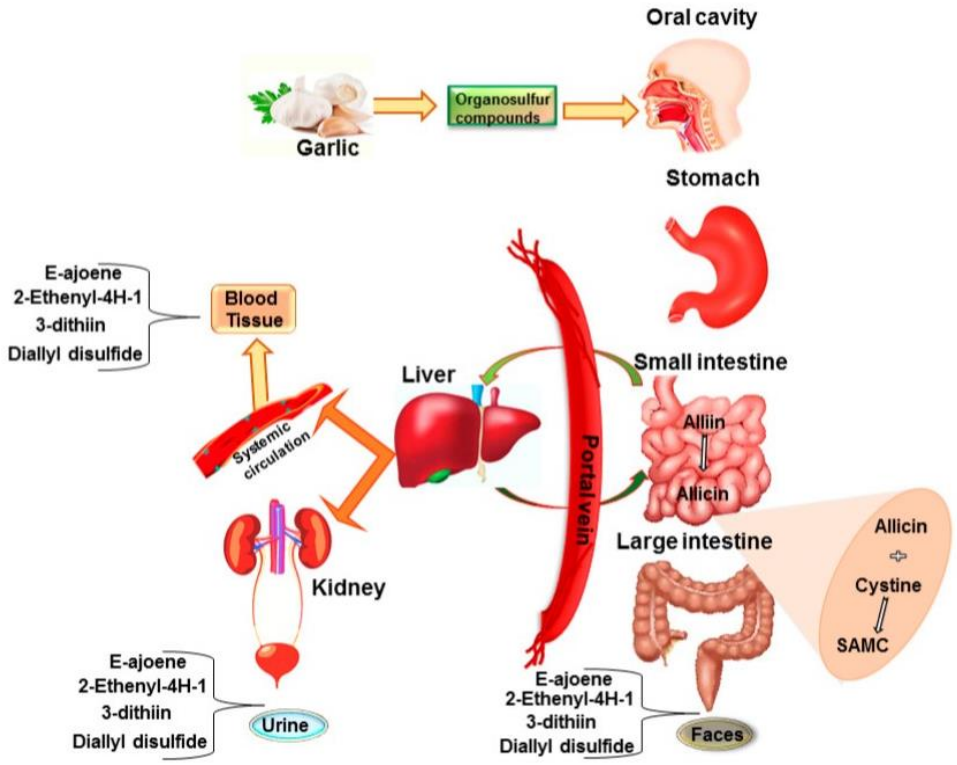

Figure 3.5: Schematic of garlic organosulfur absorption, metabolism, and distribution in the GI tract.[247]

The bioavailability of allicin varies depending on the form of garlic consumed. The findings revealed that even if alliinase is destroyed during cooking, cooked garlic still has a high bioavailability. It was also concluded that the body must have another ways to metabolise alliin.[252] When delivered intravenously, allicin was found to rapidly disappear from circulation after administration and converted to secondary metabolites, including *E*-ajoene, 2-ethenyl-4H-1, 3-dithiin, and DADS ,which can be found in blood, urine, and faeces.[247] Notably, water-soluble OSCs, such as SAC and SAMC, are found in aged garlic extract (AGE) and exhibit different pharmacokinetic characteristics to oil-soluble organosulfur compounds.[253] DADS, another allicin metabolite, was not detected in the urine but was briefly detected in the plasma. However, its metabolites, the most significant of which is allyl methyl sulfone, were detected in the urine, liver, and stomach.[254] In 2013, Wang et al. reported that the examination of volunteer's breath found allyl methyl sulfide (AMS), allyl methyl disulfide (AMDS), DAS, DADS, DATS, dimethyl sulfide (DMS), and acetone after ingesting 38 g of raw garlic.[255] Significantly, allicin, ajoene, diallyl disulfide, and 1, 2-vinyldiithin are all metabolised to allyl mercaptan in whole blood. SAMC, allicin, diallyl trisulfide, and ajoene all undergo rapid metabolism, whereas 1, 2-vinyldithin and diallyl disulfide take more time.[256] In one study, DATS was

detected in the stomach of rats up to 24 h after a single oral dosage, while rats treated with single intravenous dose of DATS (10 mg) were found to have a peak blood concentration of roughly 30 μM. Diallyl trisulfide is metabolized to allyl mercaptan, allyl methyl sulfide, allyl methyl sulfoxide, and allyl methyl sulfone, the latter of which is the most prevalent metabolite.[254]

3.7 Garlic OSCs Targeting Cancer Hallmarks

Garlic OSCs have been shown in laboratory experiments to target the hallmarks of cancer as shown in **Figure 3.6**.

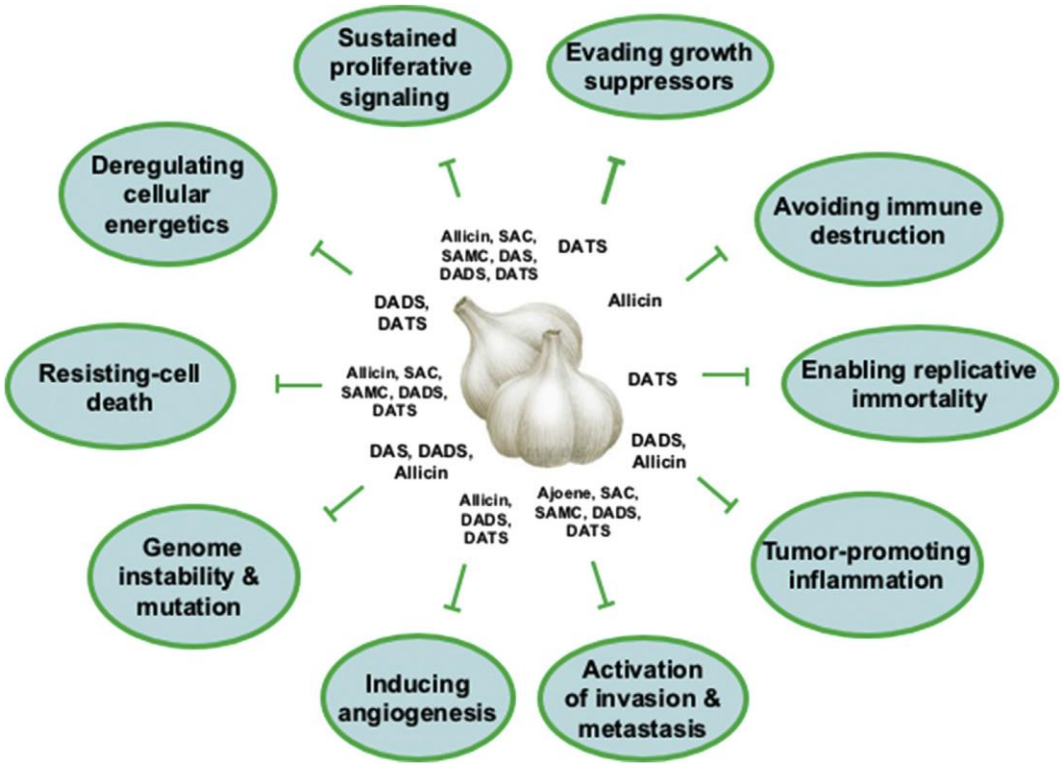

Figure 3.6: Overview of the anticancer potential of OSCs that target cancer hallmarks, taken directly from.[240]

Important aspects of garlic-derived OSCs anticancer activity is their ability to inhibit cell proliferation by causing cell cycle arrest in the G2/M phase.[257] For example Yagdi et al.[240] found that garlic OSCs caused cell-cycle arrest at the G2/M phase with changes to the microtubular network, modulation of Bcl-2 family, protein expression patterns, and changes to the redox status of the cells.[241] By activating the transforming growth factor (TGF)-β pathway, SAMC inhibited the proliferation of metastatic colon cancer cells and liver cancer HepG2 cells.[258] Similarly, DADS[259,260] and DATS[261] induced cell-cycle arrest in G2/M phase followed by apoptosis via caspase-3 cleavage and apoptotic DNA

fragmentation. In addition to altering the redox balance, the interaction of OSCs with thiol groups, such as cysteines and GSH, causes conformational changes in various protein families, including the OSC targets tubulin and Bcl-2 proteins. Because of their importance in cell proliferation and stress response, microtubules have become attractive targets in cancer therapy research.[262] For instance, DATS and DATTS have been shown to induce tubulin depolymerisation and tubulin polymerization inhibition[263] whereas DADS and DAS did not show any effect.[264] Importantly, the Bcl-2 family of proteins are an attractive target for the development of anti-cancer treatments since they participate in the mitochondrial apoptotic pathway. DATTS,[265] DATS[266] and DADS[267] reduced Bcl-2 protein expression in different cell lines leading to apoptosis in T24 bladder cancer cells. The pro-apoptotic function of garlic-derived OSCs has been identified in a variety of cancer cell lines and mitotic arrest in the G2/M phase is usually followed by apoptosis.

Many discoveries indicate kinase-dependent mechanisms precede and modulate OSC-mediated apoptosis as shown for allicin,[268] SAMC[269] and DATS.[270] For example, some studies have indicated that the production of ROS maybe important in the anticancer mechanism of garlic OSC via activating the JNK/p38 pathway, partially causing lung adenocarcinoma cells to undergo apoptosis.[271] In view of this, our research team at UCT/SU[272] reported that ajoene functions as a regulator of ER stress and the unfolded protein response (UPR). *S*-thiolation of ajoene disrupts protein folding, which causes an accumulation of misfolded proteins along with ER stress and UPR activation.[272] The underlying activities are thought to be based on thiol modification, which as a key determinant, presumably explaining regulation of the cellular targets outlined above.[240]

In conclusion, several studies have shown that OSCs derived from garlic have a wide range of anti-cancer effects due to their cytotoxic, anti-proliferative, cell cycle-regulatory, antioxidant, anti-inflammatory, anti-invasive, and antiangiogenic properties,[226] (**Figure 3.6**). The regulation of different signalling pathways and genes involved in invasion and metastasis may explain why garlic OSCs have these anti-tumour effects**.** The next section discusses the anti-cancer properties of DATS through an in-depth examination of its chemistry and biochemistry in cancer cells.

3.8 The Chemistry, Biosynthesis, and Biochemistry of DATS in Cancer Cells

Numerous studies are currently concentrating on understanding the mechanism of action of DATS's antitumor properties, which is summarised elegantly in the review by Puccinelli and Stan.[273] Proposed mechanisms include induction of apoptosis and cell-cycle arrest, the inhibition of metastasis and angiogenesis,[274,275] the migration and invasion,[276-278] the modulation of multi drug resistance (MDR),[279,280] the enhancement of cancer drug sensitivity,[281,282] the metabolism of carcinogens,[283-286] and the modification of proteins in different cell lines.[287] For instance, several investigations have shown that DATS can affect various cancer cell lines via apoptotic pathways as a result of regulating the intrinsic and extrinsic pathways in lung,[288,289] prostate,[290-293] gastric,[294] sarcoma[295-297] and bladder cancer cells.[270] DATS arrests cancer cells in the G2/M phase in prostate,[298,299] gastric,[300] colon,[301] liver,[302] bladder[303] and thyroid[304] cancer cell lines. As a whole, DATS possesses an attractive combination of sulfur content, electrophilicity, steric accessibility, and lipophilicity/cell membrane permeability, making it chemically reactive and bioavailable. These properties make DATS an attractive target compound for metastatic cancer which is more aggressive and may be located in distant areas.

Moving to DATS's derivatives, its dibenzyl counterpart DBTS, has also garnered attention for its promising anti-cancer and chemopreventive properties across various studies.[93,305] DBTS is a derivative of DATS that has been chemically synthesised[93] although it is also a natural product found in *Petiveria alliacea* L (Guinea hen weed, anamu).[306] It has been reported to have potent antiproliferative effects against triple-negative breast cancer, also effectively inhibiting their migration.[307] In other studies, DBTS has demonstrated efficacy across a range of cancer cell lines, including lung, pancreatic, breast, and prostate cancers, with nanomolar IC_{50} values in the range 340 - 840 nM.[308] Its mechanism involves activation of the MAP Kinases ERK 1 and ERK 2, which are known to influence various cellular processes associated with cancer. DBTS has also shown potent anticancer activity in murine models, as well as in leukemic cows.[309] In 2018, a proposed clinical trial (ClinicalTrials.gov Identifier: NCT04113096) carried out in the West Indies aimed to evaluate DBTS as a chemotherapeutic agent in Stage IV cancers of the breast, prostate, cervix, and colon. Following promising in *vitro* results, this randomized, placebo-controlled study administered DBTS capsules (20 mg daily for 6 months) to patients

across four experimental arms, each corresponding to a specific cancer type.[310] However, the specific results of the DBTS trial remain to be disclosed.

A study by Bhattacherjee et al. (2019),[93] examined the anti-proliferative activity of DBTS derivatives with *para*-benzyl substituents (methyl, fluoro, chloro, and bromo) as well as *ortho* or *meta* substituents (nitro, chloro, and bromo) on MCF7 cells. The cytotoxicity IC_{50} values were in the low micromolar range. Within the *para*-substituted trisulfides, the methyl derivative was the most active with an IC_{50} of 1.26 µM against MCF-7 cell lines, followed by the chloro derivative and fluoro derivatives 2.77 µM and 3.03 µM, respectively, while the bromo derivative showed a slightly reduced efficacy at 4.11 µM. It's noteworthy that the activity of the parent DBTS (sub = H) was not reported in this context. Similarly, *ortho* or *meta*-substituted trisulfides had similar activities. For example, the nitro, chloro, and bromo derivatives had IC_{50} values of 4.34, 3.75, and 3.87 µM, respectively. In addition, some derivatives demonstrated a sustained release of H_2S, indicating potential benefits for H_2S-mediated protective effects.[93]

In particular, the *para*-fluoro derivative of DBTS has been given the generic name Fluoropacin, **60** (**Figure 3.7**) and has shown promising results in a number of studies.[310] Fluorapacin significantly inhibits tumor growth by modification of β-tubulin at Cys 12 and suppression of microtubule dynamics.[311]

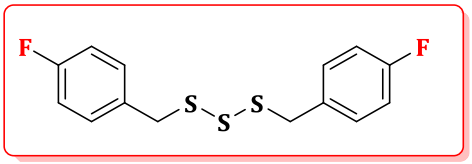

Figure 3.7: Chemical Structure of Fluorapacin, 60.[305,311]

In another a study, An et al.[118,310] investigated Fluorapacin's effects on human histiocytic lymphoma U937 cells, demonstrating that it disrupts the microtubule network by inducing tubulin depolymerization and preventing normal microtubule formation. This disruption leads to G2/M cell cycle arrest and apoptosis which is independent of reactive oxygen species (ROS) produced but rather involves the activation of c-Jun N-terminal kinase and proteolysis of the antiapoptotic protein Bcl-2. The kinetic response pattern of Fluorapacin was found to be similar to that of the cancer chemotherapeutic paclitaxel.[118] Animal model data for Fluorapacin has not emerged as yet.

Similarly, Fluorapacin has reached Phase 1 clinical trials for various advanced cancers, showing promising initial outcomes (score of 10.17).[310] A number of trials have been conducted in China by the organization ACEA. These include Phase 2 trial for Advanced Malignant Solid Neoplasm in 2022, as well as Phase 1 trials for Non-Small Cell Lung Cancer in 2013 and Advanced Cancer in 2009. Once again, Detailed outcomes for these trials are not provided by the publishers.

3.8.1 The (Bio)synthesis of DATS

DATS is not biosynthesised within the garlic plant, but is rather a chemical rearrangement of allicin, the latter produced enzymically when a garlic clove is crushed, as described in section **3.4**. The proposed steps of its biosynthesis form allicin,[312] are depicted in **Scheme 3.6** below:

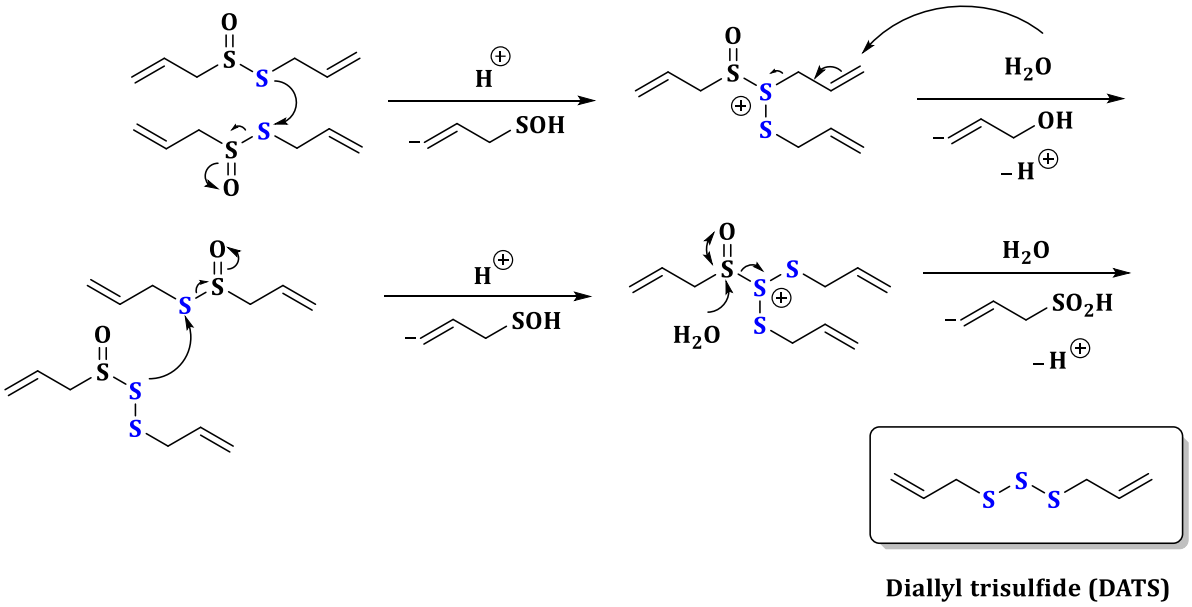

Scheme 3.6: Biosynthetic hypothesis for diallyl trisulfide.

Mechanistically, two allicin molecules are proposed to self-react to form a sulfonium ion through sulfenylation of the soft electrophilic thiosulfinate sulfenyl sulfur. Deallylation by water yields a homoelongated thiosulfinate that undergoes a further sulfenylation under acidic catalysis, resulting in the loss of allylsulfenic acid. Desulfinylation as the last step results in DATS as shown in **Scheme 3.6**. DATS may be considered as an oxidant, capable of converting two protein thiols to a mixed disulfide through a thiolation reaction (substitution of H of SH by R), which results in protein dysfunction and cell death.[313]

3.8.2 The *S*-Thiolation Reaction

According to a growing body of preclinical research,[273] once it has entered the cancer cell,[314] DATS undergoes S-S exchange (thiolysis) reactions with biological thiols such as glutathione,[315] cysteine,[316,317]or a cysteine residue on a protein.

The immediate product of this exchange is a mixed disulfide. Regioselectively, it has been shown that the first thiolysis step involves the biological thiol attacking the trisulfide terminal sulfur rather than the central one, an issue that will be covered in section **3.8.4**. As a result, this process has several consequences as depicted in **Scheme 3.7**.

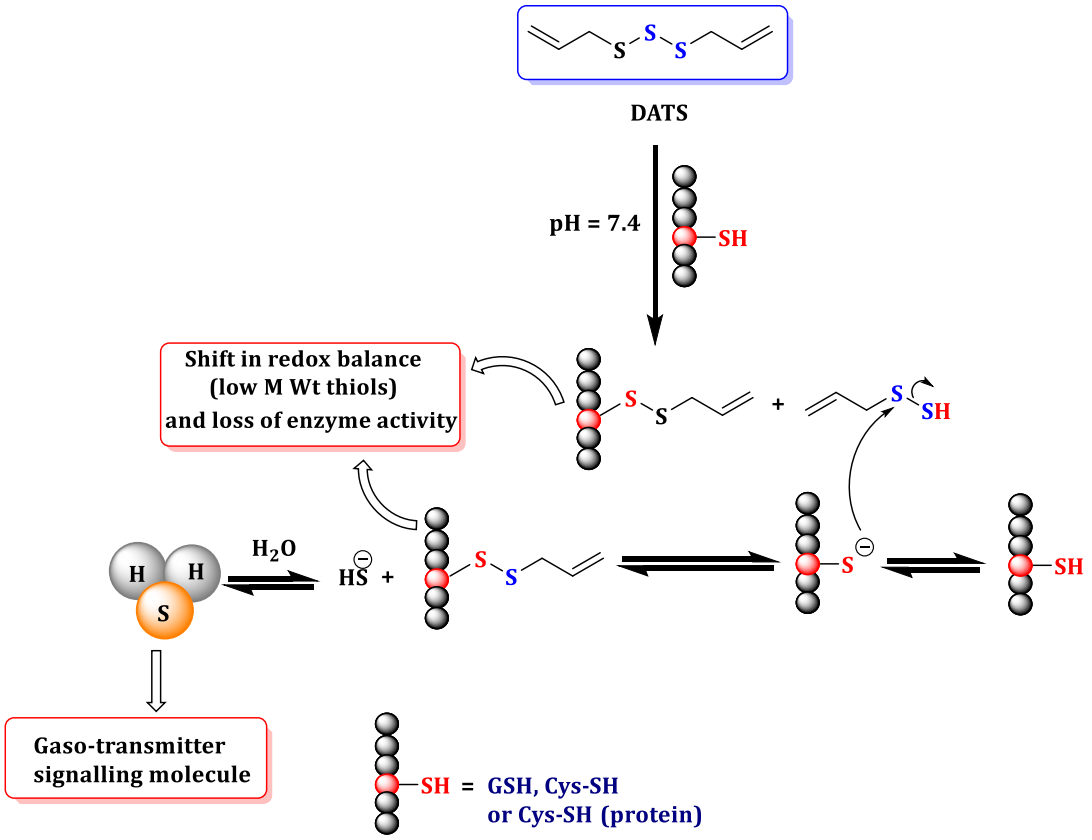

Scheme 3.7: Schematic overview of thiolysis exchange of DATS with protein thiol.

In the first step, DATS can generate *S*-allyl modified proteins by reacting with an exposed cysteine residue of a protein, which may alter protein function.[4] Because this results in a mixed disulfide (a substituted thiol) at the protein site, the process is known as thiolation (akin to a substitution of the thiol H by an SR group, which functionally constitutes an oxidation of that thiol).[239] Secondly, allylperthiol (ASSH) as a reactive perthiol (RSSH) is formed as the other thiolysis product, which can undergo further thiolysis to form another equivalent of disulfide and H_2S, the latter being an important cell signalling

molecule (details in section 3.9). In this second, crucial step, SH groups may be in their conjugate anionic form depending on their pK_a (RSH and RSSH) in which perthiols are more acidic (lower pK_a) than their thiol counterparts. The presence of both neutral and conjugate forms makes for a number of coupling possibilities. However, from a reactivity point of view, the faster reaction will be the one involving a protein thiolate (nucleophile) reacting with the perthiol (RSSH as electrophile) since this combination diminishes the $HOMO_{nuc}/LUMO_{elec}$ gap in the transition state. Hence, **Scheme 3.7** depicts it that way round (see **3.8.4.1** for more in-depth discussion on this intriguing aspect). This aspect implies that proteins with acidic cysteine residues (e.g., catalytically active ones) would be more prone towards *S*-thiolation by this pathway. The effects of mixed disulfide formation on a catalytically active cysteine could have a detrimental effect on cell function. Generation of the perthiol can also increase the production of toxic oxidants such as hydrogen peroxide and superoxide (details in **3.9.5**), with an increase in oxidative stress.[318] Simultaneously, cellular low molecular weight (LMW) thiol concentrations will decrease, making cells more vulnerable to oxidative stress. Wattenberg et al. were the first to describe the *S*-thioallylation properties of DATS in 1988. They showed that DATS reacts with the thiol group of cellular glutathione, leading to increased glutathione *S*-transferase (GST) activity in the stomach cancer tumours of mice.[319] Saturated analogues such as dipropyl trisulfide essentially had no inhibitory effect, highlighting the significance of the double bond of the allyl groups and implying that a structure-activity relationship likely exists for the R group of the trisulfide. More indication on this is that DATS, which has two allyl groups, is more active than allyl methyl trisulfide (AMT), which only has one.[319] No explanation for this intriguing selectivity has been forthcoming, but the pathway depicted in **Scheme 3.7** strongly points to an increase in *S*-electrophilicity when R = allyl. According to Pinto et al.,[320] the development of chemopreventative or therapeutic drugs that promote pro-apoptotic proteins or inactivate carcinogenic factors may well benefit from focusing on the *S*-cysteinylation of signalling proteins and transcription factors. DATS has been reported by Seki et al.[321] to directly oxidise cysteine residues on β-tubulin, resulting in microtubule network disruption during early mitosis. In a different investigation on DATS, Hosono et al. inhibition of cell proliferation and apoptosis in human colon cancer cells (HCT-15 and DLD-1) through the *S*-thioallylation of Cys-12β and Cys-354β in β-tubulin.[287,321] Similarly, the antitumor natural product trisulfide calicheamicin undergoes thiolation via reaction with GSH, producing a diradical species.

This diradical abstracts hydrogens from the deoxyribose backbone of DNA, causing DNA scission in the minor groove.[322] Together, these modifications can affect the growth of cancer cells by modifying the sulfhydryl groups of redox-sensitive signalling proteins and affecting the proliferation and apoptosis of cells. In conclusion, the chemistry of DATS in a biological environment can include several types of protein modification, H_2S release, perthiol synthesis and ROS production, all contributing to effective tumour growth suppression. In the next section, we will take a closer look at the factors that affect trisulfide *S*-thiolysis in context.

3.8.3 Factors in the Thiolysis Exchange

3.8.3.1 Thiol Nucleophilicity

As mentioned above, garlic OSCs act predominantly as oxidative thiolating agents capable of forming mixed disulfides with low molecular weight thiols such as cysteine[316,317] and glutathione.[315] Indeed, OSCs having electrophilic sulfur atoms such as allicin, ajoene and polysulfides (R_2S_n with n > 2) have been intensively studied for their *S*-thioallylation properties,[7,320,323,324] as illustrated in **Scheme 3.8** for allicin and DATS. Here, the nucleophilic cysteine residue is used in its thiolate form although the degree of ionization is obviously dependent on the biological thiol under consideration. Note here the regioselective nature of this process as already alluded to.

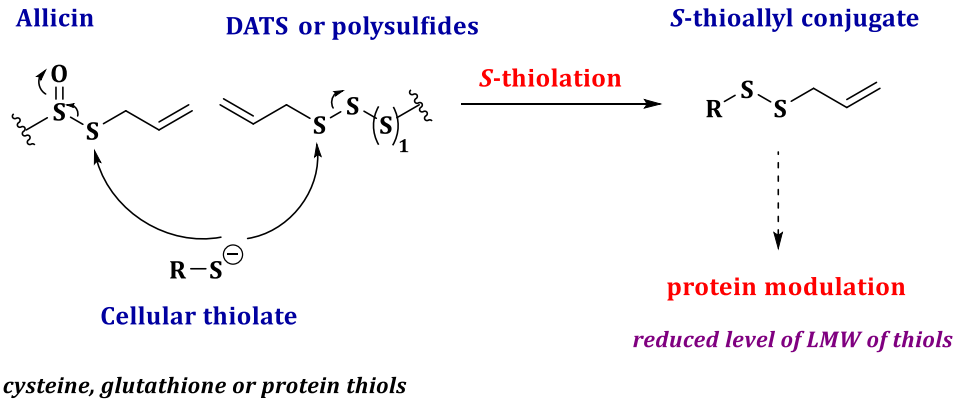

Scheme 3.8: Thiol-disulfide exchange reactions between DATS or allicin and cellular thiols to yield *S*-thioallyl conjugates.

Thiolysis exchange reactions (also referred to as thiol-disulfide exchanges) are bimolecular nucleophilic substitution processes. The kinetics of the thiol-disulfide exchange is an important determinant in cancer cell cytotoxicity and links to thiol pK_a which in turn determines the ratio of thiolate to thiol at any specific pH (7.0-7.4 for a

biological medium) in which the former is super nucleophile. The difference in nucleophilicities is so significant that in many cases, the reaction proceeds even when the thiolate is a very minor species in the equilibrium (i.e., at pH values below the thiol pK_a).[325] Using a homotrisulfide (RSSSR) (to simplify regioselectivity aspects) a thiolate nucleophile attacks a terminal sulfur atom (designated as SEN for non-sulfane electrophilic sulfur) to produce a linear, anionic tetrasulfide transition state. Ejection of a perthiolate leaving group then creates the disulfide product as shown in **Scheme 3.9**. Under conditions of excess thiol, H_2S is produced by proton-shuffle to convert the perthiolate anion RSS^- into its protonated form, which is followed by a second nucleophilic attack by the thiol anion to form hydrosulfide ion.[326-328]

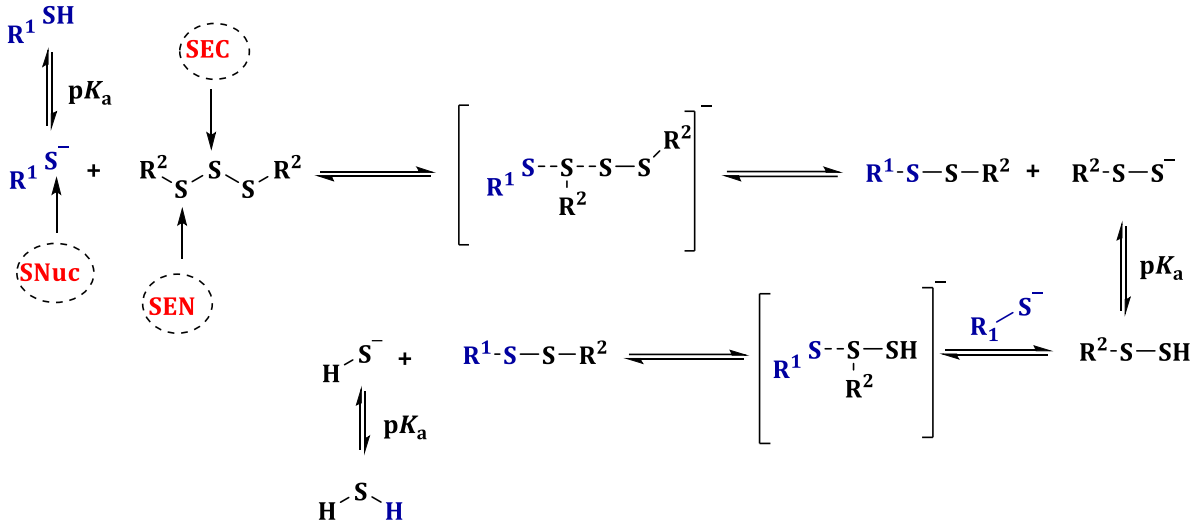

Scheme 3.9: Thiolysis sequence for DATS.

The kinetic and regioselectivity aspects of thiolysis are determined by trisulfide reactivity which in turn underpins the selectivity towards cellular thiol targets. There are three sulfur atom types involved in the exchange process as incoming nucleophilic sulfur (SNuc) from the cellular thiol, an electrophilic central sulfur (SEC), and two electrophilic non-sulfane terminal sulfurs (SEN), i.e., ones having carbon and sulfur connections rather than two sulfur connections (sulfane type), see **Scheme 3.9**. The SEN are equivalent in a homotrisulfide.

Two important aspects governing DATS thiolysis are the rate and regioselectivity. The rate is governed by two controlling factors namely thiolate concentration (versus thiol) and the thiolate nucleophilicity. A thiol RSH with R as an alkyl group is a weak acid (pK_a 9-10), but it is stronger than its alcohol counterpart ROH (pK_a 16-18) due to its bigger sulfur

atom. Cysteine, owing to the presence of electron-withdrawing groups adjacent to the thiol has a lower pK_a still of around 8.6, and in biological proteins, this can be lowered even further due to conjugate base stabilising effects through intermolecular interaction such as hydrogen bonding. Of importance here is the pH of the medium where the Henderson-Hasselbalch equation (**Scheme 3.10**) describes the relative concentrations of ionized and unionized species. The equation tells us that when the pH of the medium (7.0-7.4 in cells) equals the pK_a of the thiol, an equal concentration of thiolate to thiol will persist. However, once the pK_a of the cells drops below that pH, the thiolate concentration rises exponentially (log-dependent).

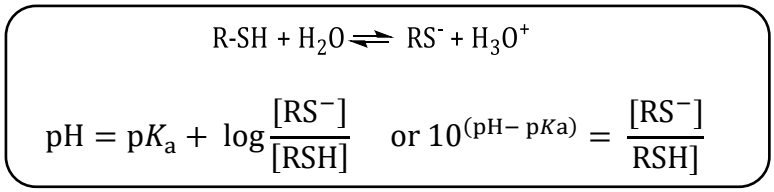

Scheme 3.10: Henderson-Hasselbalch equation relating thiolate concentration to thiol pK_a at constant pH.

For instance, Cys-SH and GSH deprotonations correlate to the second and third pK_as of Cys-SH and GSH, respectively. According to their pK_a values, 10.5 % of Cys-SH (pK_a = 8.33) and 5.2 % of GSH (pK_a = 8.66) will exist in their thiolate forms at physiological pH of 7.4.[328] Once the pK_a drops below 7, the thiolate concentration dominate over that of the thiol, indicating a considerable increase in the system's nucleophilicity and a significant increase in the rate of thiolysis exchange (relative to that due to the corresponding thiol). However, thiolate concentration isn't the only parameter, as then reactivity should rise exponentially with a lowering of thiol pK_a.

The second parameter is thiolate nucleophilicity, which can be understood through Frontier Molecular Orbital theory. Nucleophilicity, a kinetic term in organic chemistry, indicates reaction rates. Thiolates are more nucleophilic than alkoxides with soft carbon electrophiles, resulting in higher reaction rates. Within a chemotype like thiolate, nucleophilicity varies based on stability, influenced by the pK_a of the conjugate acid. According to HSAB theory, thiolates are soft nucleophiles with high-lying HOMOs that overlap well with low-lying LUMOs, such as C-Br/I bonds. The Klopman-Salem equation explains that this overlap lowers activation energy, speeding up the reaction.

However, as the HOMO energy drops, (which is the case when lowering the thiol pK_a, resulting in a more acidic thiol with a more stable conjugate base), the thiolate nucleophilicity reduces. Whiteside appreciated the oppositional nature of these two factors (thiolate concentration increasing with lowering of pK_a; nucleophilicity dropping with reducing the pK_a) in the late 1970s[329] and through experimentation established that the thiolysis rate (of a disulfide) with a thiol as the nucleophile follows a Bell-curve relationship.[325] Importantly, the apex of the curve was at a thiol pK_a of 7, which reflects the quite drastic reduction in thiolate nucleophilicity due to its stability increasing with a lowering of pK_a, Whiteside's findings[175] illustrated in **Figure 3.8**. Logically, one can anticipate a similar profile for trisulfide thiolysis with a range of protein-SH groups with varying pK_as.

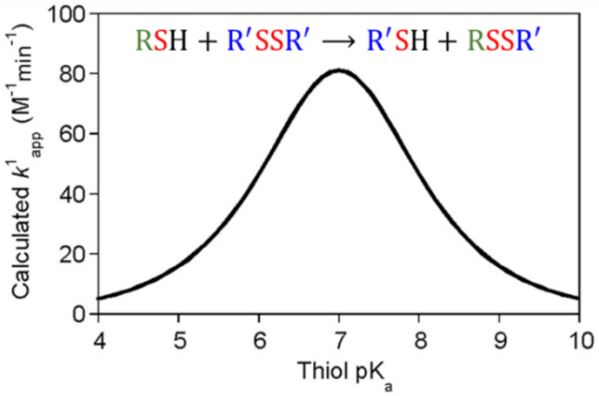

Figure 3.8: Rate constant calculated as a function of thiol pK_a for the thiol-GSSG exchange reaction at pH 7.[325,330]

The reaction is reversible (although only indicated as one-way in **Scheme 3.9**). Certainly, the back reaction will be slowed if the R'SH has a pK_a further away from 7 compared to that of the RSH. However, the position of equilibrium will depend on the normal DG thermodynamic difference in which the stability of the various species will need to be considered. Overall, the pK_as of the two thiols feature prominently since this influence both nucleophilicity (kinetic) and the leaving ability (both kinetic and thermodynamic for the equilibrium).

In summary, the pK_a of a biological thiol needs to have a pK_a of around 7 for a fast thiolysis exchange. Cysteine residues in proteins can vary significantly, depending on their environment suggesting a likely selectivity in favour of residues with pK_as at around 7.

3.8.3.2 Trisulfide Electrophilicity

Another important parameter in the thiolysis rate is the electrophilicity of the sulfur being substituted. Trisulfide electrophilicity (as with thiol nucleophilicity) is a kinetic parameter that links to sulfur regioselectivity. The regioselectivity issue dates back to the studies by Hiskey and Carroll in 1961[331] in which they carried out the first investigations into the nucleophilic cleavage of mixed disulfides RSSR'. They concluded that the regioselectivity was determined by the better leaving group, which in turn involved the thiol with the lower pK_a (more stable conjugate base). We also observed this effect in cancer cells (Smith et al 2016). More recently, Nagy[325] in 2013 and Cuevasanta *et al*.[332] in 2015, extrapolated Hiskey and Carroll's concept to the nucleophilic attack on RSSSR, concluding that substitution would be favoured at the SEN (terminal) sites because of the greater stability of the perthiolate over the thiolate (from substitution at SEC), in turn based on the lower pK_a of the perthiol compared to that of the thiol. Therefore, exchange on the trisulfide is favoured on the terminal sulfur because of an enhanced electrophilicity compared to the central sulfur.[326,328] Even in a thermodynamic and reversible scenario, this would still be expected to hold on thermodynamic grounds (RSS^- more stable than RS^-). In 2017, Cai et al. tackled the theoretical questions around polysulfide thiolysis by way of a computational calculation involving density functional theory on DATS reacting with cysteine (Cys-SH) and glutathione (GSH) in their anionic forms.[328] They reported three possibilities (**a-c** in **Scheme 3.11**). Firstly, the sulfur atoms of DATS (pathways **b** and **c**) were found to be substantially more electrophilic towards nucleophilic attack by the thiolate anions than the α-carbon of the allyl groups (pathway **a**). The study also established that nucleophilic attack of the thiolate anions on the terminal sulfurs (SEN) of DATS (pathway **c**) is more favourable both kinetically and thermodynamically than on the central sulfur atom (SEC), resulting in the production of allylperthiol anion ($AllylSS^-$ or ASS^-) rather than allylthiolate ion ($AllylS^-$ or AS^-). The three possibilities are depicted in **Scheme 3.11**.[328]

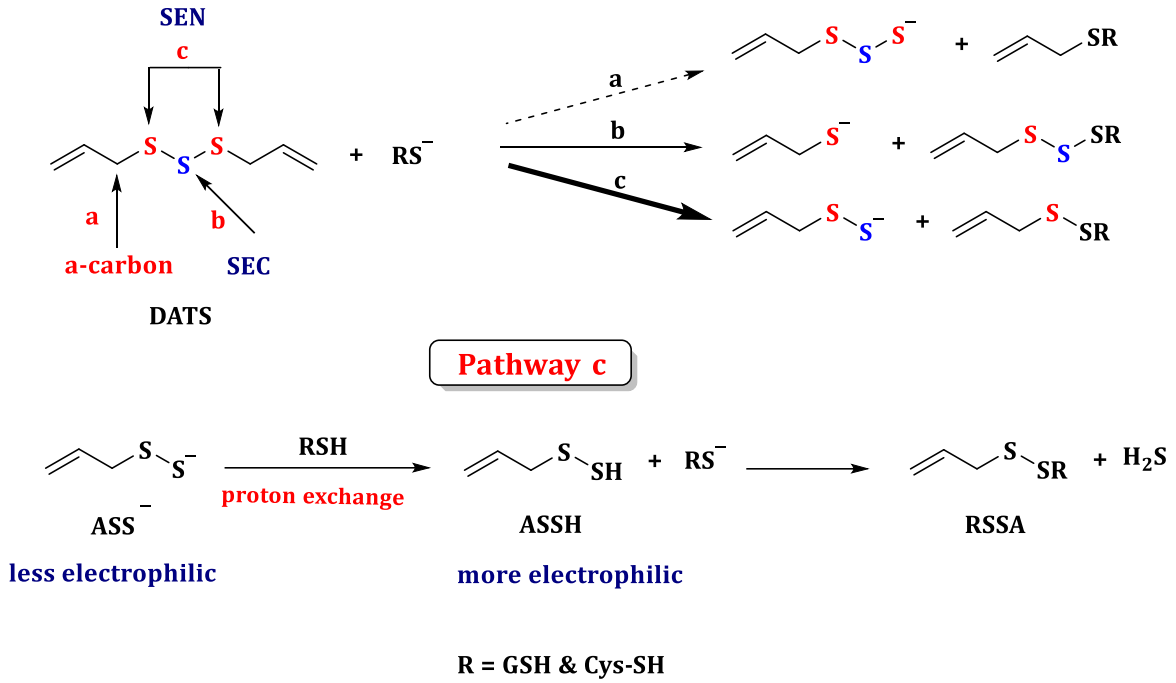

Scheme 3.11: Pathways proposed for the reactions of DATS with a thiol.[328] ***The dashed, solid, and bold arrows indicate the order of likeliness, from the least to the most likely, respectively.***

Thus, following pathway **c**, exchange is favoured to furnish ASS^- and the cysteine mixed allyl disulfide (RSSA). Thereafter, ASS^- first undergoes proton exchange with excess Cys-SH or GSH to afford ASSH, which is then in a more suitable electrophilic form for the second thiolysis with the biological thiol (now in its more nucleophilic thiolate form) to form H_2S. **Figure 3.9** shows the potential energy surfaces (PESs) of the reactions for DATS (pathways **a-c**) proceeding via pre-reaction complexes to products. The profile clearly identifies pathway **c** as having the lowest activation energy as predicted (attack at SEN) even though the lowest DG (highest numerical value as a negative) is from a pathway attacking carbon (pathway **a**).

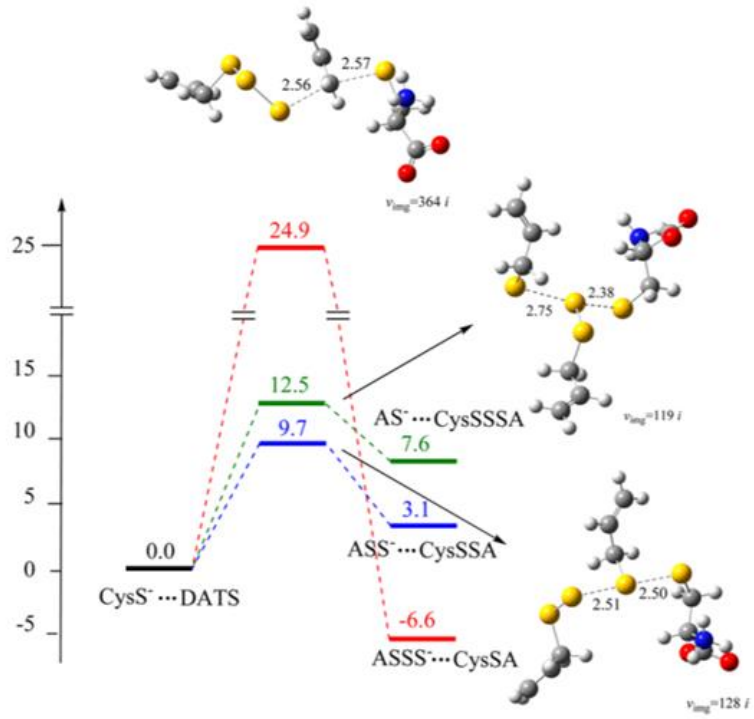

Figure 3.9: Energy profiles for the thiolysis reactions of DATS with Cys-SH. Taken from Cai et al. [328]

This theoretical finding is interesting in that it supports the findings of Huang et al. published in *Org. Lett*. in 2015 (two years before the theoretical study).[333] They reported experimentally that GSH's nucleophilic attack on DATS's allylic sulfur (here designated as SEN) generated GSSA and ASSH followed by H_2S release, making it a rapid H_2S donor. On the other hand, diallyl disulfide (DADS), as a poor perthiol source (via attack at DADS's allyl carbon), was evaluated as an extremely poor H_2S donor.

3.8.3.3 Perthiol Electrophilicity

Thiolysis exchange between SEN of DATS and a biological thiolate is only the first step in the process. In the second step, H_2S is the end product. The energy profiles of the release of H_2S by the reaction of ASSH/ASS$^-$ with Cys-SH was also explored by Cai et al. as shown in **Figure 3.10**.

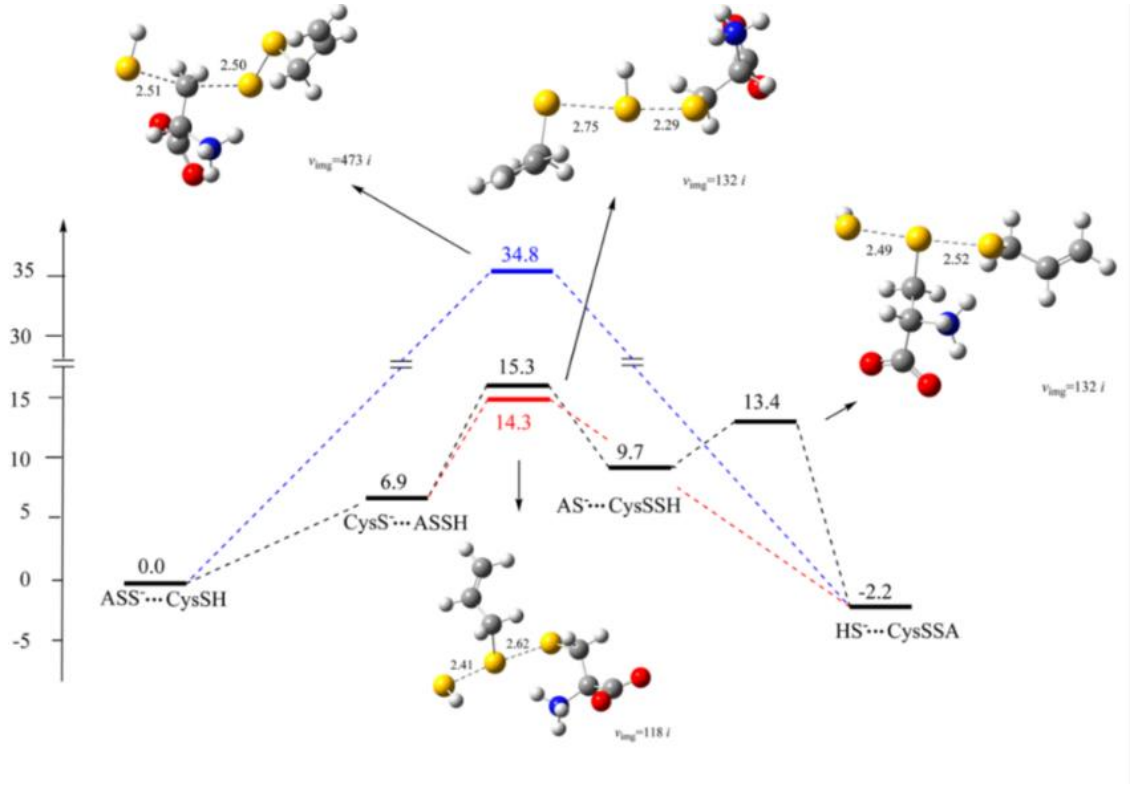

Figure 3.10: Energy profiles for the reactions of AllylSS$^-$ with Cys-SH.[328]

The profile reveals the preference for proton exchange between ASS$^-$and CysSH (encouraged by relative stoichiometry) over the attack of ASS$^-$ directly on the cysteine methylene carbon (SH bearing) to generate HS$^-$ that way (**Figure 3.10**, in blue). Once the exchange has taken place, regioselective preference of CysS$^-$ for the non-perthiol sulfur of ASSH (the sulfur attached to the carbon of the allyl group) gives HS$^-$ and cysteine allyl disulfide (TS is 14.3 kcal/mol on Photoelectron spectroscopy, **Figure 3.10**, in red) over attack at the perthiol sulfur (terminal sulfur) as a perthiol exchange (15.3 kcal/mol, **Figure 3.10,** in black). Overall, and according to these findings, biological thiols Cys-SH and GSH are able to liberate H_2S/HS$^-$ out of the central sulfur of DATS.[328] Several studies have compared the relative potency of Cys-SH and GSH for releasing H_2S from DATS. For instance, Benavides et al. demonstrated that GSH is more efficient in releasing H_2S from DATS than Cys-SH at a physiological pH.[334] According to the computational study above, the calculations predicted GSH to be more potent at liberating the perthiol anion ASS$^-$ in step 1, with Cys-SH better at liberating HS$^-$ from ASS$^-$ in step 2. The mechanism emerging from this work also implies that the rate of H_2S release is pH sensitive.[328] By comparison, DATTS (diallyl tetrasulfide) is significantly more complex because it has two potential electrophilic attack sites,[239] one at each of the two terminal S–S-bonds and the other at

the central S–S bond. Attack by a biological thiolate on the central bond resulting in the production of a trisulfide (RSSSR) and a perthiolate (RSS^-) appears to be favoured according to Munday et al.[245] In contrast to this, the production of a disulfide (RSSR) and a trisulfide anion ($RSSS^-$) from attack at the terminal sulfur should not be fully discounted at this stage. In fact, the formation of $RSSS^-$ would allow a new more complicated set of chemical reactions, such as S_2 and reductive S_2^{-2} release.[68] In addition to the aforementioned exchanges, the cytotoxicity of a trisulfide links to the chemistry of the perthiol produced, which, in turn, may link to protein S-thiolation or ROS generation. These aspects will be discussed in the next section.

3.8.4 The Chemistry of Perthiols

A perthiol (also known as a hydropersulfide), like a thiol, is able to participate in a wide range of chemical reactions, including redox reactions, radical processes, catalysis, and metal binding.[239,335] In the context of cancer biology, several studies have investigated the effect of the perthiol on ROS production and H_2S release.[245,336] However, the exact mechanism by which a perthiol attenuates ROS levels is still not fully understood and likely involves complex interactions with various cellular components. Because this thesis concerns the central role of perthiol stability in the cytotoxicity of organotrisulfides, some of the important chemistry aspects of perthiols will be reviewed in the next section.

3.8.4.1 Chemical Aspects of RSSH

A perthiol is more acidic than its corresponding thiol and its SH group is softer and hence more nucleophilic than the corresponding thiol sulfhydryl group. It also possesses an electrophilic feature (at the S bonded to the R of RSSH) that thiols lack.[337] In 1987, John L. Wood stated that a perthiol behaves like a sulfane sulfur compound with a sulfur atom bonded to an ionizable hydrogen.[338] The bifunctional chemistry of perthiols is summarised in **Scheme 3.12**.

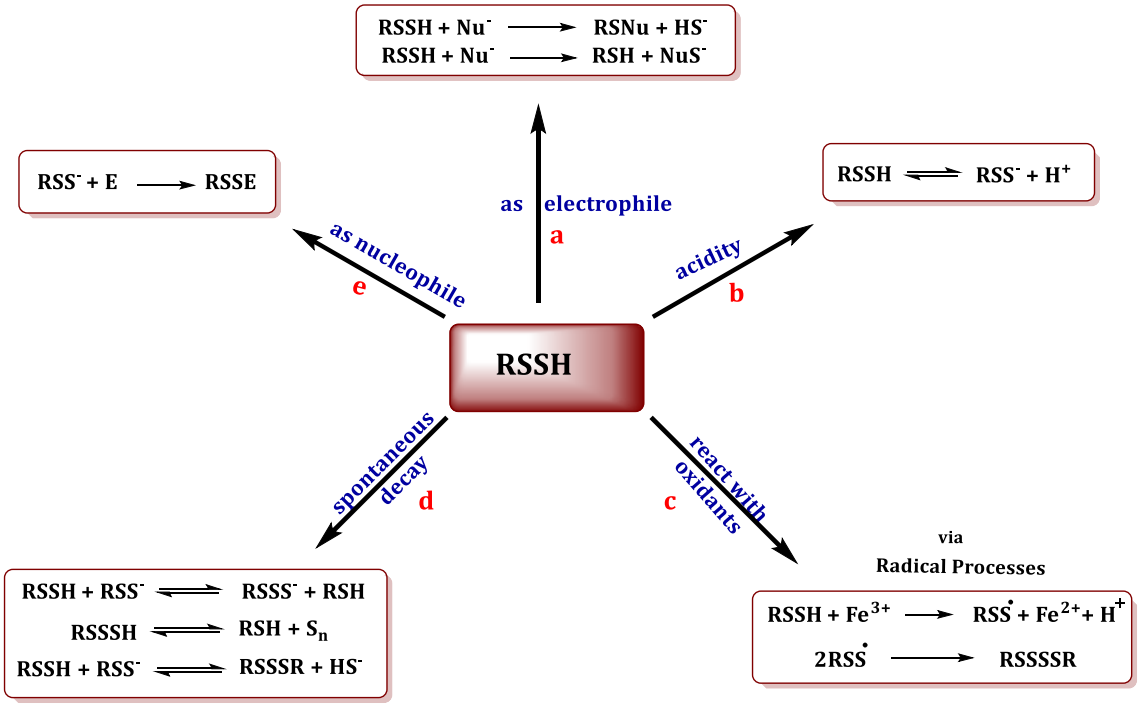

Scheme 3.12: An overview of perthiol chemical reactivity.

In the processes outlined in **Scheme 3.13**, perthiols are significantly more acidic than their corresponding thiols, with a reduction in pK_a of 1–4 units, equation **b** (e.g., pK_a of GSH is 8.94, while GSSH is 5.45).[339] This increased acidity is also observed in specific cases, such as allylmercaptan (pK_a~9.9) compared to allylperthiol (pK_a~8.5).[340] The sulfane sulfur of a perthiol has a softer nucleophilically than the sulfur of a thiol due to a hyperconjugative a-effect in which an adjacent sulfur lone pair raises the SH (or perthiolate) HOMO energy (equation **e**). Electrophilically, unhindered perthiols prefer attack at the inner sulfur as described in Michael Pluths lab, to generate H_2S as shown in equation **a**. However, steric hindrance in the R group of RSSH is a significant factor that can direct nucleophilic attack towards the outer sulfur in a transpersulfidation as a perthiol exchange.[341] In their work, they utilized a combination of computational and experimental methods to demonstrate that the presence of electron-withdrawing groups on aryl perthiols increases the kinetic and thermodynamic preference for transpersulfidation. This shift in reactivity is attributed to the stabilization of the transition state for transpersulfidation, which is favored in sterically hindered environments.[341]

Perthiols are modestly stable in aqueous solution while perthiolates are highly unstable, making them challenging as research tools.[152] This is due to their nucleophilic and

electrophilic natures, which allow interactions between them, resulting in disproportionation as depicted in equation **d**. Acting as electrophiles, different compounds can be generated depending on which sulfur is attacked. The attack of the perthiolate on the outer sulfur of the perthiol, following proton exchange, produces a thiol and hydrotrisulfide anion $RSSS^-$, the latter degrading to elemental sulfur and thiolate anion. Conversely, attack on the inner sulfur produces a trisulfide (this can go on to produce polysulfides) and H_2S after protonation.[342,343] A perthiol is also an efficient one-electron reductant[344] with generally a much stronger reducing ability than the corresponding thiol, resulting in rapid cellular SET processes. For instance, perthiolate can easily reduce ferric ion, manifesting as a yellow/orange to green colour change, see equation **c**. According to Fukuto et al.,[345] glutathione perthiol (GSSH) has a significantly greater capacity to reduce ferric-cytochrome C compared to H_2S and GSH. Despite recent research efforts to unravel many chemical aspects of perthiols, their understanding remains vague, and an improved understanding would facilitate the unravelling of the interplay between ROS, perthiols, and H_2S.

3.8.4.2 The Production of ROS from RSSH

Reactive oxygen species, abbreviated in the literature as ROS, are chemically reactive molecules that contain oxygen and are produced naturally within cells during cellular metabolism. Examples of ROS include superoxide anion (O^{2-}), hydrogen peroxide (H_2O_2), and hydroxyl and hydroperoxide radicals ($HO^\bullet$ and $HOO^\bullet$ respectively). Sulfur-containing compounds derived from garlic, such as DATS, have been shown to produce ROS and influence redox-mediated signalling pathways involved in the cell cycle, DNA repair, and cell death.[346,347] Although there is no comprehensive mechanism explaining all facets by which DATS produces ROS, Saidu *et al*.[192] in 2012 proposed a pathway depicted in **Scheme 3.13** in which superoxide (an anion radical = $O_2^{\bullet-}$) is produced in two ways.

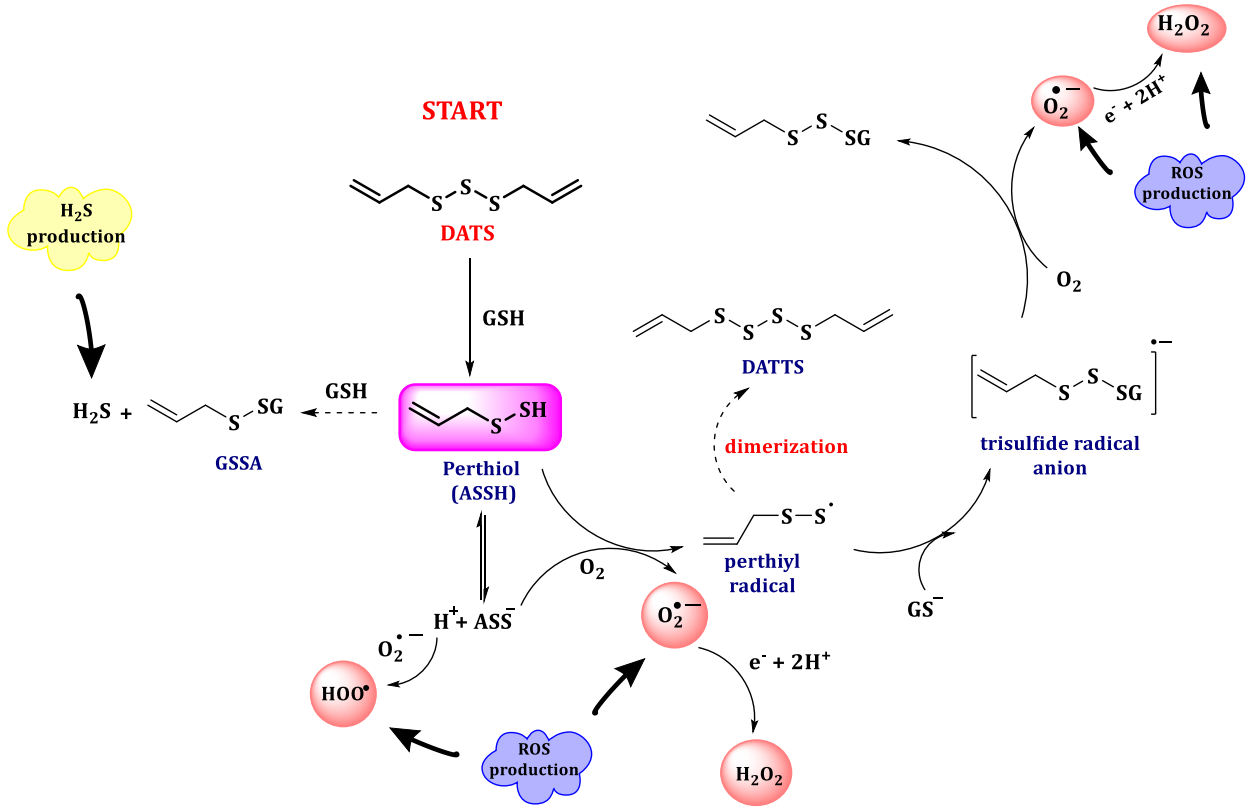

Scheme 3.13: Schematic overview of redox chemistry of DATS.

Thus, in the presence of GSH, DATS exchanges to a perthiol, which dissociates to its perthiolate anion. The latter can readily donate an electron to dioxygen (a diradical) to form superoxide ion and a perthiyl radical, the former going on to produce hydrogen peroxide radical via protonation or hydrogen peroxide via further reduction. The perthiyl radical, on the other hand, can also generate superoxide anion by first reacting with GSH in its anionic form to produce a trisulfide radical anion. The high redox potential of such a species enables the direct reduction of molecular oxygen again to produce a second source of superoxide anion, which can proceed to other ROS species as before.[347-349] Alternatively, the perthiyl radical may dimerizes to produce a tetrasulfide.[347] It is important to note that ROS production from perthiols competes with H_2S production, and the balance between the two pathways is a critical factor in the regulation of cellular redox balance, with significant implications for cellular signalling and homeostasis.[335] The relative rates of perthiol-mediated ROS and H_2S production in the cellular environment is complex and varies according to the specific conditions and the cellular context. The next subsection will explore the chemical relationship between perthiol and ROS, identifying the implications of this relationship.

3.8.4.3 The RSSH and ROS Biochemical Relationship

Compared to thiols and H_2S, perthiols (via their conjugate base) exhibit superior one-electron reducing capability, in which they react with ROS to form a variety of products that influence biological function.[350] In the study conducted by Gates *et al*., it was observed that under physiologically relevant conditions, ROS were produced due to the quick autooxidation of benzylperthiol (BnSSH). In this experiment, BnSSH and BnSH as incubated with supercoiled double-stranded plasmid DNA single-strand breaks occurred with BnSSH treatment but no with BnSH treatment under the same conditions. These results suggest that BnSSH may be a potential source of oxidative stress and DNA damage in biological systems.[351] Another study reported under certain conditions, that glutathione perthiol rapidly reacted with H_2O_2 to produce perthiosulfenic acid (RSSOH).[352] In 2022, P. Toscano *et al.,*[353] suggested that RSSH scavenges ROS or activates endogenous antioxidant pathways, rendering it as an anti-oxidant with cytoprotective character.

Although our study does not directly measure or examine the role of reactive oxygen species (ROS), it is important to recognize that their production and correlation with perthiols could provide significant insights. The interplay between perthiols and ROS, as suggested in various studies, impacts oxidative stress and cellular signaling pathways. In conclusion, it is evident that the cytotoxicity of DATS cannot be solely attributed to perthiols and ROS, which is where H_2S and its complex biochemistry comes into the play. This will be discussed in the subsequent section.

3.8.5 The Importance of H_2S

H_2S biochemistry is essential and important in the evolution of life, H_2S having emerged as the third gaseous neurotransmitter along with carbon monoxide (CO) and nitric oxide (NO).[354] It is now recognized that H_2S, whether endogenously or exogenously produced, performs numerous functions in both physiological and pathophysiological processes[355,356] in which the importance of its sulfur-containing products has lately been recognized in several reviews.[273,337,355-357] In the following section, we will summarize the biologically relevant chemistry of H_2S as well as its biosynthesis.

3.8.5.1 Chemical Aspects and Background

Hydrogen sulfide (H_2S), initially discovered in 1777 by Carl Wilhelm Scheele, has long been considered a poisonous air pollutant with an unwanted rotten-egg odour.[358,359] H_2S

is a toxic gas, and the human nose is regarded as one of the most sensitive H_2S sensors. Owing to the acidic character of its aqueous solutions, H_2S was previously known as hydrosulfuric acid or sulfhydric acid; however, dihydrogen sulfide and dihydrogen sulfane are currently the names approved by IUPAC for H_2S.[356] The word "H_2S" refers to the gas as well as the mixture of H_2S and HS^- (also known as bisulfide) in aqueous solution at a specific pH. H_2S is a covalent hydride, and its structure is similar to that of water but with lower bond angles (93° versus 104°). The H_2S molecular orbitals comprise a linear combination of the 1s orbitals of the two hydrogen atoms and the 3s and 3p orbitals of the sulfur atom.[360] The HOMO orbital of HS^- is higher in energy than that of H_2S, revealing that HS^- is more nucleophilic and basic than H_2S, which is in line with their known reactivities. H_2S has a modest water solubility at 25 °C,[356] and its solvation is dominated by dispersive forces with no hydrogen bonding to water molecules in which it behaves more like a hydrophobic solute surrounded by hydrogen-bonded water molecules.[361] **Scheme 3.14** displays the chemical reactivity and other chemical characteristics of H_2S.

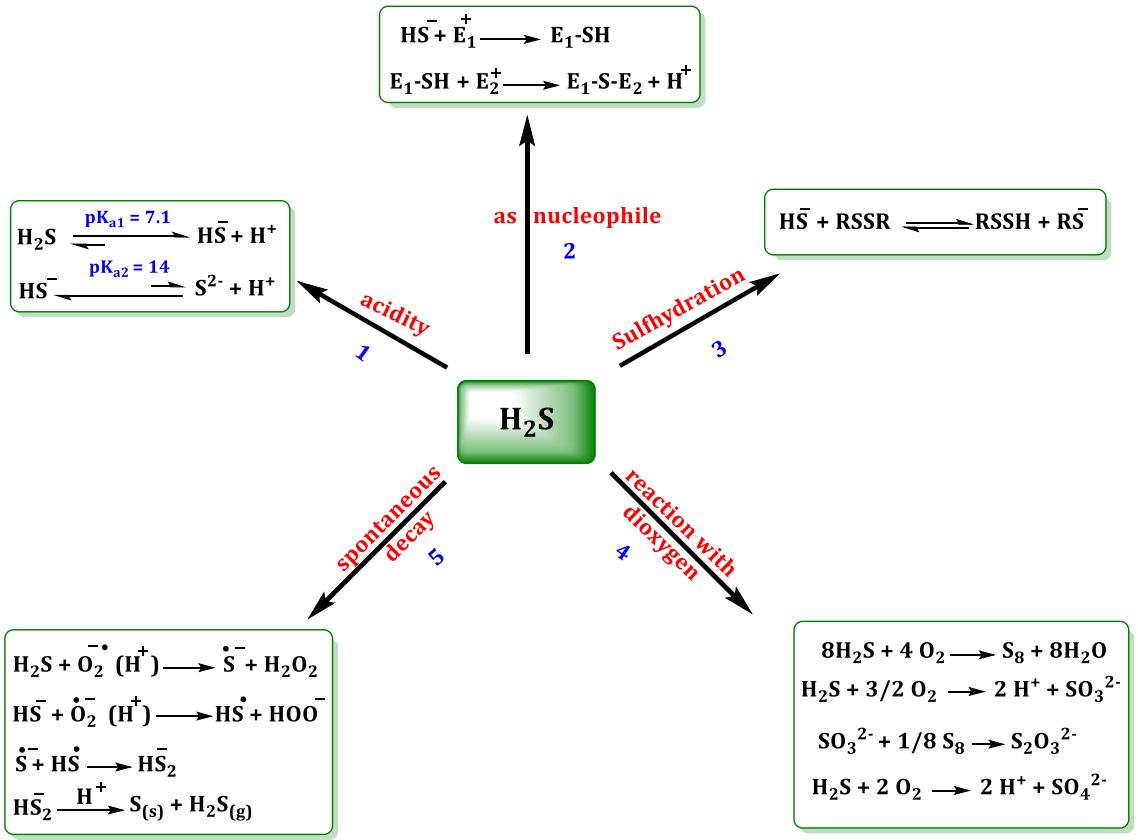

Scheme 3.14: An overview of chemical reactivity of H_2S.

H_2S is a weak diprotic acid with first and second pK_as of 7.1 and 14.[362] The fully deprotonated form as sulfide, S^{2-}, constitutes a miniscule component at physiological pH

because of the high second pK_a.[363] Under physiological conditions (pH = 7.4), HS^- and H_2S are in rapid equilibrium, with proportions of 81 and 19%, respectively (see equation **1**, **Scheme 3.14**).[364] A general reaction of HS^- with an electrophile (E_1^+ could be E_1-Lg) is shown in equation **2** in which the homosulfide is formed via two substitutions and as such acts as a surrogate for a thiolate ion.[356] Another example of nucleophilicity in context to this thesis is that HS^- can react reversibly with disulfides (RSSR) to produce a perthiol and a thiolate ion (equation **3**), which then undergoes a proton exchange due to the greater acidity of the perthiol over that of the thiol.[365] This reaction has been termed sulfhydration, which has been postulated as a unique post-translational modification capable of transducing H_2S effects.[366] Similarly, the oxidation of H_2S (HS^- and S^{2-}) by O_2 has a complex stoichiometry, producing a variety of products and metastable intermediates. Hence, oxidised polysulfide ions $S_2O_3^{2-}$, SO_3^{2-}, $S_2O_6^{2-}$ and SO_4^{2-} as well as S_8 as products involving all of sulfur's oxidation states can be generated,[367,368] see equation **4**. On the other hand, H_2S is known to decay in the atmosphere via single-electron oxidation processes to form HS_2^- (= H_2S_2 in an acidic medium) via combination of intermediate $HS^{\bullet}/S^{\bullet-}$ radicals, which in turn decomposes to generate S_n and H_2S in a self-regenerative process.[369]

However, recent research presents compelling evidence suggesting that the sulfide dianion (S^{2-}) is essentially absent in aqueous solutions.[370] This conclusion is supported by a range of spectroscopic techniques and reactivity analyses that challenge the conventional understanding of the sulfide species in water. The study indicates that under various conditions, particularly high concentrations of hydroxide ion, the formation of S^{2-} is not supported by empirical data. Instead, these findings propose that aqueous chemistry should pivot away from the assumption that S^{2-} exists, which has significant implications for the interpretation of sulfide equilibria and their broader applications in both environmental and industrial contexts.

In summary, there are still several remaining questions at the molecular level regarding how H_2S, HS^-, and S^{2-} might display a distinct chemistry and biology when surrounded by a pool of other thiols, some of which may be even more reactive (such as perthiols). The production of endogenous and exogenous H_2S within living organisms will be covered in the following sections, starting with endogenous.

3.8.5.2 Endogenous Production of H_2S

H_2S is synthesised endogenously either via a cellular enzymatic pathway, a non-enzymatic synthesis or via microbiome production.[371] In vivo, generation of H_2S via the enzymatic pathway involves the catabolism of cysteine enzymically by Cystathionine-γ-lyase (CSE), Cystathionine-β-synthase (CBS) and 3-Mercaptopyruvate sulfurtransferase (3-MST), which all utilise the reverse trans-sulfuration mechanistic pathway. 3-MST is predominantly found in the mitochondria and cytoplasm,[372] whereas CBS and CSE are only found only in the cytoplasm.[373] The usual cellular function of CBS is to catalyse the condensation of homocysteine with serine to produce cystathionine[374] as depicted in **Scheme 3.15**. Thereafter, the enzyme CSE catalyses the transformation of cystathionine into cysteine.[374] This is an important step in the biosynthesis of L-cysteine, which can then be employed as an H_2S-producing substrate. CSE can also catalyse L-cysteine to produce H_2S, with the by-products of pyruvate and ammonia. Alternatively, CBS converts cysteine into serine with H_2S generation. Cysteine aminotransferase (CAT) is another enzyme that produces H_2S by converting cysteine oxidatively to mercaptopyruvate, which is then transformed into H_2S and pyruvate by 3-MST.[375] These enzymatic conversions are summarised in **Scheme 3.15**.

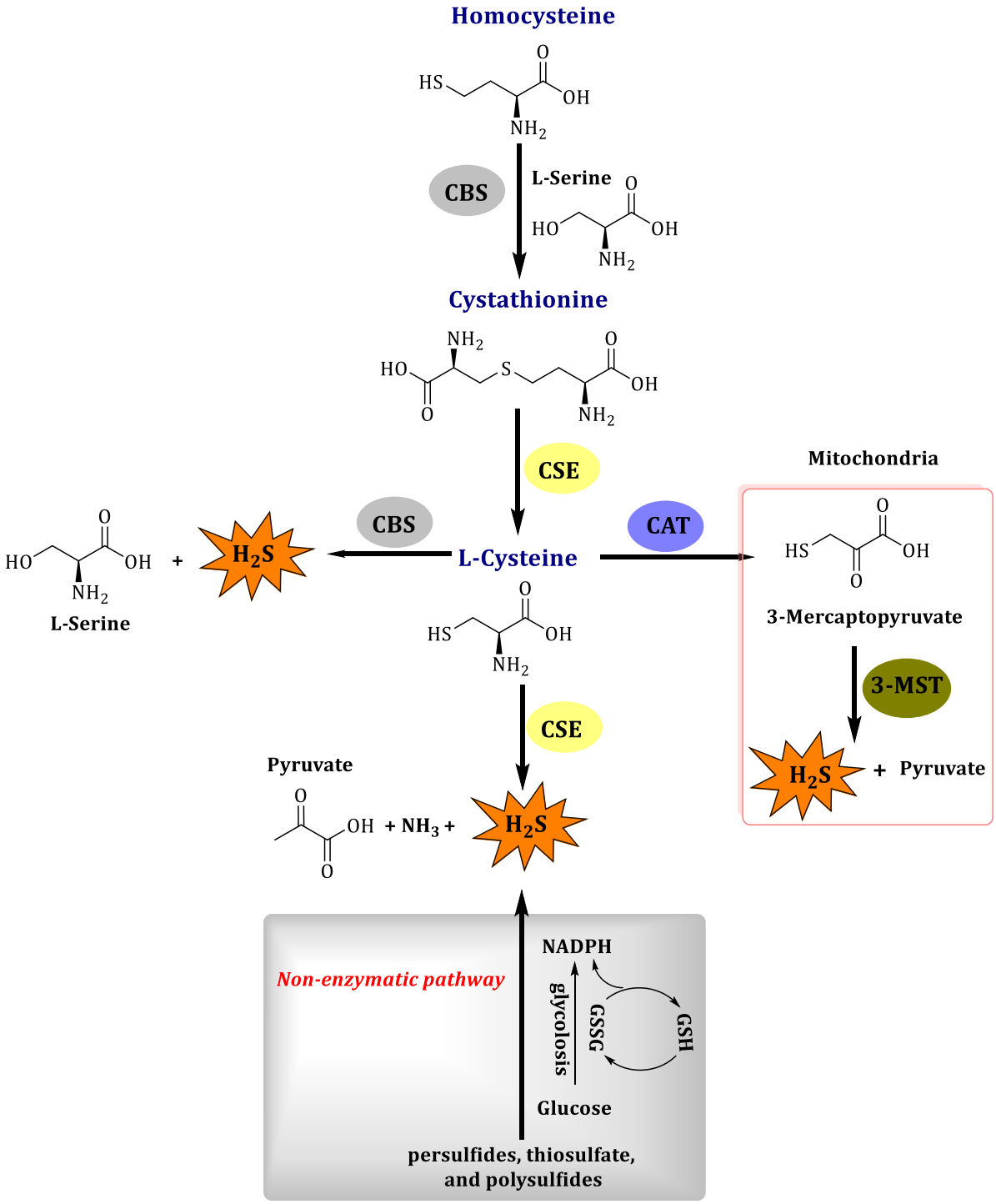

Scheme 3.15: A diagram displaying the enzymatic and non-enzymatic biosynthesis of endogenous H_2S in mammals.[355,376]

The second mode of endogenous H_2S production is via a non-enzymatic biosynthesis pathway and is also depicted in **Scheme 3.15**. Here, thiosulfate, persulfides, and polysulfides can be reduced to H_2S in the presence of reducing agents such as NADPH and NADH, which are provided from phosphogluconate and glucose oxidation in glycolysis.[376] The gut microbiota is another source of H_2S,[377] which contributes considerably to H_2S

homeostasis not only in the intestine but also in the plasma, tissues and organs.[378] The mammalian microbiome controls systemic H_2S bioavailability and metabolism. Alternatively, H_2S may be introduced into the cell exogenously, which will be discussed in the following paragraph.

3.8.5.3 Exogenous Production of H_2S

When a chemical H_2S donor, introduced into the cell undergoes a chemical reaction to produce H_2S, the literature refers to this as exogenously produced H_2S.[376] Such a compound could be a known to the cell, a natural product or a designed synthetic donor. Native compounds include the sulfide salts Na_2S and NaHS, which are fast-releasing H_2S-donors, and are associated with cancer treatments.[379] These salts demonstrated cytotoxic effects on several tumour types.[380] Synthetic H_2S donors are numerous and represent a growing field within biomedicinal applications. Some examples include the phosphinodithioate GYY4137, Lawessons's reagent, and geminaldithiol TAGDD-1 all of which exhibit strong cytotoxic effects.[381,382] Representative examples of each family are depicted in **Figure 3.11**.

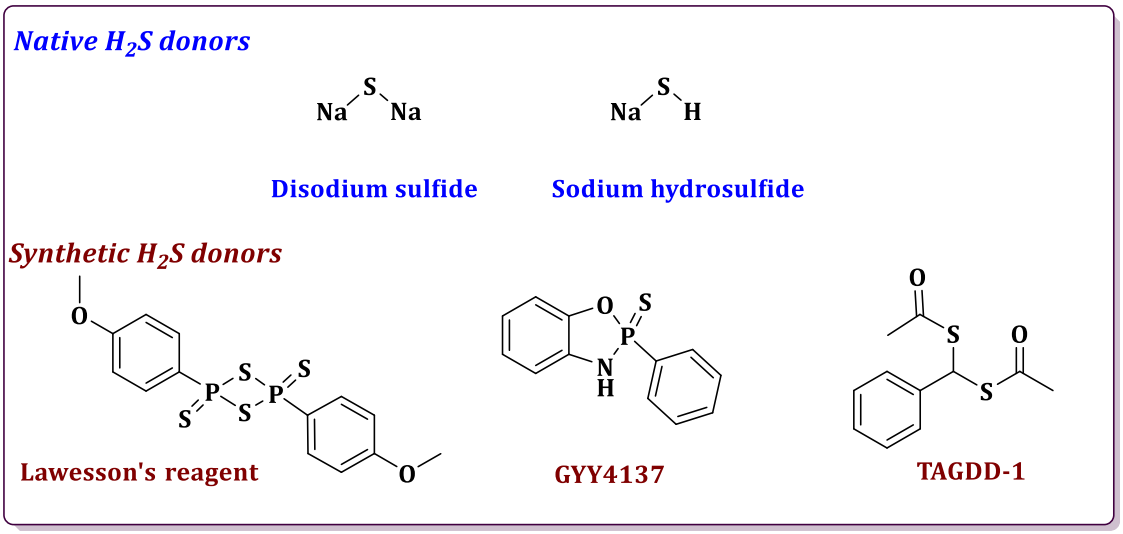

Figure 3.11: Native and synthesised exogenous H_2S-based donors.

The third class of compounds, and the topic of focus in this thesis, are naturally occurring compounds from *allium* vegetables. The most common pathway for H_2S production from the natural product H_2S donor DATS, involves thiolysis exchange. Another pathway from natural products is by raising the levels of H_2S biosynthesis enzymes in tissues,[383] an example being *S*-allylcysteine (SAC), a constituent of fresh garlic, which elevates CSE

protein expression levels in heart tissues after myocardial infarction (MI), leading to enhanced H_2S levels in animal plasma.[384] Similarly, DATS has been shown to increase the expression of CSE and CBS in isolated primary rat hepatic stellate,[385] melanoma,[386] kidney,[387] heart,[388] and liver cells.[389] Another member of natural H_2S donors are the sulfur-rich isothiocyanates such as 4-methylthiobutyl isothiocyanate (erucin), allyl isothiocyanate (AIC), sulforaphane (SFN) and benzyl isothiocyanate (BITC) found in cruciferous vegetables such as broccoli, which are all cytotoxic to cancer cells. *N*-acetyl cysteine (NAC) and *S*-propargyl-cysteine (SPRC) are other H_2S donors that have demonstrated cytotoxicity against a number of different cell lines.[390] **Figure 3.12** displays representative examples from this family.

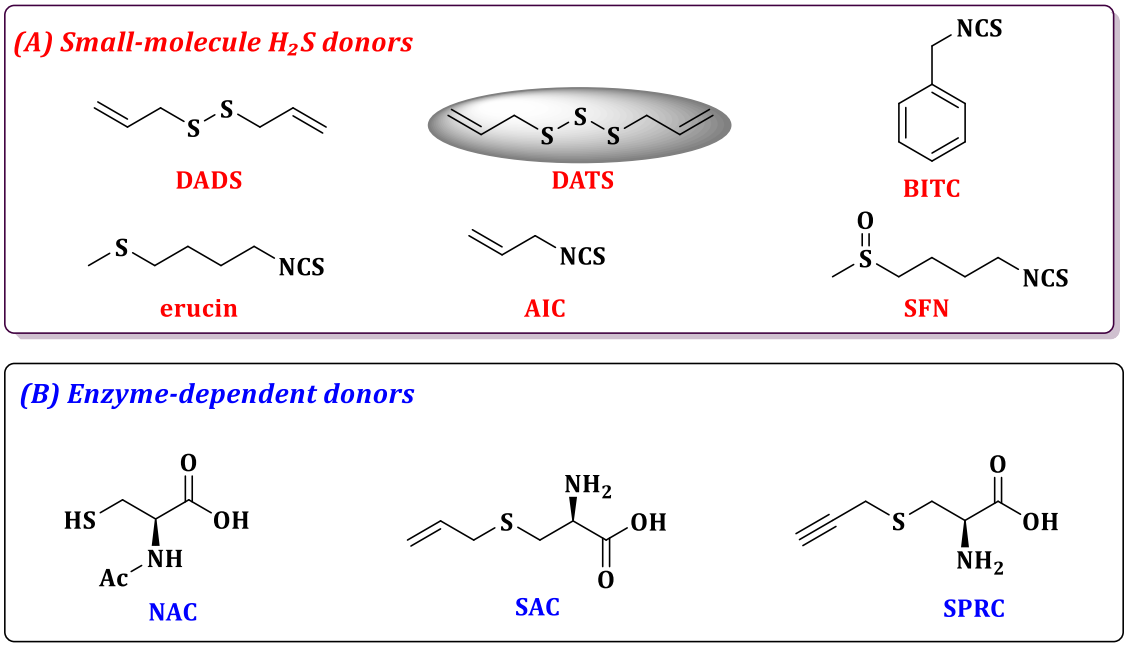

Figure 3.12: Natural exogenous H_2S-based donors.

Exogenously-produced H_2S is used to affect cell signalling, cytoprotection, inflammation, metabolism, and ion channels.[391,392] These H_2S release mechanism of one of the synthetic donors TAGDD-1 is illustrated in **Scheme 3.16** below.

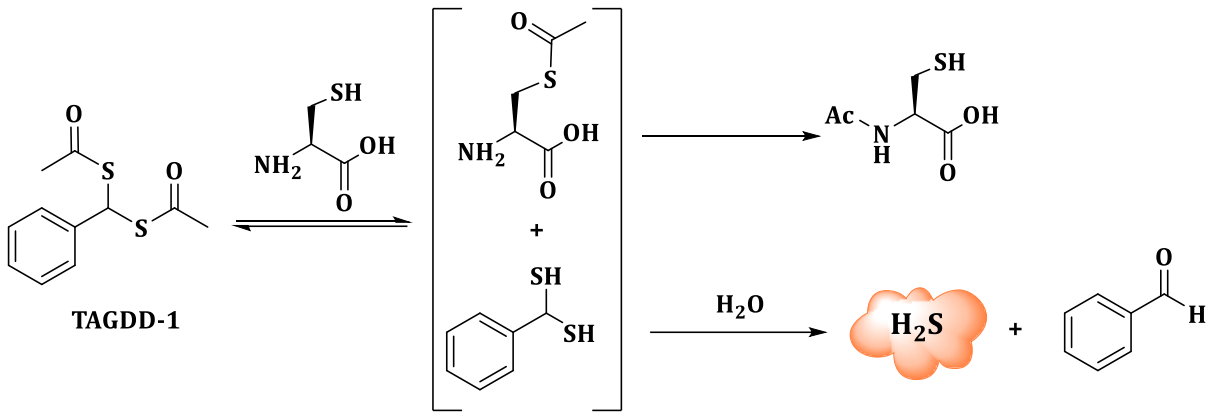

Scheme 3.16: Non-enzymatic biosynthesis of exogenous H_2S from TAGDD-1 in cells.

Currently, the mechanism of action of exogenous H_2S donors as cytotoxic agents is incompletely understood and further research is needed to evaluate their medicinal and biochemical aspects. The metabolism of H_2S will be briefly reviewed in the next paragraph.

3.8.5.4 Metabolism

H_2S is relatively short lived within the cell as it is metabolised in the mitochondria by rhodanese, bisulfide methyltransferase (BMT), and thiosulfate reductase (TSR) in the sulfide oxidation pathway,[393,394] to produce thiocyanate, thiosulfate and methanethiol.[336] The latter is then transformed into dimethyl sulfide, as illustrated in **Scheme 3.17**.

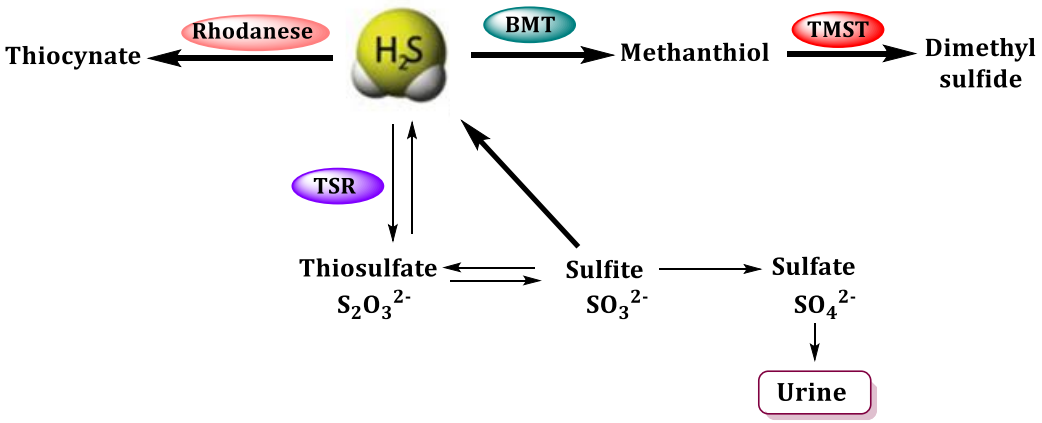

Scheme 3.17: The metabolism of H_2S.[395]

Thiosulfate can be converted to sulfite and then to sulfate *via* thiosulfate sulfurtransferase (TSST). In humans, sulfate is the primary end-product of hydrogen sulfide metabolism and eliminated in the urine[252] but a free form of H_2S can be stored inside the cell as bound sulfane sulfur for future release of H_2S.[396] H_2S endogenous concentrations are

significantly influenced by the metabolic balance between its production and clearance in which H_2S concentrations change more rapidly due to bound sulfane sulfur, which releases and absorbs H_2S.[397]

3.9 Understanding the Role of RSSH, H_2S, and ROS in DATS Cytotoxicity

This section will explore the roles of perthiols, H_2S, and ROS for providing important insight into the mechanism of DATS-induced cancer cell death.

3.9.1 Significance of RSSH in Inducing Cytotoxicity in Cancer

In a biological system, perthiol provides an essential reactive sulfur species that is relevant to hydrogen sulfide's biological activity, including its anticancer properties. **Scheme 3.18** presents an overview of the possible reactions of allylperthiol (ASSH) generated from the reaction of a biological thiol with DATS in an intracellular environment. In this depiction, we will use the protonated form rather than the anion because of its superior electrophilic nature over the perthiolate, although we appreciate that the latter is more reactive nucleophilically.

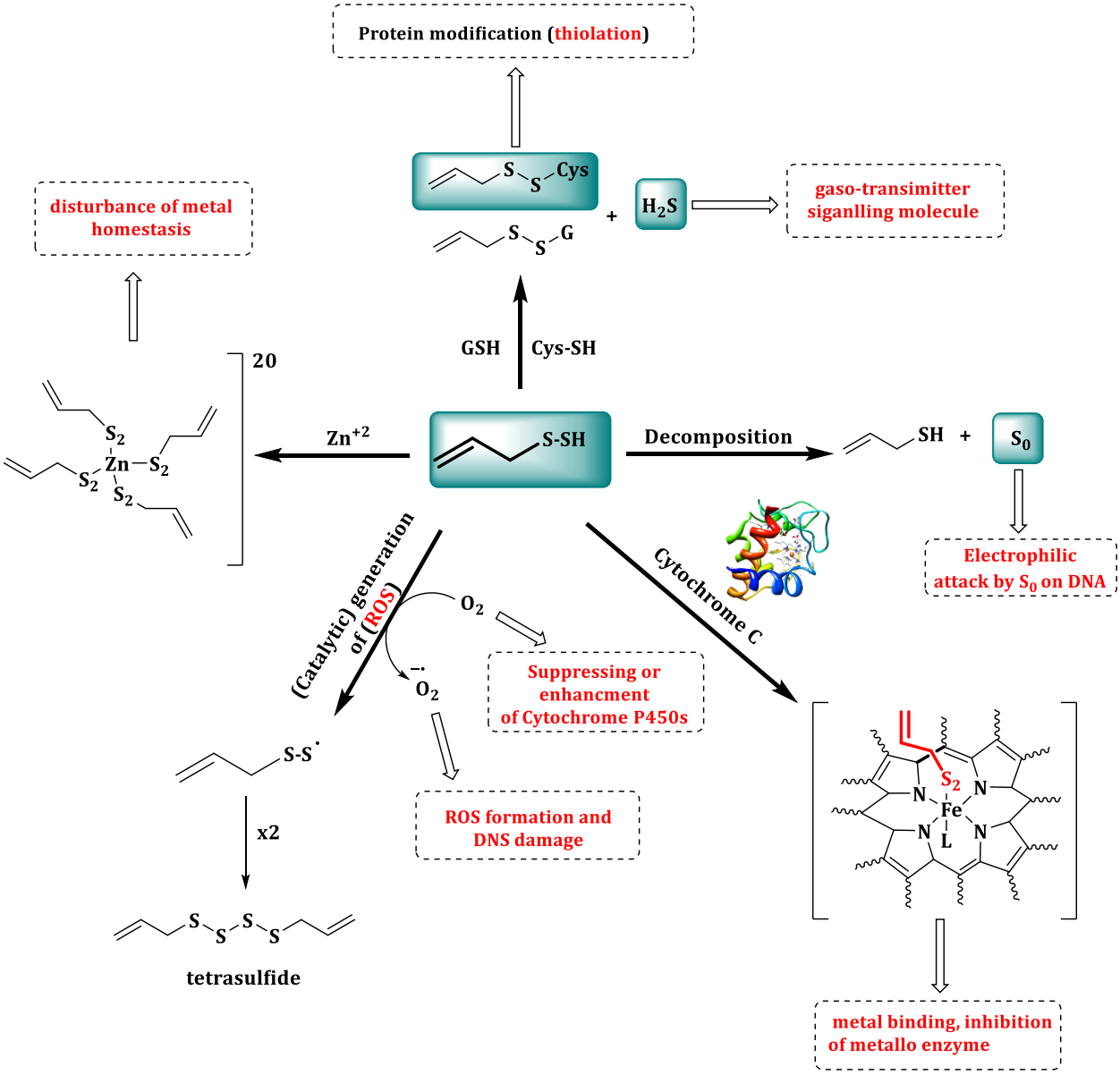

Scheme 3.18: Schematic overview of proposed biochemical activity of allylperthiols *in vivo*. Adapted from Münchberg et al. [239]

As discussed earlier in section **3.8.4.2**, the production of perthiol–perthiyl-polysulfide radicals can lead to a pseudo-catalytic redox cycle that produces ROS which can damage cell membranes and proteins.[239] A number of researchers, including Munday, Gates, and their co-workers, have interpreted this catalytic cycle as the principal explanation of polysulfide cytotoxicity involving compounds like DATS.[245,351] Perthiol reactions are not restricted, though, to oxidants such as dioxygen or haemoglobin but also include metal binding, see **Scheme 3.18**, which makes them effective ligands for transition metal ions such as zinc, copper, and iron.[239] For instance, in 1982, Sawahata and Neal demonstrated that benzyl perthiol inhibits hepatic cytochrome P450 while benzyl mercaptan does not.

They proposed that the primary reason for the cytotoxicity could be the coordination of the perthiol to the haem iron at the active site, among other possibilities such as cysteine thiolation via benzyl disulfide.[398] The soft RSSH is anticipated to bind strongly to a variety of free and protein bound metal ions due to the perthiol's low pK_a.[239] As a result, perthiols would be good inhibitors of copper, zinc, and iron enzymes, such as mitochondrial respiratory chain members, dehydrogenases, and hydrolases. Perthiols may also work as a ligands or at depleting the cytosolic pool of free metal ions.[231] In such a way, this would diminish the amount of free metal ions with disruptive consequences for protein function pertaining to cancer cell function.[239] In general, future research into enzyme inhibition by perthiols generated from natural polysulfides such as tri-, and tetrasulfides seems an appropriate topic for further investigation. Several of the bioactive properties of DATS, such as anti-inflammatory effects, blood pressure mediation, antibacterial capabilities and importantly anticancer activity overlap with the bioactivities currently attributed to H_2S, which, of course, link to release mediated by perthiol formation.

This mechanism is particularly relevant in the context of cancer biology. As previously mentioned, cancer cells, with their elevated metabolism and proliferation rates, generate more ROS than normal cells.[399] Consequently, anticancer therapies aim to disrupt this redox balance by raising intracellular ROS levels, overwhelming the cell's antioxidant defenses and triggering apoptosis.[400,401] Specifically, polysulfides (S≥2, e.g., DADS, DATS, DATTS) can produce ROS via GSH and single-electron transfer reactions, with ROS generation efficiency ranking: DATTS>DATS>DADS>DAS.[245] Notably, DATS's GSH cleavage yields one perthiol, while DATTS produces two, likely explaining DATTS's greater cytotoxicity. In contrast, DADS, lacking perthiol intermediates, produces less ROS and H_2S.[402] Additionally, DATS disrupts iron homeostasis, increases Ca^{2+} levels, and induces ROS production in cancer cells, contributing to H_2S-mediated apoptosis through mitochondrial and gene regulation pathways. [403-405]

3.9.2 Molecular Mechanisms of H_2S Activity

H_2S functions in the cardiovascular, renal, neurological, and digestive systems.[406-409] Many diseases, including metabolic and Down's Syndrome, cardiovascular disease, neurodegeneration, and cancer, are associated with dysregulated H_2S function.[410-415] H_2S easily passes across biological membranes leading to efficient intercellular signalling, which links to the high chemical reactivity of HS^-.[356,416] Importantly, H_2S itself reacts too

slowly to have any biological effect,[417] and its cellular concentration is low (10–30 nM) when compared to other thiol-based antioxidants such as glutathione (1–10 mM). However, free H_2S occurs in thermodynamic equilibrium with a variety of different sulfur species, including perthiols, polysulfides, and a variety of sulfide sulfur-containing products and has a short half-life in most tissues, lasting only a few minutes.[407] As was discussed previously, perthiols and polysulfides could react with GSH to produce a wide range of partly protonated S_n^{2-} species.[239] Given that GSH occurs in mammalian cells at millimolar quantities, the release of H_2S from DATS and DATTS becomes viable. A full mechanistic understanding of the underlying chemical processes and biochemical mechanisms behind such activities has yet to emerge, although the interaction of HS^- with metal ions, whether free or protein-bound, is seen to play a major role in the cascade of events based on the high nucleophilicity of HS^-.[239] Such biochemistry bears similarities to the chemistry of perthiolates and is summarised in **Scheme 3.19.**

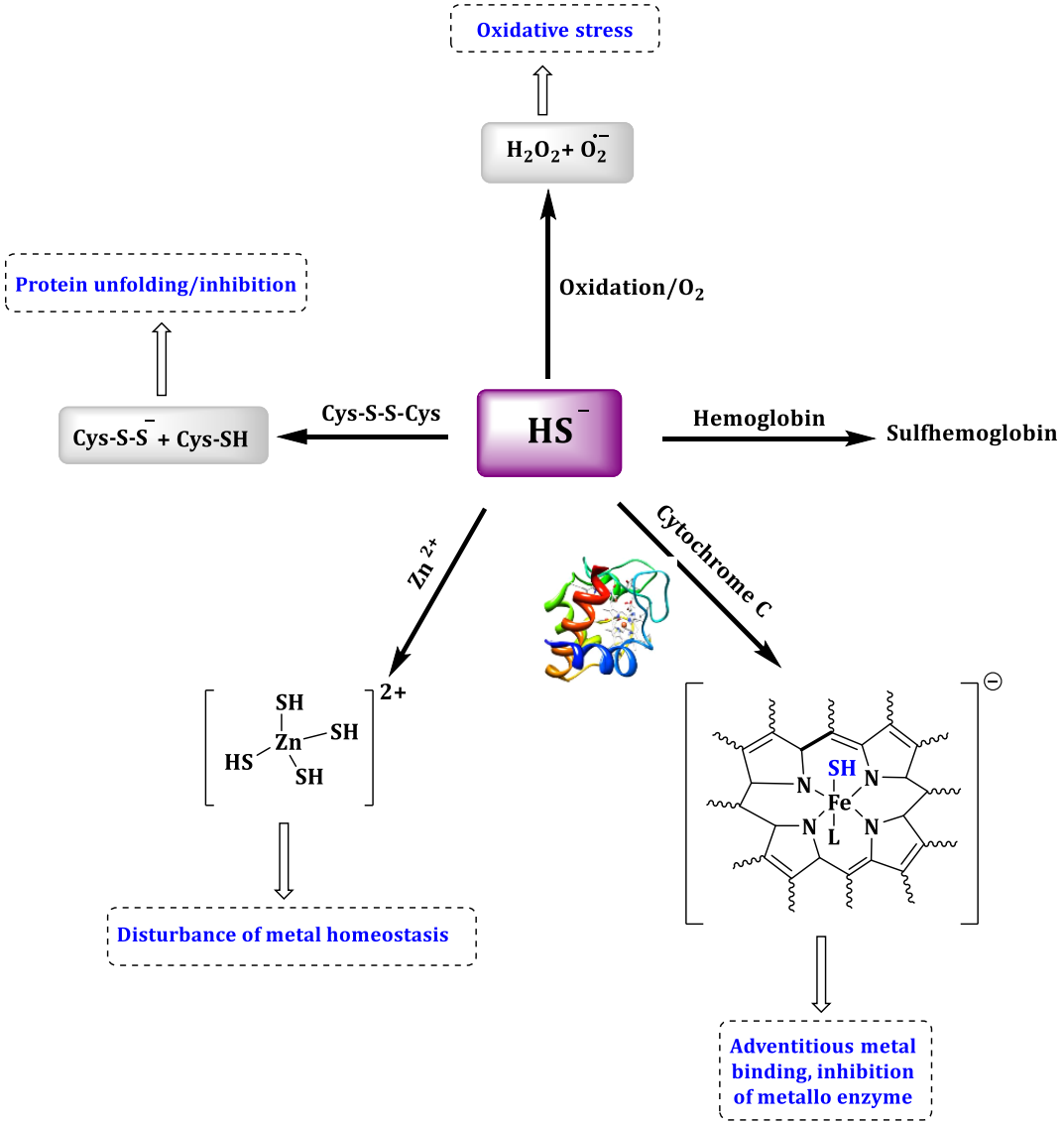

Scheme 3.19: Schematic overview of proposed biochemical activity of hydrosulfide ion. Adapted from Münchberg et al.[239]

A variety of biological responses to H_2S/HS^- are covered in several recent reviews,[391,392,418] highlighting the biological significance of H_2S. Firstly, it is known that H_2S decreases the metabolic rate of mice by approximately 90% to generate a suspended animation-like state which protects them from lethal hypoxia.[419] This is attributed to the hydrosulfide ion's suppression of the iron protein cytochrome *c* oxidase,[420] see **Scheme 3.19**. In support of these findings, HS^- has long been recognized to inhibit metalloenzymes such as carbonic anhydrase[421] by functioning as a competing ligand to the zinc metal ion.[239] It is also well established that HS^- has a strong suppressive effect on monoamine oxidase.[422] In addition, inorganic sulfide is able to exchange with disulfide bonds in proteins at the a-carbon to generate cysteine perthiolate ions (as shown in **Scheme 3.19**),

which promote protein post-translational modification leading to further modification, potentially perthiolate other SH residues in proteins.[239] Protein disulfides may thus serve as targets for polysulfide-derived sulfur species, potentially causing cancer cell damage. Further possible reaction of HS^- anion includes reaction with dioxygen to produce $O_2^{\bullet-}$ and H_2O_2 which are similar to those outlined for perthiols.[239] Lastly, H_2S could also interact with haemoglobin to form sulfhaemoglobin.

In summary, several reviews have pointed out that H_2S plays a dual role in the biology of cancer, promoting the growth of cancer cells on the one hand, while having cytotoxic effects on the other.[354,355,423] Slowing cancer-cell progression can occur by either preventing cells from producing H_2S or exposing them to exogenously supplied H_2S donors. In terms of concentration, it has been reported that endogenous H_2S or treatment with relatively low levels of exogenous H_2S for a short time may promote or maintain the growth of cancer cells, whereas treatment with a relatively high concentrations of an exogenous H_2S donor for a lengthy time has anti-cancer effects.[414] This dichotomy will be discussed in the following sections starting with endogenous H_2S.

3.9.3 Endogenous H_2S in Cancer

Endogenous H_2S is an important signalling molecule in humans and other mammals. H_2S regulation determines the normal functioning of the cells depending on the cell type, and any dysregulation in endogenous H_2S levels is associated with the development and metastasis of cancer.[355,424] Numerous cancers have been identified to have high expression levels of the three H_2S-producing enzymes CSE, CBS, and 3MST.[425] This section will briefly discuss the ways in which endogenous H_2S promotes cancer-cell growth by augmenting various cancer hallmarks as illustrated in **Figure 3.13**.

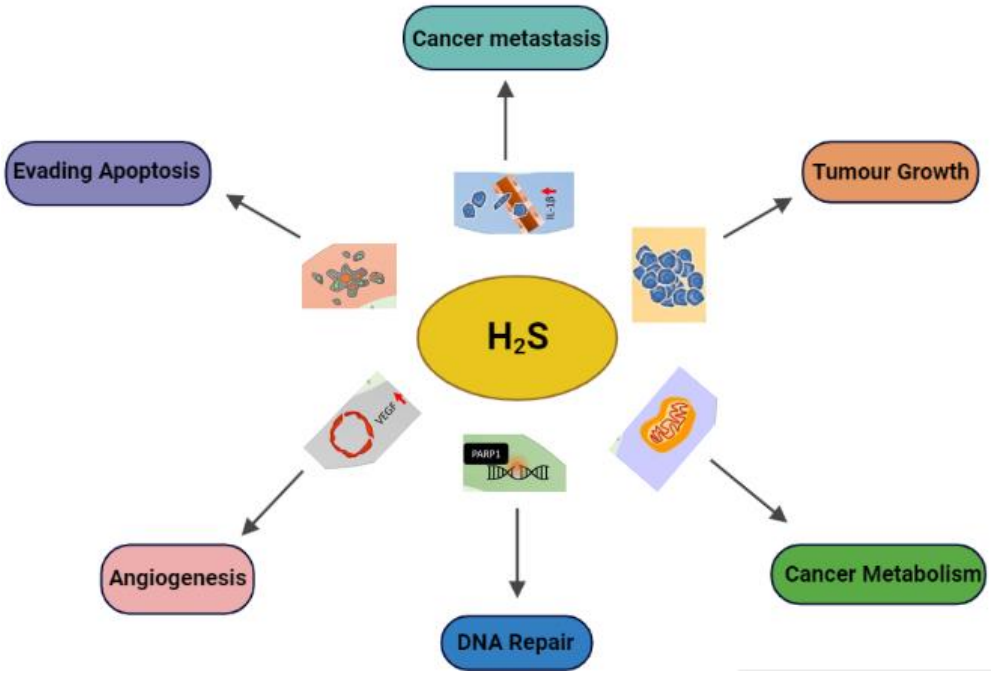

Figure 3.13: The potential role of endogenous H_2S in cancer progression.

Important empirical evidence is that growth of multiple cancer types has been linked to an increase in the concentration of H_2S-producing enzymes. Conversely, depletion of CBS or CSE activities inhibits tumour growth in breast, lung, prostate, and colon cancer.[424] For instance, CBS downregulation reduced oxygen consumption and ATP production in both colon[426] and ovarian cancer cells,[427] indicating the importance of H_2S in cancer metabolism. In addition, endogenous H_2S encourages cancer cell migration and invasion by inducing ATP citrate lyase (ACLY) to facilitate EMT,[424]processes that are important in metastasis. In addition, several in *vitro* and in *vivo* studies have established that endogenous H_2S acts as a pro-angiogenic factor.[428] As a result of the release of endogenous H_2S, high levels of antioxidants like GSH and thioredoxin (Trx) may be involved in the scavenging of ROS and RNS, providing cells with significant antioxidant protection.[429] Another aspect is that endogenous H_2S facilitates mitochondrial DNA (mtDNA) repair through persulfidation, which helps to combat chemotherapy-induced apoptosis.[430] In summary, several manifolds exist for cancer-cell protection by endogenous H_2S that include apoptosis suppression, DNA repair, tumour growth promotion, cancer metabolism acceleration, metastasis and angiogenesis promotion. There are currently a few inhibitors for suppressing endogenous H_2S production but these won't be discussed in this thesis.[424] The following section will turn towards aspects of exogenous H_2S release for suppressing cancer-cell growth and disease progression.

3.9.4 Exogenous H_2S Release in Cancer

There are a number of literature articles that have investigated the role of exogenous H_2S in tumour suppression. The aspects involve its exogenous effects on signalling pathways, angiogenesis, autophagy, proliferation, apoptosis and cell cycle. Treatment with an H_2S donor such as NaSH inhibits the migration, proliferation, and division of human hepatocellular carcinoma cells by blocking the PI3K/AKT/mTOR signalling pathway and inducing cell autophagy.[431] Exogenous H_2S is a gasotransmitter that regulates angiogenesis both in *vitro* and in *vivo* under physiological and ischaemic conditions.[432] At high concentrations, exogenous H_2S has been shown inhibit angiogensis.[355] For example, exogenously applied high concentrations of NaHS suppresses angiogenesis. Exogenously applied H_2S has also been found to induce a form of autophagy which leads to cell death in cancer cells.[433]

Exogenous H_2S can also target signalling pathways associated with proliferation.[354,434] For instance, DATS treatment reduces cell viability and proliferation in osteosarcoma,[296] glioma,[275] and gastric cancer[435] by activating MAPK and suppressing PI3K/AKT cascades. Elevated ROS levels from exogenous H_2S disrupts Ca^{2+} homeostasis, resulting in increased expression of p21 and p27,[436] which can cause cell-cycle arrest.

While several studies have explored the role of exogenous H_2S in tumor suppression, the evidence remains limited and somewhat inconsistent. The available results suggest that exogenous H_2S can affect various cellular pathways and processes such as angiogenesis, autophagy, proliferation, and apoptosis. However, these effects are highly dependent on the concentration of H_2S, the type of cancer cells, and the specific conditions of each study. Therefore, more comprehensive and well-designed studies are required to better understand the role of exogenous H_2S in cancer and to conclusively determine whether it is beneficial or detrimental in the context of cancer therapy.

DATS has been shown to cause cell death in many cancer types by enhancing mitochondria-mediated DNA damage and by controlling the signalling pathways.[240,355] **Figure 3.14** shows the various proposed effects by H_2S on the mitochondria.

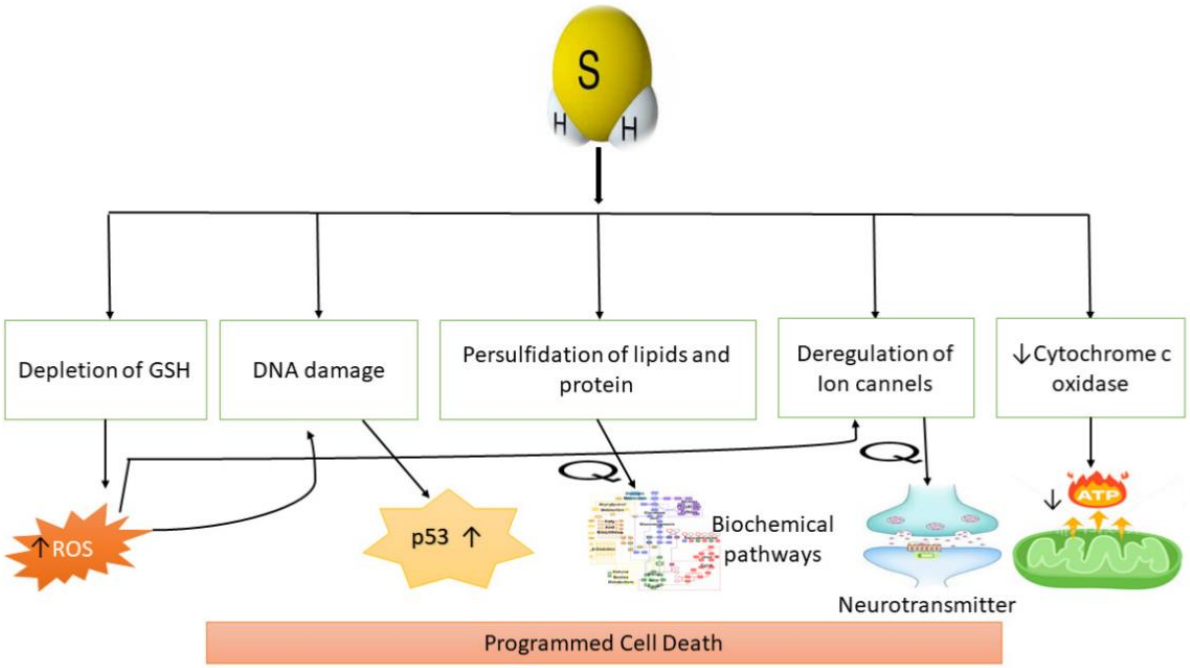

Figure 3.14: Mitochondrial cytotoxicity modes of action promoted by exogenous H_2S. Taken form Khattak et al. [355]

It has been shown that cytochrome c oxidase is inhibited by H_2S, which results in less efficient ATP synthesis. Furthermore, ROS are caused by reduced glutathione depletion[355] and high intracellular ROS levels make exogenous H_2S more likely to cause DNA damage, as well as protein and lipid persulfidation. These H_2S-induced processes may lead to apoptosis.[355]

In summary, H_2S may exert its anticancer effects through various mechanisms, such as inducing intracellular acidification, causing cell cycle arrest, and inhibiting cell survival signalling pathways to promote apoptosis although the evidence for these hypotheses is not overwhelming and there are more papers reporting the pro-survival effects of H_2S than the pro-death effects (which is of relevance to cancer treatment). Both exogenous H_2S (via H_2S donors) and H_2S biosynthesis inhibition can have therapeutic effects as described in **Figure 3.15**. Thus, low levels of endogenous H_2S produced by CBS, CSE, and/or 3-MST, have been shown to be beneficial for tumour angiogenesis and growth as depicted by the green arrow. However, inhibitors of H_2S synthesis enzymes or exogenous administration H_2S donors may inhibit cancer growth, although there is mixed evidence for this.[423,437]

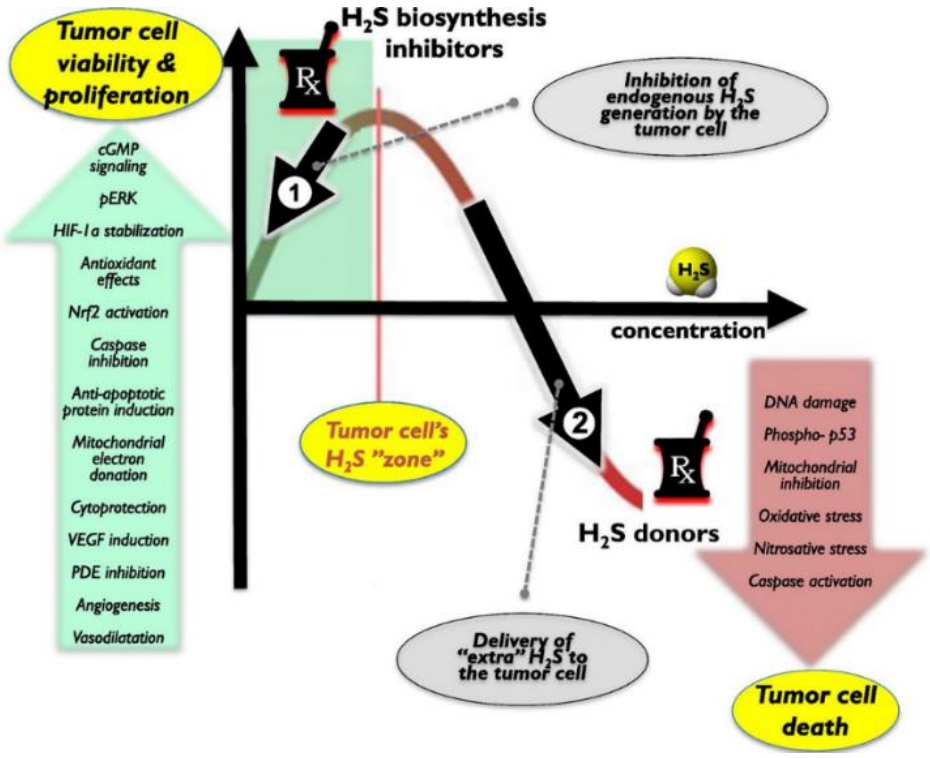

Figure 3.15: Mechanisms underlying the cancer promoting and inhibiting model developed by Hellmich et al.[382]

Thus, it is therapeutically beneficial to inhibit the endogenously produced in green pathway ①, Or to activate the red pathway ② by enhancing the concentration of exogenous H_2S.[382] Hence, H_2S donor compounds such as DATS may have an anti-cancer impact via endogenous H_2S production.[438] This model has stimulated research into agents that offer a slow release of H_2S as an anti-tumour medicine.

Overview of Literature Understanding – *the Gaps and the Objectives of this PhD*

Chapter Three of this thesis focuses on the cancer biology of organosulfur compounds (OSCs), with a particular focus on DATS as the prototypical garlic-derived organotrisulfide. As alluded to in the Chapter, more research is required to elucidate a better understanding between the role players of perthiol, ROS and H_2S from trisulfides.

Hence, to this end, the thesis is divided into the following objectives:

(i) To develop a new synthesis methodology for easy access to a range of homo- and heterotrisulfides for cytotoxicity structure-activity relationship (SAR) purposes in cancer cell lines.

(ii) To investigate the trisulfide mechanism of action for inducing cytotoxicity in cancer cells, with a focus on the effect and inter-relationship of H_2S and perthiol. The study includes in *vitro* experiments, SAR analysis, and fluorescent studies for studying the H_2S/perthiol relationship.

CHAPTER 4: Development of New Methodology for Unsymmetrical Organotrisulfide Synthesis

4.1 Overview on Unsymmetrical Organotrisulfide Methodologies

Following the literature review in Chapter Two, it was noted that most current methodologies for synthesizing unsymmetrical trisulfides suffer from notable limitations that include the use of highly toxic reagents and harsh reaction conditions, which renders them environmentally unfriendly and hence unsustainable long term. Moreover, only a limited number of these approaches qualify as a one-pot transformation with green features that can access unsymmetrical trisulfides. Based on this, it was decided to focus our efforts on developing a new methodology based on either a [1 + 2] or a [2 + 1] protocol. Recent successful methodologies of this type are summarized in **Scheme 4.1**.

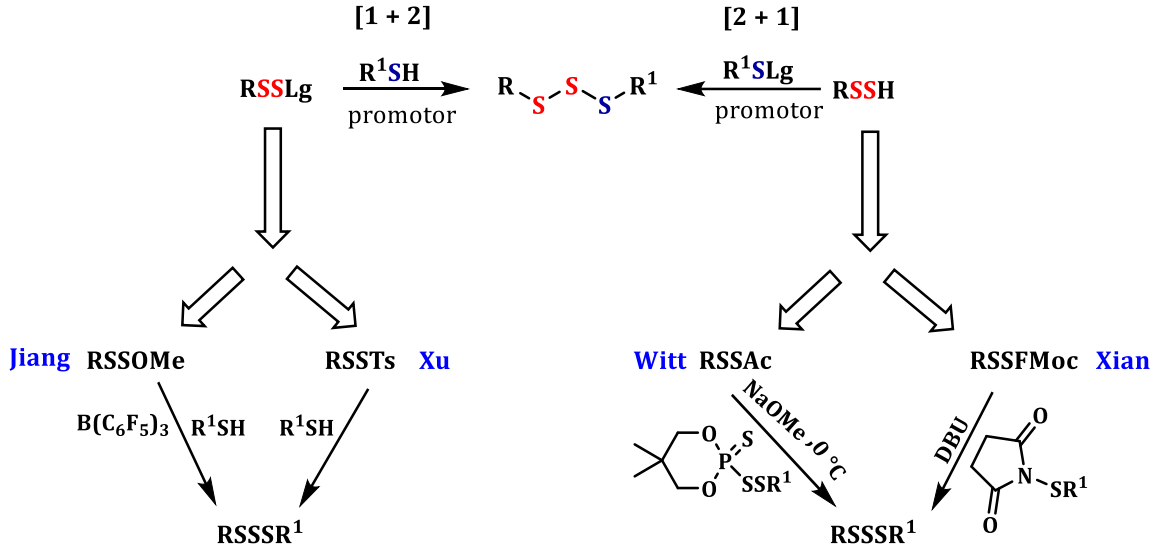

Scheme 4.1: A Summary of [1 + 2] and [2 + 1] methodologies for unsymmetrical trisulfide synthesis.

For the [1 + 2] methods, using an RSSLg species offers the advantage of utilizing a thiol as the nucleophile, with several leaving groups explored for the electrophilic disulfanyl partner such as thiocarbonate,[115] phthalimido,[128] and chloride,[126] as reported in Chapter Two. Recent research by Xu employs sulfenylthiosulfonate (with only *t*-butyl used as the R group of the RSSTs) as an electrophilic sulfur source in a [1 + 2] approach. However, it is worth noting that sulfenylthiotosylates RSSTs are generally unstable[140] and tend to expel S in polar solvents (presumably *t*-butyl as the R group retards this). Similarly, Jiang's

method utilizes methoxy as a leaving group for the two-sulfur electrophile, but a catalyst is required for S-S coupling.[1]

Moving onto the [2 + 1] approach, Xian[145] demonstrated that 9-fluorenylmethyl disulfides could serve as suitable surrogates for hydrodisulfide production under base-mediated elimination conditions (DBU) at room temperature. This nucleophilic species could then be coupled with an electrophilic sulfur source to yield organotrisulfide. On the other hand, Witt[139] and colleagues demonstrated that a perthiolate RSS^- could be generated in *situ* from the corresponding disulfanyl acetate using methoxide ion and reacted with a novel sulfanyl-2-thioxo-1,3,2-dioxaphosphorinane *S*-electrophile to produce unsymmetrical organotrisulfides.

Overall, several challenges still exist in terms of achieving high product purity and reaction scope. Moreover, all of the methods shown in **Scheme 4.1** still rely on harsh reagents such as Br_2 and $SOCl_2$[135,139] to prepare the various intermediates[135] as well as sometimes long sequences to arrive at the precursor for coupling[145,439] or involve catalysts to promote coupling.[1] Finally, none of the methods say very much about accessing aromatic-aromatic trisulfides as the most difficult class of organotrisulfides to produce. What follows is a description of our quest to develop a new unsymmetrical trisulfide methodology addressing these shortcomings.

4.2 Establishing a Prototype

We began by choosing to pursue a [1 + 2] protocol involving a thiol (or thiolate) as the nucleophile and an RSSLg species as the electrophilic partner. In part, this was to avoid proceeding via the perthiolate species (RSS^-) in the [2 + 1] equivalent. Also, our choice was inspired by previous work[440] from the group on unsymmetrical disulfide production involving BtCl as the oxidant as shown in **Scheme 4.2**, which proceeds via a less reactive (than RSCl) RSBt intermediate that minimizes homodisulfide formation.

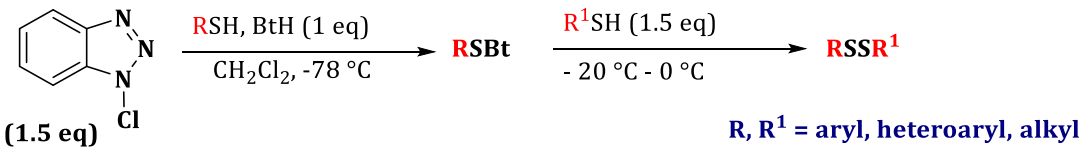

Scheme 4.2: UCT heterodisulfide synthesis methodology.[440]

Our thinking was that perhaps we could extend the BtCl chemistry to generating RSSBt as a novel S2 electrophile via reaction of a perthiol, RSSH, with BtCl. In the event, however,

reaction of BnSSAc with BtCl in the presence of NaOMe (to deprotect the disulfanyl acetate to the perthiolate) at -78 °C in THF, while providing TLC evidence for formation of BnSSBt as a TLC spot close (above) to BnSBt as a reference standard, also revealed partial loss of sulfur to form BnSBt as the reaction with BuSH as R^2SH in **Scheme 4.2** proceeded. This was confirmed by work-up and chromatography to produce a mixture of di- and trisulfides as judged by ^1H NMR spectroscopy in which BnSSSBu and BnSSBu could be differentiated by virtue of differing benzylic methylene ^1H NMR chemical shifts for di and trisulfide (2.66 and 2.87 ppm triplet in $CDCl_3$, respectively).

Thus, we turned attention to the [2 + 1] protocol involving a perthiolate or its equivalent. At this point, we were given hope by Witt's work in which methoxide had been used in *situ* (see **Scheme 4.1** for details) and wondered if this could be transposed into an *in-situ* method involving the reaction of a disulfanyl acetate (RSSAc) with a thiotosylate at low temperature (**Scheme 4.3**), each of the reactants readily accessible via standard methods.

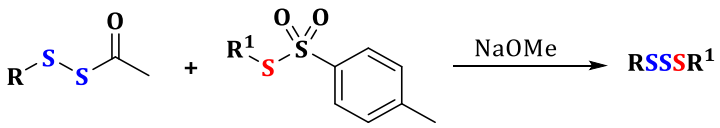

Scheme 4.3: UCT heterotrisulfide synthesis methodology.

We chose RSTs as a reliable soft and stable S1 source owing to its outstanding handling properties and facile access. For aliphatic R groups, production via alkyl halide substitution with commercially available sodium thiotosylate, the latter also accessible via reaction of sulfur with commercially available sodium *p*-tolylsulfinate salt in pyridine was used.[441-443] For aromatic R groups (not amenable to S_N2 substitution), reaction of the disulfide with iodine and sodium benzenesulfinate[444,445] could be used as shown in **Scheme 4.4**.

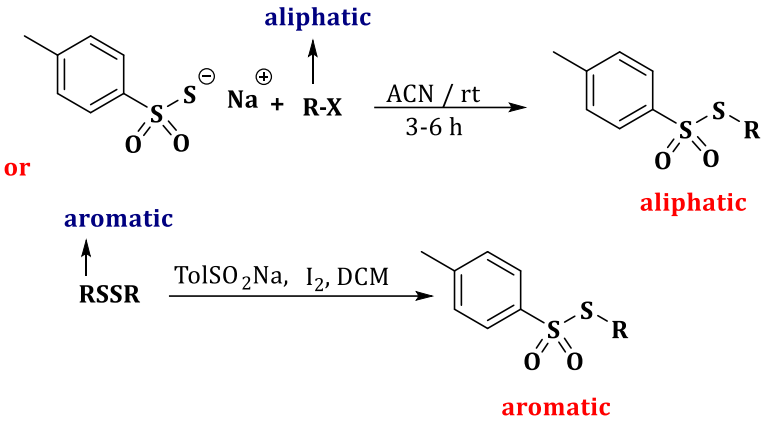

Scheme 4.4: Synthesis of RSTs.

Similarly, the disulfanyl acetate could be easily obtained via reaction of a thiotosylate (both aromatic and aliphatic) with potassium thioacetate (KSAc),[141] as depicted in **Scheme 4.5**. Hence, both reactants were envisaged as being sourced from RSTs, the latter accessed in a relatively green manner using the chemistry depicted in **Scheme 4.4**.

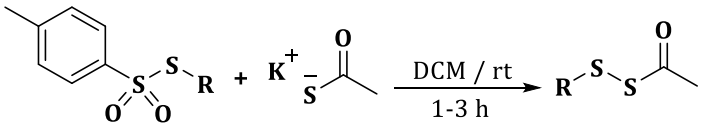

Scheme 4.5: Synthesis of RSSAc.

For the first trisulfide experiment, we decided to use the disulfanyl acetate as limiting with RSTs in slight excess (1.2 eq) in THF at – 78 °C, both reactants together in the flask. Then, once the temperature had equilibrated, NaOMe (1 eq as reagent for acetate deprotection and made up fresh from Na and dry MeOH) as a solution in dry methanol would be added slowly via syringe. We were aware of time being a crucial factor and decided to use TLC to follow the reaction. Our choice of R groups for R^1SSSR formation was based on several factors. Initially, PhSTs was selected as a starting material owing to its ready availability and strong UV activity for TLC purposes. For the disulfanyl R^1 group, a hexyl group was chosen as a typical aliphatic representative for which ^1H NMR a-methylene (attached to sulfur) chemical shifts for both disulfide and trisulfide were known.[139] The reaction is shown in **Scheme 4.6** below.

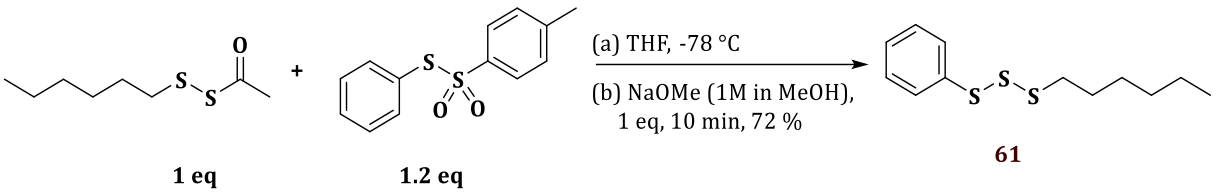

Scheme 4.6: Synthesis of HexSSSPh, 61.

In the event, the reaction was allowed to proceed for 10 minutes as a pilot run before quenching with ammonium chloride. Extraction followed by chromatography gave a product containing two closely running spots that couldn't be separated using the non-polar mobile phase of hexane with a small percentage of ethyl acetate. The yield was around 60% based on the trisulfide, and ^{1}H NMR analysis returned a ratio of 65:35 for the tri- and di-sulfides based on the known chemical shifts of the methylene hydrogens attached to sulfur of 2.66 and 2.87 ppm for disulfide and trisulfide, respectively.[139] Our first thought was that the disulfanyl anion had desulfurized to the thiolate ($HexS^{-}$), which didn't look good for our new method as it implied a competition between perthiolate sulfenylation and desulfurisation. However, we then realized that the phenyl group might also be labilising the S-S bond towards exchange reactions, leading to the disulfide ultimately (although the sequence of events involved was not clear). Thus, it was decided to change the thiotosylate R group to allyl, still maintaining a high sulfenyl electrophilicity, but with a methylene group separating the sulfur from the double bond.

Therefore, in the next experiment, HexSSAc (1 eq) was used with allylSTs (1.2 eq), and sodium methoxide (1 eq) added last as before at -78 °C. The reaction time was reduced and stirred for 5 minutes. Upon analyzing the reaction mixture using TLC, a single less-polar spot appeared to have formed, so the reaction was worked up with ammonium chloride and the product chromatographed to afford the anticipated trisulfide, HexSSSallyl, **62**, in 92% yield. The identification and characterization of HexSSSallyl were facilitated using diagnostic peaks in the ^{1}H NMR spectra. Specifically, the chemical shifts of the methylene protons in aliphatic and allyl groups served as reliable markers for trisulfide structures. According to the literature,[139] the presence of methylene protons attached to sulfur in the trisulfide structure was indicated by chemical shifts in the range of 2.87-2.92 ppm (**Figure 4.1**). Furthermore, in line with previous findings (DATS),[446] the chemical shifts of the methylene peak of allyl groups were observed to fall within the range of 3.50-3.55 ppm as doublet. This specific chemical shift range served as a distinguishing feature for identifying the presence of allyl groups attached to sulfur. These

results were summarized in **Table 4.1**, where a comparison with naturally occurring di- and tetrasulfides[446] was also provided.

Table 4.1: Literature ^{1}H chemical shifts (ppm) for the methylene protons of the allyl group for DADS, DATS and DATTS

Compounds	^{1}H NMR
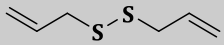	3.36
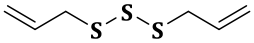	3.52
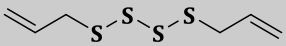	3.60

However, we identified an impurity, as shown in **Figure 4.1** of the ^{1}H NMR spectra at around 2.30 ppm, and this prompted us to plan for a future study that would involve HPLC. The other conclusion was that the phenyl group in the earlier experiment was likely responsible for formation of the disulfide via an exchange process since hexyl perthiolate had been used in both experiments (Ph to allyl).

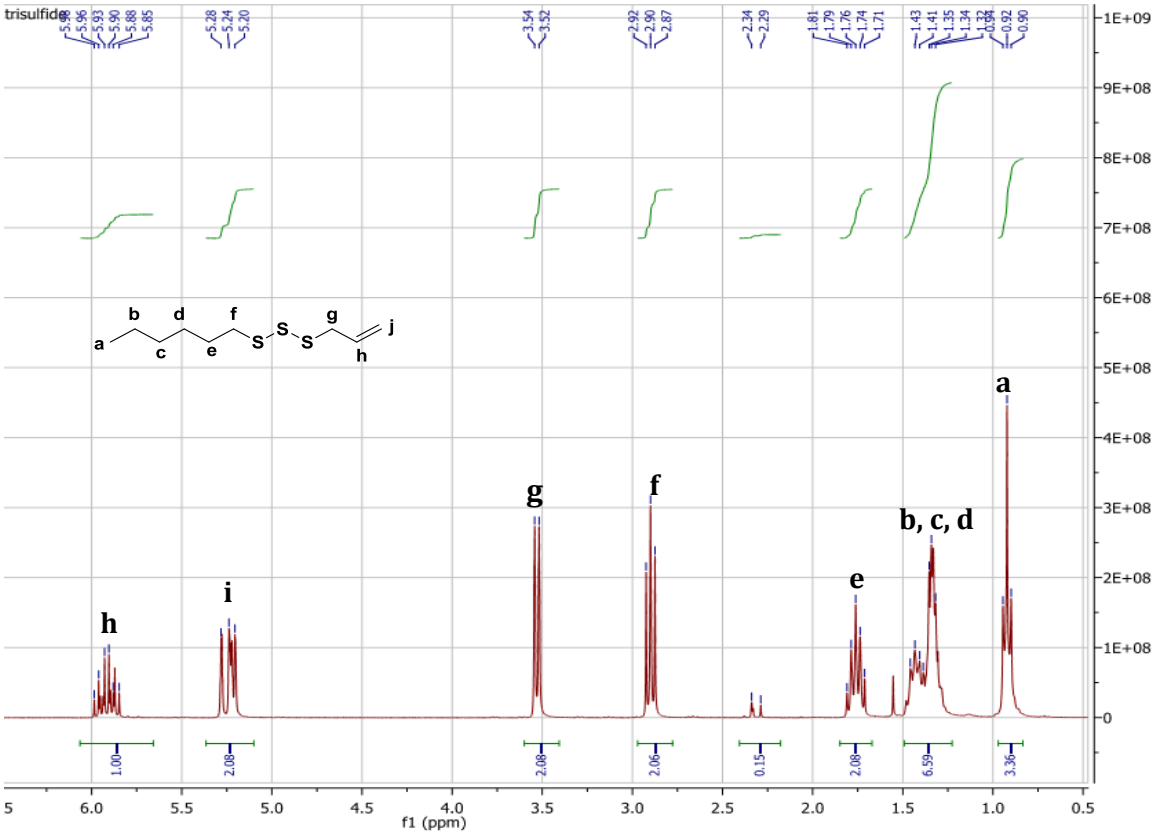

Figure 4.1: ^{1}H NMR spectrum of 3 from a 5-minute reaction time of 62.

At this point it was realized that the reaction was probably extremely fast, so a series of experiments were conducted with short time durations. The results are shown in **Table 4.2** in which yields refer to columned products and purities ascertained by C-18 reverse-phase HPLC.

Table 4.2: Screening of reaction time for the model study

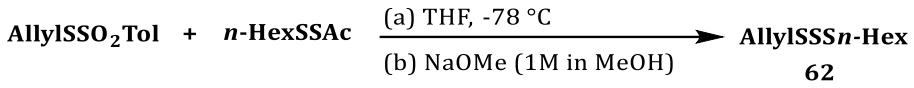

Entry	Eq. RSTs	Eq. R¹SSAc	Eq. NaOMe	Time	Yield %	Purity %
1	**1.2**	**1**	**1**	**30 sec**	**88**	**96**
2	1.2	1	1	2 min	86	95
3	1.2	1	1	5 min	92	93
4	1.2	1	1	30 min	87	85

As seen from the results in **Table 4.2**, not unexpectedly, we found that the shortest time of 30 seconds gave the highest trisulfide purity (of 96%). However, somewhat surprising was that the yield stayed relatively high throughout the timeline, indicating that S-S exchanges weren't operating to any great extent at this temperature, nor had the hexyl perthiolate desulfurized (or rearranged to other species), which was understood in terms of a fast *S*-sulfenylation. **Figures 4.2** and **4.3** below show the ^{1}H NMR spectrum and HPLC respectively for **62** from the 30 seconds run.

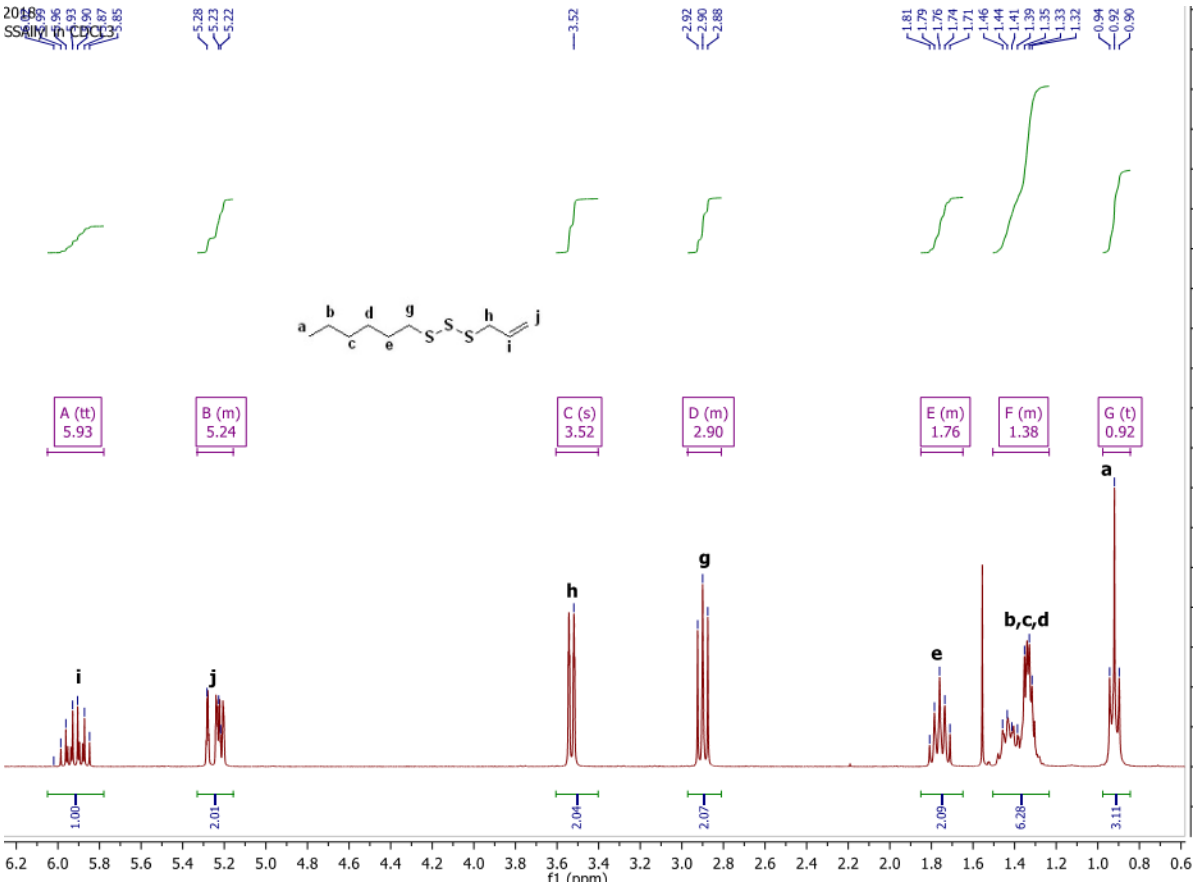

Figure 4.2: ^{1}H NMR spectrum of HexSSSallyl, 62, from a 30 second reaction time.

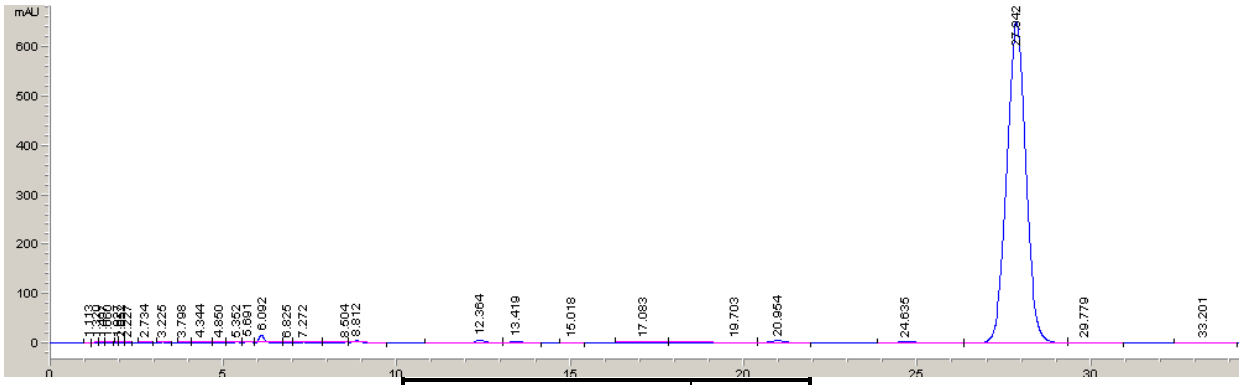

Retention time (min)	Area %
27.84	96.24

Figure 4.3: HPLC purity of HexSSSallyl, 62, from a 30 second reaction time.

In addition, it is important to note that increasing the thiosulfonate to disulfanyl acetate ratio to 1.5:1 (as shown in **Table 4.3** below), while maintaining the time and using 1 eq. of NaOMe, resulted in a decrease in both yield (to 80%) and purity (to 93%). Therefore, the optimal stoichiometry for future experiments was chosen as a 1.2:1 ratio of thiosulfonate to disulfanyl acetate.

Table 4.3: Screening of increasing thiotosylate on the reaction outcome (at -78 ºC)

Entry	Eq. R¹STs	Eq. RSSAc	Eq. NaOMe	Time	Yield %	Purity %
1	1.5	1	1	**30 sec**	80	93

Similarly, it is also worth noting that using thiosulfonate as the limiting reagent and having a slight excess of disulfanyl acetate resulted in the formation of more by-products, likely due to subsequent exchange reactions involving the excess nucleophilic disulfanyl anion. Another intriguing finding revealed that full conversion within 5 minutes could be achieved with a sub-stoichiometric amount of methoxide promoter (**Table 4.4** below), indicating that the sulfinate leaving group from the S-S coupling likely promotes acetyl deprotection via nucleophilic attack by the sulfur of the sulfinate ion (negatively charged, so relatively nucleophilic) as illustrated in **Scheme 4.7**.

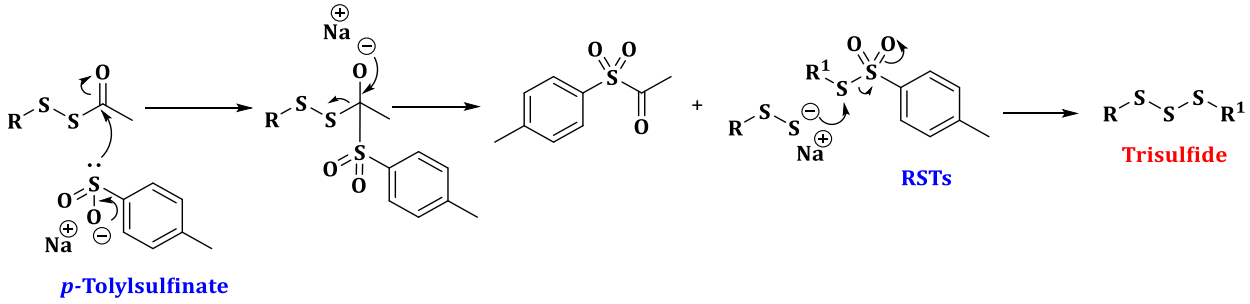

Scheme 4.7: Mechanism of the role of sulfinate ion in disulfanyl acetate deprotection.

Table 4.4: Effect of reducing the equivalents of methoxide on the reaction outcome

Entry	Eq. R¹STs	Eq. RSSAc	Eq. NaOMe	Time	Yield %	Purity %
1	1.2	1	0.7	5 min	92	95

As a result of our pilot study, we felt confident of applying the optimized conditions shown in **Scheme 4.8** below to a broader library of substrates. The results from it also suggested a mechanism as shown in **Scheme 4.8**, in which desulfurization (lower k_1) is slower than perthiolate sulfenylation (higher k_2). This was thus the major finding of the work. Also, it should be noted that *S*-sulfenylation was preferred to *S*-sulfonylation (via attack at the sulfonyl sulfur of RSTs) due to the greater softness of the sulfenyl sulfur.

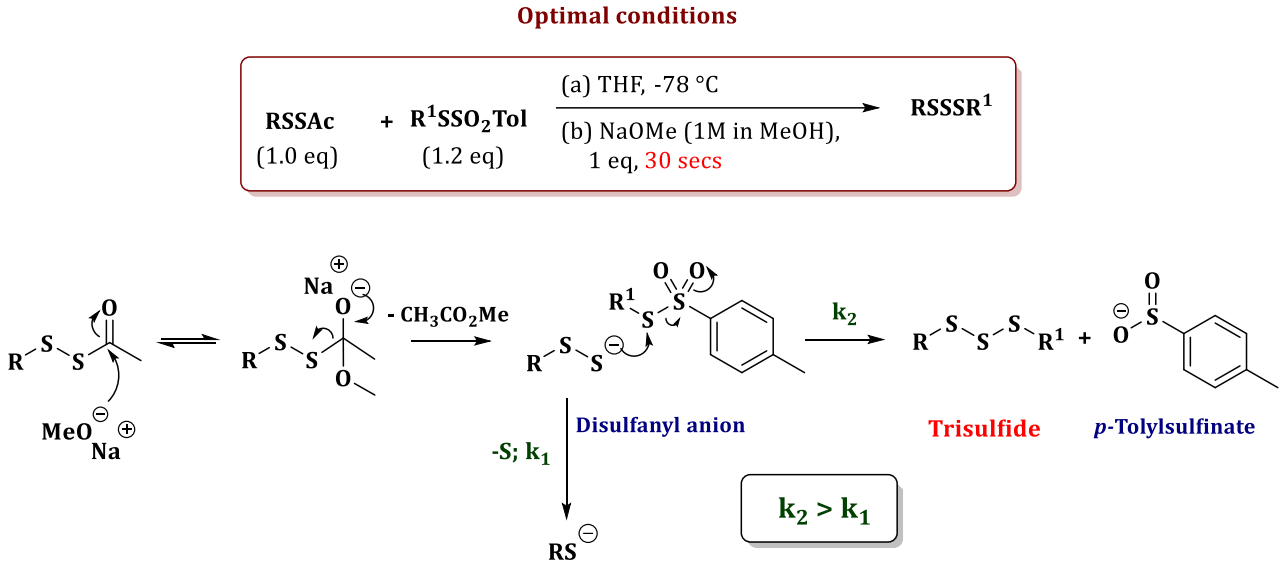

Scheme 4.8: Mechanism of our developed methodology.

In the upcoming section, we will discuss the application of this methodology in the synthesis of a diverse range of trisulfide libraries, which were designed for pursuing chemical biology studies on the cytotoxic mode of trisulfide action towards cancer cells.

4.3 Exploring the Scope of the Methodology

Having established a prototype now led us to explore the influence of the various R groups, which were chosen based on their lipophilicity, functionality, and electronic properties. Establishing scope was also important for addressing a comprehensive structure-activity relationship (SAR) trisulfide profile later in biology.

From a mechanistic standpoint, one had to take into account the influence of both R^1 (from the thiotosylate) and R (from the disulfanyl partner). Such groups, based on their influence on the reactivity of each reactant, could be classified into three main groups as: (i) aliphatic as a relatively non-activating or reactive group towards either the R^1STs sulfur electrophilicity or the disulfanyl anion nucleophilicity, (ii) allyl and benzyl as labilising groups for the R^1STs sulfur electrophilicity, and (iii) aromatic/heteroaromatic, comprising both electron-withdrawing and electron-donating groups as labilising for the R^1STs sulfur electrophilicity as well as the trisulfide product regarding exchange reactions. Our primary objective focused on targeting heterotrisulfides, which automatically encompassed homotrisulfides as a subset. However, we were already aware that category (iii) posed a challenge based on the results for HexSSSPh, **61**, in the first prototype reaction. Looking at the various combinations led us to conclude that nine were

possible as shown in **Table 4.5**, divided into three groups based on the reactivity classification above, keeping the R disulfanyl group constant for each group and varying the R^1 group within each group (one gets the same overall library the other way round). From here, each group was analysed empirically.

Table 4.5: Classification of trisulfides library based on R^1 functional groups

Entry	Type ($RSSSR^1$)
Group (i)	
1	Aliphatic-Aliphatic
2	Aliphatic-Allyl/Benzyl
3	Aliphatic-Aromatic
Group (ii)	
4	Allyl/Benzyl-Aliphatic
5	Allyl/Benzyl-Allyl/Benzyl
6	Allyl/Benzyl-Aromatic
Group (iii)	
7	Aromatic-aliphatic
8	Aromatic-Allyl/Benzyl
9	Aromatic-Aromatic

4.3.1 Group (i)

The first group studied was group (i) of **Table 4.5**, which covered three types (as entries in **Table 4.5**) of products all retaining an aliphatic R group from the disulfanyl partner while varying the three different R^1 groups of the thiotosylate. The results of yield after chromatography and purity by HPLC are given in **Table 4.6** corresponding to the various entries **1-3** in **Table 3.5** using the optimal conditions as shown in the Scheme. The scale was on mmol.

Table 4.6: Library of heterotrisulfides from group (i).

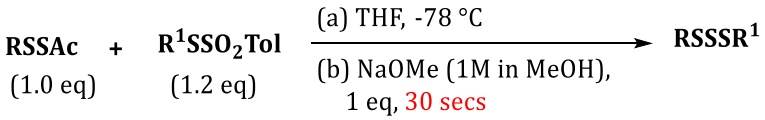

Entry	Type	R	R^1	Structure	Yield%[a]	Purity%[b]
1	Ali-Ali	*n*-Hex	$(CH_2)_3OH$	63 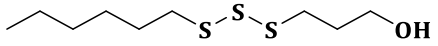	89	98
2	Ali-All Ali-Ben	*n*-Pr *n*-Hex	Allyl Benzyl	45 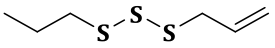 64 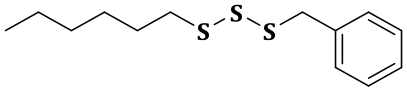	94 86	96 99
3	Ali-Aro	Dodec *n*-Pr ^{t}Butyl	Ph *p*-F-Ph 2-Pyridyl	65 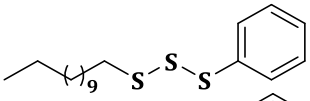 66 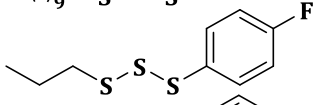 67 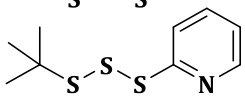	59 56 67	55, 91[c] 24, 94[c] 34, 87[c]

[a] *After column chromatography.* [b] *Measured by HPLC on a C18 column.* [c] *After preparative chromatography.*

Yields and purities with both aliphatic and allyl or benzyl thiotosylates for entries **1** and **2** were excellent, indicated that a reduction in reactivity of the thiotosylate partner in terms of sulfenylating electrophilicity going from allyl/benzyl to aliphatic (allyl contributes to positive charge stabilisation in the sulfenylation transition state) did not diminish the relative rates of sulfenylation vs desulfurisation detrimentally as depicted in **Scheme 4.8**. In confirming the structure of the trisulfide compounds, it was found that all three products were novel. However, the ^1H chemical shift data for the SCH_2 group aligned with those reported in the literature for similar structures.[115,139] Importantly, an examination of existing literature revealed a significant and trustworthy chemical shift difference in the ^1H NMR data for the methylene hydrogens of different types (allyl, benzyl, aliphatic) going from di- to tri- and tetrasulfide (the shift differences were less pronounced for the corresponding ^{13}C NMR data). A summary is given in **Table 4.7** below, showing good separation between the various classes of trisulfide. As observed, trisulfides from entries **1** and **2** (as **63**, **45** and **64**, respectively) all had their chemical shifts within the trisulfide range as illustrated in **Table 4.7**.

Table 4.7: Comparison of ^{1}H NMR chemical shifts (ppm) between synthesized trisulfide and literature values for aliphatic, allylic, and benzylic methylene protons in di-, tri-, and tetrasulfides

R of SCH_2R	Literature range of $CH_2(S)_nCH_2$ (ppm)			Compounds	δ for trisulfide (ppm)
	n = 2	n = 3	n = 4		
Aliphatic[139]	2.6-2.68	**2.85-2.90**	3.0-3.05	63 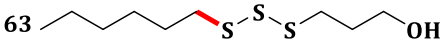 45 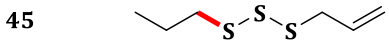 64 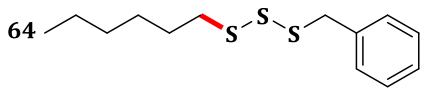	2.88 2.85 2.83
Allyl[446]	3.35-3.38	**3.50-3.55**	3.6-3.65	45 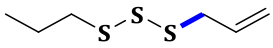	3.54
Benzyl[93,447]	3.70-3.85	**4.02-4.11**	4.16-4.24	64 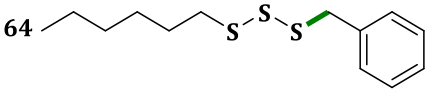	4.10

Similarly, the literature Infra-Red spectra of naturally occurring trisulfides like BnSSSBn[448] demonstrate a distinct absorption band in the range of 470-489 cm^{-1} for its S-S stretching vibrations. This differs from the corresponding disulfide BnSSBn, whose S-S stretching frequencies come higher up in the range 497-507 cm^{-1} as shown in **Table 4.8**. S-C absorptions were also considered but only values for the disulfide were found (in the 620-730 cm^{-1} range).

Table 4.8: Literature of Infrared spectroscopy absorptions for the S-S bond

Stretch	Di	Tri	Tetra
S-S	497-507[448]	470-489[448]	not reported
S-C	620-730 cm[448]	Not reported	not reported

However, the values for our compounds were generally at the upper end of this range or above (e.g., 788 cm^{-1} for **63**) as shown in **Table 4.9**.

Table 4.9: Infrared spectroscopy absorptions for the S-S bond of synthesised trisulfide

Compounds	Absorption (cm^{-1}) of the library	
	S-S	S-C

63 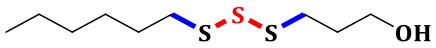	475	788
45 	476	722
64 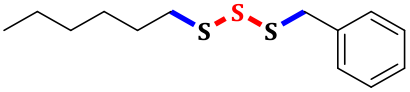	468	696

Owing to concerns about over-relying on the NMR and IR results for the analysis (remember that analytical purity data had been established using reverse-phase HPLC), an extra structure analysis technique was used in the form of high-resolution mass spectrometry (HRMS). Initially, we were concerned about instability of the S-S-S moiety during ionization, but ultimately, an atmospheric solids analysis probe ($ASAP^+$) gave a successful mass determination. The close agreement (well within the 25 mass units within 10,000) between the calculated and measured masses strongly supported the successful synthesis of the trisulfide compounds based on their $[M + 1]^+$ peaks as shown in **Table 4.10**.

Table 4.10: High-resolution mass spectrum fragments

Compound	$[M+H]^+$ obtained	$[M+H]^+$ calc.
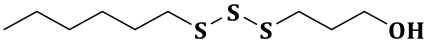	240.0677	**240.0676**
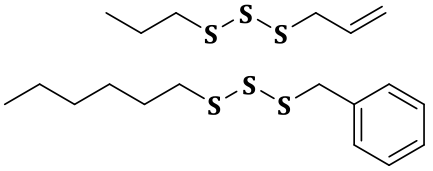	181.0186 273.0793	**181.0179** **273.0805**

Entry **3** within Group (**i**) involved one aromatic or heteroaromatic R group from RSTs, while keeping an aliphatic R group for the disulfanyl anion (with variations up to *t*-butyl) in which R was chosen as phenyl, *p*-fluorophenyl and 2-pyridyl as having an increasing degree of electron-withdrawal. The yields and purities obtained were given in **Table 4.6** before (recap below).

Table 4.11: Third class of hetero trisulfides from group (i)

Entry	Type	R	R^1	Structure	Yield%[a]	Purity%[b]

3	**Ali-Arom**	Dodec *n*-Pr ^{t}Butyl	Ph *p*-F-Ph 2Pyridyl	**65** 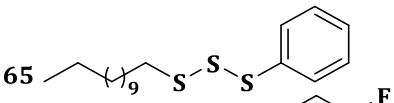 **66** 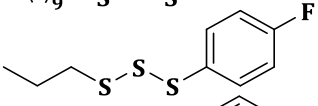 **67** 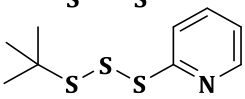	**59** **56** **67**	**55, 91**[c] **22, 94**[c] **34, 87**[c]

[a] *After column chromatography.* [b] *Measured by HPLC on a C18 column.* [c] *after plate chromatography*

As seen above, the yields ranged from 56% to 67% as significantly lower than before and also with significantly lower purities (22-55%) for the column chromatography products (as a single spot). Interestingly, the compounds on purification *via* plate chromatography gave high purities (in red in **Table 4.11**), indicating them to be stable towards the silica gel. Thus, it could be concluded that that the low purities after column chromatography were due to polysulfide by-products formed during the reaction – see the HPLC section for discussion. For characterisation, as before, the methylene chemical shifts for **65** and **66** in their ^{1}H NMR spectra (2.81 ppm for **65** and 2.82 ppm for **66**) were found to fall well within the aliphatic range of 2.85-2.90 (see **Table 4.7**). By comparison, compound **67** containing a *t*-butyl group, presented a more challenging scenario. The *t*-butyl peak in the ^{1}H NMR spectrum appeared at 1.41 ppm, which matched the range reported in the literature for trisulfides at 1.37-1.42 ppm[135] compared to disulfides at 1.31-1.34 ppm, but the difference was much smaller than the other ranges.[135,440]

In addition, distinctive peaks were observed in the IR spectra of **65**, **66** and **67** at 470 cm^{-1}, 473 cm^{-1}, and 476 cm^{-1}, respectively, which were in line with the trisulfide range as seen in **Table 4.8**. These data together with satisfactory HRMS data are shown in **Table 4.12**, all giving us confidence that the trisulfide entity in each case had been synthesised. HRMS data was not collected for the *t*-butyl derivative in view of its low purity (34% by HPLC).

Table 4.12: Characterization data: supporting trisulfides formation

RSSSR[1]	^{1}H NMR	IR	HRMS for [M+H]$^{+}$	
			experimental	calculated
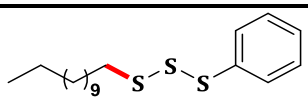	2.82	470	365.1399	**365.1407**

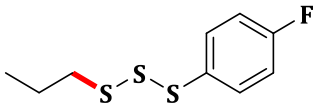	2.81	473	234.0007	**234.0010**
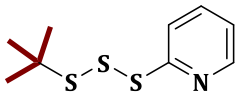	1.41	476	Not measured	**Not measured**

The HPLC data for **65-67** gave further encouragement for trisulfide synthesis as well as providing some important insights into the chemistry of these compounds. Each compound will be considered in turn, starting with the dodecyl phenyl trisulfide (DodecSSSPh) product, **65**, whose HPLC trace is shown in **Figure 4.4** below. It is important to highlight that the HPLC analysis throughout this thesis was conducted using reverse-phase HPLC in which separation was achieved through an isocratic solvent elution consisting of 70% acetonitrile (ACN) and 30% water, with a constant solvent composition throughout the analysis. Furthermore, apart from the aromatic ring in these compounds, UV-detection was also provided by the SSS chromophore, so homosulfides with R = dodecyl could also be picked up on the trace.

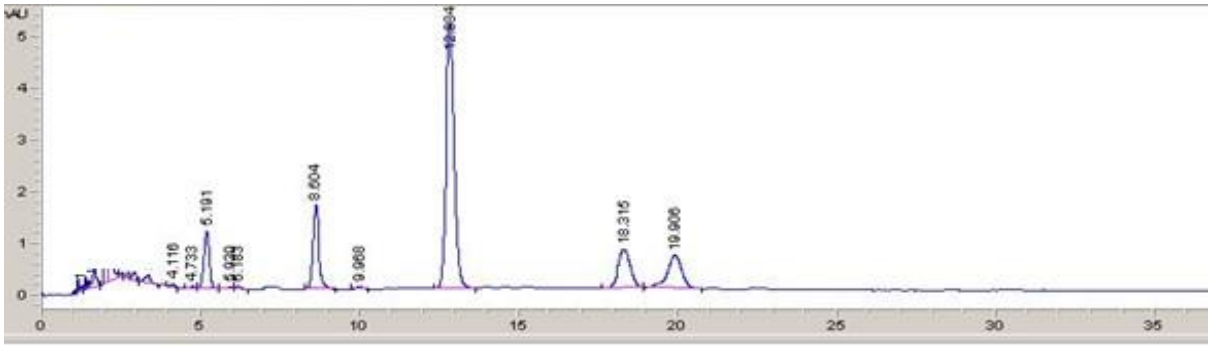

Retention time (min)	Height	Area %
5.19	4.54	7.34
8.6	21.3	13.02
12.8	61.6	55.18
18.3	6.95	11.46
19.9	7.23	11.27

Figure 4.4: HPLC purity of 65 purified with column chromatography.

The HPLC trace as shown in **Figure 4.4** above revealed five components in the single spot that eluted off the column. Subjecting a sample of it to plate chromatography improved the purity to 91% (in red in **Table 4.11**) as shown by its HPLC trace shown in **Figure 4.5**

below, revealing that the peak at 12.8 mins of the mixture was indeed the trisulfide, DodecSSSPh (seen as the major component in the ^{1}H NMR spectrum too).

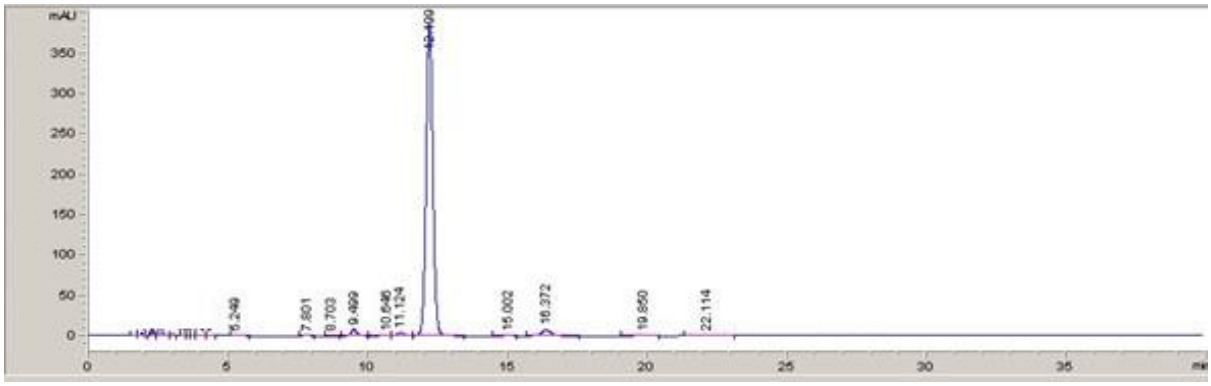

Retention time (min)	Height	Area %
8.5	101	1.5
12.8	412.0	91.2
19.4	153.8	2.3

Figure 4.5: HPLC trace of purified 65.

That left assignment of the other four components. The first rationale brought to bear was that entries **1** and **2** from group (i), also involving an aliphatic disulfanyl anion (RSS$^-$) as with entries **3** involving an aromatic/heteroaromatic group (from R^{1}STs), had returned extremely high purities of > 96% (**Table 4.6**) by HPLC of the single spot off the column. This was extremely important because it allowed desulfurization of the aliphatic disulfanyl anion being a contributory factor to by-product formation to be eliminated. This left the cause of by-product formation to be due to the presence of an aromatic group in the trisulfide product in which S-S exchanges would be driven by the stability of any aryl- or heteroarylthio group as a leaving group. Putting all this together led to the following mechanistic interpretation shown in **Scheme 4.9** for primary and secondary product formation.

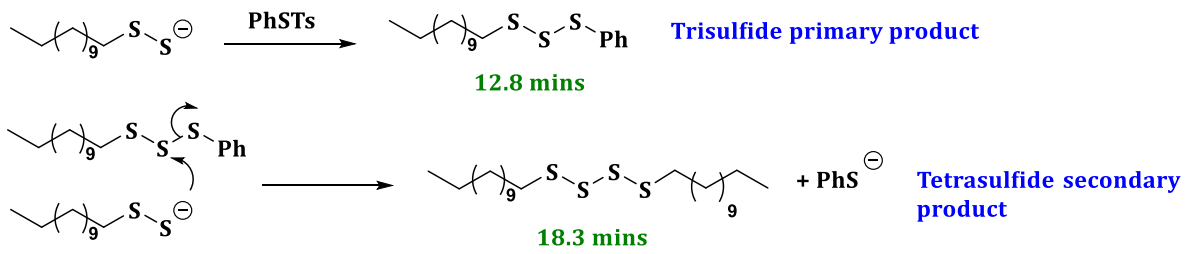

Scheme 4.9: Mechanism of primary and secondary product formation in reaction of 65.

Hence, the second HPLC peak assigned was for the dodecyl homotetrasulfide, eluting at 18.3 mins (11.5% peak area). The relatively large difference in retention time going from the heterotrisulfide to the homotetrasulfide was due to a decrease in polarity exchanging phenyl for dodecyl as well as the addition of an extra sulfur. That left the peak at 19.9 mins with the longest retention time and the two peaks with short retention times. Given that retention times increased with the number of sulfurs due to being reverse phase, the former (long retention time) was assigned as the aliphatic homopentasulfide while the former two both as disulfides, with the most polar 5.2 mins component assigned as diphenyl disulfide. A possible mechanistic rationalization of tertiary product formation is shown in **Scheme 4.10.**

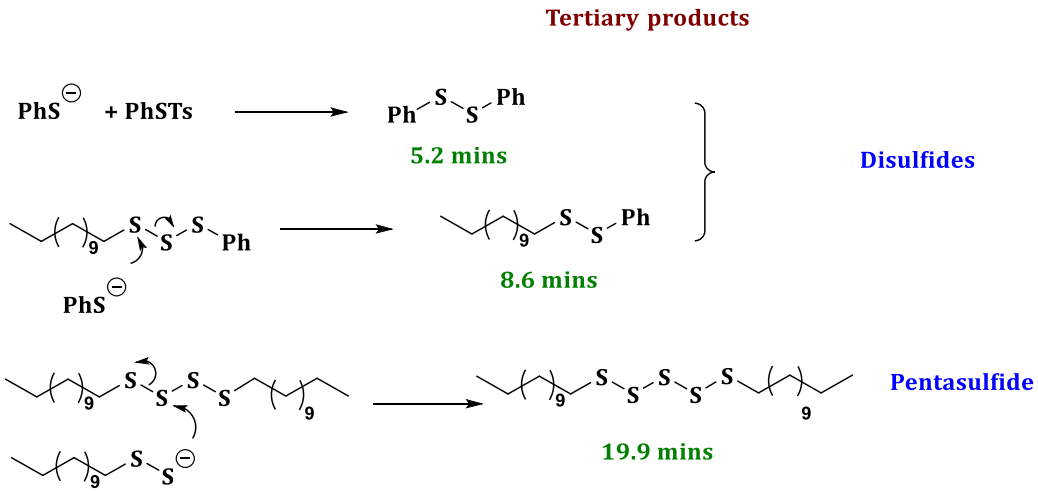

Scheme 4.10: Tertiary product formation for 65.

Clearly, a more exhaustive analysis could have been carried out bringing in mass spectrometry (LCMS) to verify product structures. Nevertheless, the use of polarity on the reverse phase as indicator in conjunction with mechanistic considerations provided a fairly comprehensive picture of the likely ongoings during the 30 seconds reaction time.
In a similar fashion, the HPLC data for the second compound, **66** for *p*-FPhSSSPr, which was isolated by column chromatography as a single spot provided additional understandings into the exchange mechanisms. The HPLC trace for **66**, obtained using an isocratic solvent elution of 70% acetonitrile (ACN) and 30% water as for **65**, is depicted in **Figure 4.6** below, revealing four main components.

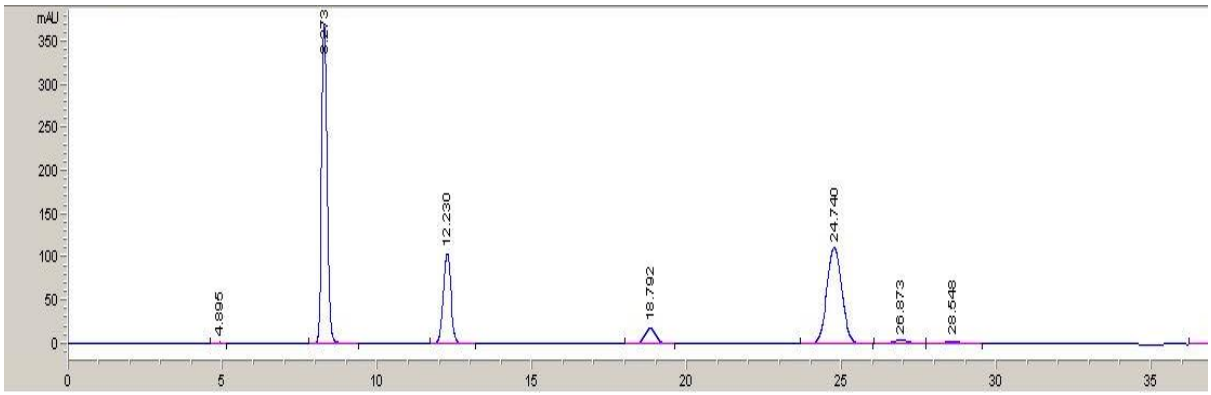

Retention time (min)	Height	Area %
8.2	369.5	38.1
12.2	179.4	23.9
18.7	69.1	4.85
24.7	111.6	32.3

Figure 4.6: HPLC purity of 66 purified with column chromatography.

As before with **65**, plate chromatography (its HPLC is shown in **Figure 4.7**) identified (by ^{1}H NMR and mass spectrometry) the trisulfide **66**, *p*-FPhSSSPr, as the 12.2 mins component, with a slightly lower HPLC retention time compared to that of **65** (12.8 mins) due to the presence of the fluorine.

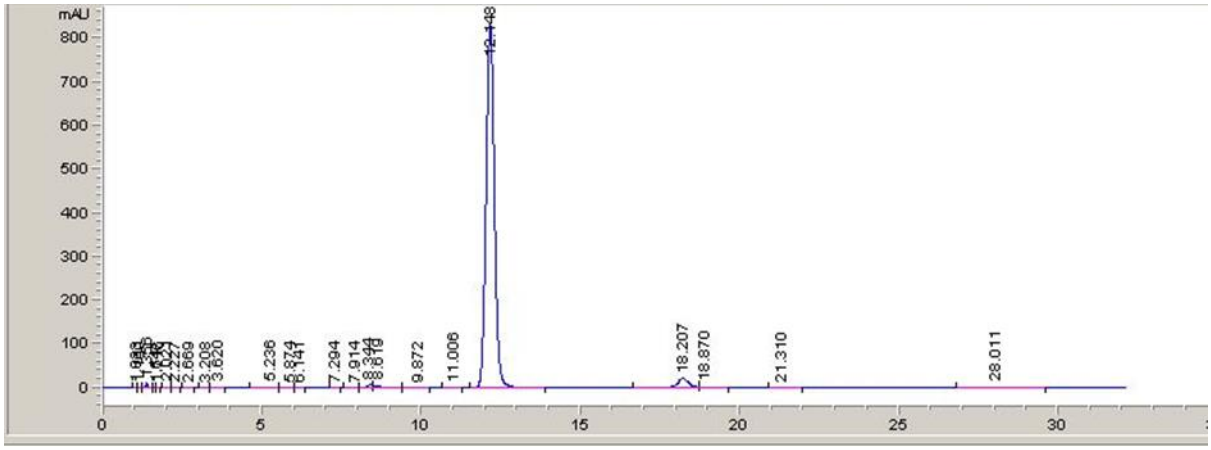

Retention time (min)	Area (mAU's)	Area %
5.3	15.2	0.5
12.14	2659.4	94
18.2	30	3.5

Figure 4.7: HPLC trace of purified 66.

However, what was noticeable from the trace was that the more polar component in the disulfide region was the dominant product at 38% (8.3 mins). By analogy to the trace for **66**, this component could be assigned as *p*-FPhSSPr. It was at this point that a second mechanistic idea emerged – that this disulfide could originate from the desired trisulfide via either a desulfurisation or an exchange with the perthiolate. Such mechanisms would take advantage of the fluorinated ring's ability to stabilise negative charge (Meisenheimer S_NAr type), with entropic release of sulfur as a major thermodynamic driver. The mechanisms are shown in **Scheme 4.11**. Given that the neutral trisulfide is relatively stable, we concluded that the perthiolate anion exchange is the one occurring.

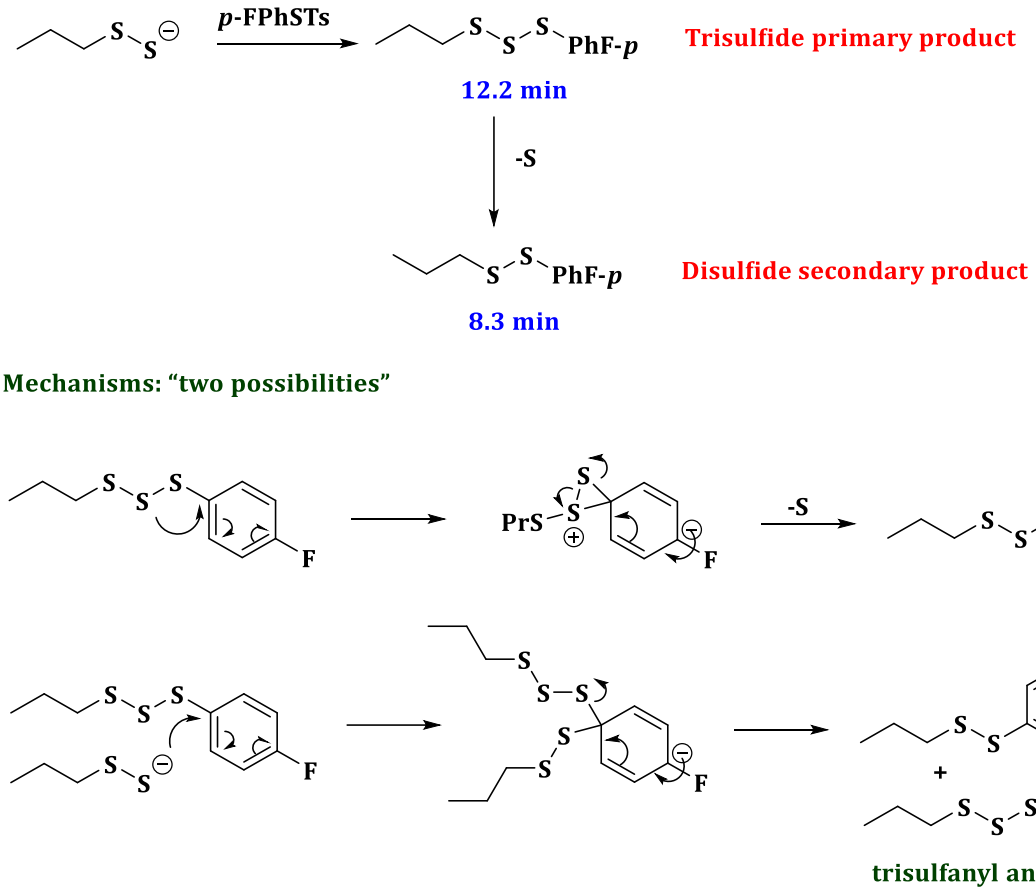

Scheme 4.11: Exchange mechanism for disulfide formation for 66.

In retrospect, it was realized that the disulfide PhSSDodec from **65** could also have arisen via the same exchange mechanism in which both *para*-carbon electrophilicity and stabilization of the negative charge in the Meisenheimer complex would have been lower (no fluorine). This would then account for the lower percentage of disulfide observed (13% at 8.6 mins).

The less polar (reverse phase) components eluting at 18.7 mins (5%) and 24.7 mins (32%) in **66** could be assigned as higher polysulfides, with the 18.7 mins component as the tetrasulfide (PrSSSSPr) in keeping with assignments made for **65** and formed via exchange involving the disulfanyl anion on the trisulfide. The 24.7-minute component suggested a much higher polysulfide such as a hexasulfide in view of its retention time, which invited the possibility of S-S (thiolysis) exchanges involving a polysulfide anion formed from disproportionation of the trisulfanyl anion from the disulfide reaction from **Scheme 4.11**. **Scheme 4.12** depicts these ideas.

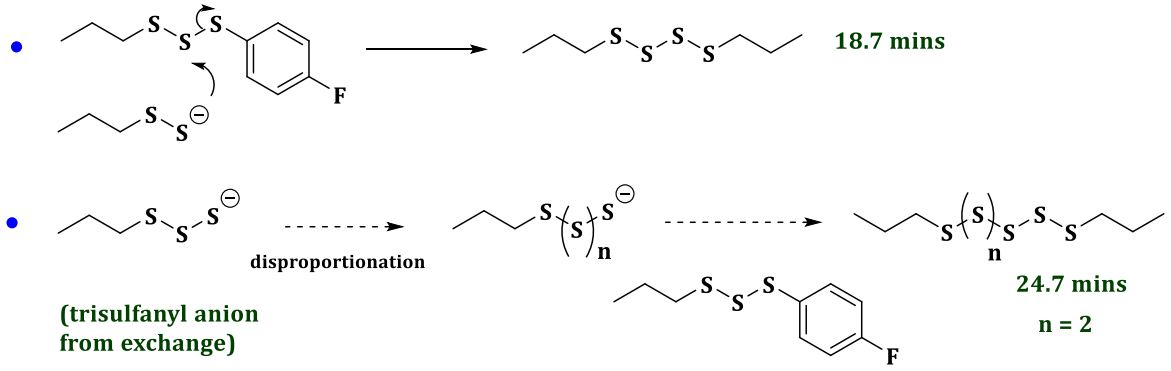

Scheme 4.12: Disproportionation of 66 to higher polysulfides.

The final aromatic case was the pyridyl *t*-butyl trisulfide target, **67**, made using *t*-butyl disulfanyl acetate and 2-pyridyl thiotosylate. The *t*-butyl disulfanyl acetate, **70**, was prepared using the "aromatic" method from *t*-butyl thiol, which was oxidized to the disulfide, **68** and reacted with iodine and sodium benzenesulfinate followed by reaction with potassium thioacetate. Meanwhile, 2-pyridyl thiotosylate, **72**, was produced via a similar procedure using the commercially available 2,2'-dipyridyl disulfide (aldrithiol-2), **71**, under the same conditions. Both preparation steps are depicted in **Scheme 4.13** below.

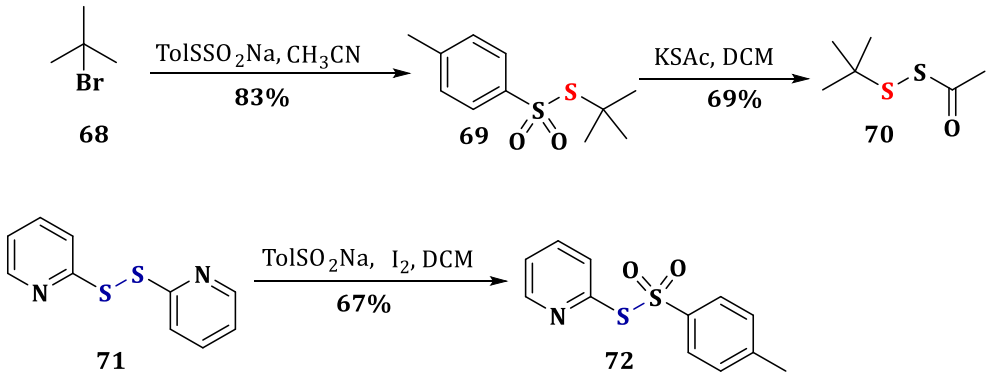

Scheme 4.13: Synthesis of RSSAc and RSTs of 67.

As before, a reaction was carried out at -78 °C for 30 secs and the major product isolated via column chromatography following a conventional extractive work-up to produce the HPLC trace shown in **Figure 4.8**, revealing two major components eluting at 5.8- and 8.8-mins accounting for more than 90% of the material.

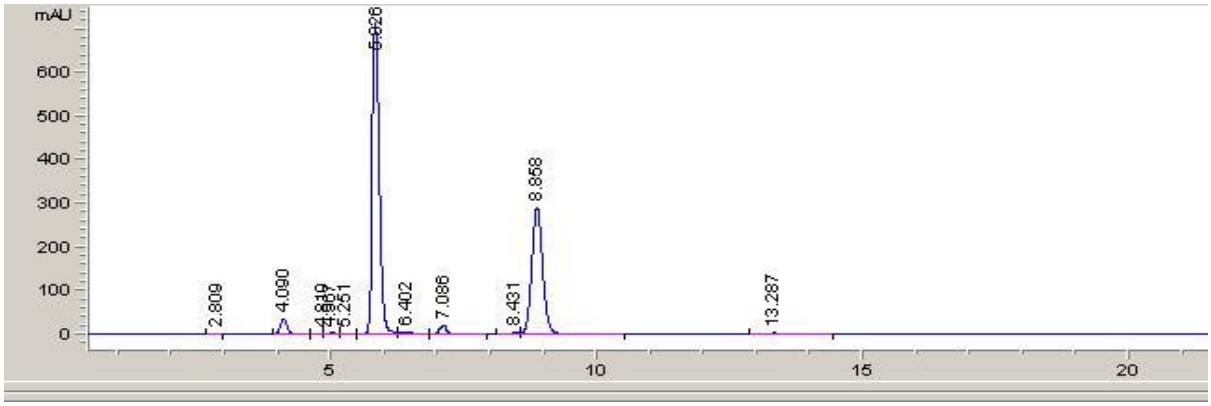

Retention time (min)	Area (mAU's)	Area %
4.1	316.5	2.68
5.8	716.6	58.6
7.0	65.6	2.02
8.8	3986.6	33.8

Figure 4.8: HPLC purity of 67 purified with column chromatography.

After preparative TLC analysis, the compound **67** eluting at 8.8 minutes (with a purity of 87) as shown in **Figure 4.9** was shown by spectroscopic analysis discussed on page **116** to be the desired trisulfide. The faster eluting component at 5.8 mins was assigned as *t*-butyl 2-pyridyl disulfide rather than di-*t*-butyl disulfide because of the polarity on TLC, and the three-minute difference between them was consistent with loss of a sulfur (making it more polar) in keeping with data from **65** and **66**.

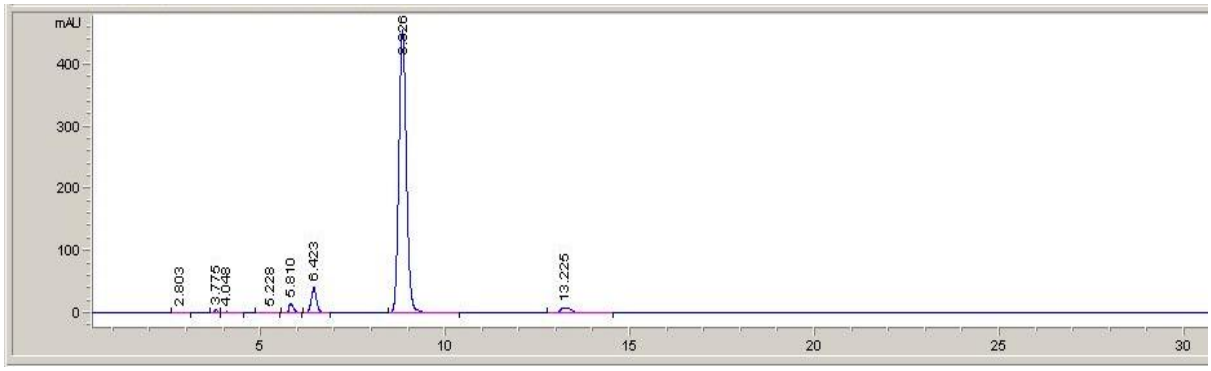

Retention time (min)	Area (mAU's)	Area %
5.8	27.3	2.11
6.4	472	6.7
8.8	6185.1	87.3
13.2	179.7	2.54

Figure 4.9: HPLC purity of 67 after preparative chromatography.

4.3.2 Group (ii)

Building upon the classifications in **Table 4.5**, we next studied Group (**ii**), keeping the disulfanyl R group as allyl or benzyl and varying the R^1 group as before from aliphatic to allyl/benzyl, propargyl and finally aromatic. In this part of the work, we also sought to explore functionality in the R^1 group using cysteine and sugar-based starting materials because of their relevance to the biology. The structures and results are shown in **Table 4.13**. As before, yields were based on column chromatography only without resorting to using preparative TLC. The purities were obtained from reverse-phase HPLC.

Table 4.13: Functional groups explored in aliphatic compounds

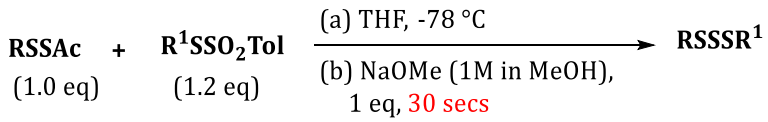

Entry	Type	R	R^1	Structure	Yield%[a]	Purity%[b]
4	**Allyl-Ali**	*n*-Allyl	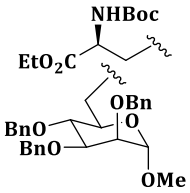	73 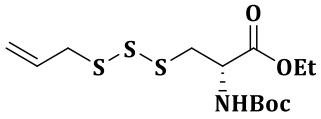	**97**	**98**
				74 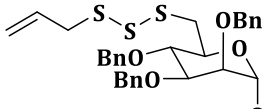	**63**	**84**
	Progyl-Ali	Proparg	n-Dodec	75 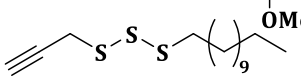	**52**	**96**
5	**All-Ben**	*n*-Allyl	Benzyl	76 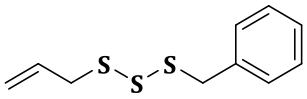	**76**	**91**
	Ben-Ben	Benzyl	Benzyl	54 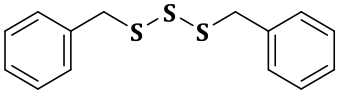	**89**	**95**

6	**Allyl-Arom**	*n*-Allyl	*p*-OMe-Ph	**77** 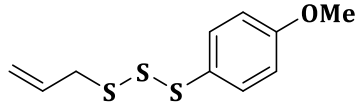	**64**	**97**

[a] *After column chromatography.* [b] *Measured by HPLC on a C18 column.*

We will start with the entries in **4** involving an allyl R group and an aliphatic R^1 group to give the same type of target trisulfide as those in entry **2** from group (i) (aliphatic - allyl). Target **73** was chosen based on having R^1 as the *S*-thiotosylate of cysteine, **79**, protected as its *N*-Boc and methyl ester. The thiotosylate is novel and its synthesis is shown in **Scheme 4.14** below using the tolylsulfinate disulfide (cystine) cleavage method.

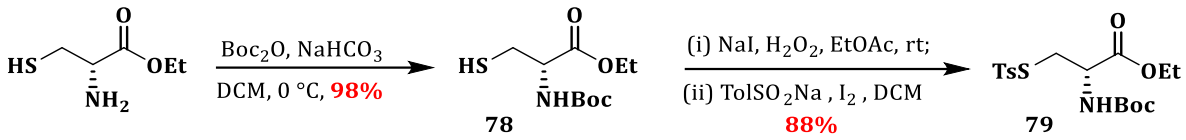

Scheme 4.14: Synthesis of CysSTs N-Boc, Me ester, 79.

By comparison, the mannose *S*-thiotosylate, **86**, synthesis for trisulfide **74** was a lot longer, involving six steps using the S_N2 substitution method with thiotosylate salt for thiotosylate formation. The required 6-iodide could be accessed using a literature sequence[449] as shown in **Scheme 4.15**. All synthesized compounds gave satisfactory NMR and HRMS data in accordance with literature data.[449,450]

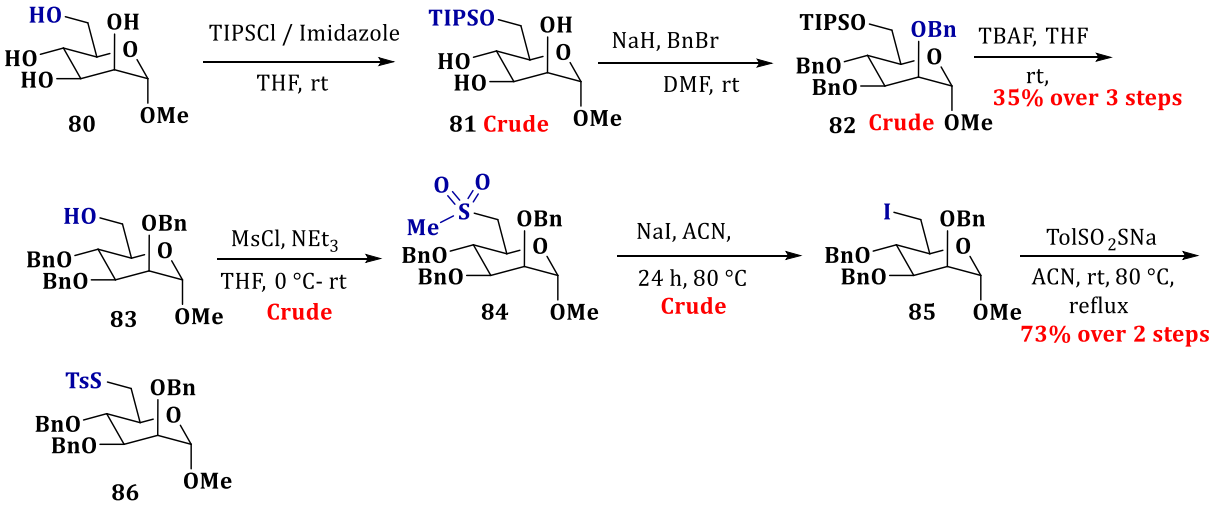

Scheme 4.15: Synthesis of mann-STs, 86.

Thereafter, each *S*-thiotosylate was used in slight excess (1.2 eq) under the standard conditions (30 sec run for each) with allyl disulfanyl anion in each case to generate the

trisulfide product after chromatography in 97 and 63% yield for **73** and **74**, respectively. In the Mannose case, despite achieving a full conversion of the limiting reagent, the yield was lower than expected, likely due to the small-scale reaction employed. Compounds **73** and **74** were new compounds for which the *S*-allyl methylene for each fell in the range expected for a trisulfide (3.52 ppm vs 3.36 ppm for a disulfide – see **Table 4.1**). Similarly, both ^{1}H and ^{13}C NMR data correlated for a trisulfide based on trends observed thus far. Finally, HRMS data as shown in **Table 4.14** gave definitive support for our trisulfide structures.

Table 4.14: Characterization data of compound 73 and 74

RSSSR[1]	^{1}H NMR		IR	HRMS $[M+H]^+$	
	$-SCH_2$	$-SCH_2$	S-S	calc.	obtained
73 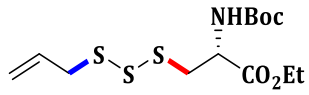	3.50	3.33	481	354.0869	**354.0867**
74 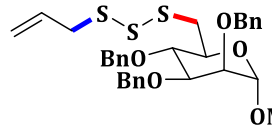	3.49	3.42	477	585.1813	**585.1803**

Finally, regarding purity, while cysteine derivative **73** returned an excellent single peak at a 98% purity, the mannose derivative, **74**, showed small slower eluting peaks as shown in the HPLC trace shown in **Figure 4.10** in a purity of 84%. This profile is reminiscent of the earlier aromatic-aliphatic trisulfides, suggesting some exchange reactions to furnish less polar homopolysulfides, possibly driven by steric strain release in the sugar.

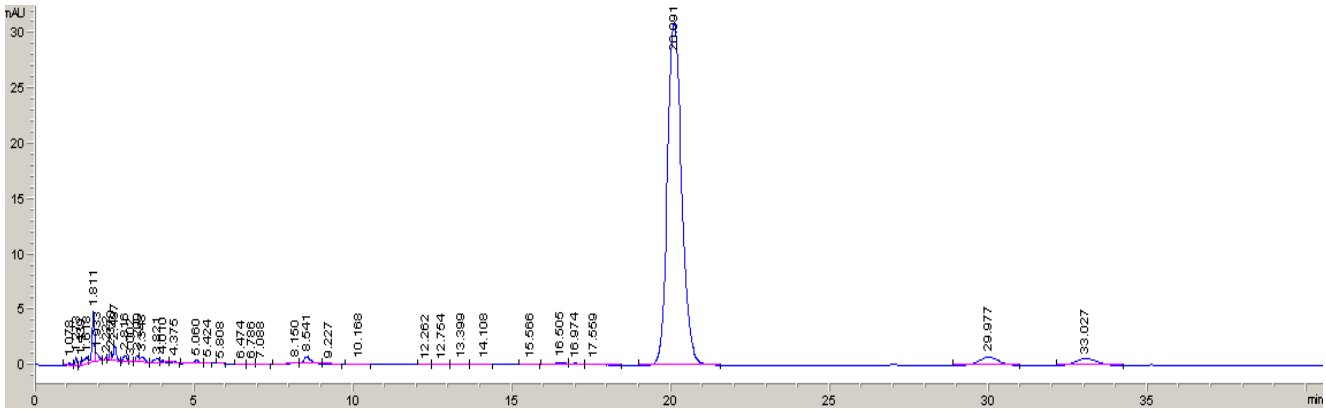

Retention time (min)	Area	Area %
1.81	17.2	2.38
8.51	11.7	1.02

20.1	961.2	84.1
29.9	32.4	4.83
33.0	29.2	4.56

Figure 4.10: HPLC purity of 74 purified with column chromatography.

Within the allyl-aliphatic variants, it was decided to extend the group for R to a propargyl as shown in **75** involving propargyl and dodecyl for the trisulfide groups, which was obtained in 52% yield and 96% purity, the lower yield probably reflecting the greater reactivity of the propargyl disulfanyl anion. Propargyl disulfanyl acetate, **88**, was synthesised by reacting propargyl bromide with the thiotosylate salt as shown in **Scheme 4.16**. This new compound, along with dodecyl thiotosylate, was thoroughly characterized.[451]

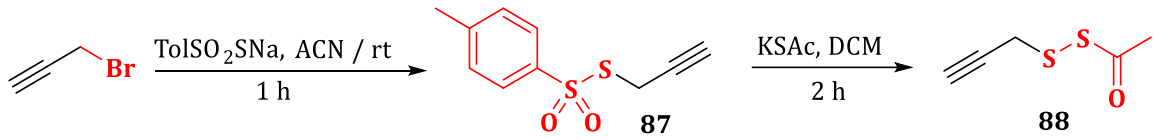

Scheme 4.16: Synthesis of propargyl disulfanyl acetate, 88.

Characterisation data for trisulfide product **75** as shown in **Table 4.15** supported trisulfide formation. Noticeably, the propargyl *S*-methylene was even more downfield compared to the equivalent allyl case (about 0.1 ppm) and ~ 0.7 ppm compared to an aliphatic methylene in keeping with the greater deshielding effect of the triple bond.

Table 4.15: Characterization data of compound 75

RSSSR¹	¹H NMR		IR	HRMS [M+H]⁺	
	-SCH₂	-SCH₂	S-S	calc.	obtained
75 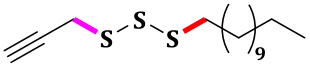	3.62	2.91	477	305.1431	**305.1429**

In summary for entry **4**, switching the groups round from entry **2** from an aliphatic disulfanyl anion / allyl/benzyl thiotosylate to an allyl disulfanyl anion and an aliphatic thiotosylate, perhaps unsurprisingly, gave a similar outcome.

Moving on to entry **5** involving the coupling of allyl with benzyl, we anticipated a routine set of coupling results, which was indeed what was observed. The allyl benzyl trisulfide **76** was, perhaps surprisingly a new compound and fully characterised (see **Table 4.16**),

while the homotrisulfide **54** (dibenzyl trisulfide) was a known compound, with the ^{1}H NMR methylene chemical shift agreeing with known data (see **Table 4.7**). Interestingly, the methylene chemical shifts were almost 0.5 ppm downfield going from allyl to benzyl (**Table 4.7**).

Table 4.16: Characterization data of compound 76 and 54

RSSSR[1]	^{1}H NMR		IR	HRMS [M+H]$^+$	
	-SCH_2	-SCH_2		calc.	obtained
76 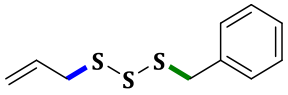	3.45	4.10	469	228.0114	**228.0100**
54 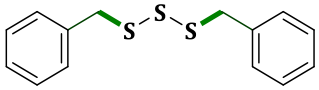	4.02		462	known[1]	**Not measured**

Finally, in entry **6** as the third and final variant of Group (**ii**), the R^1 group was chosen as an aromatic in the form of *p*-methoxyphenyl. One will recall that the aliphatic-aromatic category from Group (**i**) (entry **3**) had given issues with S_NAr product exchange reactions onto the aromatic ring, so we were interested to see what would happen now changing the disulfanyl partner from aliphatic to allyl.

Compound **77** (see Table 4.13) represented a new compound according to the Scifinder database. While its yield, as perhaps expected, was modest at 64%, notably, the HPLC purity was 97% as shown by the trace in **Figure 4.11** below. Importantly, this result supported conclusions reached on entries **3** in Group (**i**) in that the S_NAr exchange involving the disulfanyl anion onto the ipso aromatic carbon of the trisulfide is presumably disfavoured by the electron-donating *p*-methoxy group. Moreover, allyl disulfanyl anion was certainly not expected to have a reduced nucleophilicity compared to a saturated counterpart.

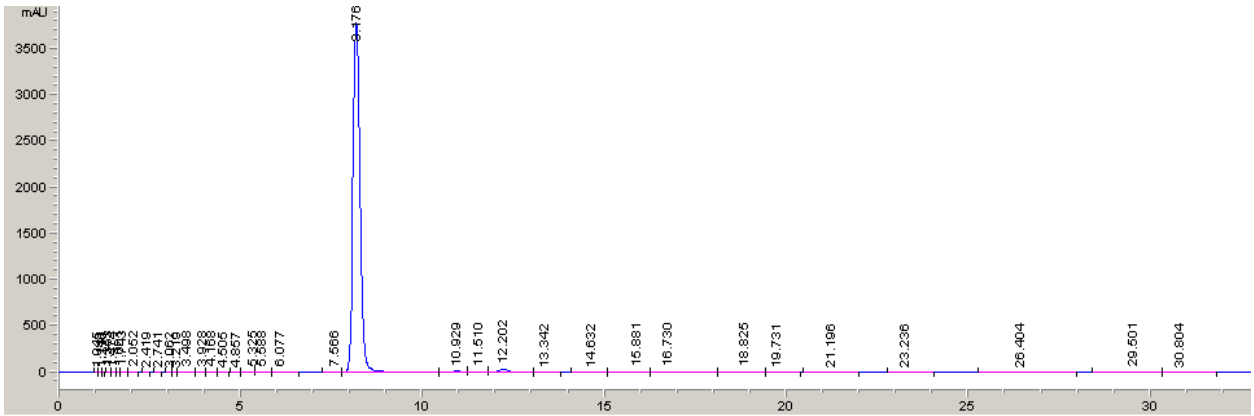

Retention time (min)	Area	Area %
8.20	3785.6	97.1
12.2	602.5	1.15

Figure 4.11: HPLC purity of 77 purified with column chromatograph.

For characterisation, while the methylene chemical shift for the *S*-allyl methylene was a tad low for a trisulfide at 3.43 ppm, the HRMS confirmed the structure, as demonstrated in **Table 4.17**.

Table 4.17: Characterization data of compound 77

RSSSR[1]	^{1}H NMR	IR S-S	HRMS [M+H]$^+$	
			calc.	obtained
77 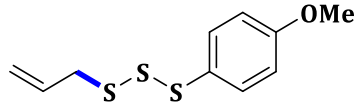	3.43	467	245.0100	**245.0129**

In this upcoming section, we will conclude using an aromatic disulfanyl anion.

4.3.3 Group (iii)

The final Group (**iii**) involved having the disulfanyl anion bearing an aromatic R group. Here, given our previous experiences with the aliphatic-aromatic results in entry **3** of Group (**i**), it was of interest to investigate how altering substitution within the aromatic R group impacted the stability and performance of the disulfanyl anion, as well as the product(s) outcome. Naturally, some of these couplings gave the same types of products described in groups (**i**) and (**ii**). The structures and results are displayed in **Table 4.18**.

Table 4.18: Functional groups explored in aromatic compounds

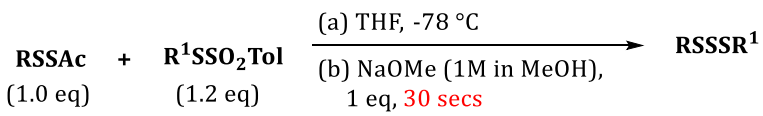

Entry	Type	R	R[1]	Structure	Yield% [a]	Purity %[b]
7	Arom-Ali	*p*-Tolyl	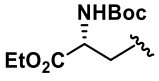	89 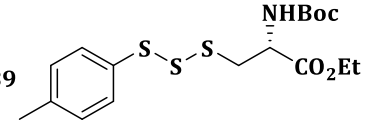	70	97

8	**Arom-All/Ben**	-	-	-	-	-
9	**Arom-Arom**	*p*-OMe-Ph *p*-OMe-Ph *p*-Me-Ph	Ph *p*-F-Ph *p*-F-Ph	**90** 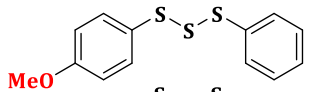 **91** 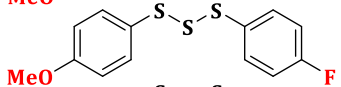 **92** 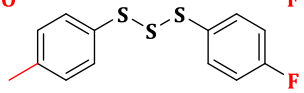	**64** **81** **89**	**78** **91** **60, 90[c]**

[a]After column chromatography. [b]Measured by HPLC on a C18 column. [c]After preparative chromatography.

Entry **7** marks the beginning of our exploration involving tolyldisulfanyl acetate, which was difficult to prepare from thiotosylate **94** (formed via the disulfide method) as shown in **Scheme 4.17** in 28% yield.

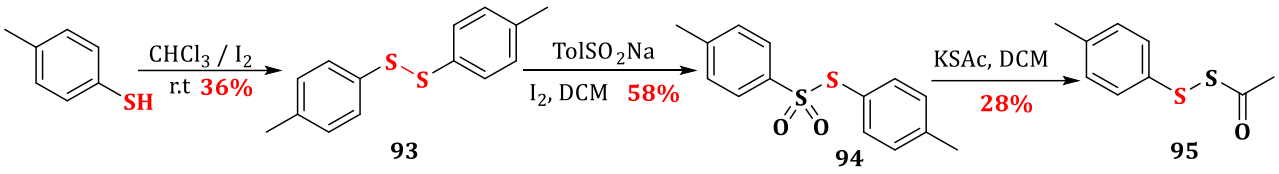

Scheme 4.17: Synthesis of tolyl disulfanyl acetate, 95.

Using the standard trisulfide formation conditions yielded a 70% yield of **89** after chromatography accompanied by a very high purity of 97%. As a new compound, **89** was fully characterized, with the main data shown in **Table 4.19**. Similar to its allyl counterpart, compound **73**, the *S*-cysteinyl methylene chemical shift of **89** of 3.36 ppm fell close to that of **73** at 3.33 ppm (refer to **Table 4.14**), which was somewhat downfield compared to that of simple alkyl methylene groups (2.85-2.90 ppm), presumably due to an inductive effect exerted by the cysteine moiety. However, the correct mass for the trisulfide was observed in the HRMS ($[M+H]^+$).

Table 4.19: Characterization data supporting trisulfide formation

RSSSR[1]	-SCH$_2$	IR	HRMS $[M+H]^+$	
			calc.	obtained
89 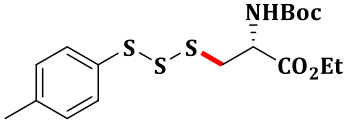	3.36	481	404.1024	**404.1018**

Finally, the high purity of 97% (trace not shown) for **89** deserves mentioning. In this case, the aromatic group was contained within the disulfanyl anion partner rather than the thiotosylate. For comparison purposes, it is fitting to compare this result with that of **65** from **Table 4.11** shown below in **Figure 4.12** formed via a dodecyldisulfanyl anion, and in which by-products were rationalized as being formed via S_NAr-type exchanges of the disulfanyl anion onto the *ipso* aromatic carbon of the trisulfide product.

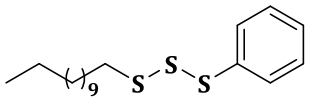

59% yield
55% purity

Figure 4.12: Results of Compound 65.

Hence, for entry **7**, although *p*-tolyl does have a modest electron-releasing group (Me) for suppressing any S_NAr exchange, it is considered more likely that the main reason for attaining high purity is that the nucleophilicity of the aromatic disulfanyl anion is reduced compared to that of an aliphatic case. This would be due to the lowering of its HOMO energy due to the aromatic ring.

Moving to entry **8** of (Arom-All/Ben) shows a blank in **Table 4.18** indicating that this combination was not attempted. Hence, for this type, we opted to leave access to this structural type using "the other way round" as R = allyl/benzyl and R^1 = aromatic as described in entry **6** (**Table 4.13**).

Finally, turning to the aromatic-aromatic trisulfide variants, which were expected to be the most challenging group to access in high purity, it is worth once again mentioning that these compounds are rarely discussed in the literature. As shown in entry **9**, **Table 4.18**, all three products (**90-92**) in this category yielded entirely new compounds, despite their relatively simple substitution patterns, with moderate to very good yields (64-89%) after column chromatography.

Their ^1H NMR spectra showed aromatic signals in the range of 6.80-7.50 ppm, showing correct proton integrations between the rings, but proof of obtaining the trisulfide once again required mass spectrometry in the form of HRMS for analysis as indicated in **Table 4.20**.

Table 4.20: Characterization data for 90, 91, 92

RSSSR^1	IR	HRMS [M+H]$^+$

		calc.	obtained
90 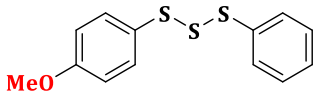	469	280.0050	**280.0053**
91 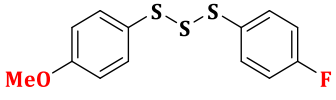	463	297.9956	**297.9957**
92 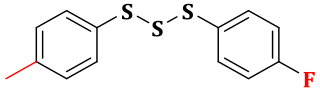	502	282.0007	**282.0026**

Ideally, we would have liked to have accessed aromatic disulfanyl anions (the RSS^- component) with an aromatic R group bearing either a strong electron-withdrawing group (F) or releasing one (OMe) with something in the middle (CH_3), but the *p*-fluorophenyl disulfanyl acetate couldn't be prepared; hence, only the methoxy and methyl variants for R were used. Equally, for the thiosulfonate component, *p*-fluorophenyl and phenyl (as a mid-way variant) were used. These research endeavours came relatively early in the PhD during method development, and in retrospect, it would have been more informative to have studied a broader range of substituents in both partners.

Following the normal reaction conditions and isolation by column chromatography as single spots, HPLC data again was needed to gain insight into the nature of the side reactions.

Starting with **90** from *p*-methoxyphenyldisulfanyl anion and phenylthiotosylate**,** the HPLC trace shown in **Figure 4.13**, returned a modest (and intermediate in relative terms) purity of 78% of the trisulfide, which eluted at 11.6 minutes. This was accompanied by a faster eluting by-product at 7.8 min and a slower eluting one at 17.7 minutes. Based on previous structural analyses, these were hypothesized to be a di- and tetrasulfide, respectively.

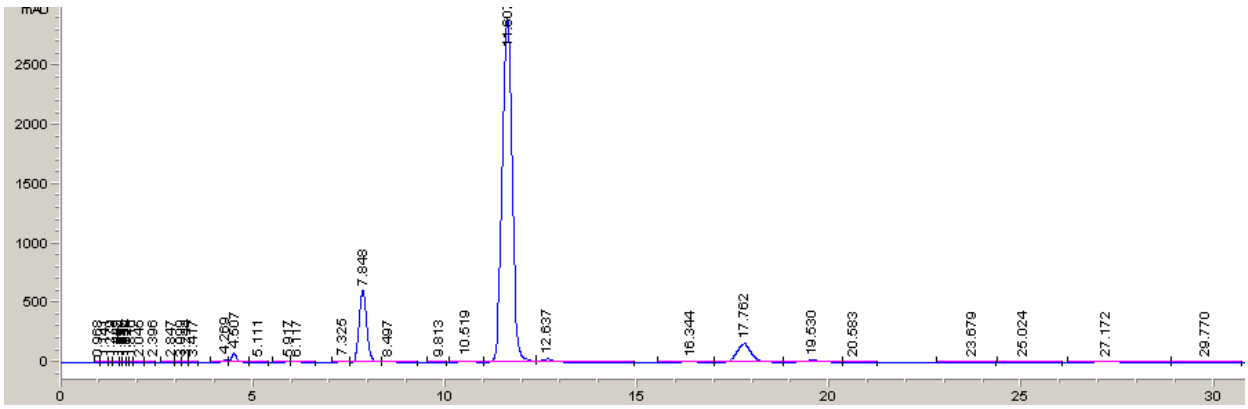

Retention time (min)	Area	Area %
7.8	7727.4	11.9
11.6	50715	78.2
17.7	3970	6.12

Figure 4.13: HPLC purity of 90 after purification with column chromatography.

Compared to the analysis on aliphatic-aromatic byproducts in entry **3**, it was even harder to know exactly what the structures were. However, in keeping with our ideas on S_NAr exchange, the disulfide may well have been due to S_NAr exchange by the methoxydisulfanyl anion at the phenyl ring of the trisulfide product rather than at the less stabilising methoxy-bearing ring as illustrated in **Scheme 4.19**. This would have generated *p*-methoxytrisulfanyl anion, which could have reacted with the thiotosylate to give *p*-methoxyphenyl phenyl tetrasulfide (not shown). Alternatively, the tetrasulfide might have arisen by an S-S exchange reaction between the disulfanyl anion and the middle sulfur of the trisulfide (with phenylthiolate as the leaving group) to furnish the homotetrasulfide (with *p*-methoxyphenyl groups), but as stated, these ideas were not followed up and are not represented schematically below in **Scheme 4.18**.

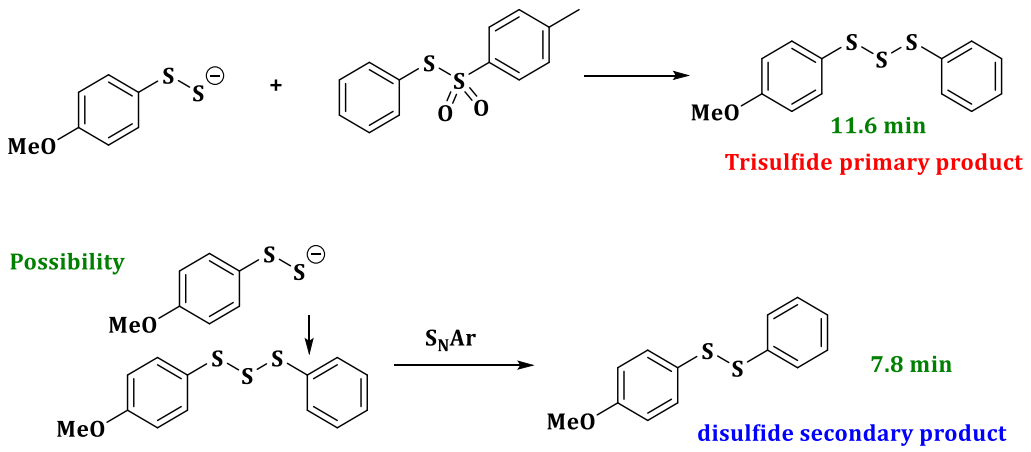

Scheme 4.18: Mechanism of primary and secondary product formation in reaction of 90.

In some contrast, the HPLC data for the second compound, **91**, revealed a significantly higher purity of 91% (see **Figure 4.14**). A likely explanation here is that sulfenylation by the highly electrophilic *p*-fluorothiotosylate is much faster, thus consuming the limiting and highly reactive disulfanyl anion much faster, resulting in less of the S_NAr exchange product. Equally an additional inference is that the *p*-methoxydisulfanyl anion is relatively

stable and reluctant to desulfurise to *p*-methoxphenylthiolate in which the charge would be in resonance with an electron-rich aromatic ring. This has important implications for results in the biological section.

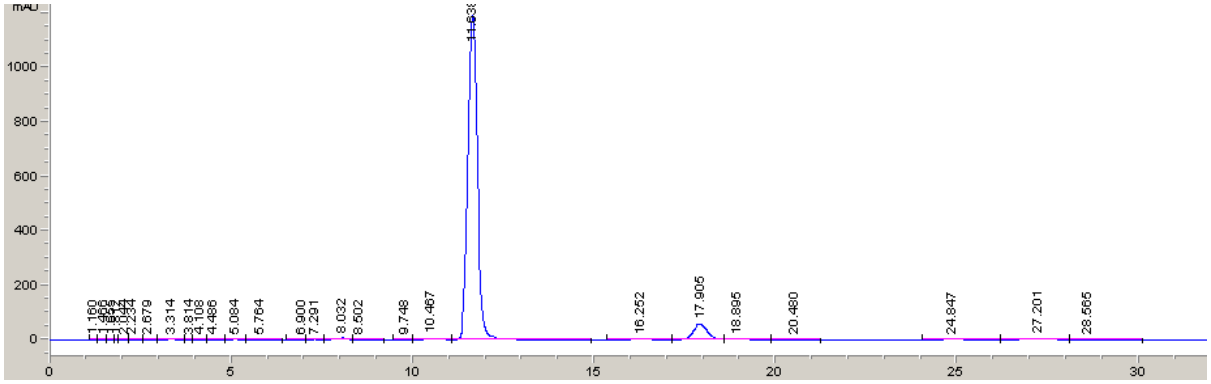

Retention time (min)	Area	Area %
11.6	21366	91.9
17.9	1481.8	6.37

Figure 4.14: HPLC purity of 91 after purification with column chromatography.

Finally, compound **92** was also isolated as a single spot off the column but HPLC revealed it to be only 60% pure, see **Figure 4.15**.

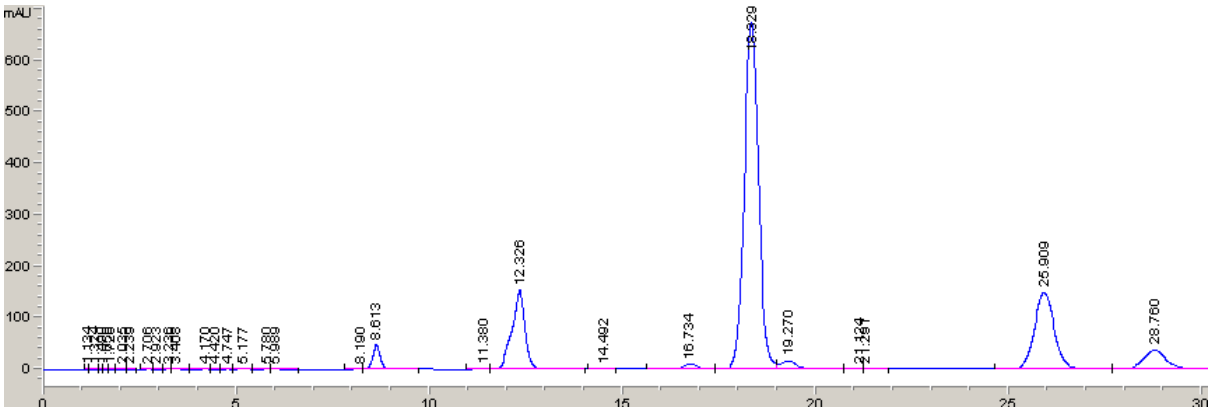

Retention time (min)	Area	Area %
8.61	660	2.28
12.3	3601	12.4
18.3	17301	59.7
25.9	5252	18.4
28.7	1482	5.12

Figure 4.15: HPLC purity of 92 purified with column chromatography.

The unexpected retention time of compound **92**, eluting at approximately 18.3 minutes, indeed raised questions about its classification as a trisulfide. Aromatic-containing sulfides are typically slightly more polar than their aliphatic counterparts and thus expected to elute faster on reverse phase as here; not slower. Given that throughout the study, the aliphatic trisulfides eluted between 11 and 12 minutes suggested that the 60% peak eluting at 18.3 minutes was in fact a tetrasulfide. Mass spectrometry in the form of HRMS did give the correct peak for **92** being a trisulfide (see **Table 4.20**) though, so at this point we decided, given this conflict of data, that further analysis could not be done as with the other cases. The compound could be purified using plate chromatography to a > 90% level as indicated by HPLC purity and retention time (18.2 mins) but noticeably was relatively more unstable than the other aromatic-aromatic trisulfides when stored at low temperature (-20 ºC) in the refrigerator.

Clearly, a follow-up study needs to be carried out to fully establish a complete mechanistic picture. However, a baseline picture on mechanism was generated and the primary aim of developing a new methodology for the chemical biology component of the study achieved. This revealed that our new method worked well with a range of R groups for both disulfanyl anion and thiotosylate components. Admittedly, the case of R = aromatic posed some challenges, but this was more to do with the lower stability of the products than the method itself. Finally, and importantly for the chemical biology aspect of the study, disulfanyl anions were shown to withstand a range of R groups in which dianion integrity was put down to the very low temperature employed of -78 ºC. This, we could see, was not going to hold for room temperature studies in which desulfurisation was expected, amongst other transformations.

CHAPTER 5: Structure-Activity Studies into the Cytotoxicity of Organotrisulfides in Cancer Cells

5.1 Trisulfide Cytotoxicity SAR Studies

Garlic-related trisulfides have emerged as promising candidates for both cancer prevention and treatment, demonstrating good anti-cancer activity in both *in vitro* and *in vivo* systems.[273,275,435,452] Their efficacy emphasizes the need for an understanding into their biological mode of action in cancer cells, which is the objective of this Chapter. Their cancer cell cytotoxicity is thought to proceed on a chemical level through thiolysis exchange with intracellular thiol targets, a process that in turn is dependent on a number of factors, some of which include the thiolysis reactivity, the resulting perthiol stability, and H_2S production. Thus, in the current chapter, the trisulfides synthesised in Chapter 4, separated into three small libraries, were investigated for structure-activity effects at inducing cytotoxicity in WHCO1 oesophageal and MDA-MD-231 breast cancer cells. We then directed our attention towards exploring the hypothesis of intracellular thiolysis exchange with a biological thiol. The common structural feature in trisulfides is the presence of the S-S-S functional group, which is the bioactive pharmacophore and central to its chemistry. As discussed in Chapter 3 (section **3.1**), once DATS (as a representative trisulfide prototype) enters the cancer cell, it modulates several cancer hallmark processes, most likely by *S*-thiolation.[310]

In Chapter 4, we synthesised many unsymmetrical trisulfide analogues (RSSSR') that contained a range of different R/R' groups, covering aliphatic, aromatic, and functionalized ones including sugar and an amino acid. These broad variations were intended to not only test out the methodology, but also to generate a variable trisulfide library for cytotoxicity studies. The next section will describe our findings on such studies.

5.1.1 Initial Cytotoxicity Screening

To start the study, a broad range of derivatives from the methodology study were selected. WHCO1 cells from an oeseophageal cancer cell line were chosen for the cytotoxicity studies, because of their relevance to the targeted cancer type and their established use in our previous research.[272,453-455] The cells in question were derived from esophageal squamous carcinoma cells of South African origin.[456] The MTT assay is a commonly used colorimetric method developed by Schemenn in 1983,[457] which involves the reduction

of yellow tetrazolium MTT to purple formazan by metabolically active cells as shown in **Scheme 5.1**.

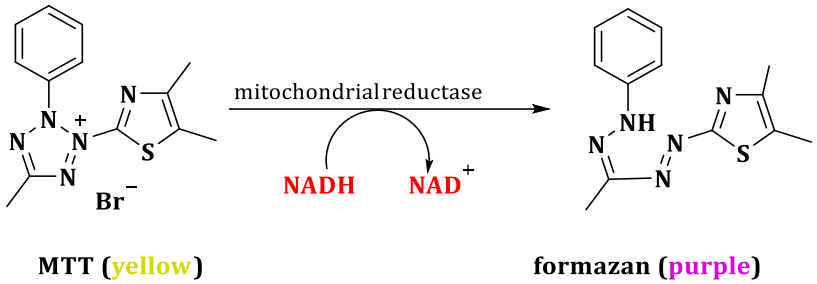

Scheme 5.1: MTT reduction in live cells: formation of purple formazan with absorption at 570 nm.

Despite its widespread application, the MTT assay has limitations; notably, the insolubility of the purple MTT-formazan (MTT-F) in aqueous media and the inherent toxicity of MTT.[458] This can be overcome by using the more recent XTT assay, but because of cost factors, we used the original MTT reagent in a 96-well assay format to test the cytotoxicity of our library. After seeding at a specific density, the cells were placed in an incubator overnight to allow for adhesion and progression to the growth phase. Each compound was added in two-fold dilutions and incubated with the cells for 48 h, after which the MTT solution was added to allow the viable cells to produce the MTT-F crystals. These crystals were then solubilized to give a purple solution which was quantified spectrophotometrically and analysed by fitting to a dose-response curve.

The selection of concentrations and the 48-hour incubation time for the MTT assay (**Table 5.1**) was based on prior findings that the cytotoxicity (IC_{50}) of ajoene derivatives decreases over time, indicating an increased cytotoxic effect with prolonged exposure. To capture a strong effect, the 48-hour timepoint was chosen. This timeframe aligns with previous studies on garlic-derived compounds, allowing for meaningful comparisons with existing data.

Table 5.1 and **Figure 5.1** show the IC_{50} values obtained for the sixteen-member library (Entries **1-16**) of heterotrisulfides. The IC_{50} values presented are an average of three to five independent determinations in which the relatively narrow standard deviations obtained affirm the reproducibility of our results. The numbering corresponds to Chapter 4 and the compounds are ordered in the Table generally in the order of aliphatic, functionalised aliphatics and aromatics for the R/R' groups of RSSSR' respectively. The

cytotoxicity IC_{50}s, defined as the concentration found to inhibit 50% of cell growth, are also shown.

Table 5.1: Cytotoxicity IC_{50}s of the unsymmetrical trisulfide library 1 in WHCO1 esophageal cancer cells

Entry	Compound No.	Structure	$IC_{50} \pm SD$ / µM*
1	**64**	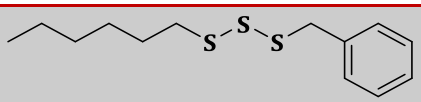	**2.5 ± 1.4**
2	**62**	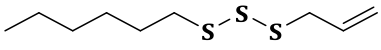	11.4 ± 14.5
3	**75**	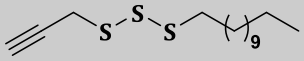	>200
4	**36 (DATS)**	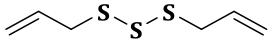	6.3 ± 4.4
5	**45**	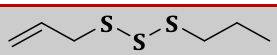	22.7 ± 13.8
6	**73**	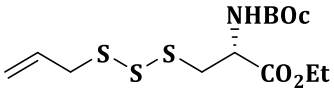	26.5 ± 12.9
7	**74**	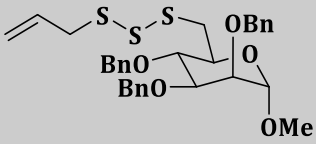	>200
8	**77**	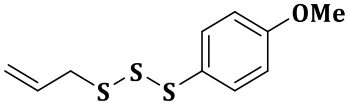	5.4 ± 7.8
9	**63**	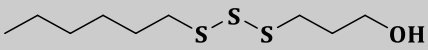	49.3 ± 14.6
10	**96**	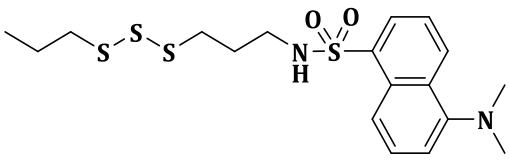	54.6 ± 29.3
11	**65**	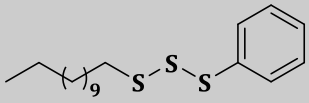	>200
12	**66**	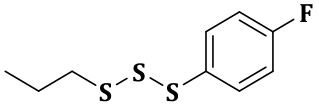	11.0 ± 4.4

13	**89**	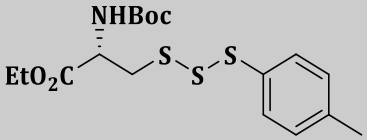	66 ± 45
14	**90**	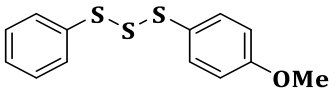	9.5 ± 1.1
15	**91**	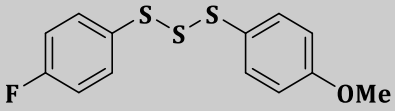	66 ± 19
16	**92**	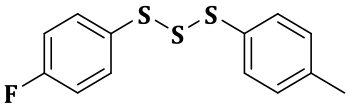	10.3 ± 2.1

** Each IC_{50} value represents the mean of three to five independent experiments*

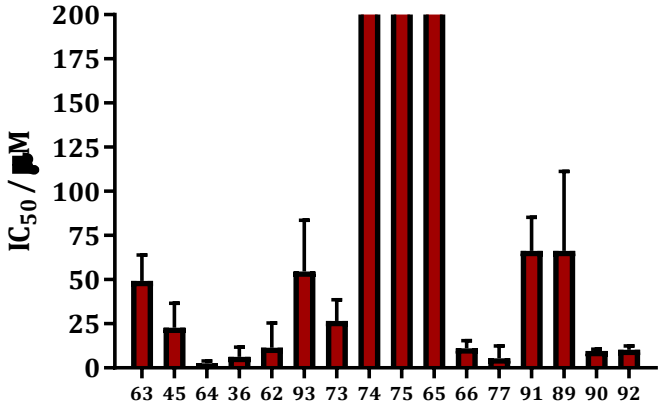

Figure 5.1: Cytotoxicity IC_{50}'s of the unsymmetrical trisulfide library 1 in WHCO1 cancer cells by the MTT assay. IC_{50} values as the mean ± SD from at least three independent determinations.

The cytotoxicity IC_{50}'s of the compounds covered a broad range of values from > 200 µM (for **65**, **74**, and **75**, compounds only tested up to 200 µM) to 2.1 µM for the most active analogue **64**. This is an interesting finding as all the compounds have a trisulfide functional group and yet the activity varies greatly depending on the side groups present. When attempting to fit the > 200 µM data to a dose-response curve, there was an indication that these IC_{50}s may lie around 2000 – 3000 µM (although such high concentrations can't be achieved in the assays and the fit is an estimation). Thus, it appears that the activity of the analogues may range some 1000-fold. Within the active analogues, the IC_{50}'s varied from 2.5 – 66 µM, some 30-fold.

Active compounds **62**, **63**, and **64**, all had a single hexyl substituent. The most active analogue of the series **64**, contained a benzyl substituent as the other R group, returning

an IC_{50} of 2.5 μM. Analogue **62**, with an allyl/hexyl combination (similar to DATS) was still very active with an IC_{50} value of 11.4 μM, while **63**, with a 3-hydroxypropyl substituent, displayed a reduced cytotoxicity of 49.3 μM, suggesting that hydrophilicity disfavours cytotoxicity. Within this series, compound **64** (entry 1) exhibited a 20-fold enhanced activity over compound **63** (entry 9), highlighting the superior effect of a benzyl over the hydroxy-bearing group.

Examination of compounds all featuring an allyl group as in **45**, **62**, **73**, **74**, and **77** revealed further insights. This functional group is present in the parent natural product trisulfide DATS (compound **36** as entry 4), with an IC_{50} value of 6.3 μM. Analogue **45**, with a propyl group on the other side, displayed a 4-fold decreased cytotoxicity (22.7 μM) compared to DATS, and was similar in activity to the amino-acid-bearing derivative **73** (entry 6), whereas the benzylated sugar derivative **74** (entry 7) was inactive. The most active analogue, close in activity to that of DATS, was the *p*-methoxy substituted phenyl trisulfide **77** (entry 8), although generally, aromatic trisulfides are more unstable.

Comparing derivatives with a propyl group on the one side with allyl, dansyl, and fluorophenyl on the other side (compounds **45, 96** and **66** respectively), showed the dansyl analogue **93** to be the least active and the fluorophenyl derivative, **66**, to be quite active at 11 μM.

Within the aromatic compounds, no clear trends emerged. Most of the phenyl-substituted analogues were quite active with IC_{50} values around 10 μM, except for **91**, which had a reduced activity of 66 μM, which appears to be an outlier compared to the other phenyl trisulfides. However, it is pertinent to emphasize that phenyl-bearing trisulfides are far less stable than their aliphatic counterparts and thus less attractive for further studies in cancer cells.

Since the very inactive compounds all had long aliphatic side groups, we wondered if lipophilicity may be playing a determining role in the cytotoxicity trends. To test this, we plotted compound Log IC_{50} vs LogP (as the Log of the partition coefficient of the compound between octanol and water, which increases, therefore, with increasing lipophilicity) as seen in **Figure 5.2**. It can be seen that no correlation was observed between cytotoxicity and the LogP, although very inactive compounds (**65**, **74** and **75**) appeared to be above a lipophilicity threshold, which is probably important. LogP values of each derivative are depicted in **Table 5.2.**

Table 5.2: Lipophilicity LogP values of unsymmetrical trisulfides from library 1

Compd no	**62**	**63**	**45**	**64**	**65**	**66**	**73**	**74**	**75**	**77**	**89**	**90**	**91**	**92**	**36**	**96**
Lipophilicity	5.1	4.0	3.8	6.1	8.6	5.0	3.8	7.6	7.1	4.6	5.0	4.6	5.7	6.3	3.7	5.7

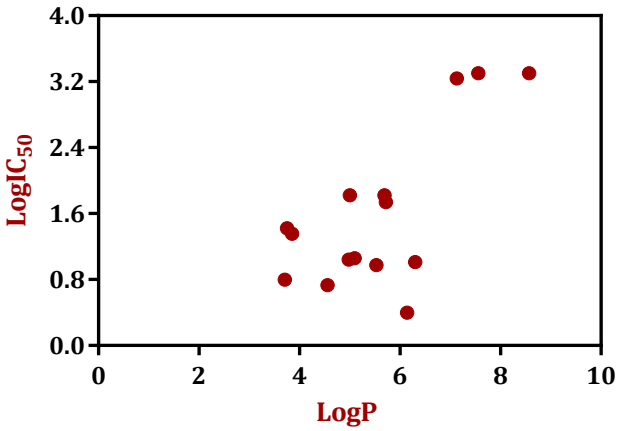

Figure 5.2: Plot of Log IC_{50} against Log P for the 16 unsymmetrical trisulfides in Library 1.

The poor IC_{50} results of compounds **65**, **74**, and **75** are likely attributed to their high lipophilicity, as indicated by their LogP values. These compounds cluster together as the least active, suggesting that their increased solubility in lipids rather than in aqueous environments may negatively impact their cytotoxicity. In summary, there does not appear to be an activity trend from this data that can be linked to an obvious structural parameter. Thus, apart from lipophilicity, the chemical reactivity of the SSS moiety (i.e. its electrophilicity) and its dependency on the R groups is probably a key factor in determining cytotoxicity trends. This came across as somewhat surprising since electronic transmission effects into the trisulfide moiety didn't look to be that varied. However, this notion was taken forward to the subsequent chemical biology design phase. On lipophilicity, the most active trisulfide, hexyl-benzyl **64**, was the only analogue in the series with a benzyl group. Benzyl groups are considered somewhat lipophilic which enables interaction with hydrophobic regions of biological membranes.[305,459] In biological systems, lipophilicity plays a crucial role as it influences a compound's permeability across cell membranes and its distribution within tissues. Hence, higher lipophilicity often correlates with increased cellular uptake and bioavailability; however, excessively high lipophilicity can lead to poor solubility, metabolic instability, and potential toxicity.[460] All things considered, though, benzyl looked to be an interesting candidate for trithio-reactivity modulation via substitutions in the aromatic ring.

5.1.2 Refining the Library

Next, we directed our attention towards the development of a more focused library to produce more active trisulfides, and also to gain further structure-activity insights. Since the benzyl derivative was the most active in the previous series, we designed our next library around this substituent. The allyl group was also selected as it returned active analogues and is found in the natural trisulfide DATS (**Figure 5.3**). Indeed, dibenzyl trisulfide is also a naturally occurring trisulfide called DBTS (**Figure 5.3**). Thus, we synthesised a hybrid of the two called ABTS (allyl benzyl trisulfides).

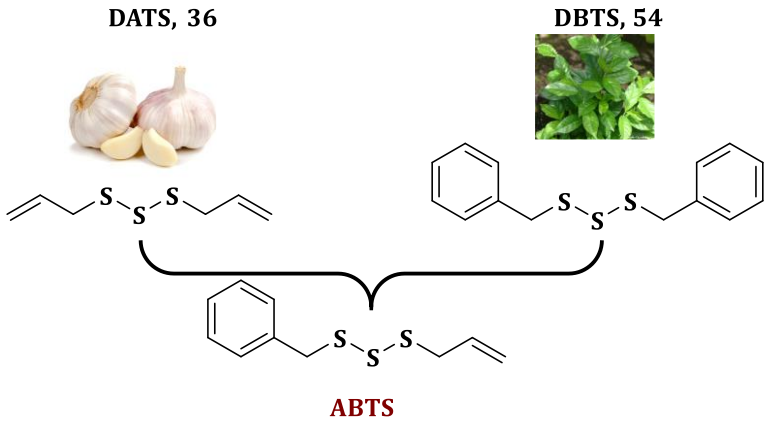

Figure 5.3: Backbone to the new library as a hybrid of two naturally occurring trisulfides DATS, 36 and DBTS, 54.

There is a large body of literature supporting the anticancer activity of DATS, both in in *vitro* and in *vivo* models (summarised in section 3.9 of the literature review). Similarly, the natural product trisulfide DBTS also shows impressive activity. Indeed, evidence indicates that DBTS is a superior anti-cancer agent to DATS where DATS is reported to have IC_{50}s in the micromolar range (56.1- 31.6 μM)[461] on various in vitro cancer cell lines, DBTS is reported to be approximately 100-fold more active with IC_{50}s in the nanomolar range (around 340 – 840 nM).[308]

5.1.3 Structure-Activity Studies into Benzyl-Allyl Hetero Trisulfides

The ABTS library was synthesised first with substituents at the *para*-position as hydrogen, fluorine, chlorine, bromine, methyl, methoxy, and trifluoromethyl based on their range of electronic and steric effects as well as commercial availability of the benzyl halide or thiol (for preparing BnSTs). *p*-Nitro as substituent was identified, but *p*-nitrobenzyl thiotosylate was unstable, a chemical feature of some significance later. The synthesis of this library followed our established methodology in Chapter 4 as shown in

Scheme 5.2 in which using the benzyl component as the thiotosylate partner worked the best.

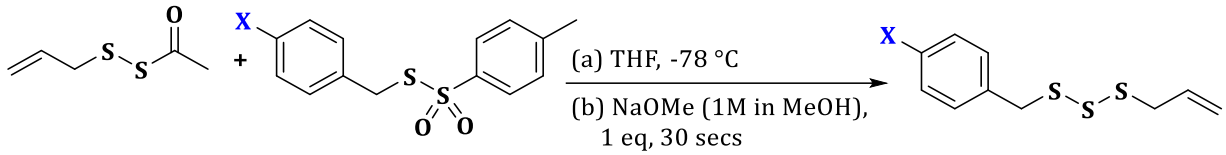

X (H;76: 66%, **F;97:** 51%, **Cl;98:** 93%, **Br;99:** 42%, **Me;100:** 75%, **OMe;101:** 71%, **CF_3;102:** 76%**).**

Scheme 5.2: Synthesis of the heterotrisulfide library 2 analogues containing benzyl-allyl substituents.

All of the trisulfides were characterized using a combination of NMR, HRMS, IR, and HPLC spectroscopy. The diagnostic feature in the ^{1}H NMR spectrum, indicating formation of the trisulfide, was the presence of the benzylic methylene singlet in the range 4.00-4.05 ppm[93,447] as well as an allyl methylene peak in the range 3.46-3.54 ppm[446] according to the literature as summarised in **Table 4.7** in Chapter 4. Shown below in **Figure 5.4** is a representative ^{1}H NMR spectrum obtained for the benzyl-allyl derivative, **76**.

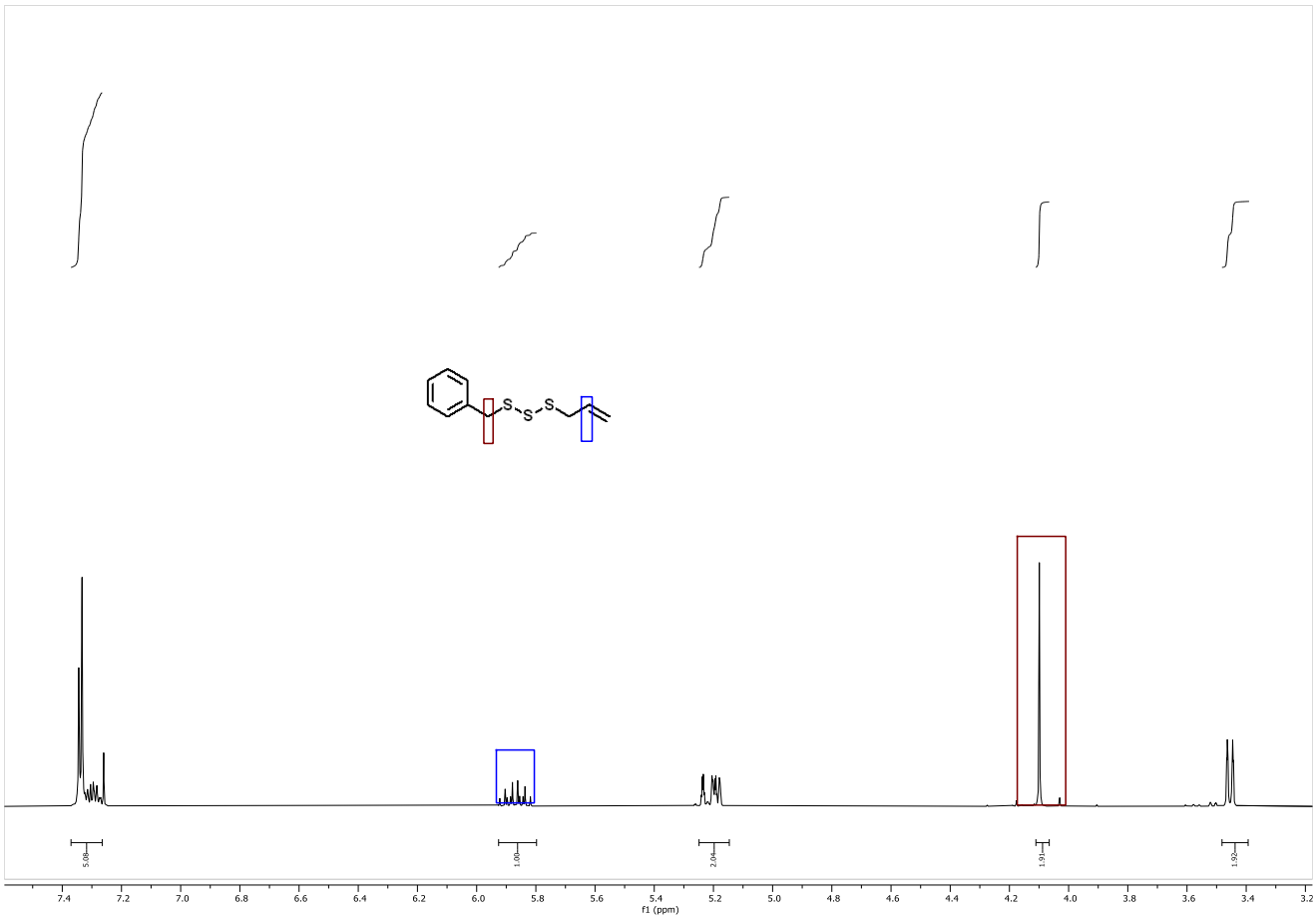

Figure 5.4: ^{1}H NMR spectrum of 76.

Following synthesis and characterization of the library (see experimental section in Chapter 6), we proceeded to explore their cytotoxicity effects on WHCO1 cancer cells. As before, the IC_{50}s obtained are displayed as an average and SD of three to five independent determinations (**Table 5.3** and **Figure 5.5**), but this time with lipophilicity (p), size (MR), and Hammett constants (σ_p) indicated for SAR purposes.

Table 5.3: Library 2 of benzyl-allyl trisulfides: WHCO1 cytotoxicity IC_{50}, Hammett Constant (σ_p), lipophilicity (π), and size (MR)

No.	Structure	IC_{50} (Ave ± SD (μM) *	σ_p	π	MR
76	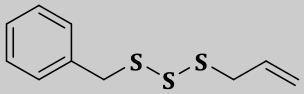	**1.7 ± 0.79**	0	0.00	0.103
97	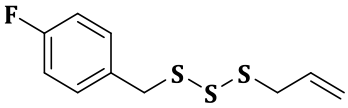	**1.2 ± 0.12**	0.062	0.15	0.092
98	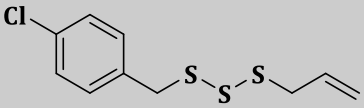	**1.4 ± 0.34**	0.227	0.70	0.603
99	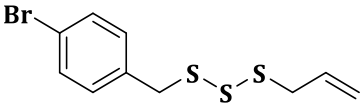	**3.4 ± 2.1**	0.232	1.02	0.888
100	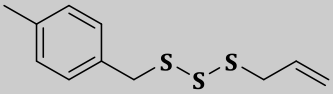	**0.47 ± 0.15**	-0.17	0.52	0.565
101	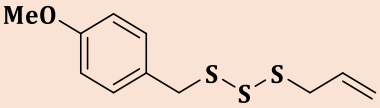	**0.16 ± 0.07**	-0.268	-0.02	0.787
102	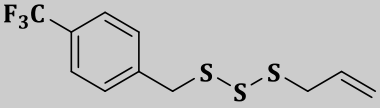	**6.5 ± 1.03**	0.54	0.88	0.502

** Each IC_{50} value represents the mean of three to five independent experiments*

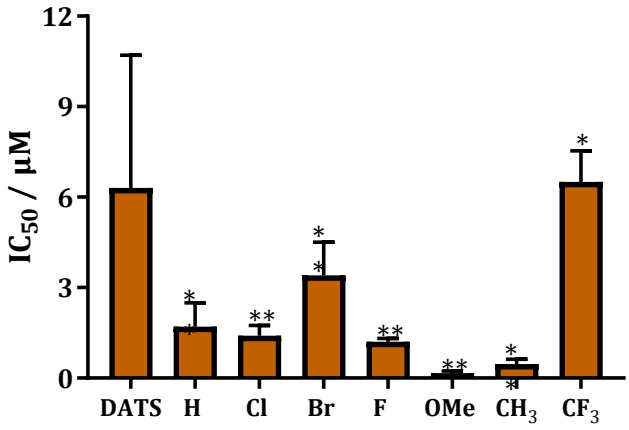

Figure 5.5: IC_{50} values for the benzyl-allyl Library 2 trisulfides.

The cytotoxicity IC_{50} values within the compound library were found to range some 40-fold, from 0.16 to 6.5 µM, indicating a substantial effect imparted on trisulfide activity from the *para*-substituent attached, vindicating conclusions reached from the basic SAR study that reactivity of the SSS moiety as modulated distally was key. Comparing these values to those in the larger, more diverse Library 1, some compounds in this set exhibited even more superior activity to the lead compound **64** (see **Table 5.1**). In this case, the benzyl-allyl derivative had similar activity to the benzyl-hexyl derivative **64** in Library 1, indicating a comparable potency going from hexyl to allyl (2.5 to 1.7 mM respectively).
The introduction of fluorine or chlorine substituents in **97** and **98**, returned similar cytotoxicities of 1.2 µM and 1.4 µM, respectively. However, the bromine substituent in **99** led to a slight reduction in activity of 3.4 µM. Conversely, the introduction of a methyl group in **100** significantly increased activity with an IC_{50} value into the nanomolar range of 0.47, while the methoxy group in **101**, exhibited the highest activity of 0.16 µM. These findings indicate that electron-donating groups enhance cytotoxicity in these benzyl-allyl trisulfides. Both methyl and methoxy are electron donating groups with methoxy being strongly electron donating due to n-p_p resonance. In support of this hypothesis, incorporation of an electron-withdrawing trifluoromethyl substituent in **102** notably reduced cytotoxicity, making it the least active in the series at 6.5 µM. To explore the role of electronic effects further, we looked at the Hammett constant as a likely quantitative marker. We also looked at other physical parameters that might be important such as lipophilicity (π) and molecular refractivity (MR) as an indication of size.

5.1.4 SAR Analysis of the Benzyl-Allyl Library 2

The lipophilicity (Fig 5.6**A**), molecular refractivity (Fig 5.6**B**) and the *para*-Hammett constant (Fig 5.6**C**) was plotted against the $LogIC_{50}$.

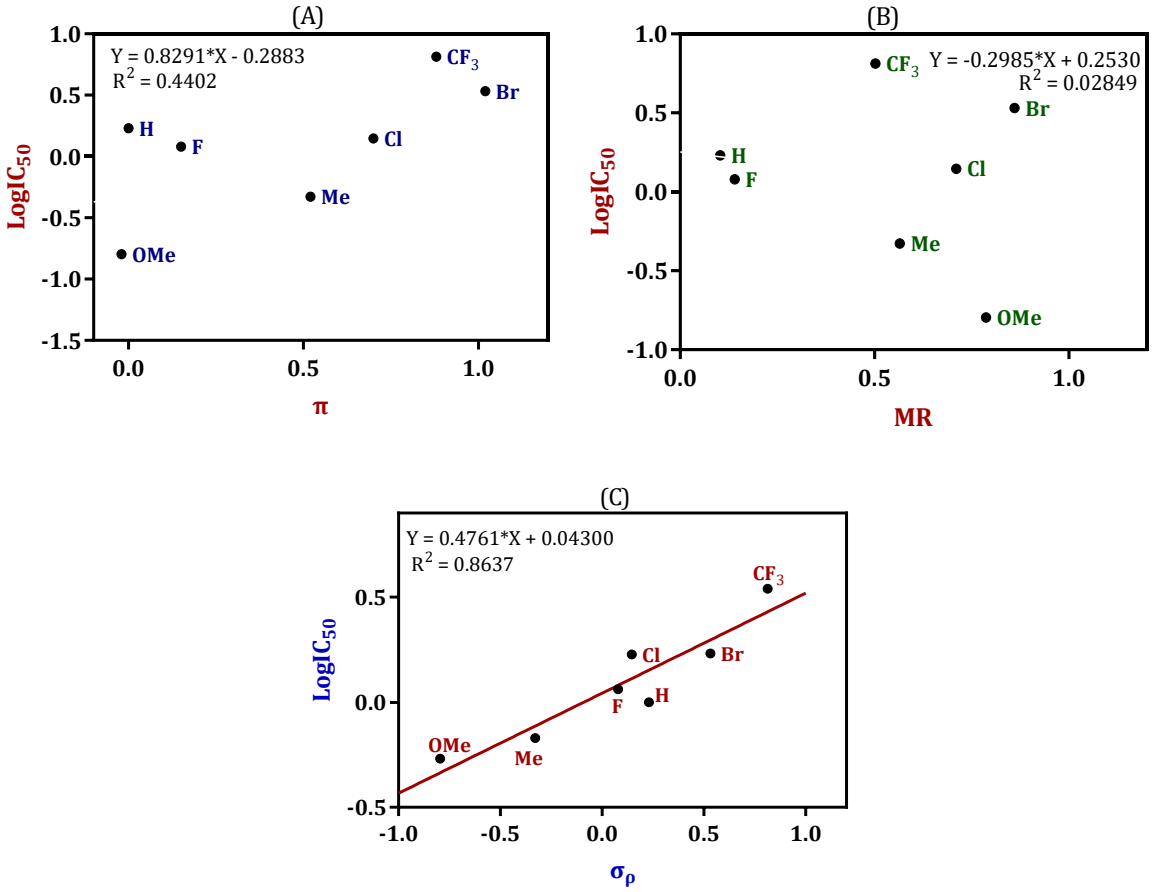

Figure 5.6: Plot of (A) lipophilicity (π), (B) Molar refractivity (MR) and (C) *p*-Hammett Constant (σ_p) of the *p*-benzyl substituent vs $LogIC_{50}$ of the benzyl-allyl trisulfide Library 2.

No trend was observed for the lipophilicity (**Fig 5.6**A, R^2 = 0.4405, p = 0.1040, ns) or substituent size MR (**Fig 5.6**B, R^2 = 0.02849, p = 0.7175, ns). However, a strong linear relationship was observed between $LogIC_{50}$ and the *para*-Hammett constant, conforming to the equation $LogIC_{50} = 0.47\sigma_p + 0.043$, with an R^2 value of 0.864 and a *p*-value of 0.0025 (***). This significant correlation indicates that ring activating substituents enhance cytotoxicity against WHCO1 cancer cells.

5.1.5 Structure-Activity Studies into Library 3 of Benzyl-Benzyl Homo Trisulfides

Next, we investigated structure-activity relationships in homotrisulfides that contained only a *para*-substituted benzyl R group on both sides of the trisulfide. This was chosen in view of the emerging medicinal chemistry prominence of DBTS and fluoropacin. Consistent with our structural design in the hetero series, we opted for the same analogous substituents for the homo-Library 3. Again, the synthesis of compounds **54**, **103-108** followed our established methodology, using identical conditions as outlined in Chapter 4. **Scheme 5.3** provides a summary of the structural details and yields achieved in the synthetic process.

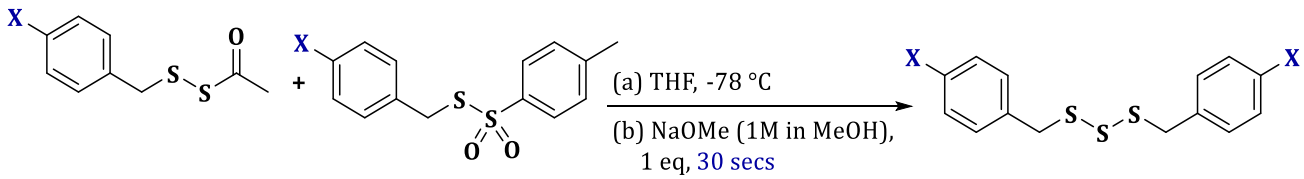

X (54 (H; 89%), 103 (F; 77%), 104 (Cl; 67%), 105 (Br; 68%), 106 (Me; 93%), 107 (OMe; 78%), 108 (CF_3; 62%)

Scheme 5.3: Synthesis of the benzyl-benzyl homotrisulfide Library 3.

As anticipated, the homobenzyl trisulfides only exhibited a benzylic methylene singlet, which was in the range 4.00-4.05 ppm consistent with literature trisulfide data as before.[93] **Figure 5.7** depicts a representative ^{1}H NMR spectrum of the *p*-OMe derivative, **107**, showing key features that confirm its structure and purity. The benzylic singlet appears at 4.02 ppm, as well as a signal for the *p*-methoxy group and an AB system for the 1,4-disubstituted aromatic hydrogens. These spectral features are consistent with the expected structure of the trisulfide, indicating a high level of purity.

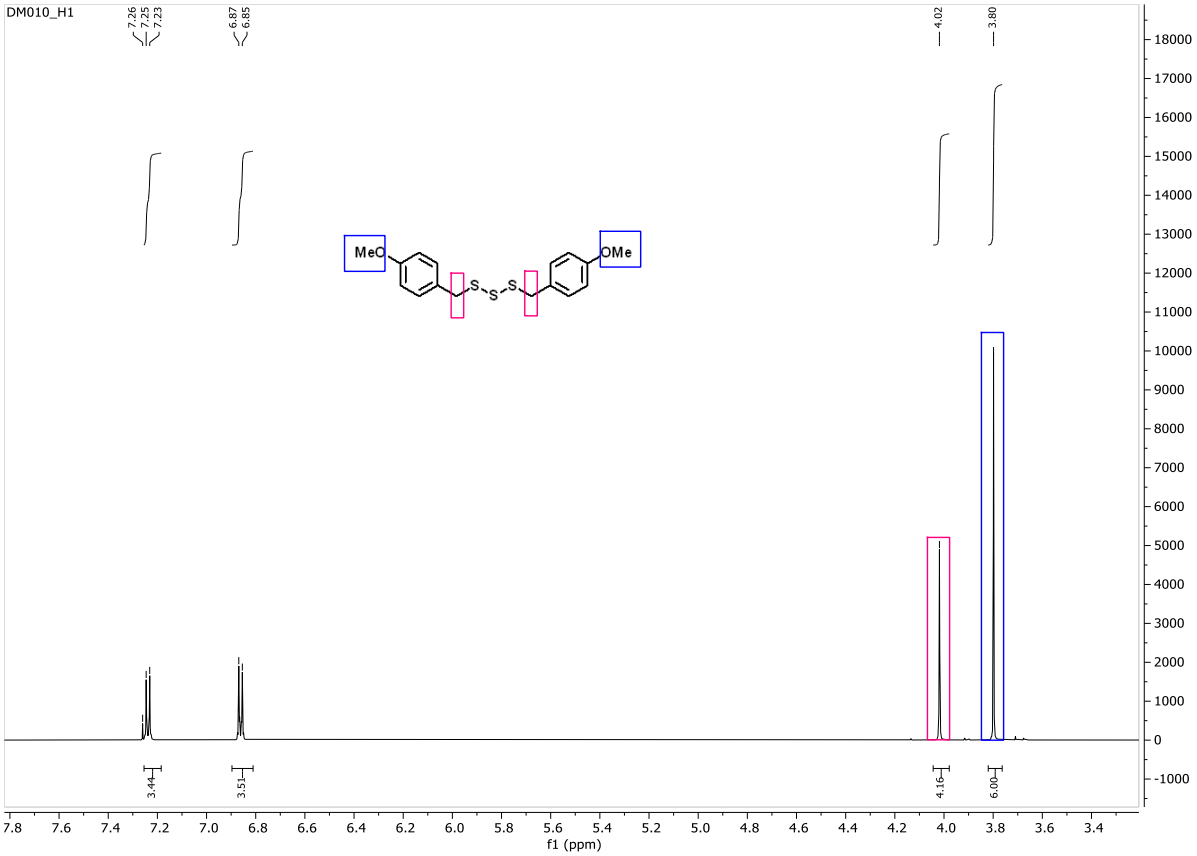

Figure 5.7: ^{1}H NMR spectrum of 107.

Following the successful synthesis and characterization of Library 3, we conducted the cell proliferation assays on WHCO1 cells. **Table 5.4** and **Figure 5.8** show the results.

Table 5.4: Cytotoxic IC_{50s} of homobenzylic Library 3 trisulfides against WHCO1 cell proliferation

No	Structure	IC_{50} (Ave ± SD (µM) *	σ_p	π	MR
54	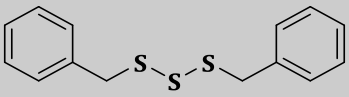	0.47 ± 0.08	0	0.00	0.10
103	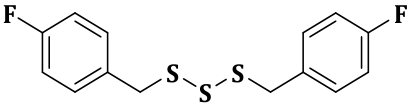	0.29 ± 0.08	0.06	0.15	0.09
104	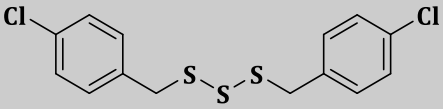	0.97 ± 0.44	0.23	0.70	0.60
105	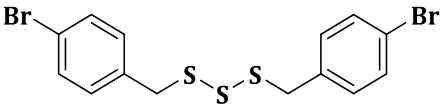	2.44 ± 1.20	0.23	1.02	0.89

106	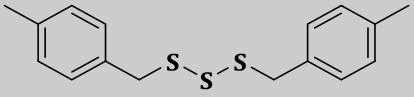	0.69 ± 0.07	-0.17	0.52	0.57
107	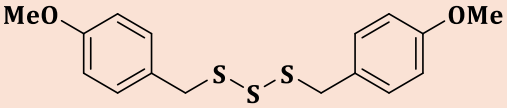	0.053 ± 0.024	-0.27	-0.02	0.79
108	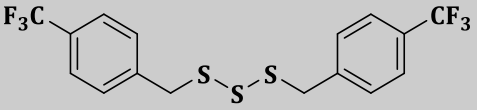	3.83 ± 1.25	0.54	0.88	0.50

** Each IC_{50} value represents the mean of three independent experiments*

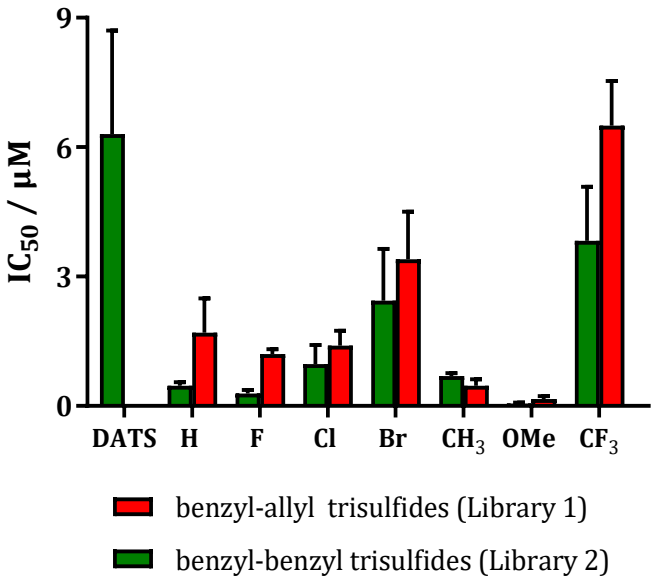

Figure 5.8: Comparative histogram of IC_{50} values for homo- and hetero-benzyl trisulfides against WHCO1 proliferation.

As seen from the comparative **Figure 5.8**, overall, the homo analogues (benzyl-benzyl, Library 3) demonstrated a higher cytotoxicity compared to their hetero counterparts (benzyl-allyl, Library 2), which reflects the superior activity of benzyl over allyl. The low nanomolar (53 nM) IC_{50} of the *p*-OMe derivative, **107**, was particularly pleasing and considered to be highly significant mechanistically as we shall see later. Secondly, apart from the methyl- and H-substituted derivatives, the trend of IC_{50}s followed the same order, i.e. (by substituent) OMe < F < C l< Br < CF_3.

Excited by the low nanomolar IC_{50}s now on offer, we decided to undertake cell morphology studies using visual imaging in which 0.1% DMSO (as a negative control) revealed no observable effect in line with the MTT assay results. However, upon treatment

with compound **107** (*p*-OMe) and **105** (*p*-Br) separately, notable differences in cellular morphology were observed, (see **Figure 5.9**).

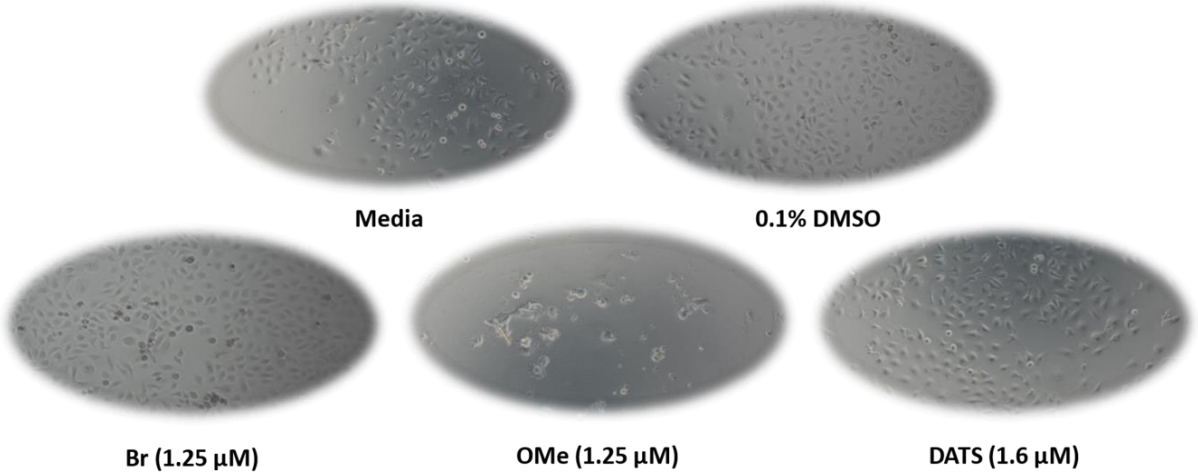

Figure 5.9: Comparative cellular imaging of WHCO1 cells treated with trisulfides *p*-Br, (105); *p*-OMe (107) and DATS (36) for 24 hours at the concentration shown.

Cells treated with the more potent trisulfide **107** (*p*-OMe), displayed signs of stress and potential apoptosis based on the shrunken shape which occurs when the chromatin shortens and the cytoplasm contracts. Conversely, cells treated with **107** and DATS, with higher IC_{50} values, exhibited lesser changes in cellular morphology, suggesting a milder impact on cell viability. This observation aligns with our quantitative data, highlighting the cytotoxic effect of **107** in WHCO1 cells.

5.1.6 SAR Analysis of the Benzyl-Benzyl library

Similar to Library 2, we plotted the lipophilicity (π) (Fig 5.10**A**), molecular refractivity (MR) (Fig 5.10**B**), and the *para*-Hammett constant (σ_p) (Fig 5.10**C**) against the $LogIC_{50}$.

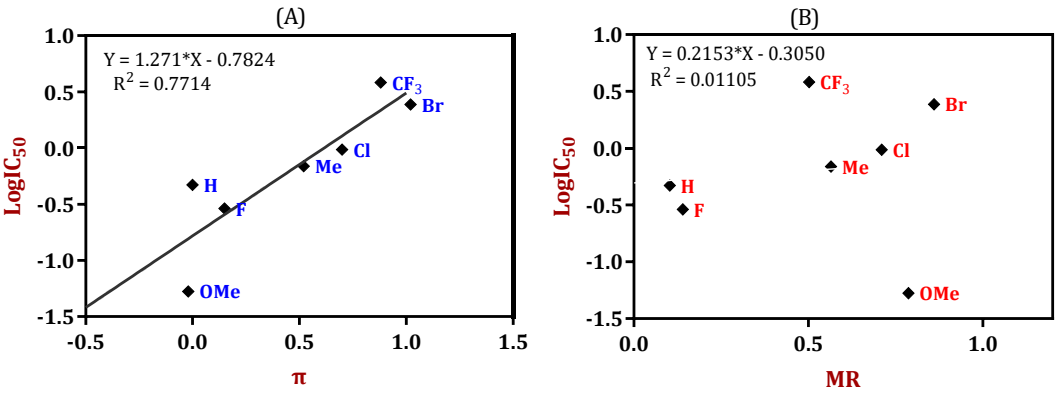

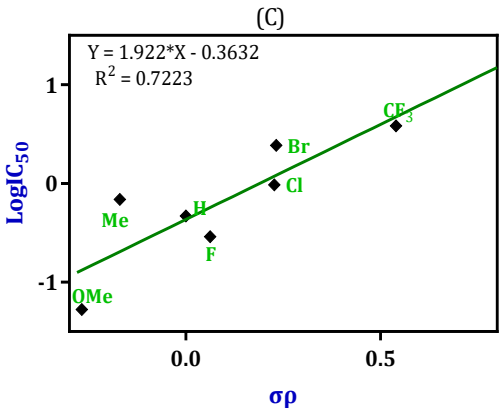

Figure 5.10: Plot of (A) lipophilicity (π), (B) Molar refractivity (MR) and (C) *p*-Hammett Constant (σ_p) of the *p*-benzyl substituent vs the $LogIC_{50}$ of the benzyl-benzyl trisulfide library.

In the homo series, lipophilicity was significantly correlated to $LogIC_{50}$, with the relationship $LogIC_{50}$ = 0.607 π + 0.581 (R^2 = 0.7714, p = 0.0093, ***), suggesting that compounds with higher lipophilicity exhibit greater activity against the target in this library. Interestingly, this trend contrasts starkly with the hetero series, where no noticeable relationship between lipophilicity and activity was identified. By comparison, as with the hetero series, MR showed no correlation with $LogIC_{50}$ (R^2 = 0.011, p = 0.8226, ns).

Finally, as perhaps expected, a significant linear correlation was found between the $LogIC_{50}$ in the homo series and the Hammett constant with an equation of $LogIC_{50}$ = 0.3758 σ_ρ + 0.1612 (R^2 = 0.7223, p = 0.0154, *), indicating a notable correlation between σ_p and cytotoxicity, akin to the findings in the hetero series. The negative coefficients associated with the electron-donating groups (CH_3, OMe) again indicated that these groups favoured cytotoxicity.

The data from the two libraries presents the first in-depth Hammett correlation between a benzyl *para*-substituent and the cytotoxicity IC_{50}, aligning with the findings of Bhattacherjee et al.,[93] indicating that *p*-fluoro- and methyl-substituents in the dibenzyl series enhance activity (but OMe was not evaluated by them). As detailed in section 3.8, their findings showed IC_{50} values in the low micromolar range. The *para*-substituted methyl derivative was the most active (IC_{50} 1.26 µM), followed by the chloro and fluoro derivatives (2.77 and 3.03 µM, respectively), with the bromo derivative having slightly reduced activity (4.11 µM) against MCF-7.

Our results show a similar trend, particularly highlighting the enhanced activity of *p*-fluoro- and methyl-substituents. This consistency reinforces the notion that these substituents are critical for potent cytotoxic activity. Additionally, our study's in-depth Hammett correlation provides a more comprehensive understanding of the electronic effects of these substituents on cytotoxicity, complementing Bhattacherjee et al.'s findings.

Our findings, yet, aligned with studies on Fluorapacin with a *para*-fluoro substituent, which has shown promising anti-cancer activity and undergone Phase 1 clinical trials for advanced cancers, demonstrating encouraging initial outcomes (see section 3.8 for more details on this).[310]

In conclusion, our exploration of both the hetero and homo libraries of trisulfides yielded important insights into structural features affecting the cytotoxicity of trisulfides. Both libraries displayed similar trends, with potency-enhancing effects due to electron-donating groups at the *para*-position of the benzyl group that were supported by the Hammett s_p correlation to the IC_{50}. However, while no significant correlations were found between molecular size and the IC_{50} for either library type, lipophilicity correlated well in the homo-series and not in the hetero one. These results now encouraged us to find explanations, starting with an investigation into perthiol stability in view of its pivotal role in the trisulfide thiolysis sequence as discussed in the review section of Chapter 3.

5.2 Stability Studies on Perthiols

Perthiols are postulated as being thiolysis intermediates in the cytotoxicity of trisulfides, they are known to be reactive species with limited stability, as summarised in the literature review of Chapter 3 in section 3.8.3. Thus structure-activity relations that govern perthiol stability may play into the cytotoxicity of trisulfides in cancer cells. While perthiol is typically a stronger nucleophile than its thiol counterpart, perthiols can also function as electrophiles in their neutral or protonated state under specific conditions. Both sulfur atoms within a perthiol possess electrophilic character, enabling reactions with thiolates to yield either hydrogen sulfide (H_2S) and a disulfide or a transpersulfidation product.[341] However, perthiols are highly reactive species that can undergo various degradation processes in which their soft nucleophilicity leads to high reactivity towards electrophilic species both in a reaction flask and in biological systems. In this, the perthiolate is much more reactive and unstable than the perthiol, which brings

perthiol p*K*a under the spotlight for determining the degree of ionisation at the physiological pH of 7.4. Furthermore, while the perthiolate is clearly nucleophilic, the perthiol can act as both electrophile and nucleophile.[462] **Scheme 5.4** summarises the chemistry involving the perthiolate.

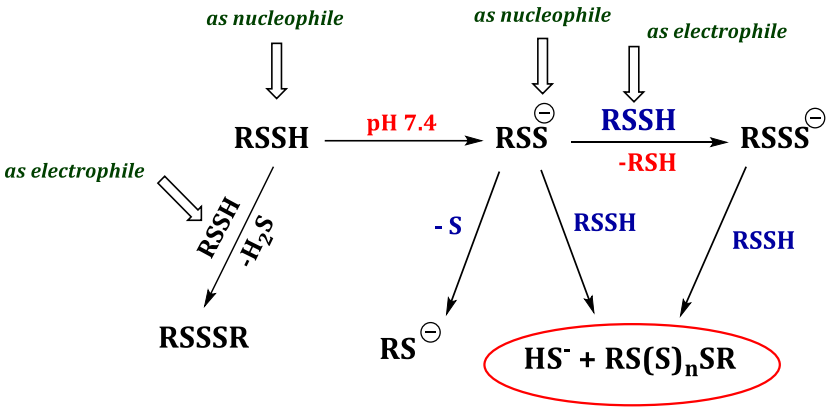

Scheme 5.4: Biologically important reactions of the perthiol and its perthiolate.

Thus, to commence the study, a comparison of the stability of three perthiols, of relevance to the study, was made.

5.2.1 The Choice of Perthiol Substrates

Three perthiols from the benzyl-allyl heterotrisufide library were chosen because of their having only one aromatic group. A *para* substituent on the phenyl ring was incorporated for developing an SAR comparison, chosen as *p*-OMe and *p*-Br substituents because of their opposing electron-donating and withdrawing properties, respectively. Benzyl perthiol (*p*-H) was included as a reference. For the *p*-OMe and *p*-Br perthiols, despite the substituents not being resonance-connected to the disulfide functionality because of the sp^3 benzyl methylene group, we surmised that there might be a level of transmission between the aromatic ring and the dithio functionality based on inductive considerations. These substituent choices were further based on the contrasting variations in cytotoxicity observed in WHCO1 cells in which the cytotoxicity of the *p*-bromobenzyl-allyl trisulfide (IC_{50} = 3.4 ± 2.1 μM) was approximately 21-fold less active than that of the *p*-OMe trisulfide (0.16 ± 0.07 μM). Similarly, in the case of the corresponding homobenzyl trisulfides, the cytotoxicity of the *p*-Br derivative was 46-fold less (2.44 ± 1.20 μM) than the *p*-OMe trisulfide (0.053 ± 0.024 μM), suggesting that the *p*-OMe trisulfide in each case produces more "thiol equivalents" than its bromo counterpart. Thus, these two compounds provided a good contrast for the stability study.

5.2.2 Protocols for Accessing Perthiol Substrates

The overall protocol as shown in **Scheme 5.5** for perthiol production involved acid hydrolysis of a disulfanyl acetate to generate the perthiol. Although a disulfanyl acetate can be rapidly hydrolysed using base, it is well known from Pluth's work[462] as well as our own (trisulfide methodology) that perthiolates are extremely unstable, so this manifold was not available.

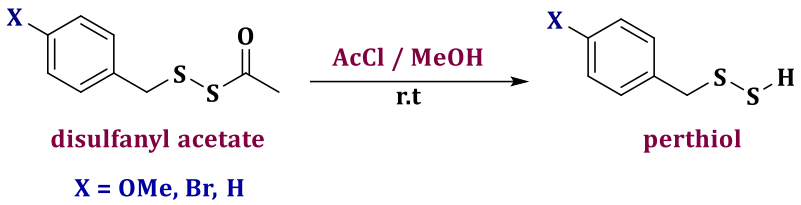

Scheme 5.5: Synthesis of the perthiol via acid hydrolysis.

Regarding the hydrolysis step, it was envisaged that acetyl chloride in methanol would generate HCl *in situ*, which would protonate the disulfanyl acetate carbonyl oxygen, inducing methanol addition followed by liberation of the protonated perthiol with proton transfer. Such an approach has been documented by Chatterji et al.[351] During the experiment, reaction progress was carefully monitored using thin-layer chromatography (TLC). This showed a spot-to-spot conversion to the less polar perthiol for each compound. However, it is worth noting that trisulfide and perthiol exhibited the same Rf value on TLC which became relevant later. At room temperature, the reactions were completed within 29 minutes for the bromine-substituted compound (Br), 25 minutes for the methoxy-substituted compound (OMe) and 20 minutes for the benzyl (H) compound on a 0.025 mmol scale in 2 mL of solvent (12.5 mM overall). Upon completion, the solutions were immediately evaporated using a rotary evaporator without a work-up or chromatography to avoid further decomposition followed by a brief exposure to the high vacuum, which lasted approximately ten minutes. Because we didn't have immediate access to running the ^{1}H NMR spectra, the samples were then stored in the -20°C freezer. However, once access became available, the samples were run immediately.

5.2.3 ^{1}H NMR Analysis of Perthiol Compounds

Benzylperthiol (**109**) was used as a positive control, whose spectrum is shown in **Figure 5.11** (all spectra were run in $CDCl_3$), which strongly indicated the presence of the perthiol based on singlets at 3.90 ppm and 2.89 ppm for the benzylic methylene hydrogens and

the perthiol proton, respectively. Minor by-product signals could be observed, but all things considered, the purity was quite good.

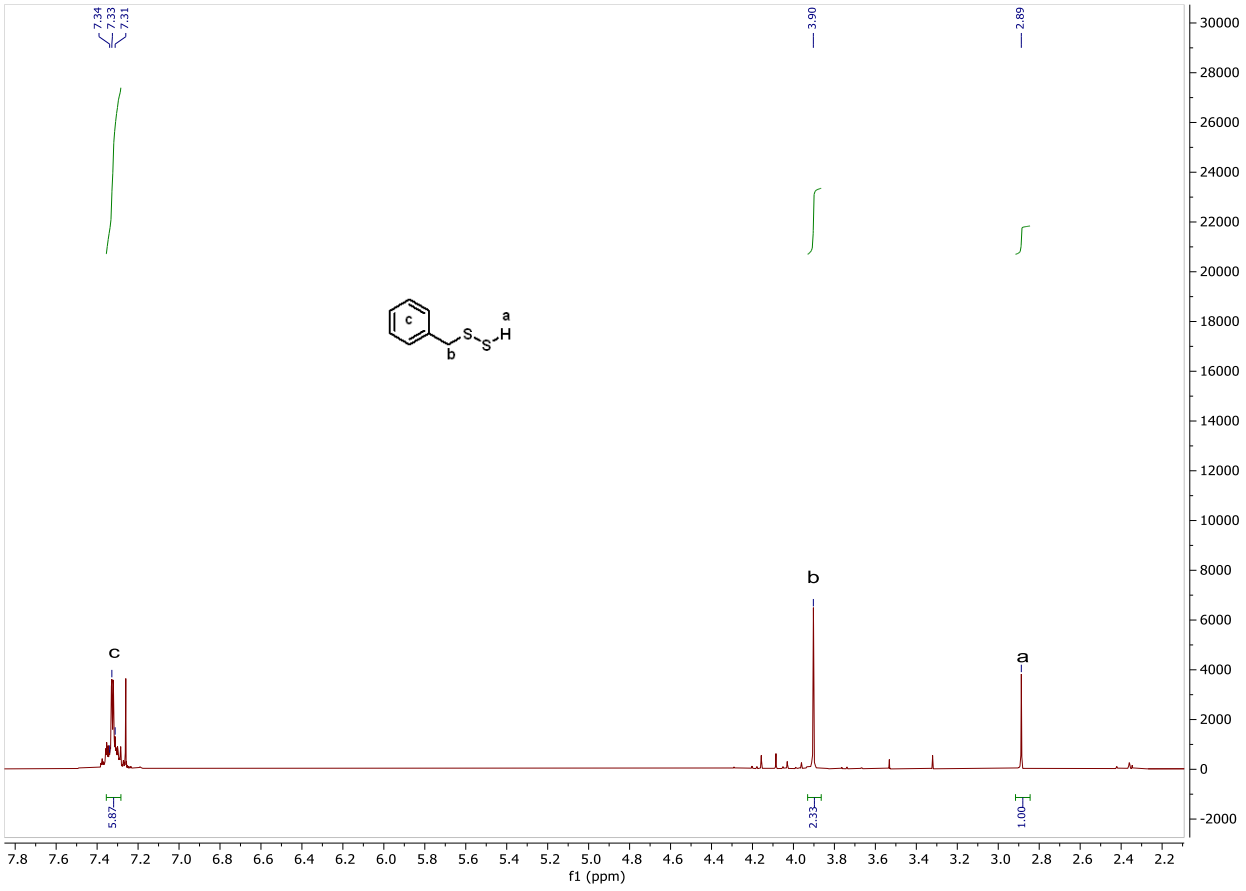

Figure 5.11: ^{1}H NMR of BnSSH, 109.

The chemical shift of the perthiol sulfhydryl hydrogen was compared with that of its benzyl thiol counterpart in which the perthiol proton was observed downfield. The overlayed spectra shown below clearly show this shift, with the SH proton converting from a singlet in the perthiol to a triplet in the thiol as illustrated in **Figure 5.12**. Furthermore, the benzyl methylene also shifts downfield in the perthiol, which is well known for organosulfides of this nature as the number of sulfurs increases (cf. the methodology section).

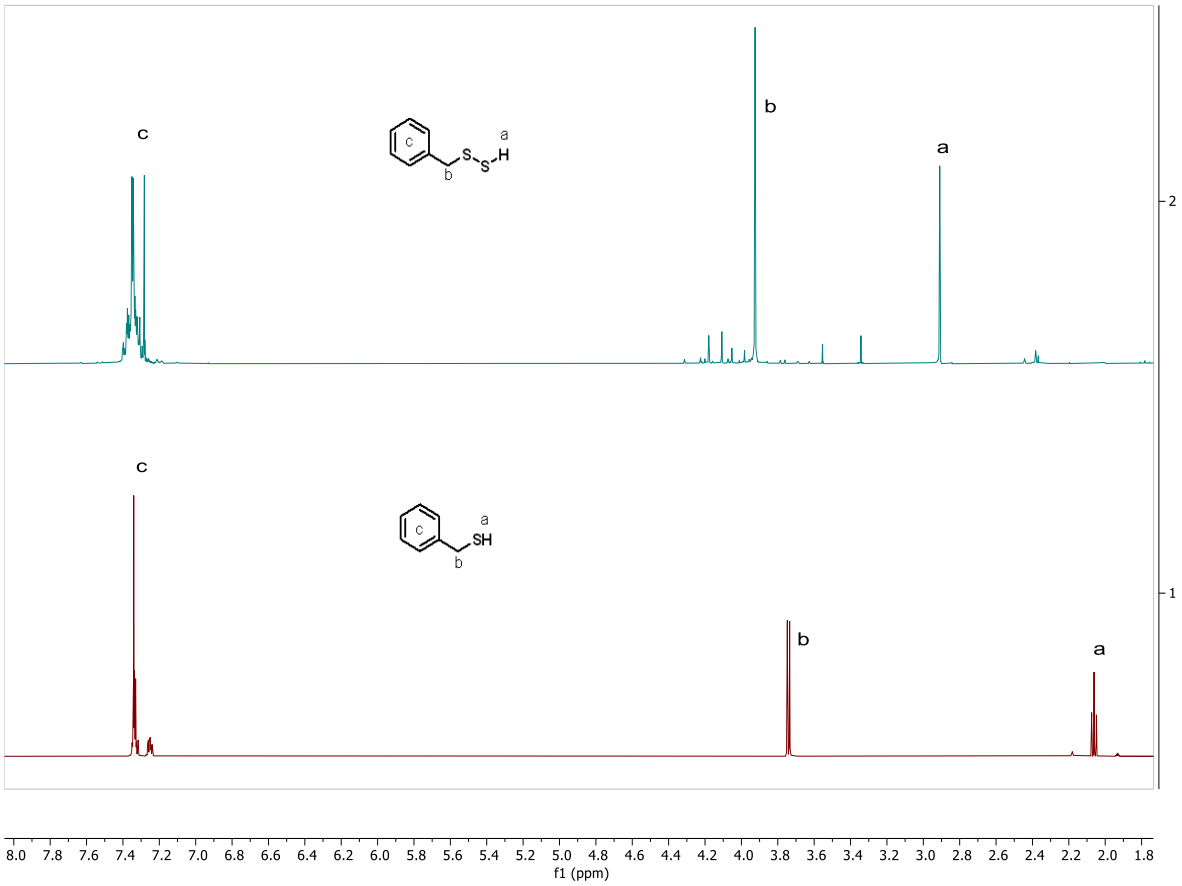

Figure 5.12: Overlayed ^{1}H NMR spectra of BnSSH, 109, and BnSH.

Next was the *p*-OMe perthiol, **110**, as shown in **Figure 5.13**, showing the benzyl singlet at 3.91 ppm. Here, an extra signal for the *p*-methoxy group (as well as an AB system for the 1,4-disubstituted aromatic hydrogens) could be seen, and the spectrum indicated a similar purity level to that of BnSSH. The perthiol hydrogen could once again be seen at just under 3 ppm (2.92 ppm). However, a significant extra singlet was noted slightly upfield to the methoxy singlet, which wasn't assigned.

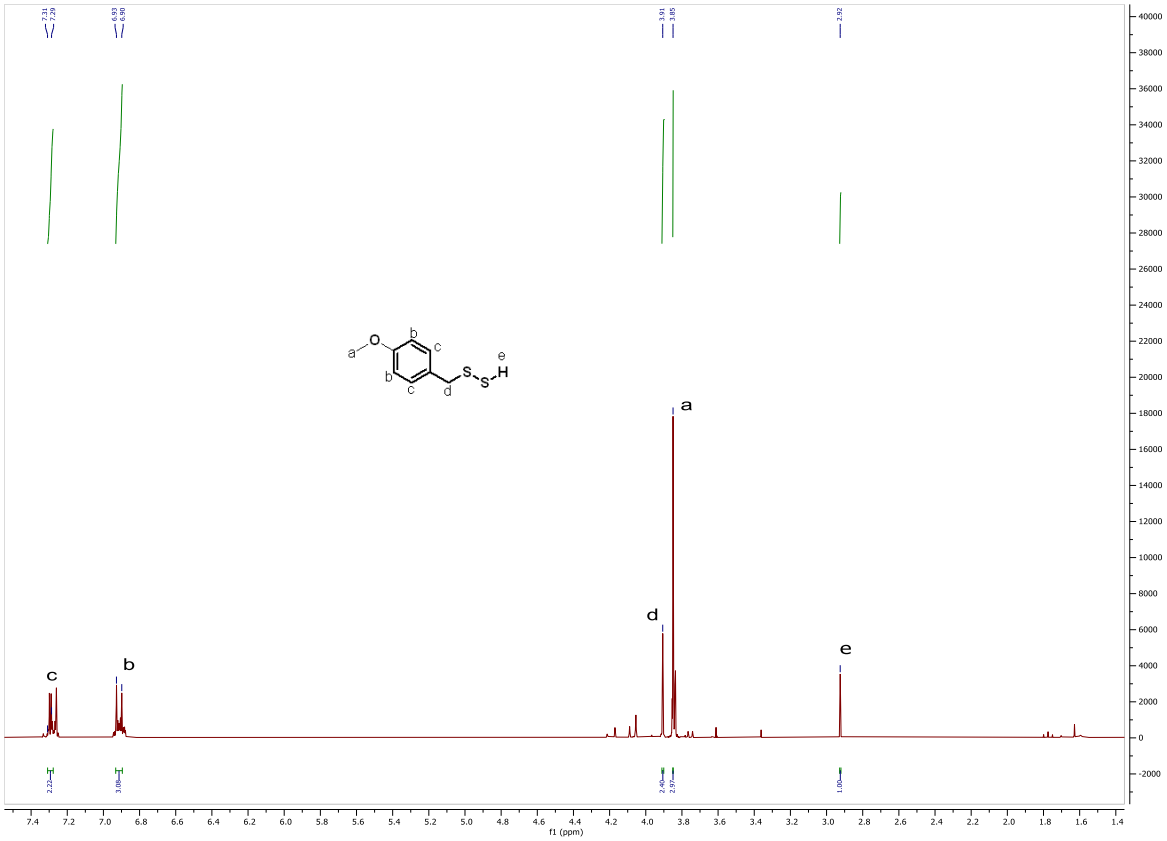

Figure 5.13: ^{1}H NMR spectrum of *p*-MeOBnSSH, 110.

Then, for the bromo derivative, **111**, two compounds could be clearly discerned; one as the perthiol (methylene at 3.83 ppm; perthiol H at 2.86 ppm), and the other as the trisulfide based on previous data in the methodology project (here, a singlet at 4.05 ppm for the trisulfide methylene was observed) as shown in **Figure 5.14**. Based on the integration and taking into account that the trisulfide to perthiol necessitates a benzyl methylene ratio of 4:2 in the spectrum integration for a 1:1 molar ratio, the ratio of trisulfide to perthiol came out as 40:60. The formation of the trisulfide indicates a self-condensation reaction (disproportionation) of the perthiol that illustrates the ambident nature of the perthiol as both nucleophile and electrophile as depicted in **Scheme 5.5**.

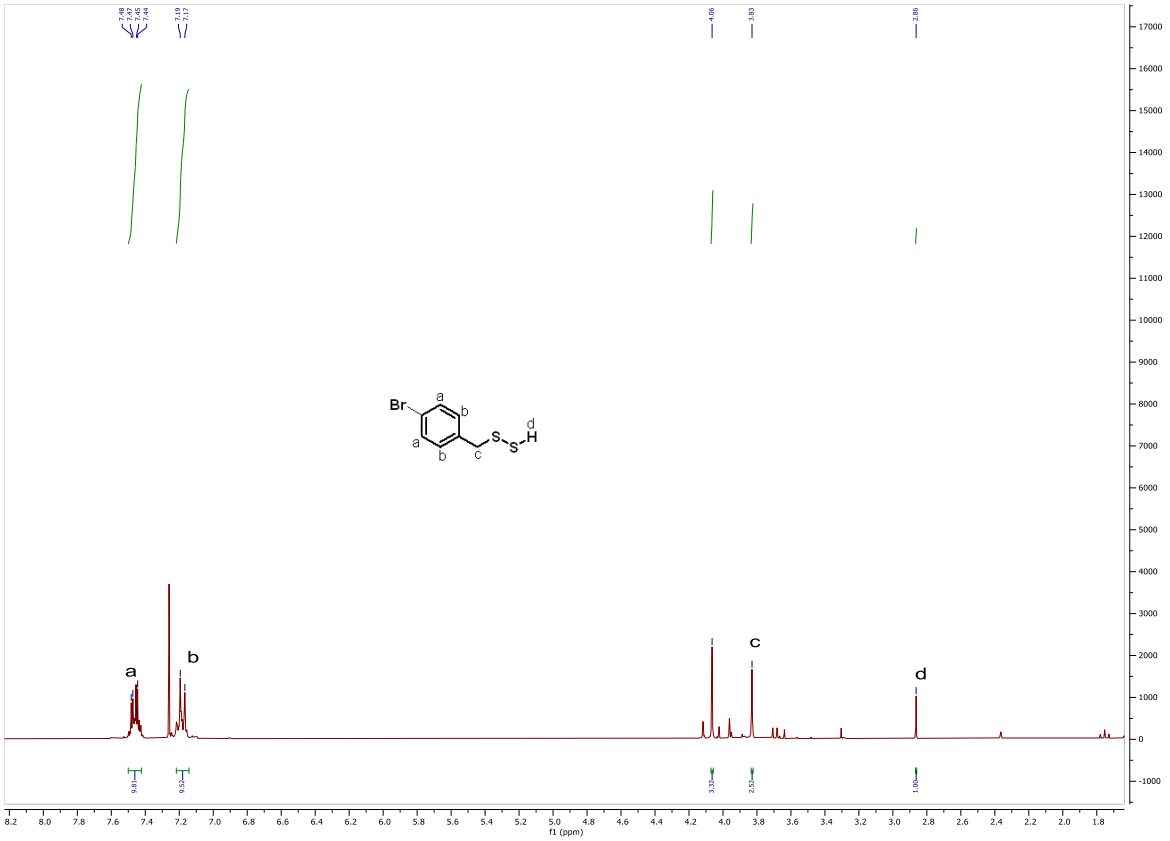

Figure 5.14: ^{1}H NMR spectrum of *p*-Br-BnSSH, 111.

The greater reactivity of the *p*-bromo compound presumably arises from its benzyl group sulfur being more electrophilic due to the inductive withdrawing effect of the bromine. This interpretation is further investigated in the upcoming section. **Scheme 5.6** shows the disproportionation mechanism via the perthiol rather than the perthiolate (not in an aqueous medium).

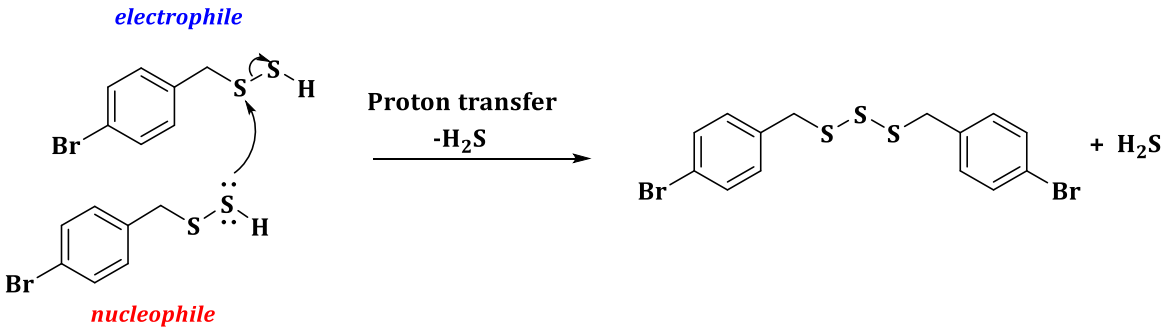

Scheme 5.6: Proposed mechanism for the self-condensation of the Br-perthiol, 111 (in organic solvent).

5.2.4 Perthiol Evaluation using an Ellman's Assay

The second technique for perthiol stability evaluation chosen was the Ellman's assay, albeit with some reservations that will emerge in the theory discussion. Importantly, the intention was to use the Ellman's assay to monitor perthiol stability over time. First the theory.

The Ellman's assay is a well-known assay for sulfhydryl groups[463] involving thiolysis exchange with the Ellman reagent 5,5′-dithiobis-(2-nitrobenzoic acid) or $DTNB^{2-}$. Exchange is relatively fast, simple to carry out, reproducible, and DTNB is commercially available.[463] The chemistry for a thiol evaluation participating in an Ellman's thiolysis exchange is illustrated in **Scheme 5.7**.

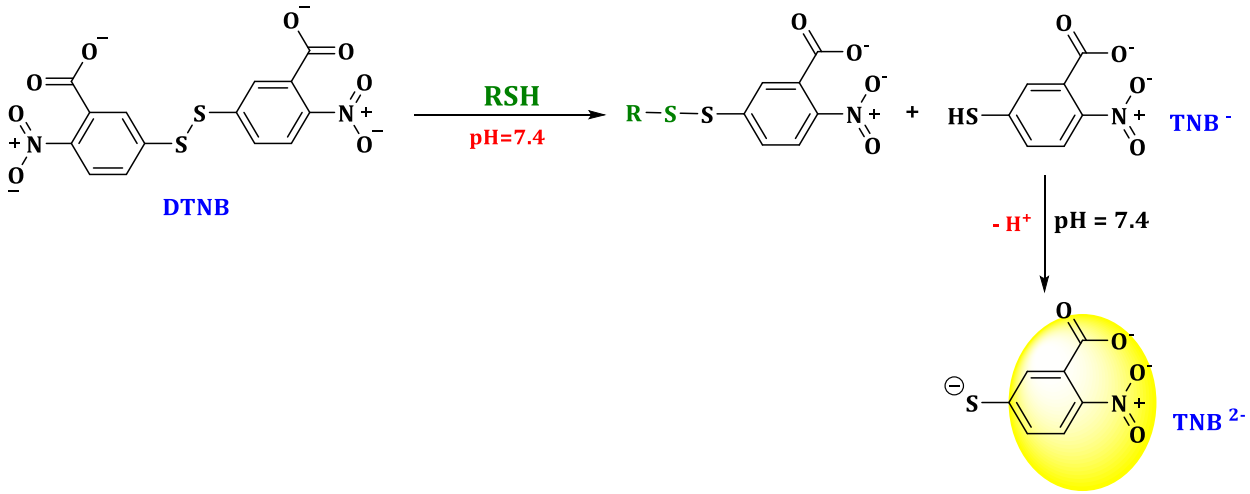

Scheme 5.7: The thiolysis exchange chemistry with a thiol in an Ellman's assay.

Hence, the exchange is driven by the electrophilicity of the disulfide group due to the electron-withdrawing *p*-nitro groups on the phenyl rings. This affords a mixed disulfide and the TNB^{-} thiol, which at pH = 7.4, deprotonates on the thiol (due to its low pK_a caused by the nitro group) to generate the yellow TNB^{2-} dianion, absorbing at 412 nm. Measuring this absorbance allows for the quantitative evaluation of thiol equivalents. Thus, overall, one TNB^{2-} corresponds to one sulfhydryl (SH) equivalent.

Similarly, Carroll et al. has demonstrated that a protein perthiol concentration can also be evaluated by the Ellman's assay,[464] in which the same type of exchange chemistry operates except to give a mixed trisulfide rather than a disulfide as shown in **Scheme 5.8.** However, importantly, once again, one perthiol equates to one $DNTB^{2-}$. However, in this case, further reaction of the mixed trisulfide is to be expected such as formation of PSSSSP with TNB^{2}

or PSSSP with S extrusion to form TNB^{2}. Importantly, the 1:1 stoichiometry is still maintained in these various possibilities.

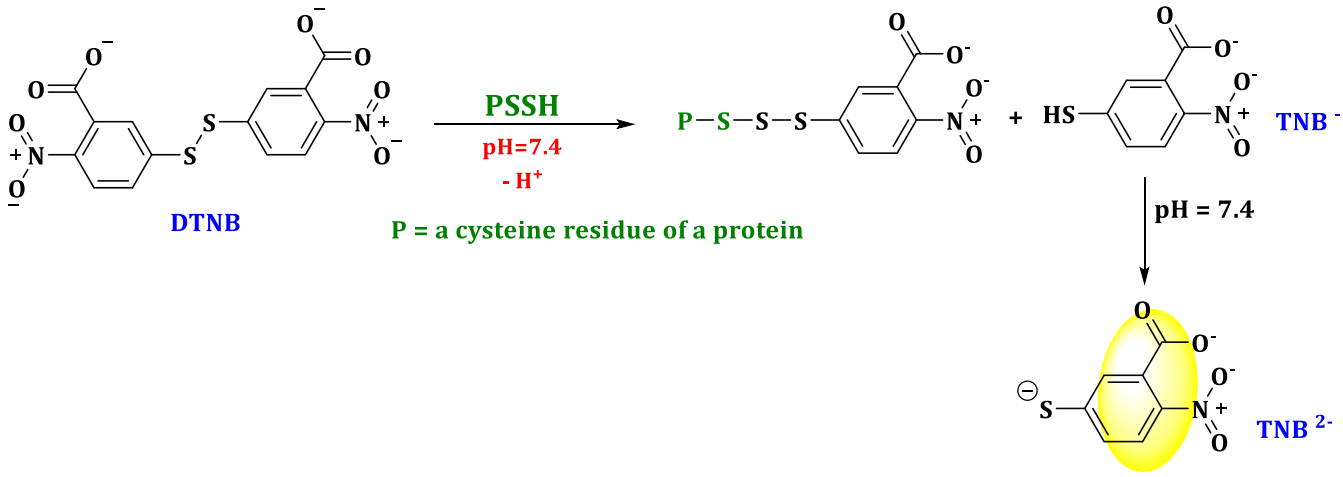

Scheme 5.8: The chemistry of a perthiol in an Ellman's assay.

Now to the question of decomposition, for which the literature identifies a number of possibilities and in which a self-condensation (disproportionation) is one of them. Since the latter was identified for the *p*-bromoperthiol in the ^{1}H NMR study, it was important to consider the impact such a self-condensation would have on the Ellman's assay. As shown in **Scheme 5.1** pertaining to the perthiol self-condensation, 2 perthiol equivalents give one equivalent of H_2S. But 1 equivalent of H_2S, as shown by reports in plant samples,[465] undergoes thiolysis exchange with 2 DTNB to give 2 $DTNB^{2-}$, reducing once again to a 1:1 relationship between perthiol and $DTNB^{2-}$. Similarly, reductive elimination of sulfur from the perthiol (or perthiolate) to afford thiol plus sulfur would also retain a 1:1 ratio between perthiol and $DTNB^{2-}$. **Scheme 5.9** summarises the self-condensation chemistry with DTNB.

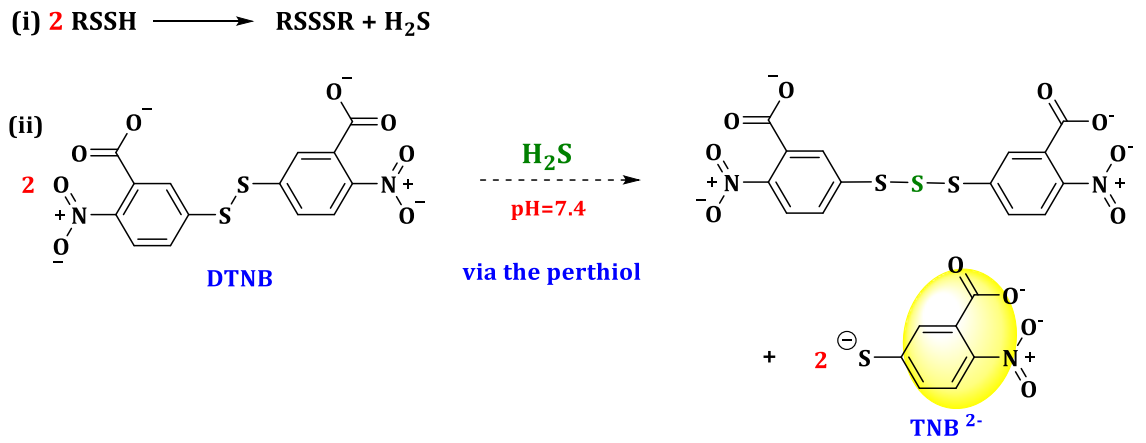

Scheme 5.9: The chemistry of perthiol self-condensation product (H_2S) in an Ellman's assay.

Thus, assuming that the only decomposition pathway (more on this later) was the self-condensation pathway would imply that perthiol decomposition could ***not be followed*** using an Ellman's assay. We decided to go ahead with the experiment anyway, particularly in pursuit of any other pathways in which the thiol to $DTNB^{2-}$ relationship would be interfered with. One possibility that came to mind in this regard was perthiol oxidation by oxygen to afford the tetrasulfide in which thiol equivalents would be lost (O_2 reduced to water or H_2O_2).[465]

5.2.5 Stability Analysis of Perthiol Compounds

To start the study, a calibration curve was first constructed by reacting different concentrations of *N*-acetyl cysteine (NAC), a biological thiol, with excess DTNB in PBS buffer (see the Experimental section for full details). Standard solutions of NAC were prepared at concentrations ranging from 0 - 1.5 mM. These were diluted further to obtain NAC solutions in the 0 - 15 mM range. Importantly, Ellman's reagent was present at a concentration of just under 200 mM (178.6 mM) as a large excess to the thiol to push the equilibrium over. Based on the literature,[466] the solutions were incubated at room temperature for 15 and 30 minutes following a thorough mixing and then the absorbance measured at 412 nm using a UV-Vis spectrophotometer. **Figure 5.15** shows the plot of the absorbance (A412) vs [NAC] for the reactions following 15 minutes (red) and 30 minutes (blue; tend to be obscured by the red) incubation with DTNB. The equation corresponds to the blue line

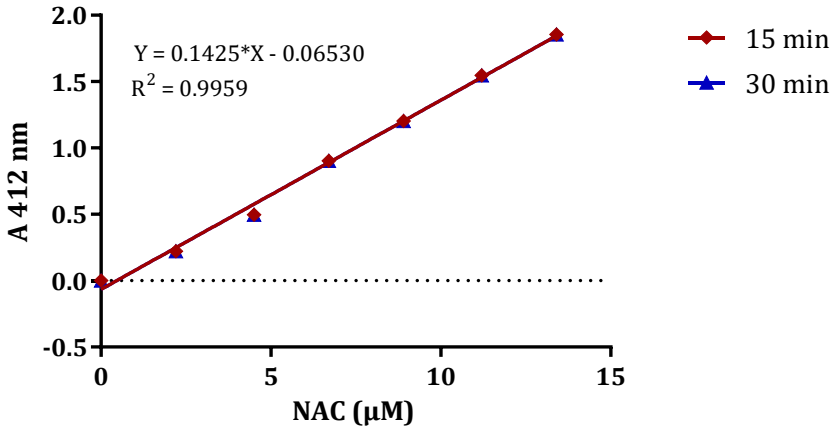

Figure 5.15: Calibration curve of DTNB with NAC.

The graph obtained showed a linear relationship between [NAC] and the absorbance of TNB^{2-} produced at 412 nM, demonstrating, as anticipated, that absorbance can be used as a direct measurement of thiol concentration (NAC here). Since there was no difference between the 15- and 30-minute incubation times, we decided to opt for 15 minutes in the hot run. In retrospect, the incubation timeline should have been studied at shorter times. For the perthiol stability study, the focus now was to study a single concentration of the chosen Br and OMe derivatives that would be aged for a certain time and then trapped with DTNB. For this, the DTNB concentration was kept at 178.6 mM, while the perthiol was present in the solution at 89 mM as a 2:1 DTNB: perthiol ratio, which was considered to be sufficient. As with the calibration cure, the incubation time with DTNB was kept at 15 minutes, and time increments of 10 minutes were used to age the perthiol up to 70 minutes. One must bear in mind that time zero on the graph is not the true time zero since following the synthesis of the perthiol, there was an isolation step which was approximately 10 minutes involving a quick rotary evaporation and high vac, after which the clock was started. The two graphs are shown in **Figure 5.16**.

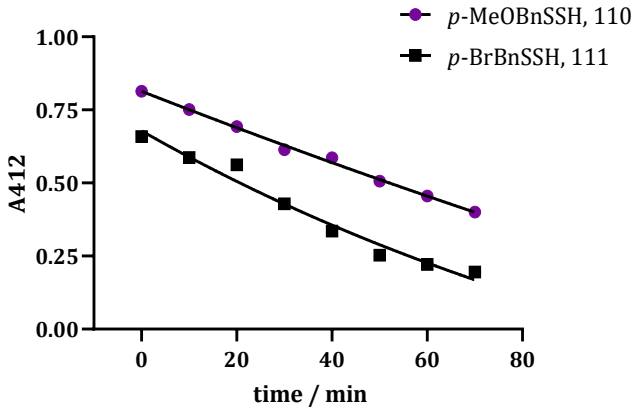

Figure 5.16: Timeline study of perthiol stability for *p*-OMe (110) and *p*-Br (111).

Both profiles exhibited decay over time, whose decay kinetics were investigated by fitting to a first-order exponential decay model using Prism 9. For the equation $y = y^0e^{kt}$, where y^0 is the amount of substance at t=0 and y is the amount of substance at t=t, and k is the exponential rate constant, the following parameters were obtained:

Nonlin fit	***p*-MeOBnSSH, 110**	***p*-BrBnSSH, 111**
Y_0	0.8139	0.6786

NS	-2.130	-0.5962
K	0.002165	0.007296
Half-life	320.2	95.00

Thus, the exponential rate of decay of **110** (*p*-MeOBnSSH) was found to be 0.002165 min^{-1} and that of **111** (*p*-BrBnSSH) was found to be 0.007296 min^{-1}. Thus **110** decays at a slower rate compared to **111**. From the equation, the half-life of **110** (OMe) is 320 minutes whereas that of Br (**111**) is 95 minutes under these conditions.

The R^2 values of 0.9964 for **110** and 0.9737 for **111** indicated a good fit to the data. Owing to the approximately 10-12 minutes required for solution preparation, which likely included perthiol degradation, obtaining an exact time zero was impractical.

The rate data agrees with that of the ^1H NMR data where the *p*-bromo derivative showed some degradation to the trisulfide whereas the *p*-OMe was more stable. Although the ^1H NMR experiment was performed in $CDCl_3$ which is an organic medium, whereas the Ellman's study was run in buffered aqueous solution. Hence, the different profiles for the two media presumably involve disproportionation in the organic medium (*p*-Br perthiol only) proceeding via the perthiol, whereas in the aqueous Ellman's case, reaction proceeds primarily via the perthiolate. The latter being more reactive now converts the *p*-OMe derivative. Furthermore, it is reasonable to assume that the same self-condensation occurs in the Ellman's reactions as in the NMR studies, with both perthiol *S*-electrophilicity and perthiol pK_a playing a role. Here, the data indicates a superior electrophilicity and lower pK_a (hence more perthiolate) for the *p*-Br perthiol vs its *p*-OMe counterpart respectively. **Figure 5.17** summaries these important structural influences.

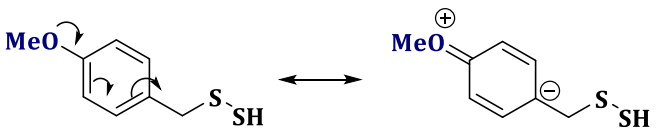

n-pπ release decreases benzyl *S*-electrophilicity and raises the perthiol pK_a (destabilization of the conjugate base), limiting the percentage of reactive perthiolate in the buffer.

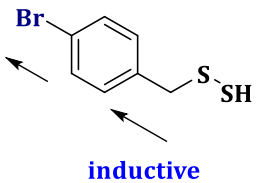

inductive withdrawal increases benzyl *S*-electrophilicity and lowers perthiol pK_a (conjugate base stabilisation), increasing the percentage of reactive perthiolate in the buffer.

Figure 5.17: A comparison of the electronic factors influencing reactivity for perthiols *p*-OMe (110) and *p*-Br (111).

Reducing reactivity down to such electronic factors bodes well for future perthiol design for cytotoxicity enhancement. A remaining question is why a reduction in absorbance over time when the number of thiol equivalents was not changing. For this, we postulated the gradual seepage of H_2S from the reaction mixture with the timeline greater for the assay than in the ^1H NMR study. We appreciate that other factors and reaction types might also be at play such as perthiol oxidation, but the overall picture emerging was an exciting one to take into the next phase of the study regarding understanding the structural features at play in perthiol stability and their relationship to cancer cell cytotoxicity.

5.3 Calculation of Perthiol p*K*a's using Density Functional Theory

From the previous section, it is evident that perthiol can degrade through disproportionation, and that the perthiolate and perthiol exhibit different reactivity preferences. Thus, perthiol pK_a may be important as a perthiol stability factor, so it made sense to investigate how we might measure the perthiol pK_a. Experimental perthiol pK_a determination is challenging because of perthiol instability, making titration-based approaches impossible. Therefore, we considered instead using computational modelling as an alternative method for their pK_a determination, despite its limitations.

This computational work was conducted with the invaluable assistance of Dr. Willem Gerber from Stellenbosch University, who set up the calculations using Density Functional Theory (DFT) with ORCA 5.0.1. The procedure employed the B3LYP functional with a D3 atom-pairwise dispersion correction,[467,468] a RIJCOSX algorithm, and a def2-TZVP basis set utilizing the auxiliary basis def2/J.[469,470] The protonated and deprotonated perthiols underwent geometry optimization using an implicit SMD solvation model[471] with the parameters of water. All the obtained structures were characterized as potential energy surface (PES) minima by analysing the respective Hessian matrix for each structure, i.e. no negative vibrational frequencies were involved. The optimized geometries for the protonated perthiols are shown in **Figure 5.18**.

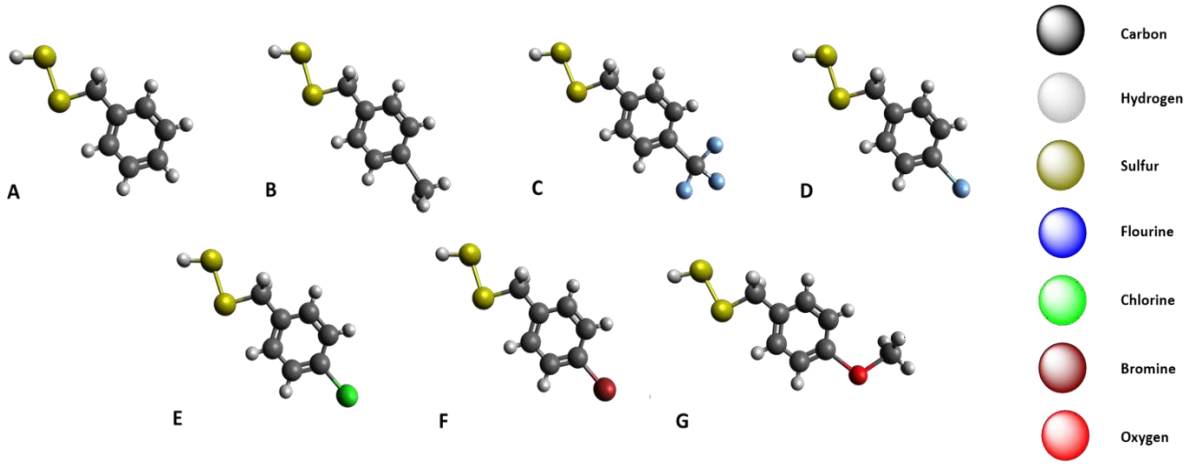

Figure 5.18: The structures of *p*-substituted benzyl perthiols, modeled using Avogadro. The perthiol data set includes A. benzyl perthiol, B. 4-methylbenzyl perthiol, C. 4-trifluoromethylbenzyl perthiol, D. 4-fluorobenzyl perthiol, E. 4-chlorobenzyl perthiol, F. 4-bromobenzyl perthiol, and G. 4-methoxybenzyl perthiol. Avogadro was used to generate the visual representation of structures from Orca output files.

From the Orca output files, we could determine the relative thermodynamic parameters (Gibbs free energy, enthalpy, and entropy) for perthiol ionization. In view of the stability study to date, our aim was to elucidate the electronic factors influencing perthiol acidity, particularly the impact of substituents on the aromatic ring of our benzyl perthiols. As described before, electron-withdrawing or -donating substituents were expected to influence the pK_a values. The computationally predicted pK_a values for a series of para-substituted benzyl perthiols is presented in **Table 5.5**. These values are compared against the Hammett constant of the para-substituent in **Figure 5.19**.

Table 5.5: pK_a values determined computationally for a series of *para*-substituted benzyl perthiols vs the *para*-Hammett Constant (σ_p)

Substituent	Predicted pK_a	Hammett Constant (σp)
***p*-F**	8.99	0.062
***p*-Cl**	8.85	0.227
***p*-Br**	8.81	0.232
***p*-CH_3**	9.30	-0.170
***p*-OMe**	9.49	-0.268
***p*-CF_3**	8.54	0.540

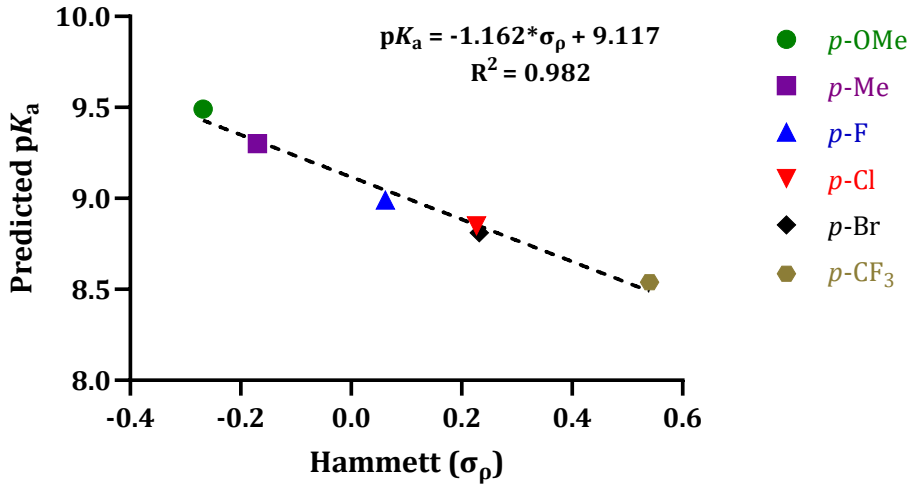

Figure 5.19: Plot of the calculated perthiol pK_a vs the *para*-Hammett constant of the substituent.

The analysis of this relationship revealed a significant linear correlation conforming to the equation pK_a = -1.162 σ_p + 9.117, with a correlation coefficient R^2 of 0.98 and a *p*-value of 0.0001, indicating a highly significant relationship as shown **Figure 5.19**. The negative slope demonstrates that as the electron-withdrawing character of the substituent increases (higher σ_p), the predicted pK_a of the perthiol decreases, leading to an increase in acidity. This observed correlation is encouraging as it provides confidence in the predicted values, as the electronic nature of substituents is known to play a role in modulating the stability of the conjugate base in an acid deprotonation equilibrium, in line with the principles of the Hammett equation. The relationship offers confidence in the predicted values; however, the accuracy of these absolute values relative to the true pK_a values remains uncertain. For instance, perthiols are typically 1–4 pK_a units more acidic than their corresponding thiols, such as glutathione (GSH) with a pK_a of 8.94 compared to its persulfide form (GSSH) with a p*K*a of 5.45. Given the low pK_a of GSSH, our predicted values might be overestimated, especially considering that the pK_a of benzyl mercaptan is 9.43.[472]

In addition to this established relationship, we now turned our attention to exploring how these parameters correlated with the cytotoxicity of benzyl-allyl and benzyl-benzyl trisulfides from Library 2 and 3 respectively. The data and plots of pK_a vs LogIC_{50} are given in **Table 5.6** and **Figure 5.20** below.

Table 5.6: pK_a values determined computationally for a series of *p*-substituted benzyl perthiols and LogIC_{50}s of hetero and homotrisulfides from libraries 2 and 3 respectively

Substituent	Predicted pK_a	LogIC$_{50}$ (hetero)	LogIC$_{50}$ (homo)
***p*-F**	8.99	0.08	-0.54
***p*-Cl**	8.85	0.15	-0.01
***p*-Br**	8.81	0.53	0.39
***p*-CH$_3$**	9.30	-0.33	-0.16
***p*-OMe**	9.49	-0.79	-1.28
***p*-CF$_3$**	8.54	0.81	0.58

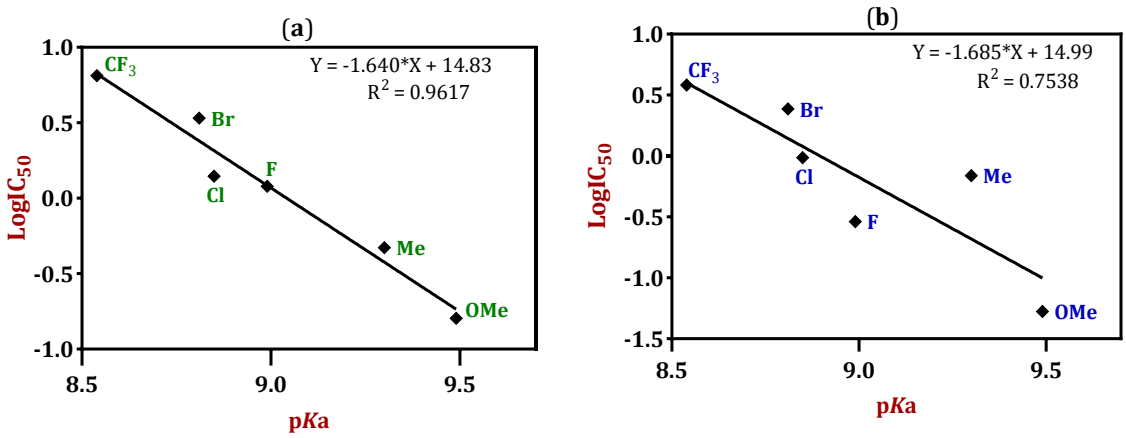

Figure 5.20: Plot of calculated perthiol p*K*a vs the LogIC$_{50}$ of the corresponding (a) benzyl-allyl and (b) benzyl-benzyl trisulfides from Libraries 2 and 3 respectively.

The equation for the hetero benzyl-allyl series as shown in **Figure 5.20** (a) described a strong linear relationship as LogIC$_{50}$ = -1.640 p*K*a + 14.83, with an R^2 value of 0.962, and a significant *p*-value of 0.0006 (****). Similarly, the equation for the homo benzyl-benzyl series was found to be LogIC$_{50}$ = -1.685 p*K*a + 14.99, with an R^2 value of 0.754, and a significant p-value of 0.0249 (*). In both cases, the trend in cytotoxicity correlated well with the predicted p*K*a of the perthiol where more acidic perthiols such as *p*-Br and *p*-CF$_3$ show reduced cytotoxicity, and less acidic perthiols such as *p*-CH$_3$ and *p*-OMe show enhanced cytotoxicity. Thus, this impressive pattern links perthiol acidity to modulating trisulfide cytotoxicity.

Overall, these results aligned with findings from the ^{1}H NMR and Ellman's assay studies in terms of a dependency between the *para*-substituent on the benzyl group and the corresponding perthiol acidity, which in turn, has a bearing on overall trisulfide cytotoxicity. Specifically, perthiols with higher p*K*a values exhibited enhanced trisulfide

cytotoxicity, suggesting that a greater perthiol lifetime translates to an increase in cytotoxicity.

In summary, several correlations emerged from the study of *p*-substituted benzyl-allyl and benzyl-benzyl trisulfides, an important one being between cancer cell cytotoxicity and the Hammett constant of the substituent in which activating groups led to more cytotoxic analogues. This correlation strongly pointed towards a link between cytotoxicity and the stability of the perthiol released after thiolysis exchange on the trisulfide within the cancer cell, resulting in the perthiol acting as the primary driver of trisulfide cytotoxicity. Assuming that the perthiol does not link directly with cytotoxicity, based on mechanistic considerations as described in Chapter 3, the implication from these results was that cytotoxicity increases with perthiol stability and concomitant increase in oxidised protein thiol/glutathione and H_2S production. **Scheme 5.10** summarizes these ideas in terms of perthiol characteristics.

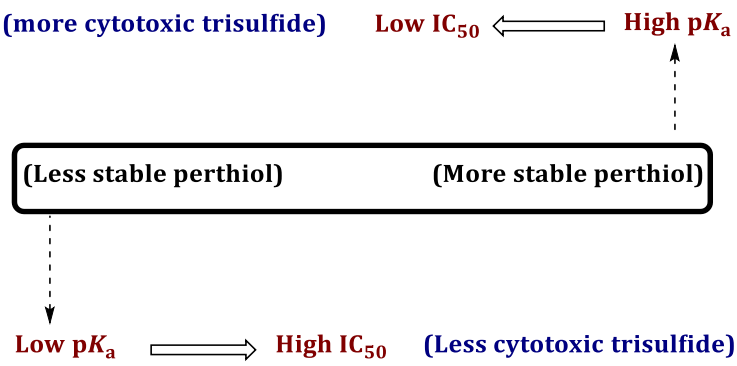

Scheme 5.10: Summary of the correlation between the trisulfide cytotoxicity, and perthiol pK_a and stability.

Hence, at this stage of the project, we concluded that perthiol stability mediates cancer cell cytotoxicity in an indirect way rather than a direct one. Our next aim was to seek validation of this hypothesis in cancer cells.

5.4 Sulfhydryl Chemical Biology in Trisulfide-treated Cells

The next phase of the project focused on now looking at trisulfide substrates in cancer cells and using Ellman's assay previously described for scrutinising ***relative*** levels of sulfhydryl equivalents produced. However, in this case, because cells were being used rather than a cuvette, it is first important to describe the literature's understanding of the processes involved.

5.4.1 The Fate of a Trisulfide in a Cancer Cell

It is first important to summarise the trisulfide cancer cell journey based on current literature. Recent work by Lin, Fukumoto and Kumagai groups in 2019 explored cysteine trisulfide (CysSSSCys) as a trisulfide cell probe,[473] and established that the perthiol, CysSSH, generated following thiolysis exchange between the trisulfide and a biological thiol (R'SH in the Figure below), acts as the pivotal intermediate in a number of intracellular processes. However, importantly in the context here, they established that cells with increased intracellular perthiol levels could export CysSSH into the extracellular space. Interestingly, while CysSSH was the major perthiol exported perthiol, GSSH (formed via exchange between GSH and CysSSH) was shown to be the predominant intracellular species.[473] An overall picture of pertinent events is given in **Figure 5.21.**

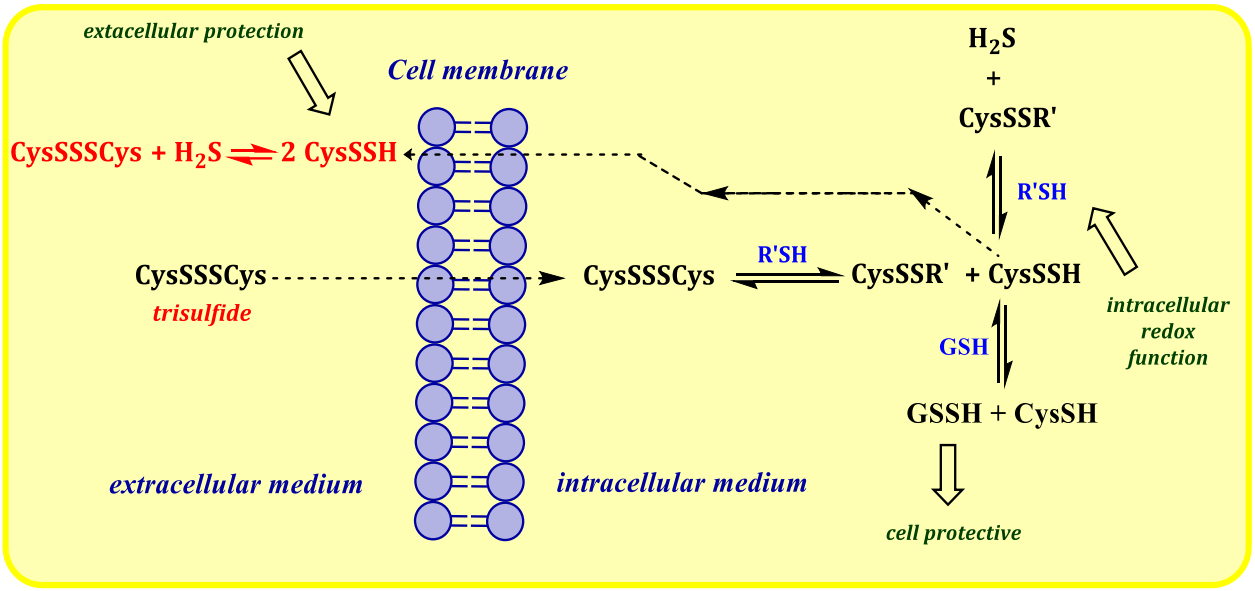

Figure 5.21: The proposed fate of a trisulfide entering a cell.[473]

In this somewhat complex milieu, it is essential to differentiate between intracellular and extracellular processes because the cellular environment influences perthiol function.[473] Intracellularly, perthiols participate in signalling pathways and modulate protein function. Extracellularly, their S-S bond reduction by reductants present in the extracellular matrix[16] (or secreted by cells) to form a thiol and H_2S can result in a variety of different physiological effects such as vasodilation and antimicrobial activity.[474] Such processes are promoted by extracellular reductants like ascorbate or glutathione.

Since trisulfides produce these species as a byproduct following thiolysis within the cancer cell, we were interested to assess their extent of production and to investigate how

these species affect cancer cell cytotoxicity, which is the biological activity of interest in this study.

Given the results in the project thus far, we found the issue of perthiol transport intra- to extracellular offered a possible opportunity for monitoring perthiol presence in the extracellular space of cancer cells by the Ellman's assay through the assay of the cell culture media.

5.4.2 Rationale for Trisulfide Selection

The selection of the trisulfides for this experiment was guided by the cytotoxicity results obtained previously, where electron-donating substituents on the benzyl ring demonstrated the highest activity (as seen with *p*-OMe, **107**), while the bromo substituent, **105**, exhibited reduced cytotoxicity. Hydrogen substitution, **54**, showed moderate activity between these extremes. **Figure 5.22** depicts the structures as well as their IC_{50}s for a mini-library of homobenzyl trisulfides, which were selected in preference to the hetero analogues (benzyl-allyl) in view of their superior cytotoxicity.

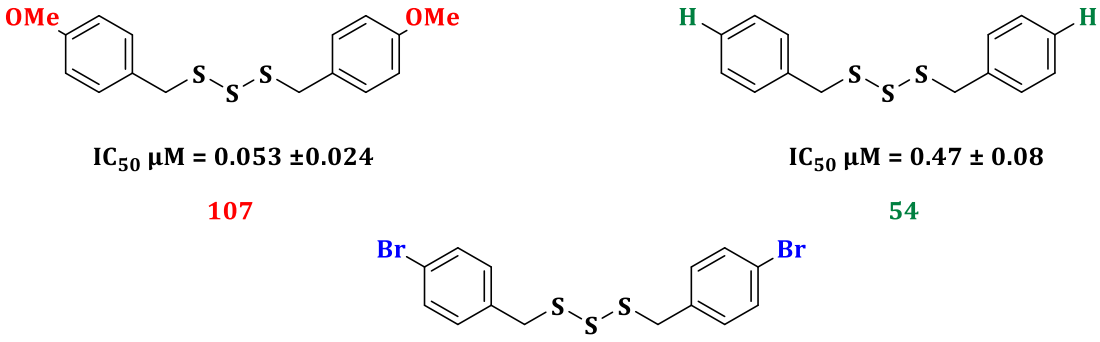

Figure 5.22: Cytotoxicity IC_{50}'s of 54, 105 and 107 in WHCO1 cancer cells.

Regarding the assay component, the Ellman's assay was performed as before by incubating the reagent with the "thiol source" for 15 minutes to develop the colour and form the TNB^{2-}.

5.4.3 Experimental Protocol for Sulfhydryl Level Assessment

To start the experiment, WHCO1 cells were plated in 24-well plates at a density of 50,000 cells per well and allowed to settle overnight. The following day, they were treated with 100 µM of each of the three trisulfides for 3 hours. Untreated cells were included as

controls to determine baseline thiol levels, and a 0.1% DMSO control was included to account for any solvent effects on thiol levels. Dibenzyl disulfide (BnSSBn) was also used as a control for disulfide. Each experiment was conducted independently in triplicate.

After the 3-hour incubation period with the trisulfide, 100 µL of the culture media was removed and added to 100 µL of DTNB (1 mM) to give a molar ratio of DTNB to trisulfide of 10:1 (see the Experimental for a full analysis of concentrations). The DTNB was incubated with the culture media for 30 minutes, after which 1.8 mL of PBS buffer was added, and the absorbance was measured at 412 nm using a UV-Vis spectrophotometer. The experimental workflow is outlined in **Scheme 5.11**.

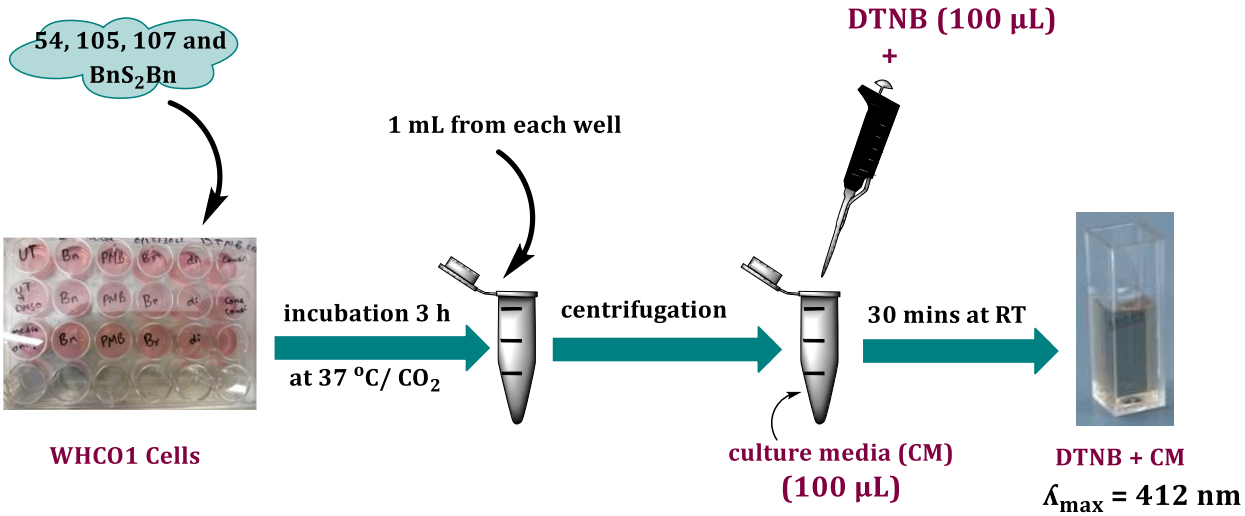

Scheme 5.11: Experimental workflow for quantification of DTNB-reactive sulfhydryl groups in the culture media of WHCO1 cells following treatment with trisulfides.

5.4.4 Results and Interpretation

The results revealed varying levels of DTNB-reactive sulfhydryl groups in the cellular media of the WHCO1 cells following treatments with the trisulfides. Treatment with *p*-OMe, **107**, produced the greatest amount of TNB^{2-}, followed by *p*-H (**54**) and then *p*-Br (**105**) (see **Figure 5.23**). Noteworthy, this trend mirrored that of the cytotoxicity findings, indicating that the higher levels of sulfhydryl groups or "thiol equivalents" in the extracellular media (which could be RSH/RSSH or H_2S according to "Ellman's") is a marker of cytotoxicity. Hence, the term "thiol equivalents" refers to the DTNB-reactive species detected rather than the direct presence of thiols. As discussed in section 5.2.4, DTNB reacts with RSH and RSSH to produce only one equivalent of TNB^{2-}, whereas H_2S yields two equivalents.

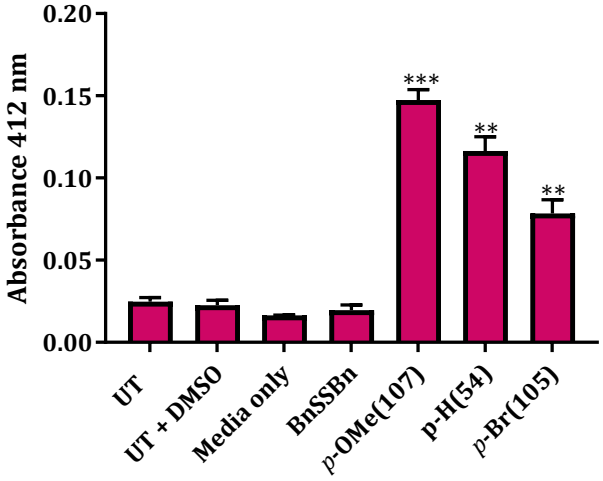

Figure 5.23: Measurement of reactive sulfhydryl groups in the culture media following treatment with organosulfur compounds BnSSBn, *p*-OMe (107), *p*-H (54) and *p*-Br (105). UT = untreated cells.

Quantitatively, *p*-OMe (**107**) produced 2-fold more DTNB-reactive sulfhydryl species compared to *p*-Br (**105**), with absorbance values of 0.147 ± 0.006 and 0.078 ± 0.008, respectively. It is likely that these differences may be higher at a lower timepoint compared to the 3-hour incubation period used in this study, but additional timepoints were not investigated. Trisulfide *p*-H (**54**) was found to have a mean absorbance of 0.116 ± 0.008. The disulfide, BnSSBn produced the same level of TNB^{2-} as the control (untreated cells) as expected since simple disulfides do not readily undergo thiolysis exchange.

Regarding interpretation, once again, perthiol stability in terms of *S*-electrophilicity (both sulfurs) and its pK_a seem to be pivotal. The higher concentration of sulfhydryl equivalents in the cell's supernatant (extracellular space) for the *p*-OMe derivative, **107**, indicates a higher perthiol stability in keeping with our earlier results. This gives the perthiol from **107** time to cross the membrane back into the extracellular domain. Similarly, the lower levels of perthiol from the *p*-Br derivative, **105**, indicates its perthiol in the intracellular space to be shorter-lived. However, the lower cancer cell cytotoxicity of these more reactive perthiols, assuming H_2S (formed via exchange on the said perthiol by RSH as glutathione or a cysteine residue on a protein) to be the principal cytotoxic agent, reveals that such perthiols degrade, at least in part, via a non-cytotoxic pathway. The latter, we suggest involves two key structural features. The methoxy perthiol, being less acidic, remains predominantly as a perthiol at physiological pH, allowing for a sustained release of H_2S. In contrast, the more acidic bromo perthiol may exist as a perthiolate, which degrades more rapidly through disproportionation.

Interestingly, the bromo perthiol might exhibit a shift in regioselectivity, leading to thiolysis at the external sulfur, a shift that has recently been shown experimentally by the Pluth group.[341] In this case, a bulky or electron withdrawing group (i.e. Br) was shown to switch the electrophilicity preferences to the external sulfur leading instead to transpersulfidation which may be a non-productive reaction in terms of cytotoxicity as this shift does not lead to further mixed disulfides or H_2S release. Indeed, transpersulfidation generates a non-cytotoxic thiol and a biological per hthiol that is cytoprotective. Thus, the underlying cause of cytotoxicity in cancer cells could stem from the formation of mixed disulfides and H_2S. These ideas are summarised in **Scheme 5.12**.

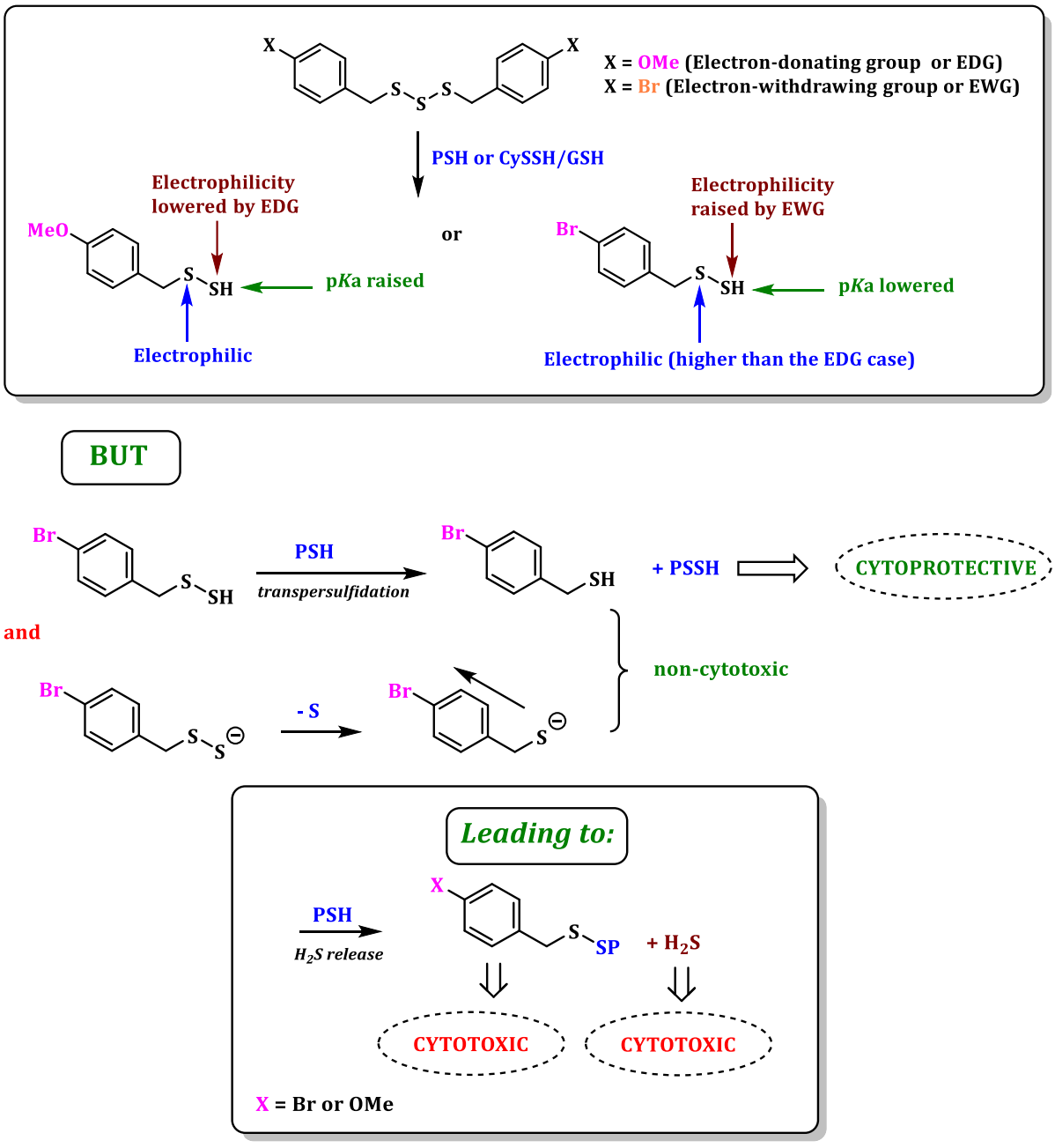

Scheme 5.12: A rationale for perthiol stability affecting H_2S production and ultimate cytotoxicity.

In summary, a convincing picture had emerged – that the key to trisulfide-based cytotoxicity is producing a stable perthiol following thiolysis exchange with a biological thiol leading to a sustained release of H_2S and also sustained oxidative modification of proteins or consumption of GSH intracellularly. To further explore this hypothesis, we next examined the H_2S release in cancer cells using an H_2S probe.

5.5 Exploring the Role of H_2S in Trisulfide Cytotoxicity

Having explored perthiol levels in cells and their role in trisulfide cytotoxicity, our attention turned to hydrogen sulfide (H_2S) as the final product in the thiolysis end game. We thus investigated H_2S release from *p*-substituted homodibenzyl trisulfides within WHCO1 cells using an H_2S probe. This research links to previous probe studies demonstrating the potent anti-cancer effects of H_2S release from various trisulfides in different cancer cell lines,[93,357,475] which will be discussed in the next section.

5.5.1 Detecting H_2S Release using an Azide Fluorescent Probe within the Cancer cell

Although a review was presented in Chapter 3, first it is important to focus on the details of recent probe studies on H_2S produced in cancer cells treated with organotrisulfides. A recent review[476,477] highlights the various options in terms of the functional chemistry, but in this study, it was decided to use an azide-based probe because of its ease of synthesis and reliable usage in cells.

In 2017 and 2020, Quinn et al.[357,475] in two different publications investigated PEG-trisulfides as H_2S donors in cancer cells using a fluorescent probe for H_2S detection, which revealed a steady increase in fluorescence over time in HEK293 cells. Similarly, Bhabak et al. and Pluth et al. in two separate publications used an azide probe to measure H_2S release from trisulfide donors in cancer cells. Bhabak et al.[93] examined the H_2S release profiles of dibenzyl trisulfide derivatives in MCF-7 cells, revealing differences in cytotoxicity and dynamic H_2S release patterns. Among the derivatives studied, di-(*p*-methylbenzyl) trisulfide exhibited a unique and potent H_2S release profile, correlating with significant cytotoxic effects. This derivative demonstrated a dynamic and sustained release of H_2S, leading to a pronounced anti-proliferative activity. Similarly, Pluth et al.[478]

recently used the same azide probe to quantify H_2S release from bis (morpholinomethyl coumarin-based) trisulfide showing a strong and specific response to H_2S and the ability to localize within the lysosome of cells.

There are several fluorescent probes that have been developed that use different chemistries for detecting H_2S in a biological sample. For instance, metal-ion indicators indirectly detect H_2S by monitoring changes in fluorescence properties in the presence of metal ions.[479] Cyanine-based probes enable sensitive detection in complex biological environments, while BODIPY-based probes ensure reliable quantification of H_2S levels owing to their high photostability as summarised in the review by Matson et al.[480] However, the probe that caught our attention was the fluorescent azide probe 1,8-naphthalimide (NAP), **112**, and the coumarin-based scaffold SF_4, **113**, both with a reducible azide-group, **Figure 5.24**.

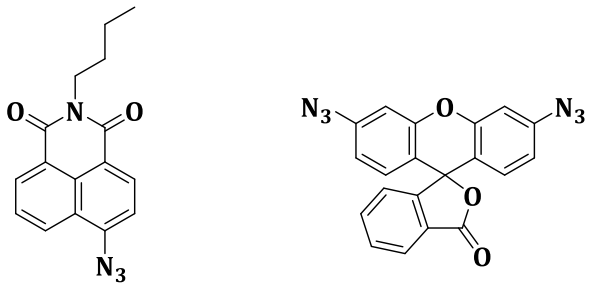

NAP, 112 SF_4, 113

Figure 5.24: Chemical structures of two azide-fluorescent probes used for H_2S detection.

The reduction of the azide group by H_2S results in a fluorescence signal. The transition from a non-fluorescent to a fluorescent state allows for naked-eye detection of H_2S, which can also be measured quantitatively.[477,481] Current thinking based on the experimental evidence points towards trisulfide cytotoxicity mode of action involving a reaction with a biological thiol to form a perthiol, which reacts further to generate H_2S in the second step. Any probe experiment relies on the chemical reaction of a functional group in the probe, which in the case of an azide-probe involves azido group reduction to an amino group by the H_2S with a change in the fluorescence. The relevant chemistry is depicted in **Scheme 5.13**.

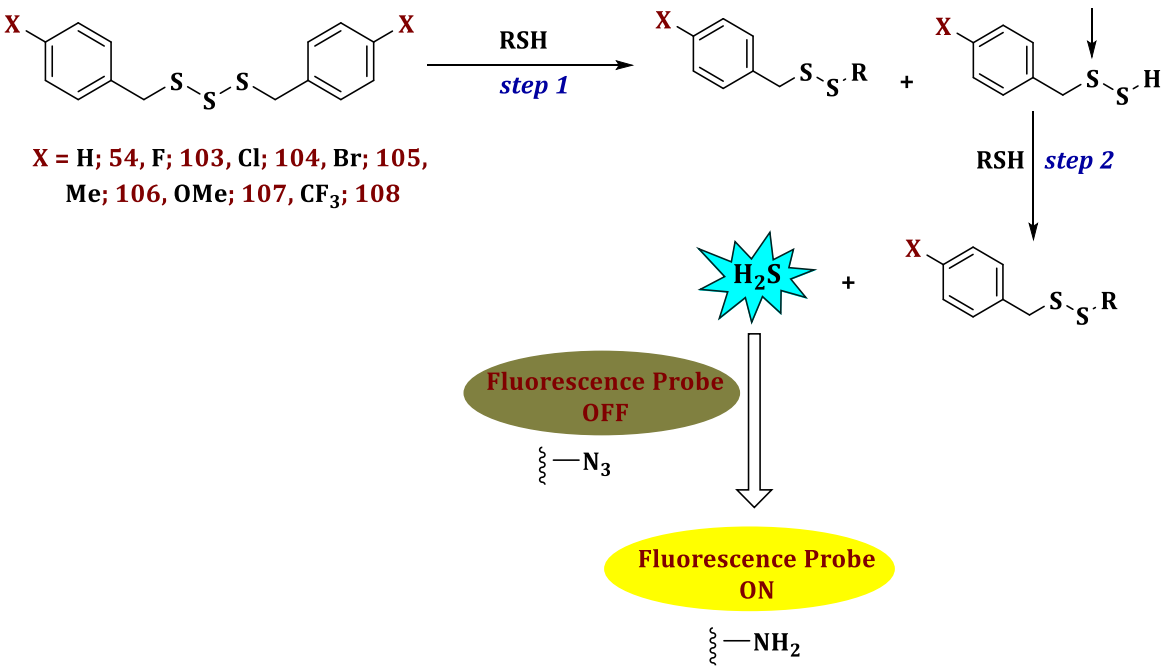

Scheme 5.13: Proposed thiolysis exchange reactions of trisulfides in cancer cells, resulting in H_2S production as an end product detectable by an azide fluorescent probe.

Hence, in keeping with previous studies, the research now turned towards studying the influence of a *para*-substituent on the aromatic rings of a small library of homobenzyl trisulfides on H_2S production in cancer cells using an H_2S azide-probe, which is the topic of the next section.

We aimed to synthesize the NAP probe using the commercially available NAP starting material. NAP synthesis appeared to be straightforward, and the probe is reported to manifest a high reactivity towards H_2S. In a study by Ling Zhang et al.,[477] NAP, **112**, was used for the detection and imaging of endogenous H_2S in MCF-7 cells via ratiometric fluorescence imaging. The probe's ability to visualize and quantify H_2S levels in living cells showcases its utility for studying H_2S-related processes at the cellular level. Mechanistically, azide reduction by H_2S has been studied by Pluth[482] and shown to involve the hydrosulfide ion as the key intermediate, adding to the azide terminal nitrogen to form an intermediate that eliminates nitrogen and elemental sulfur in an intramolecular process or nitrogen and HS_2^- via an intermolecular one as depicted in **Scheme 5.14**.

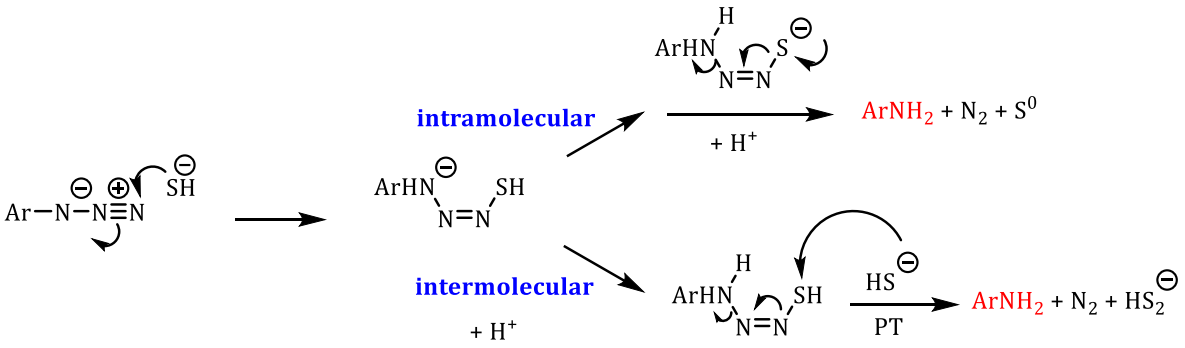

Scheme 5.14: Pluth's mechanism for azide reduction.[482]

Once reduced, the electron-releasing amino group formed promotes fluorescence that can be measured quantitatively,[477] as shown in **Scheme 5.15**.

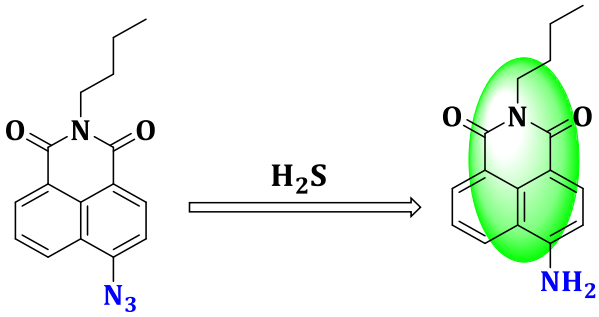

Azide, 112 (non reduced) **Amine, 114 (reduced)**

non-Fluorescent ***Fluorescent***

Scheme 5.15: Reduction of Azide to Amine in the NAP Fluorescent Probe for H_2S Detection.

5.5.2 Synthesis of the NAP Fluorescent Probe

The NAP azide probe was synthesized following Song et al.'s method,[483] via a condensation between *n*-butylamine and the naphthoic anhydride, **115**, shown in **Scheme 5.16** followed by an S_NAr of the bromine with an azide ion. The chemistry involved refluxing **115** with *n*-butylamine in ethanol for 6 hours, which proceeds via S_NAc to the amido-acid, which then cyclises with loss of water to the imide, **116**. Following removal of solvent (and reagent), the product was colourless and crystalline, which was purified by crystallization. Subsequently, imide **116** was reacted with sodium azide in dimethylformamide (DMF) at 40 °C for 4 hours, resulting in the formation of a yellow precipitate, **112**, that could be filtered on cooling, washed and crystallized. **Scheme 5.16** illustrates these synthetic steps.

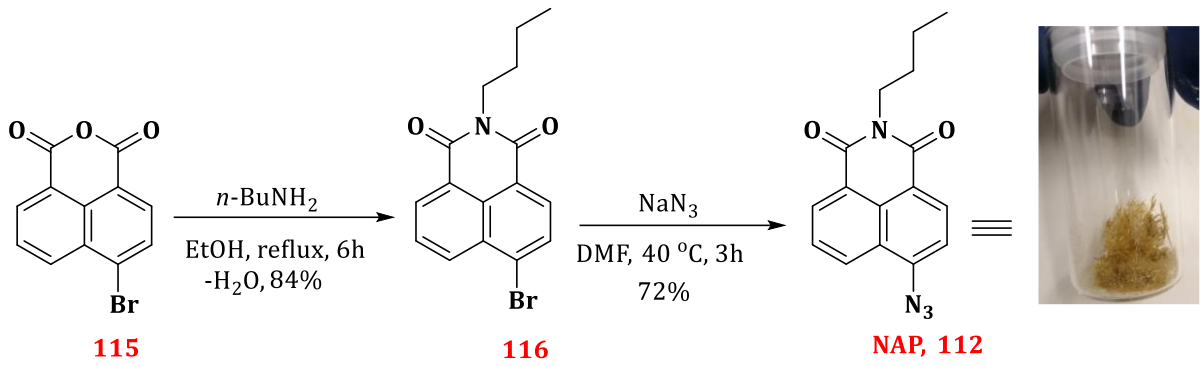

Scheme 5.16: Synthesis of NAP (113) using the method of Song et al.[483]

5.5.3 Validation of NAP: NMR, Fluorescence Studies, and Calibration Curve

The NAP probe was characterized by NMR spectroscopy. The ^{1}H NMR spectrum of the non-reduced azide probe exhibited characteristic peaks consistent with its structure (see **Figure 5.25**). Specifically, we observed distinct signals corresponding to the butyl group in the aliphatic region as well as aromatic protons, each displaying correct integrations agreeing with literature.[483]

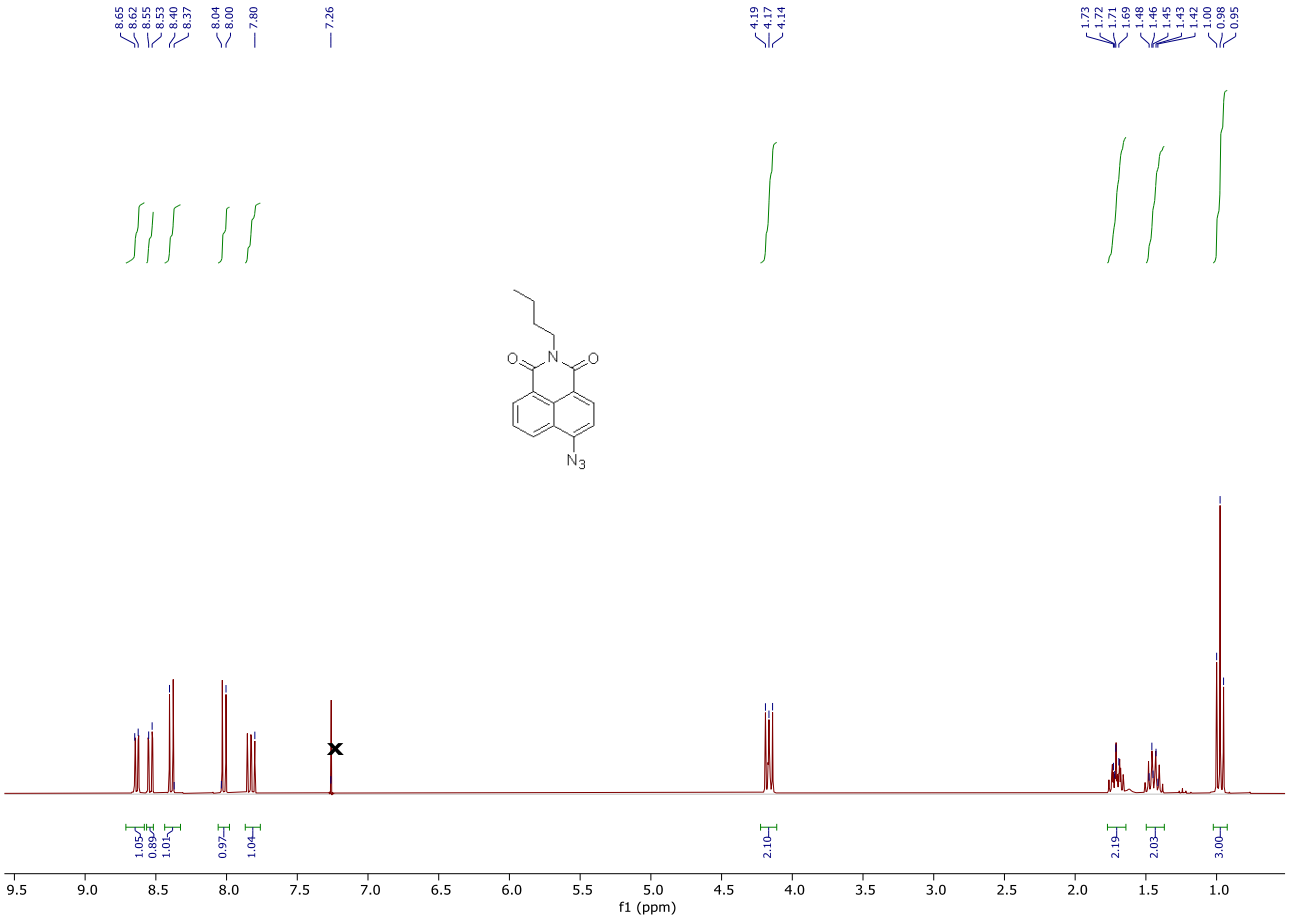

Figure 5.25: ^{1}H NMR spectrum of NAP, 112.

After successfully characterizing the probe, we proceeded to confirm its functionality through a series of tests. Initially, we investigated its reduction using Na_2S as a model sulfide reductant for H_2S. NAP (44 mg, 0.10 mmol) was dissolved in acetonitrile (15 mL, 6.7 mM), and a solution of $Na_2S•9H_2O$ (80 mg, 0.33 mmol) in PBS buffer (16.5 mL, 20 mM, pH = 7.4) was added. The relative concentrations were carefully chosen to ensure the homogeneity of the solution, considering that NAP is insoluble in water. The mixture was stirred at room temperature for 3 hours, resulting in the formation of a visibly fluorescent product. Subsequently, the product was extracted into EtOAc and purified via column chromatography. The reduced product was then analysed by ^1H NMR spectroscopy.

The spectrum (run in $CDCl_3$) showed an -NH_2 peak integrating for 2H as a singlet at 7.41 ppm, with aliphatic signals shifted slightly downfield in agreement with the literature.[483] Thin-layer chromatography (TLC) further corroborated these findings by showing the formation of a more polar and fluorescent product spot. **Figure 5.26** shows both azide and amine spectra.

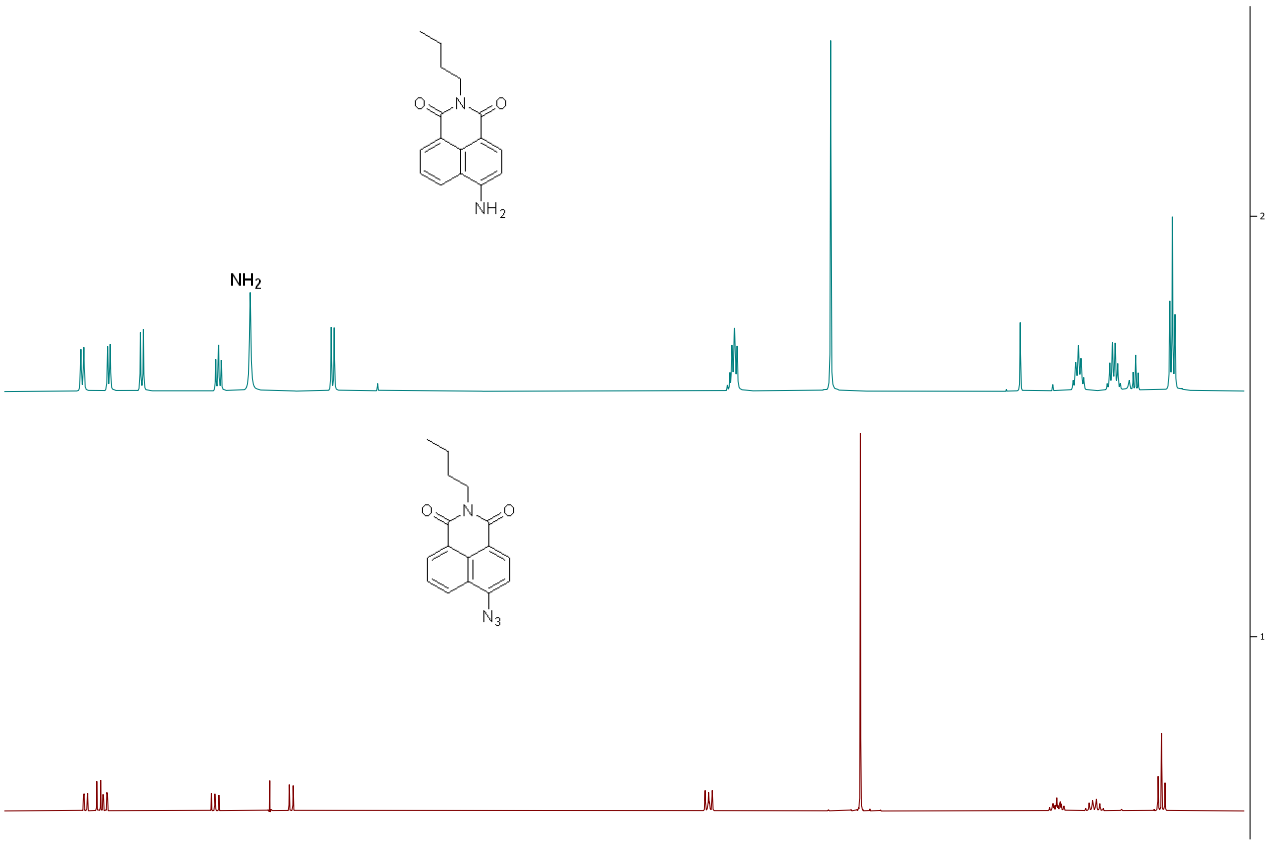

Figure 5.26: ^1H NMR overlay of non-reduced (TOP) and reduced (BOTTOM) probe versions of NAP, 112.

Next, excitation and emission spectroscopy were conducted on the probe. The non-reduced probe exhibited a baseline level of fluorescence with an excitation at 330 nm and emission at 661 nm. Upon reduction to the amine form, a notable enhancement in fluorescence intensity was observed, with strong excitation and emission spectra recorded at similar wavelengths. Specifically, a major emission peak was detected at 520 nm as shown in **Figure 5.27**.

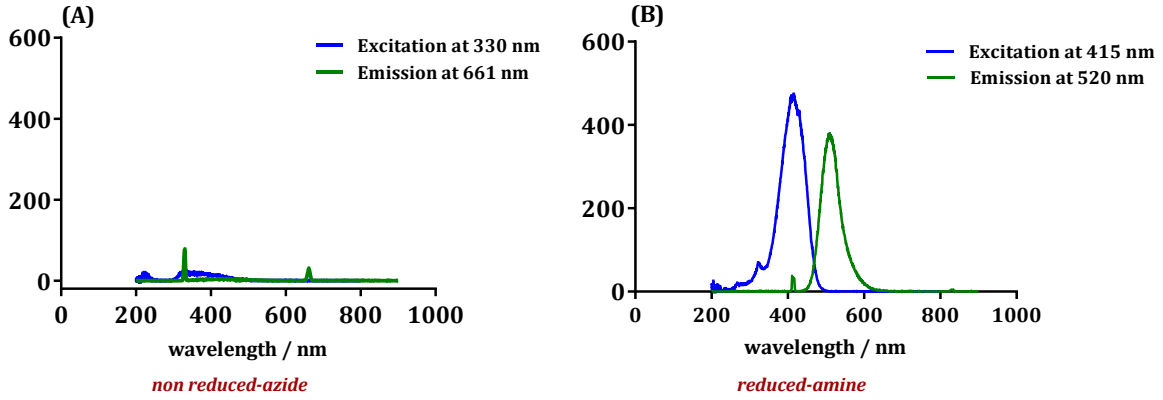

Figure 5.27: Excitation and emission spectra for (A) non-reduced, 112, and (B) reduced, 114 probe.

Having established the probe's fluorescent properties, we went on to create a calibration curve using Na_2S. Thus, a 10 µM solution of probe **112** was treated with Na_2S at concentrations ranging from 0 - 50 µM. The fluorescence emission intensity at 509 nm was measured for each solution. A plot of [Na_2S] vs E_m509 revealed a linear relationship (**Figure 5.28**) between the fluorescence emission intensity and Na_2S concentration, with the relationship $E_m509 = 0.358\ [Na_2S] - 0.268$ with $R^2 = 0.9869$, and *p*-value < 0.0001, indicating a significant correlation and the probe ready for use in H_2S evaluation for the trisulfide study.

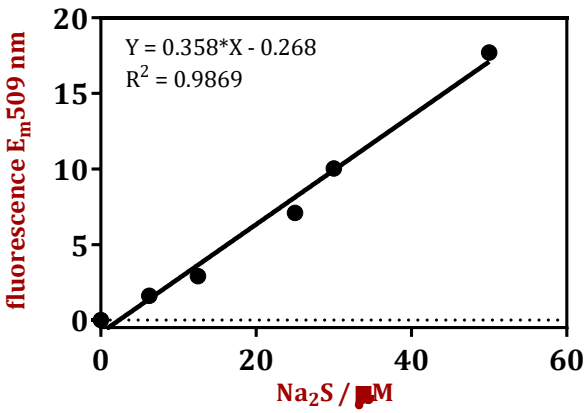

Figure 5.28: Calibration curve of [Na_2S] vs fluorescence at E_m509.

Importantly, the correlation covered the active concentration range of the trisulfides used in cancer cells from 50 nM – 10 μM.

5.5.4 Cellular Experimental Design and Timeline Analysis for H_2S Release

At this stage of the project, armed with our newly synthesized probe, we applied our small library of *p*-substituted homobenzyl trisulfides to measuring H_2S release in WHCO1 cancer cells.

Thus WHCO1 cells were cultured in 12-well plates and treated with either trisulfides *p*-OMe (**107**) or *p*-Br (**105**) at a concentration of 10 μM. Additionally, cells were treated with NAP alone or with Na_2S + NAP (both at 10 μM) for 10-minutes incubation time to allow for any H_2S production , which according to the literature[483] is the optimal timeline for incubating with the azide probe to trap all the H_2S, the culture media was then removed from each well, leaving the cells attached. The cells were then dried for three hours. Note that this step is reported not to affect the fluorescence intensity,[481] as the fluorescence signal has been shown to remain stable once the probe is reduced, regardless of the drying duration. One must also note here that these experiments aimed to target intracellular events regarding H_2S production rather than extracellular ones studied with the Ellman's perthiol study in section 5.4. Fluorescence measurements, expressed in arbitrary units (a.u.) reflect the relative brightness of the signal, and were captured using a Nikon fluorescence microscope at an excitation wavelength of 440 nm and an emission wavelength of 509 nm. The results of these measurements are shown in **Figure 5.29**.

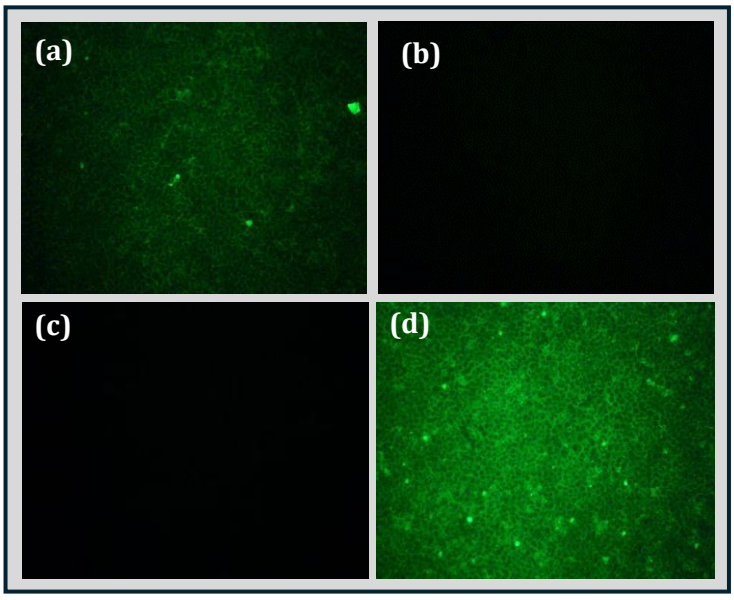

Figure 5.29: Fluorescence Images of the positive and negative controls for WHCO1 cells treated with (a) 112 NAP (b) 107 (*p*-OMe), (c) 105 (*p*-Br), and (d) NAP+ Na_2S. Cells were imaged on using a Nikon fluorescence microscope.

As seen in frame (a), a small amount of background fluorescence was produced by the probe alone, which agreed with the fluorescent spectrum of NAP **112** where a small amount of fluorescence was also detected (see **Figure 5.29**) and is indicative of the background reduction of the probe over time by cell reducing enzymes. Nevertheless, the background fluorescence was minimal compared to that generated from the NAP **112** in combination with Na_2S (frame d) due to reduction of the azide in **112**. Finally, the cells treated with the trisulfides alone as shown in panes (b) and (c) for the *p*-OMe and *p*-Br respectively showed no fluorescence as expected since no probe was present.

Next, our investigation focused on monitoring H_2S release in cells from trisulfides *p*-OMe (**107**) and *p*-Br (**105**) in the presence of NAP. The experiment followed the same protocol as the controls where WHCO1 cells were plated in 12-well plates and treated with trisulfides at a concentration of 10 μM. This time we did a short time course and allowed for three incubation times namely 10 minutes, 1 hour, and 3 hours. After each incubation period, the culture media was removed, and the cells were treated with NAP at 10 μM for 10 minutes. The cells were then dried, and the fluorescence was measured using a fluorimeter. **Figure 5.30** presents the results obtained from these experiments.

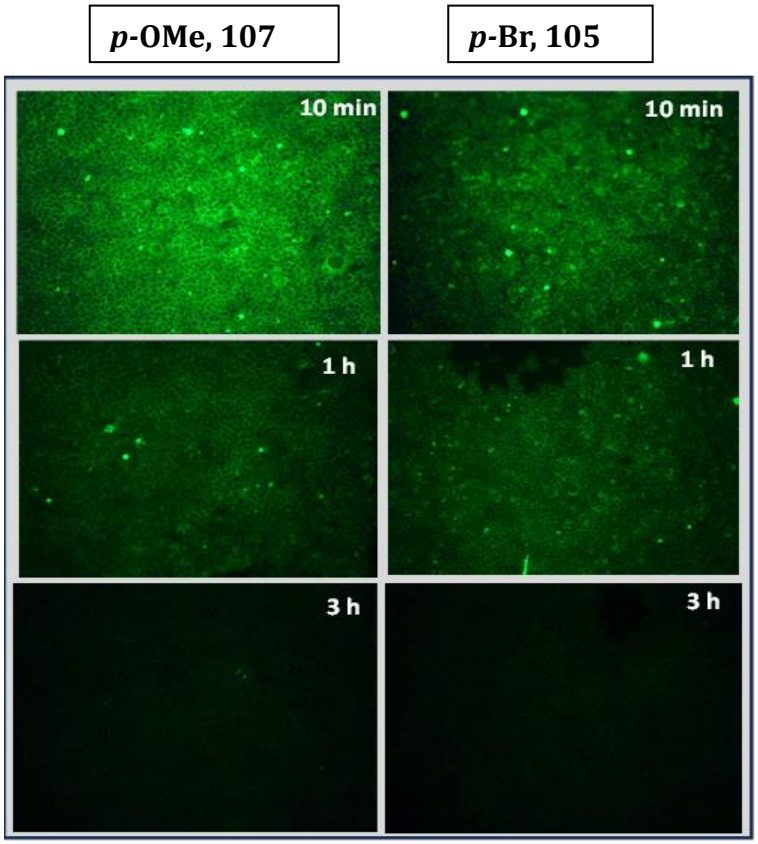

Figure 5.30: Fluorescence Images of WHCO1 cells treated with trisulfides 107 (*p*-OMe) or 105 (*p*-Br) for timepoints 10 min, 1 h and 3 h, followed by NAP, 107 H_2S monitoring. Cells were imaged using a Nikon fluorescence microscope.

The rapid intracellular thiolysis exchange reaction, enabling H_2S production, was observed as early as 10 minutes post-treatment, with fluorescence intensity diminishing over the following 3 hours. These findings indicate that substantial H_2S production begins as early as 10 minutes after treatment, with potential for an earlier detection point based on observed trends.

In addition, trisulfide **107** (*p*-OMe) resulted in significantly higher NAP-detectable fluorescence compared to trisulfide **105** (*p*-Br) under identical conditions. This result is encouraging as it is in line with the cytotoxicity trends observed of the parent trisulfides where the greater H_2S producer is also the more cytotoxic trisulfide i.e. **107**, *p*-OMe.

5.5.5 Evaluating the Correlation between Cytotoxicity and H_2S Release

Next, we examined the influence of additional homobenzyl trisulfides in an expanded library on H_2S production at 10 minutes. Employing the same method as that used for benzyl-benzyl trisulfides **105** (*p*-Br) and **107** (*p*-OMe), the other derivatives analysed were **54** (*p*-H), **103** (*p*-F), **104** (*p*-Cl), **106** (*p*-Me), and **108** (*p*-CF_3). Again, Na_2S and probe-only treatments served as controls. The fluorescence images obtained from WHCO1 cells treated with the trisulfides are presented in **Figure 5.31**.

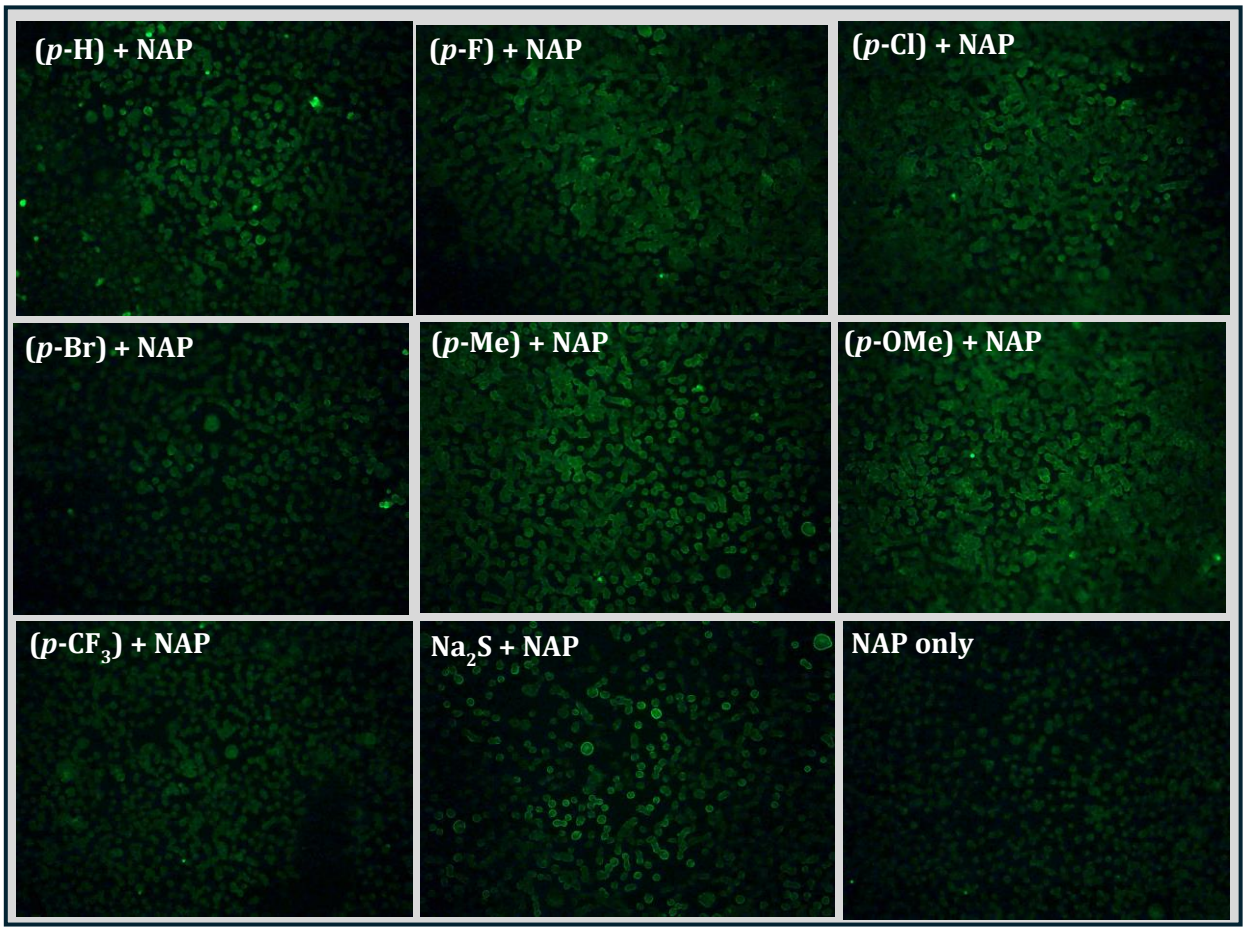

Figure 5.31: Fluorescence Images of WHCO1 cells treated with 54 (*p*-H) and 103 (*p*-F), 104 (*p*-Cl), 105 (*p*-Br), 106 (*p*-Me), 107 (*p*-OMe), and 108 (*p*-CF_3) trisulfides for 10 minutes followed by NAP. Cells were imaged using a Nikon fluorescence microscope.

The fluorescence intensity in this experiment was quantified using ImageJ software. The experiment was conducted once, with three biological repeats. For each well, three regions of interest (ROIs) were selected from each of three images, resulting in nine ROIs per experiment. This process was repeated for three determinations, leading to a total of 27 measurements per compound. All the trisulfides **54**, **103**, **104**, **105**, **106, 107** and **108** were found to have fluorescence intensities higher than the control group, albeit to varying degrees as shown in **Figure 5.32**.

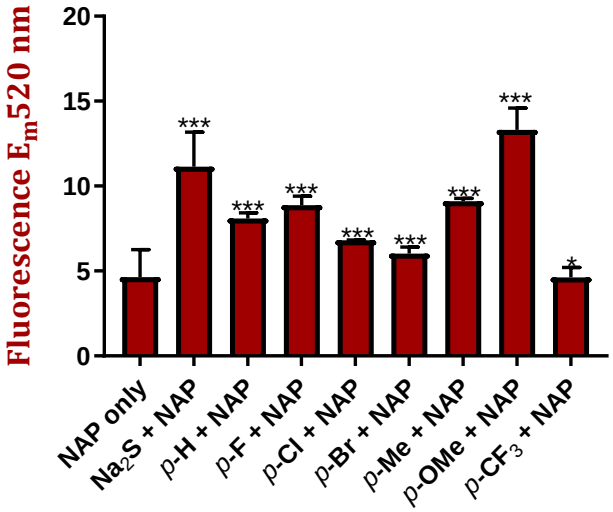

Figure 5.32: Fluorescence intensity of the homo benzyl-benzyl trisulfides in WHCO1 cells following a 10 min incubation followed by NAP treatment.

The t-test analysis revealed a significant increase in fluorescence relative to the untreated cells when comparing the NAP-only control to cells treated with trisulfides and Na_2S. A significant increase in fluorescence was observed for all treated groups with *p*-values < 0.001.

Once again, these results suggested a relationship between the electronic characteristics of the substituent and the fluorescence intensity, so a graph of fluorescence against the Hammett constant (σ_p) was plotted as shown in **Figure 5.33**.

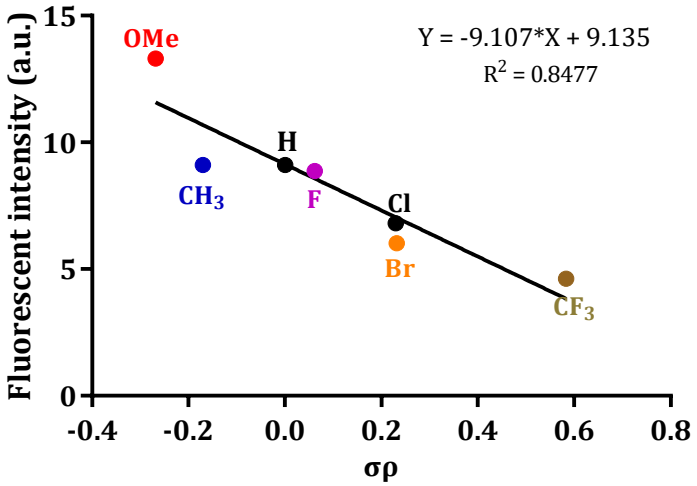

Figure 5.33: Plot of Fluorescence intensity vs the Hammett constant (σ_p) of the substituent in the benzyl-benzyl trisulfide library.

A correlation was observed between the fluorescence intensity produced and the *para*-Hammett constant of the substituent on the benzyl-benzyl trisulfide conforming to the equation: Em = -9.107σp + 9.135. The analysis indicates a negative gradient, with a *p*-value of 0.0033 and R^2 of 0.8477. Such a relationship demonstrated that as the electron-withdrawing capacity of the substituent increases (σ_p), the fluorescence intensity decreases, reflecting lower H_2S production. Notably, the group treated with **107** (*p*-OMe) exhibited the highest fluorescence intensity among all the experimental groups in line with its superior electron-donating character and its superior cytotoxicity. By comparison, **105**, bearing a *p*-CF_3 group as a strong inductive deactivator, showed the converse.

Additionally, it seemed logical to extend these results further to graphing fluorescence intensity vs trisulfide cytotoxicity as an IC_{50} as shown in **Figure 5.34**.

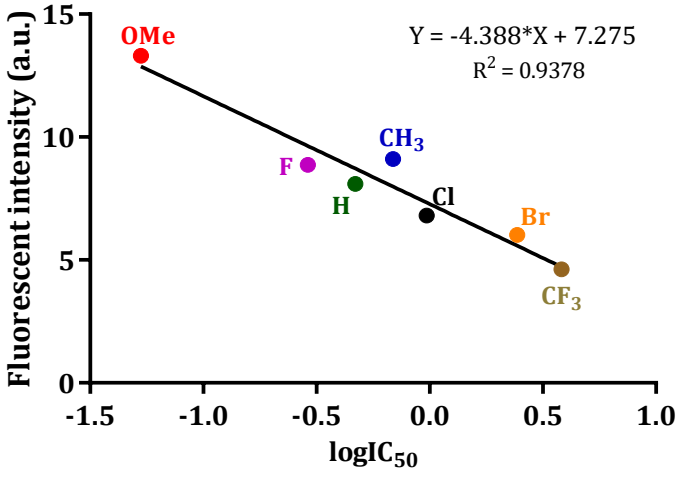

Figure 5.34: Plot of Fluorescence intensity vs the Log of the cytotoxicity IC_{50} of the benzyl-benzyl trisulfide.

Pleasingly, although not completely unexpected given the other correlations observed so far, a strong correlation was observed conforming to the equation Fluorescence AU = -4.388LogIC_{50} + 7.275. A highly significant *p*-value of 0.0003 and a robust R^2 value of 0.938 indicated a strong relationship. Once again, the negative trend held, with fluorescence intensity decreasing with higher IC_{50} (reduced cytotoxicity), Notably, the halogens followed their deactivating trend of Br > Cl > F, with Br with the lowest fluorescence intensity and the highest IC_{50} (less potent). The *p*-fluoro derivative, **103**, recorded a relatively higher fluorescence value compared to its other halogen counterparts, which may be accounted for by its stronger n-pp resonance donating effect (F is the least deactivating of the four halogens as F, Cl, Br, I). This correlation emphasizes the significant impact of the *p*-substituents on the amount of H_2S produced at 10 minutes. The results also agree with the Ellman's study on trisulfides in cancer cells, showing that activating substituents increase the pK_a, prolonging the perthiol lifetime and increasing its concentration in both extracellular and intracellular spaces. A higher perthiol concentration intracellularly as here, also links higher H_2S production with a more cytotoxic trisulfide.

5.6 Investigation into the Accumulation of Trisulfides in Cancer Cells

In the next section, we extended our mechanistic investigations of trisulfides in cancer cells in an attempt to track its intracellular localisation and to identify its targets. To this end, we synthesised a fluorescently labelled trisulfide which was tracked by confocal laser microscopy. The selection of this dansyl label,[272] was based on previous findings in our lab[484] in which the garlic compound ajoene was tagged and found to accumulate in the endoplasmic reticulum (ER) of breast cancer cells.[310,484]

5.6.1 Synthesis of a Fluorescent Dansyl-Tagged Trisulfide

The aim here was to synthesize a fluorescently labelled trisulfide by incorporating a dansyl fluorescent tag as one of the side groups, the target structure is shown below in **Figure 5.35** with a pointer for the biology rationale. This target was synthesised using our trisulfide synthesis methodology as described in Chapter 4. Although two different perthiols would presumably be produced from thiolysis, the dansyl group would

ultimately end up attached to GSH or a nucleophilic cysteine residue of an intracellular protein. Propyl spacer groups flanking the trisulfide were chosen based on their activity observed in Library 1. Notably, the versatility of our methodology for accessing hetero-trisulfides came into play, as is shown in **Scheme 5.17**.

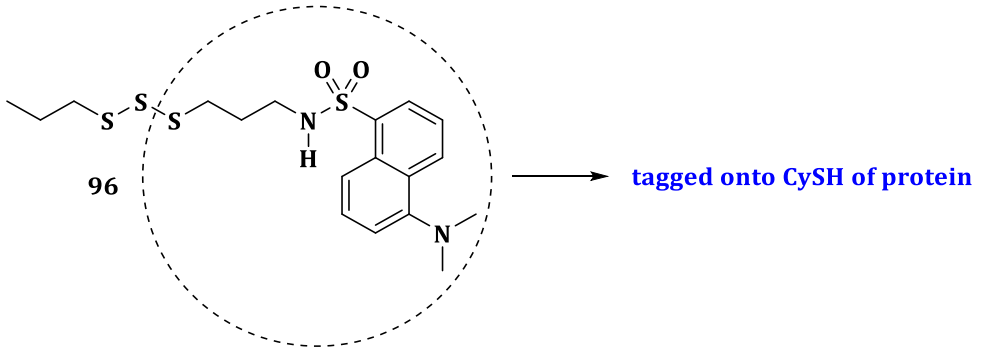

Figure 5.35: Structure of dansyl propyl-trisulfide (DPTS), 96.

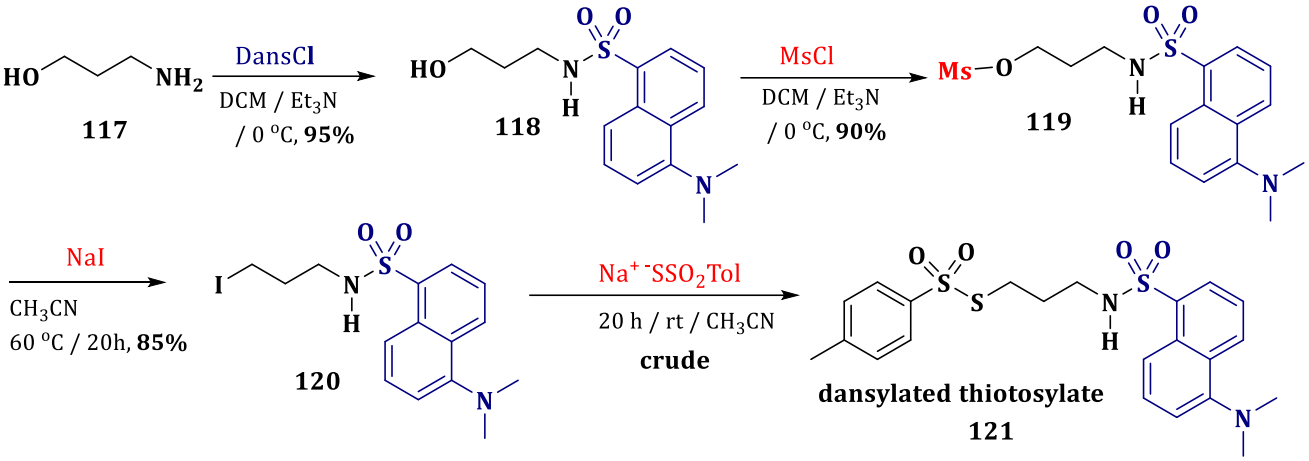

Scheme 5.17: Synthesis of the dansyl thiotosylate, 121.

Thus, nucleophilic substitution of dansyl chloride with the amino group of 3-aminopropan-1-ol, **117**, using triethylamine as a base for the HCl generated resulted in the formation of dansyl alcohol **118**. The reaction took place rapidly and efficiently on ice to produce **118** in 95% yield after column chromatography. Structural confirmation for **118** was obtained by ^{1}H NMR spectroscopy, in which the aromatic region (range 7.18 - 8.56 ppm) showed the six hydrogens of the dansyl moiety as an individual multiplet, while the NMe_2 moiety resonated as a singlet at 2.89 ppm as expected (see the appendix for the spectral data).

Next, we needed to transform the hydroxyl group into a leaving group for which the mesylate (methylsulfonate ester) and chosen and formed via slow addition of mesyl chloride to a solution of **118** and triethylamine in anhydrous dichloromethane (DCM) on

ice. After 30 minutes, TLC analysis showed complete conversion of **119** to the less polar mesylate, **119**, which was obtained as a luminous green oil in 90% yield after work-up and chromatography. The introduction of the mesylate group was confirmed by a significant downfield shift of the methylene hydrogens adjacent to oxygen, as well as a singlet for the three hydrogens of the mesyl group at 2.92 ppm in the ^{1}H NMR spectrum. Both these compounds had been made before in the ajoene project[272] and the spectroscopic data agreed with the published data. To increase the leaving group ability further, we converted mesylate **119** to the iodide. This was accomplished by heating **119** in 20 equivalents of NaI in acetonitrile for 24 hours at 60 °C (see **Scheme 5.1**). Successful conversion to a less polar spot assumed to be iodide **120** was observed by TLC in which **120** was obtained as a luminous green oil in 85% yield following purification by silica-gel chromatography. Thereafter, we attempted the iodide substitution with potassium *p*-toluenethiosulfonate using sodium thiotosylate in acetonitrile at room temperature. Under these conditions, a more polar fluorescent product appeared on TLC more or less spot-to-spot. However, this product degraded on silica, so was used in the next step without purification. Although quantifying the latter conversion was not possible, the intensity of the TLC spot suggested more than 60% conversion. Although not ideal, we were hopeful that full characterisation of the trisulfide could be achieved at the synthesis end.

With the dansylated thiotosylate in hand, we could now proceed to using our new trisulfide synthesis methodology. To this end, propyl disulfanyl acetate (1 eq.), **122**, and thiotosylate, **121** (1.2 eq.), were coupled in THF at -78 °C using sodium methoxide as a promoter and using a 30 second reaction time. Work-up and chromatography produced the target dansyl propyl trisulfide (designated as **DPTS**) **96**, as shown in **Scheme 5.18** in 71%. Unlike thiotosylate, **121**, trisulfide **96** was stable towards chromatography and stored in the refrigerator similar to other aliphatic trisulfides from before. Achieving a 71% yield in the final step was based on using the disulfanyl acetate partner as limiting and the thiotosylate in excess.

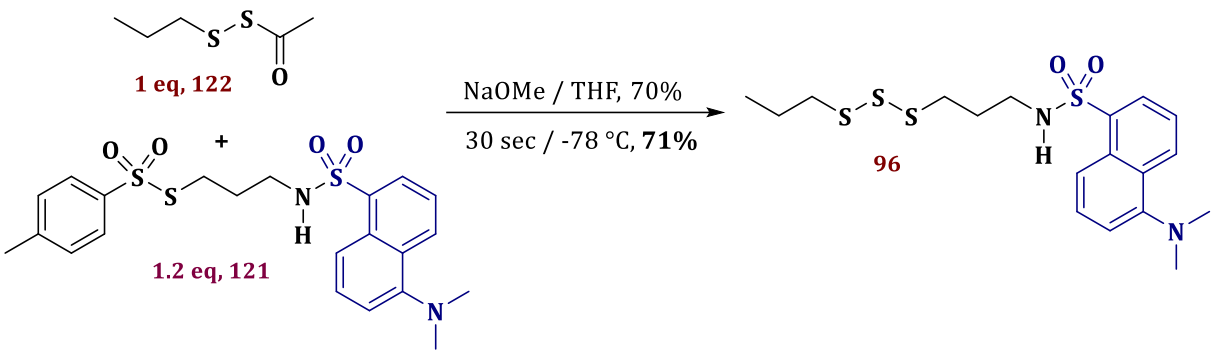

Scheme 5.18: Synthesis of dansylated-trisulfide (DPTS), 96.

The ^{1}H NMR spectrum of **96** is shown in **Figure 5.36** below with all resonances assigned. Of note was the appearance of the two methylene groups flanking the two trisulfide sulfurs in the range 2.70 - 2.80 ppm, consistent with **96** being an aliphatic trisulfide rather than a di- or tetrasulfide.

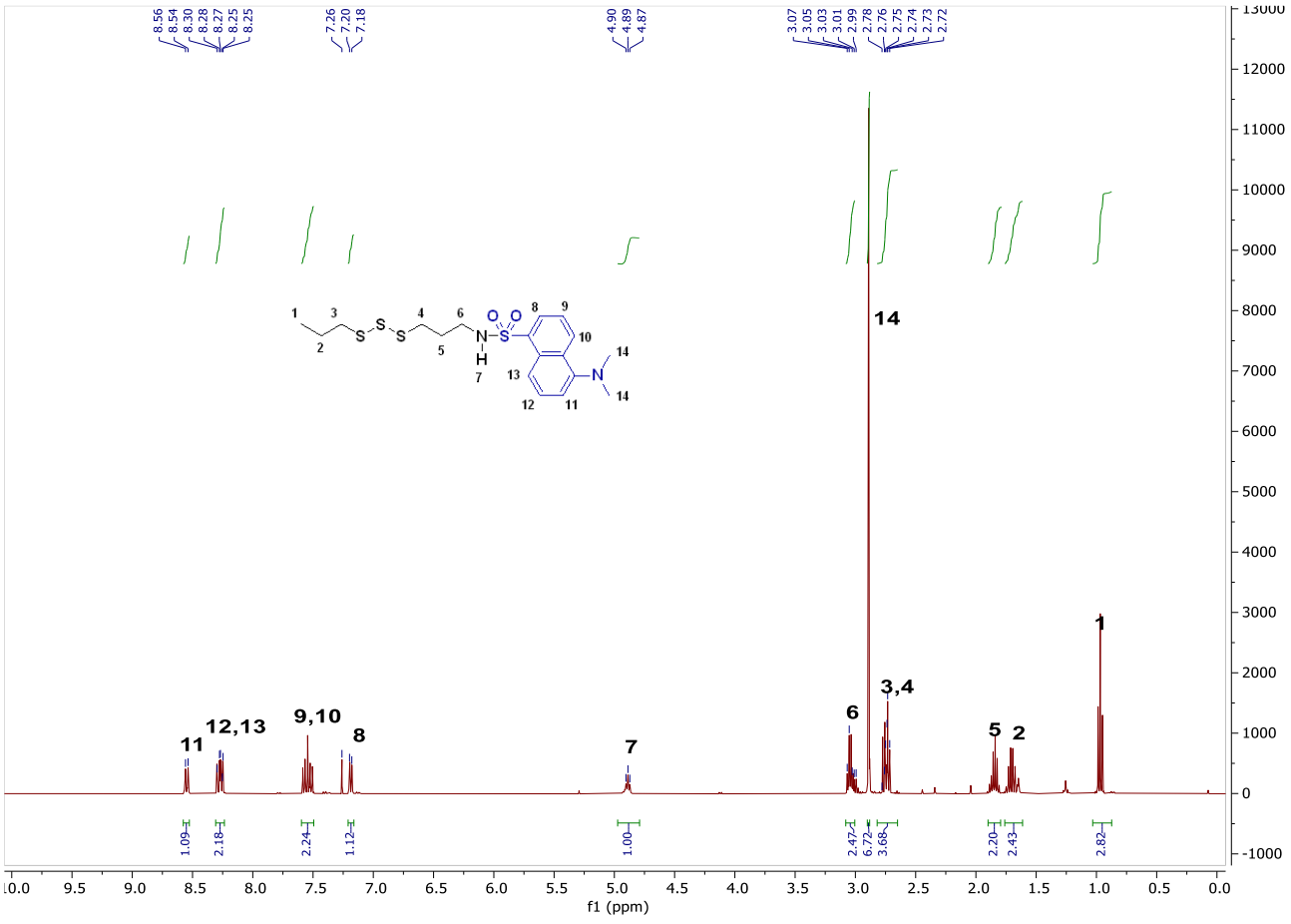

Figure 5.36: ^{1}H-NMR spectrum of dansylated trisulfide (DPTS), 96.

High-resolution mass spectrometry confirmed a molecular ion of 431.0952, aligning reasonably well with the expected 431.0980 for $[M + H]^+$ for $C_{18}H_{28}N_2O_2S_4$. The diagnostic

spectroscopic characterisation for **96** is presented in **Table 5.7**, including an IR stretching peak for S-S, providing us with the confidence that dansyl trisulfide **96** had been successfully synthesized.

Table 5.7: Spectroscopic data supporting dansyl trisulfide (DPTS), 96, formation

Structure	^{1}H NMR -SCH_2	IR S-S	HRMS for $[M+H]^+$	
			experimental	calculated
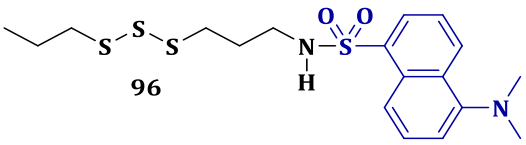 96	2.70-2.82	468	431.0952	431.0980

5.6.2 Absorption and Emission Properties of DPTS

To confirm the dansyl-trisulfide's suitability as a fluorophore for fluorescent studies, we investigated its absorbance and emission properties as shown in **Figure 5.37**. A suitable fluorophore must absorb and emit light with non-overlapping signals, which would cause quenching. A solution of 5 µM DPTS was prepared in DMSO, and the absorbance and emission spectra were recorded. The absorbance was recorded in the range 200 - 520 nm, and the emission spectra from 0 - 800 nm. DPTS was found to have two absorption peaks at 263 and 338 nm (**Figure 5.37A**), and non-overlapping emission peaks at 522 and 523 nm (**Figure 5.37B** and **5.37C**) for the two absorption wavelengths respectively, accounting for its blue-green fluorescence.

(**A**)

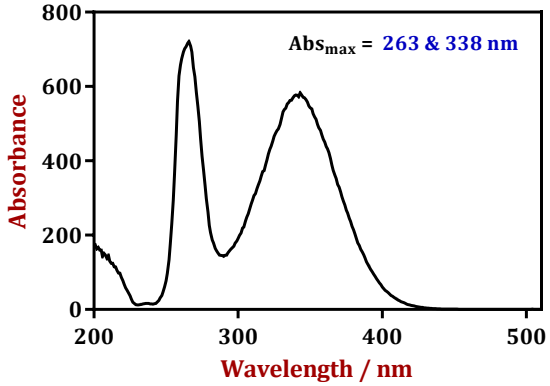

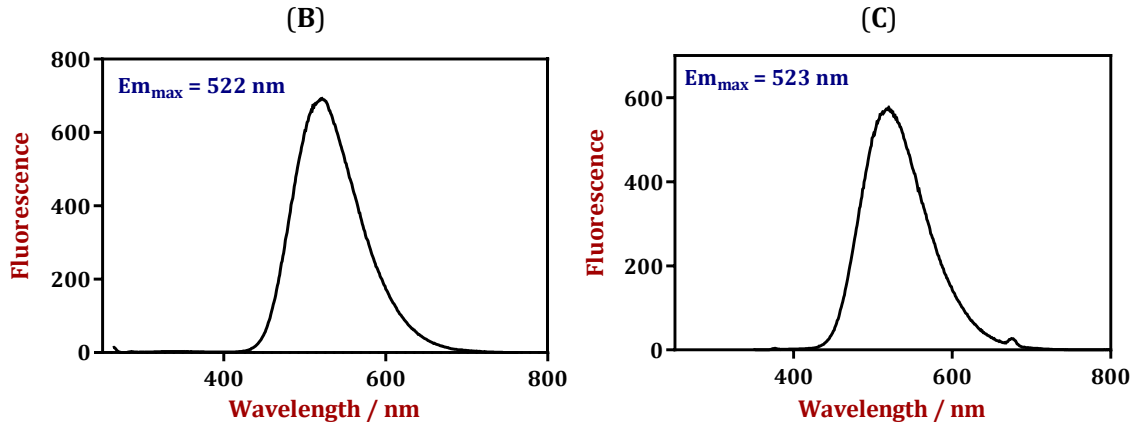

Figure 5.37: Absorption and Emission spectra of DPTS. (A) UV-Vis spectrum of DPTS (B) Fluorescence spectrum of DPTS, Ex = 263 nm; Em = 522 nm (C) Fluorescence spectrum of DPTS, Ex = 338 nm, Em = 523 nm.

5.6.3 Cytotoxicity of DPTS in Cancer Cells

In order to establish whether DPTS had any cytotoxicity to cancer cells, it was incubated with WHCO1 cells for 48 hours as described before (section 5.1.1) and evaluated using the MTT assay. The fluorophore alone, as dansyl chloride, was also investigated as well as DATS (diallyl trisulfide), *E/Z*-ajoene and DP (dansyl ajoene) as comparisons. The cytotoxicity IC_{50}s are shown in **Table 5.8**.

Table 5.8: Cytotoxicity IC_{50}'s of DPTS and related garlic compounds against WHCO1 esophageal cancer cells

Compound	IC_{50} ± SD (μM)
DPTS	**54 ± 29**
DATS	**6.3 ± 4.4**
DP	**21 ± 6.2**[272]
Z-ajoene	**25 ± 2.8**[272]
E-ajoene	**39 ± 7.8**[272]
dansyl chloride	**>200**[272]

DATS was found to have the most potent cytotoxicity with an IC_{50} value of 6.3 ± 4.4 μM against WHCO1 cells, with dansyl chloride found to be inactive (IC_{50} > 200 μM). As established previously, the ajoenes were somewhat less potent (IC_{50} in the 20 - 40 mM range), while our dansylated trisulfide, **DPTS**, came out as the least active at 54 ± 29 mM. From other studies[317] and the current work (Library 1), the allyl group has similar activity

to propyl but clearly the dansyl group was lowering the cytotoxicity. Nevertheless, its IC_{50} of around 50 mM was considered to be sufficient to carry on with. In a comparative study, **DP**, a dansylated ajoene analogue previously synthesized and evaluated,[272] provided valuable insights into the targets of ajoene in cancer cells, although admittedly, its IC_{50} was just over two-fold greater than that of **DPTS** with an IC_{50} of 21 mM.

5.6.4 Laser Scanning Confocal Imaging (LSCM) as a Tool for Studying Intracellular Dynamics

Laser scanning confocal microscopy (LSCM) can allow for the exploration of protein-drug interactions within complex biological systems.[484] This technique can provide detailed 3D images by capturing thin sections of the biological sample, enabling the study of molecules in their complex environments.[485] We employed commercially available organelle dyes to fluorescently label the ER, mitochondria, and lysosomes. These dyes emit fluorescence in distinct channels, enabling their visualization.

Colocalization refers to the phenomenon where two or more fluorescent signals overlap.[486] This occurs when emissions originate from distinct fluorescent sources, such as an organelle dye and a labelled drug; and the signals emanate from the same location.[10] Thus colocalization indicates close proximity. However, the overlap of two signals does not necessarily imply that the two fluorescent emitters directly interact (i.e. through a chemical bond or electrostatic interaction); rather, it signifies their coexistence within the same location. Analysis of colocalization can take place both by visual inspection and quantitatively. In this context, colocalization is an overlap of pixels acquired from two emission channels.[487]

The dansyl-tag has desirable characteristics, being excited at 350 nm, and emitting at 520 nm in the blue-green range with a favourable duration of approximately 10 ns[488] in which emission characteristics are affected by the specific molecule to which it is attached, as well as the surrounding solvent.[489] Notably, the blue-green emission spectrum of the dansyl-tag does not overlap with the commercially available organelle trackers which we had on hand, which are red. Laser scanning confocal microscopes use focused laser beams to scan a specimen's surface, collecting and processing emitted or reflected light to create high-resolution 2D or 3D images (**Figure 5.38**).

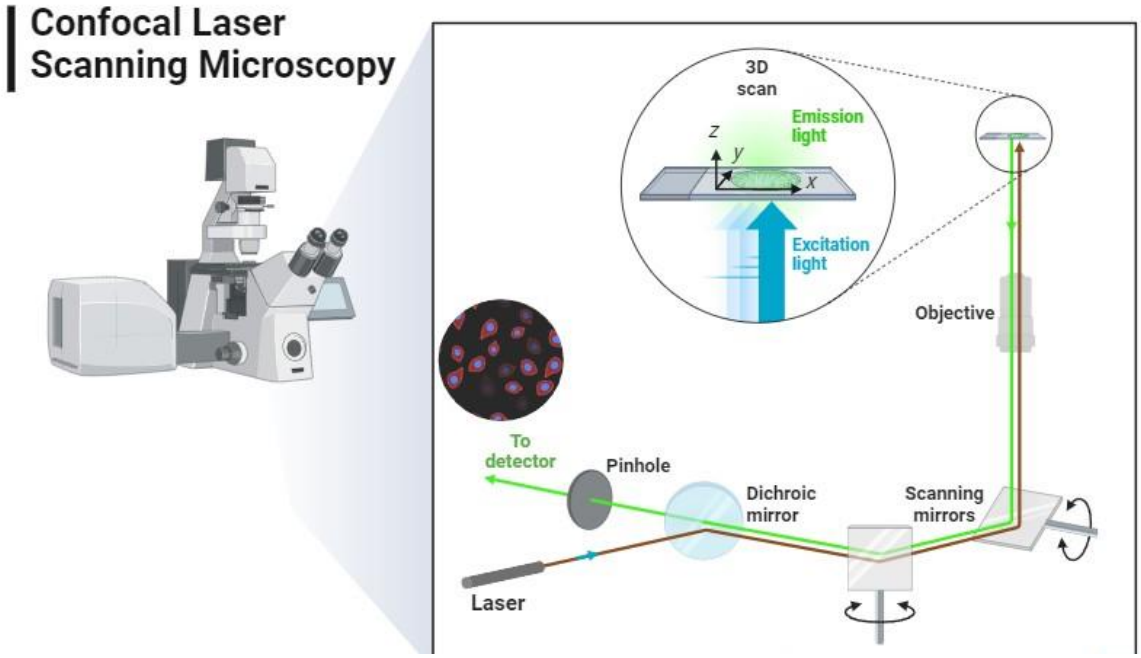

Figure 5.38: The principle of Scanning Confocal Laser Microscopy. A cross-section of the specimen is excited at a specific wavelength to obtain fluorescence in a specific focal plane. The integration of essential components, including scanning mirrors, a dichroic mirror, objective lens, and a confocal pinhole, contributes to enhanced lateral and axial resolution. The result is a high-contrast, finely detailed image that allows for precise three-dimensional visualization of the specimen's structure.

We selected MDA-MB-231 breast cancer cells for the confocal experiment owing to their tendency to spread out with their large cytoplasm, enabling for an easier visualisation of intracellular compartments. In contrast, WHCO1 cells are smaller in size, and have a small cytoplasm and large nucleus which is more difficult to see.

5.6.5 Live Cell Confocal Images of MDA-MB-231 Cells Treated with DPTS and Trackers

For our study, we used the following live cell tracking dyes: ER-tracker red (Invitrogen E34250), Lyso-tracker red (Invitrogen L7528), and Mito-tracker red (Invitrogen M22425). These stains accumulate in living cells and selectively stain these organelles. The organelle dyes were added 30 minutes before imaging to allow for accumulation within their respective organelles.

Upon treatment of the cells with DPTS for 30 minutes, a distinct blue fluorescence was observed as shown in panel **B**, **Figure 39**, indicating drug penetration into the cells with prominent accumulation in the cytoplasm with an apparent perinuclear distribution. Notably, fluorescence was not observed in the membrane or nucleus. As shown in Figure

5.39, the transmitted light channel (**T**) revealed a healthy cell morphology, while the overlay (**O**) illustrates the drug's localization within the cell. However, no fluorescence was observed in the red channel (**R**).

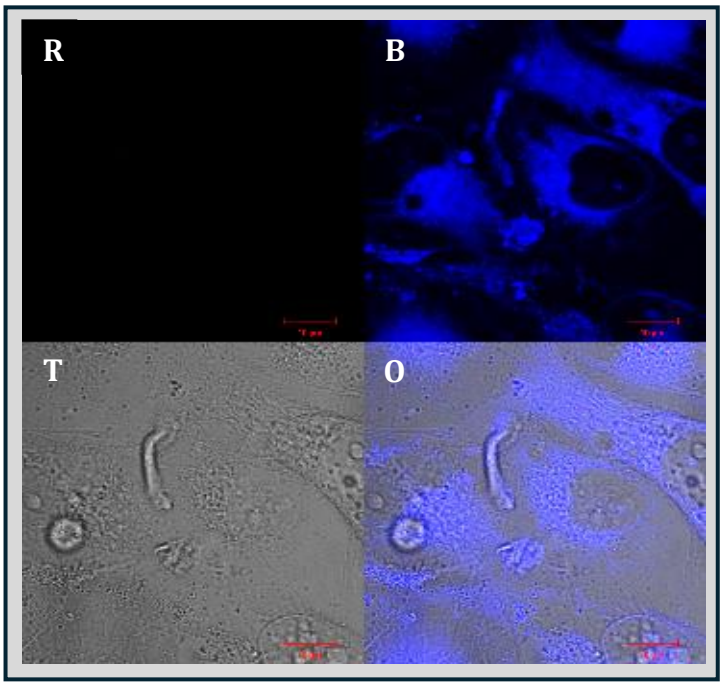

Figure 5.39: Live cell confocal images of MDA-MB-231 cells treated with DPTS. Cells were treated for 30 minutes and then imaged. (R) No fluorescence detected in the red channel (B) fluorescence is observed in the blue channel (T) transmitted light channel only to show cell morphology. (O) overlay of all three channels.

Next, the MDA-MB-231 cells were treated with the organelle trackers to generate images shown in **Figure 5.40**. All of the trackers were found to only fluoresce in the red channel with nothing coming through in the blue channel. In addition, the distribution of signals was different between the trackers, with the ER as expected being perinuclear and cytoplasmic, the mitochondria as mainly rod-like structures within the cytoplasm, and the lysosomes dispersed and globular-like. Owing to the lack of any blue fluorescence emanating from the trackers, they could be used together with the DPTS probe which fluoresced blue but not red.

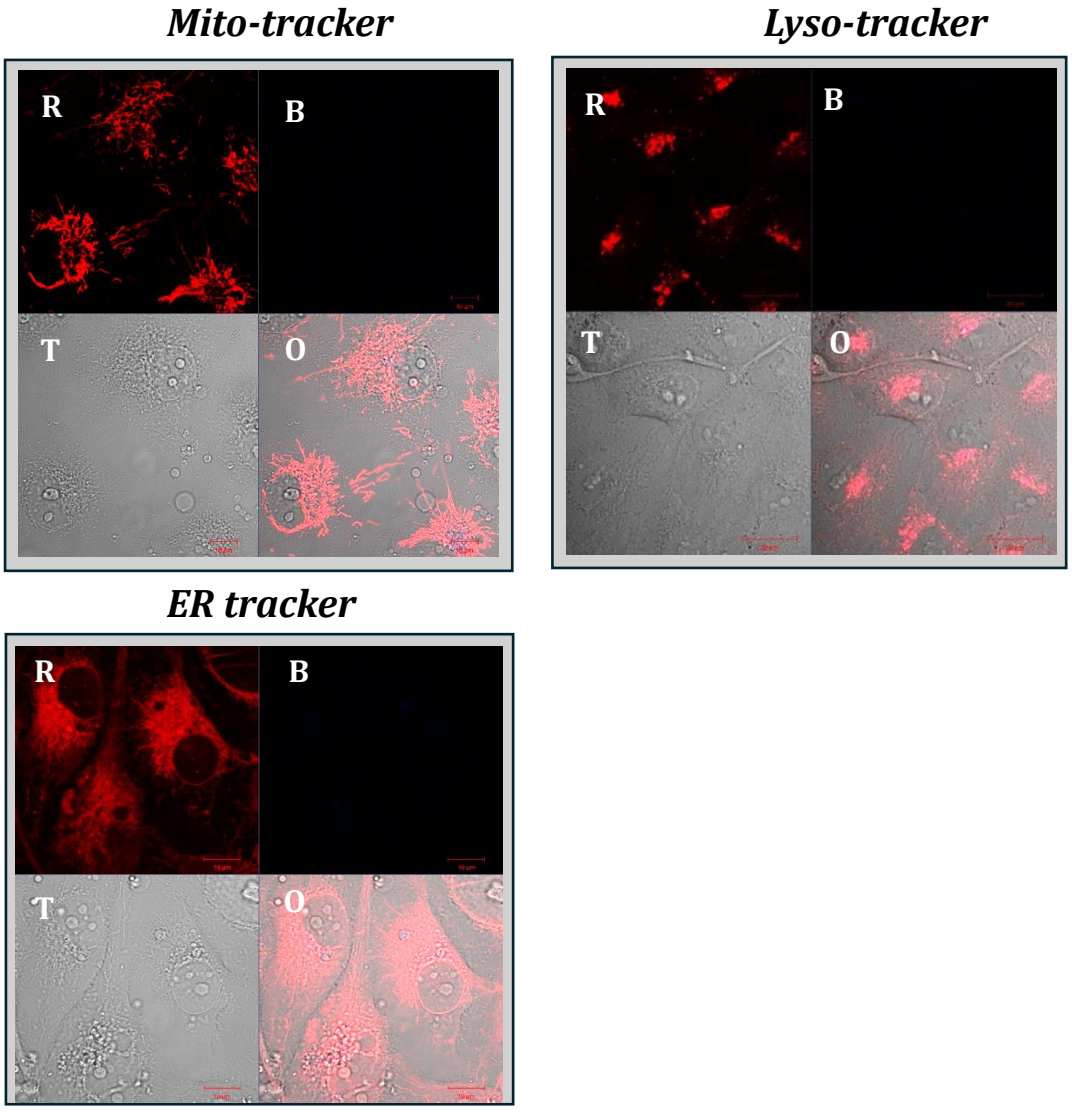

Figure 5.40: MDA-MB-231 cells incubated with Mito-tracker, Lyso-tracker, and ER-tracker. Cells were pre-treated for 30 minutes with the tracker and then imaged**. (R)** Red Channel**. (B)** blue channel**. (T)** transmitted light**. (O)** overlay of all signals.

The transmitted light and overlay images for the mitochondrial, lysosomal, and ER trackers all revealed MDA-MB-231 cells with normal morphology, indicating that none of the trackers had induced adverse effects on cellular structure. The absence of any apparent abnormalities in cell morphology supports the suitability of the chosen concentrations and incubation times for the trackers in live cell imaging experiments.

Having established the effects of compounds and trackers on the cells independently, we next looked at combinations. We first investigated whether DPTS might accumulate in the regions of the mitochondria, an organelle involved in cellular processes, including energy production, calcium homeostasis and apoptosis.[490] **Figure 5.41** shows the images obtained from DPTS together with the mitotracker organelle stain.

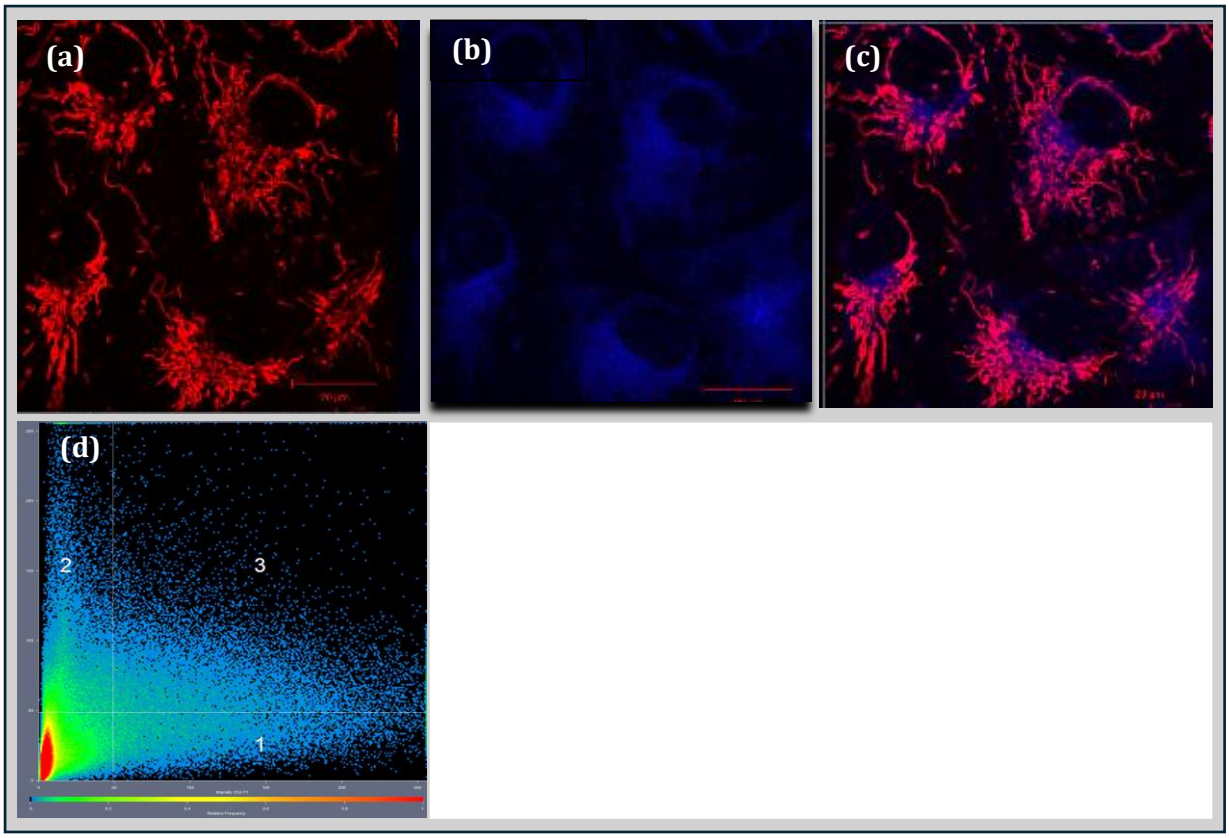

Figure 5.41: Confocal microscopy of MDA-MB-231 cells treated with DPTS and stained with mitotracker red: (a) Mitotracker (Red channel) **(b)** DPTS (Blue channel) **(c)** Overlay **(d)** Scatterplot**.**

From visual inspection, the combined fluorophores from mitotracker and DPTS (**Figure 5.41c**) do not appear to be in the same location of the cell, i.e. DPTS doesn't appear to be localising in the mitochondria. Quantitation was then performed using a pixel-by-pixel approach with Zen Black® software. Each pixel is plotted in a scatter diagram based on its intensity level from each channel with the blue intensity on the x-axis, and the red intensity on the y-axis. The pixels are designated into four quadrants, defined by crosshairs within the scatterplot (see **Figure 41d**). Quadrant 4, lower left, denotes pixels with low intensity in both channels and is considered background, excluded from colocalization analysis. Quadrants 1 and 2 contain pixels with high blue or red, respectively. Quadrant 3 contains colocalized pixels, visualized as purple blending in the colocalization image.

In order to quantify the colocalization, we examined pixel distributions within defined Regions of Interest (ROI). From this, a colocalization coefficient (cc) was calculated for each channel to give a pixel overlap value in the range 0 to 1.[491] This was done for three replicates from which an average and standard deviation was obtained. Another

parameter that was obtained was the weighted colocalization coefficient (wc), which considers pixel intensity. Here, a lower wc for the red channel suggests more red pixels outside the colocalization area. The overlap coefficient (oc) assesses perfectly colocalized pixels, and the Pearson's[491] correlation coefficient (R) provides a quantitation of the relationship between the two signals ranging from -1 to 1. The colocalization analysis for mitotracker and DPTS is shown in **Table 5.9**.

Table 5.9: Colocalization analysis of DPTS and mito-tracker in MDA-MB-231 cells

Organelle	wc (blue)	wc (red)	oc	Pearson's Correlation R
Mitochondria	0.470	0.329	0.55	- 0.02

The weighted colocalization coefficients indicate that 47% of the mitochondrial red pixels overlap with the DPTS, while 32% of the DPTS overlaps with the Mito-red. This suggests some overlap; however, the correlation coefficient with a value of -0.02 does not support any colocalization. Since the blue fluorescence in these images is weak and close to background, it is possible that the wc and oc are picking up background pixels which makes the colocalization look more than it is but when taken together with the visual inspection of the images which do not show any overlap, and with the lack of correlation in the Pearsons correlation constant, we can conclude that DPTS does not localise in the mitochondria.

The second organelle we investigated were the lysosomes, which are membrane-bound organelles containing hydrolytic enzymes involved in intracellular digestion and waste material degradation.[492] The cells were treated with DPTS in combination with lysotracker red as depicted in **Figure 5.42**.

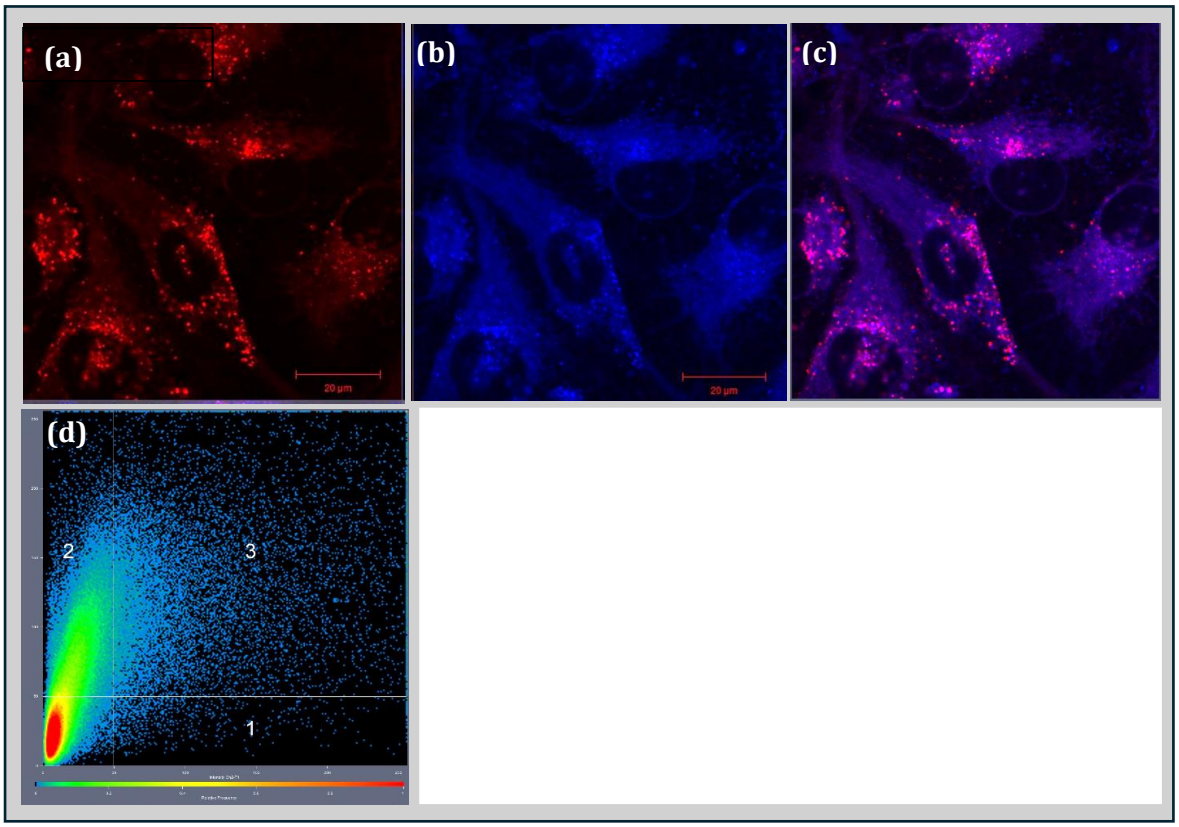

Figure 5.42: Confocal microscopy of MDA-MB-231 cells treated with DPTS and stained with lyso-tracker red: (a) Lyso-tracker (Red channel) **(b)** DPTS (Blue channel) **(c)** overlay **(d)** Scatterplot.

Visually there appears to be a substantial overlap between the blue (DPTS) and red (lysotracker) channels in Panel 3 (**c**). All of the red signals appear to coincide with the blue signal, although much of the blue is outside of the red. In this image, the lysotracker dots appear pink, indicating signal overlap and colocalization. Examining the scatter plot, there are substantial pixels in quadrant 3, indicating colocalization. Quantification of the data is shown in **Table 5.10.**

Table 5.10: Colocalization analysis of DPTS with Lyso-tracker in MDA-MB-231 cells

Organelle	wc (blue)	wc (red)	oc	Pearson's Correlation R
Lysosome	0.947	0.239	0.66	0.21

The weighted colocalization coefficient is significantly higher in the blue channel (DPTS) compared to the red channel (lysotracker), with values of 0.947 and 0.239, respectively. This supports the visual inspection in which some of the blue overlaps with the red. However, while all of the red overlaps with the blue, only some of the DPTS are in the lysosome. The overlap coefficient (oc) of 0.66, and the Pearson's correlation coefficient of

0.21 support some colocalization. The accumulation of DPTS within the lysosome suggests that some of it may be targeted for degradation or processing within this organelle.

We next investigated the endoplasmic reticulum (ER). The ER is an organelle responsible for the biosynthesis, folding, assembly, and modification of most secretory and transmembrane proteins within eukaryotic cells. The ER is the main site for the biosynthesis of lipids such as phospholipids, cholesterol, and ceramides, which are transported to other organelles and cellular membranes via vesicles of the secretory pathway.[493] **Figure 5.43** shows the fluorescence images acquired when the MDA-MB-231 cells were stained with ER tracker-red and treated with DPTS for 30 minutes.

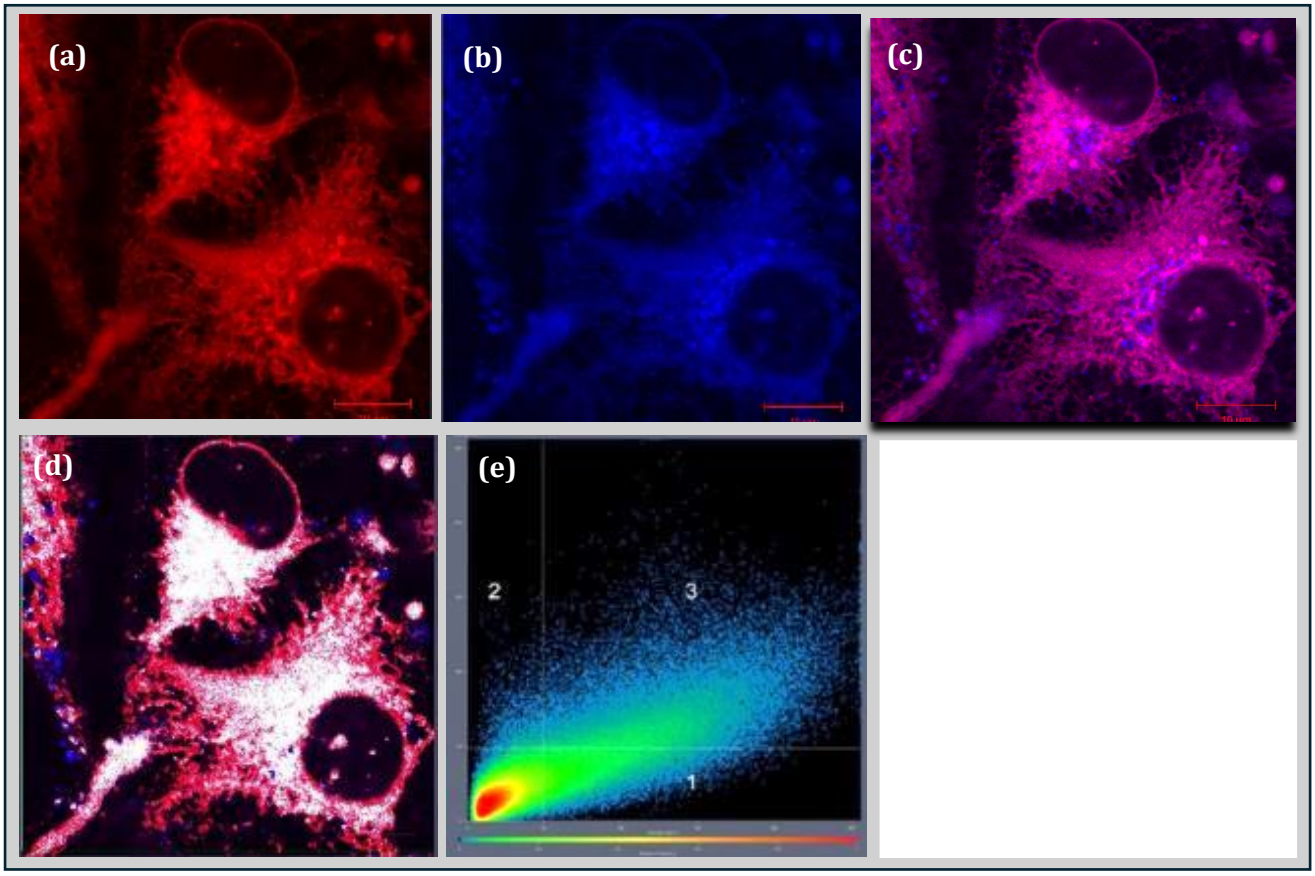

Figure 5.43: Confocal microscopy of MDA-MB-231 treated with DPTS and ER tracker. (a) ER tracker (Red channel) **(b)** DPTS (Blue channel) **(c)** overlay **(d)** colocalisaiton map **(e)** Scatterplot.

At first glance, the blue and red signals appear to exhibit a remarkably similar distribution. Indeed, we had shown in the control experiments, that ER tracker fluoresces red and does not bleed through into the blue channel. Together DPTS and ER tracker produce strongly overlapping signals as seen from the pink overlay in Figure **5.43c,** and

the colocalisation map **d**. In the scatter plot (**e**), the blue and red signals exhibit a strong co-distribution, depicted by the concentration of pixels along the diagonal. This suggests that the signals from DPTS (blue channel), and the ER tracker (red channel), are emanating from the same cellular locations. Furthermore, the presence of pixels above the diagonal line indicates regions where the blue signal is higher than the red, suggesting localization of DPTS also in some areas of the cell other than the ER. The quantitation analysis for ER tracker and DPTS is presented in **Table 5.11.**

Table 5.11: Colocalization analysis of DPTS with ER-tracker in MDA-MB-231 cells

Organelle	wc (blue)	Wc (red)	oc	Pearson's Correlation R
Endoplasmic reticulum	0.985	0.766	0.88	0.59

The weighted colocalization coefficient shows that 99% of the red pixels colocalize with the blue, and 77% of the blue pixels colocalize with the red. In addition, a Pearsons correlation is 0.59 is obtained. Thus, DPTS appears to be strongly localising in the ER, with some also in the lysosome.

These results of DPTS in MDA-MB-231 breast cancer cells present new insights into the intracellular targets of trisulfides in cancer cells. Comparing the degree of colocalization among the three organelles studied, the ER exhibits excellent colocalization with DPTS, suggesting a targeted affinity for this organelle, while the mitochondria is not targeted, with the lysosomes showing some targeting. The presence of DPTS in the lysosome suggests that it may be cleared through this route.

We have previously found similar findings for dansyl-tagged and fluorescein-tagged ajoene, another garlic organosulfur compound although a different chemotype with a vinyl disulfide functional group instead of a trisulfide. Importantly it also has an electrophilic sulfur. Since dansyl-trisulfide also targets the ER, it is likely that there may be overlapping modes of action between the two chemotypes in cancer cells. Based on our findings for ajoene, we can propose a similar mechanism of action, although in the case of the trisulfide, thiolysis exchange also produces a reactive perthiol which leads to the production of H_2S – a key aspect that will be discussed later on. Taken together, we propose a general hypothesis for the mode of action of trisulfides in cancer cells shown in **Figure 5.44**, which takes into account the ER targeting. Presumably the protein

cysteine can also attack the sulfur adjacent to the propyl group, but this won't lead to visualisation.

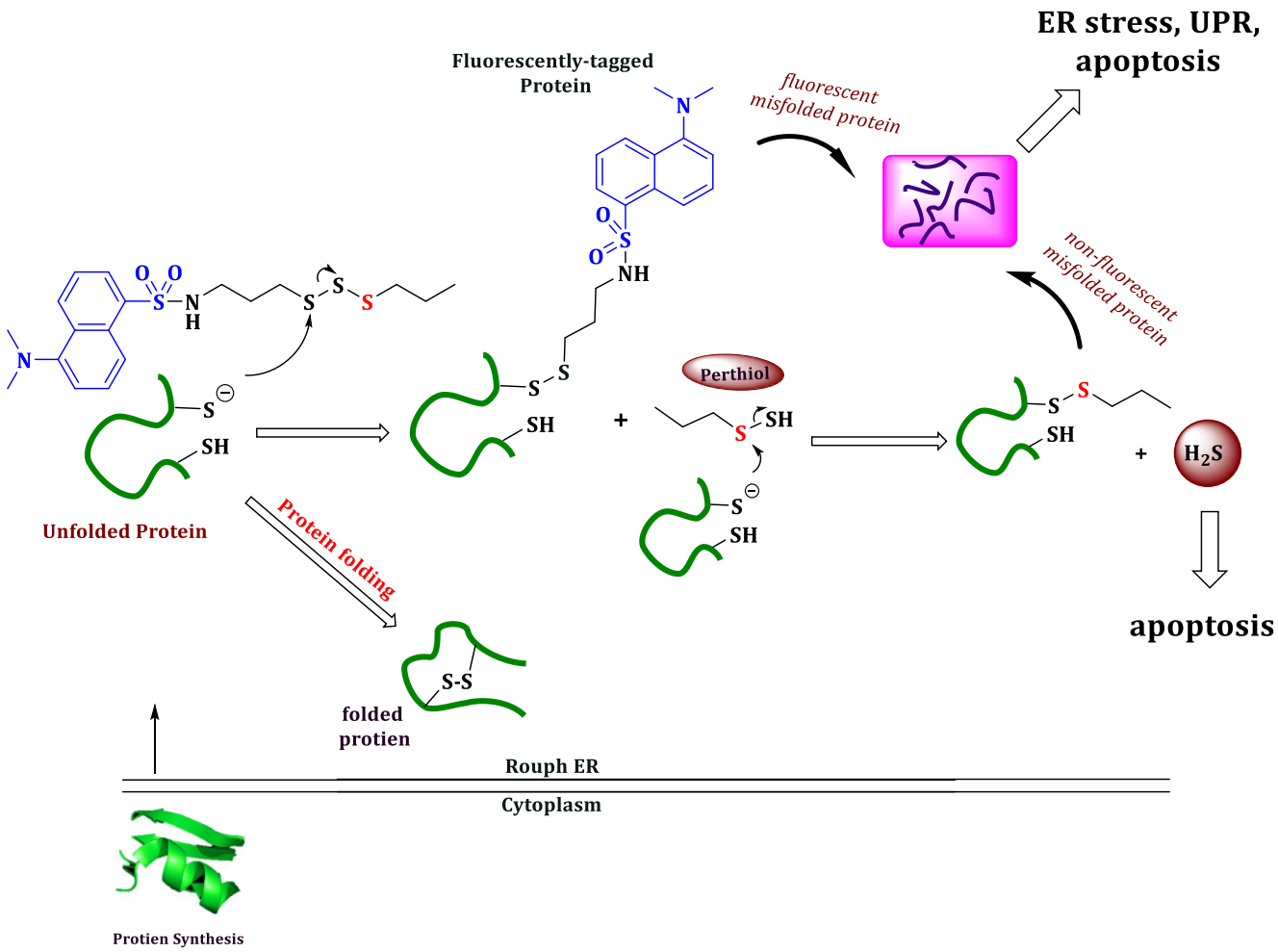

Figure 5.44: A hypothesis on the cytotoxic mechanism of action of trisulfides in cancer cells based on the ER targeting mechanism.

Our hypothesis, depicted in **Figure 5.44**, suggests that the cytotoxicity of trisulfides may result from two pathways; the one involving protein folding processes, akin to the mechanism observed with ajoene, and the other with H_2S signalling. Our previous studies on ajoene revealed its ability to induce misfolded protein aggregates and to activate the Unfolded Protein Response (UPR) by perturbing protein folding processes in the ER.[272] Therefore, we propose that trisulfides, at least in part, exert their cytotoxic effects by disrupting protein folding, similar to ajoene. This may be complemented by an apoptosis mechanisms involving H_2S. Further investigations are needed to validate this hypothesis and elucidate the specific molecular mechanisms underlying the interplay of these two manifolds.

5.7 Summary and Outlook

This Chapter has presented an investigation into the perthiol chemical biology underpinning organotrisulfide cytotoxicity in cancer cells, building a cohesive narrative from initial screening to detailed mechanistic insights. Our journey began with an initial screening of a library of derivatives prepared by using our new heterotrisulfide methodology that revealed a poorly defined set of structure-activity relationships between cytotoxicity and structure. However, this initial ambiguity led us to investigate further, focusing on substituted benzyl trisulfides in both a hetero (benzyl-allyl) and homo (benzyl-benzyl) series bearing *para* substituents on the phenyl ring, with the anticipation that there might well be transmission effects that could result in generating mechanistic insight. This refined approach revealed a much clearer SAR and a tool for chemical biology investigation both in the test tube (e.g. Ellman's) and in vitro in cells. A summary of these achievements follows.

Once we had latched onto the importance of varying the substituent in different benzyl trisulfides, the focus of attention first turned to perthiol stability. Here, it was found that electron release into the benzyl group phenyl ring stabilises the perthiol and restricts its disproportion into the homotrisulfide via self-condensation. This was explained in terms of electron release raising the perthiol p*K*a, reducing the concentration of perthiolate in solution, which was corroborated by computational studies. A further factor was the reduction of benzyl *S*-electrophilicity by the electron-releasing substituent. This was the first evidence within the project that we had uncovered an important design factor for prolonging perthiol lifetime in cells, which needs to be exploited further in the future in the quest for more cytotoxic trisulfides.

From here, we took the mini-library into cancer cells, knowing (from literature) that a perthiol would be formed via thiolysis exchange with a biological thiol such as glutathione or a cysteine residue on a protein. Pleasingly, once again, a higher perthiol concentration extending to the extracellular space via passage back across the cell membrane (where it was measured using an Ellman's assay) was found for the *p*-OMe derivative, again corroborating results from the perthiol stability study in the test tube as described in the paragraph above.

Finally, our library was used for monitoring H_2S production in a WHCO1 cancer cell line using a fluorescent (azide) probe. Here, using an expanded library now covering a broader range of electron-withdrawing and releasing substituents, the same SAR was

pleasingly established – that fluorescence intensity (as a measure of H_2S concentration) increased with increasing electron release from the *para*-substituent, again tracing back to an enhanced perthiol stability. In turn, the trisulfide cytotoxicity potency increased with increasing H_2S production. Importantly, these results not only corroborate the general view on the thiolysis-based mechanism of a trisulfide cytotoxicity leading to H_2S but have also provided a crucial design principle for engineering optimal agents. Unfortunately, aromatic trisulfides – in which electronic effects could be directly transmitted to the trithio moiety – are relatively unstable as a result, but the benzyl chemotype at this stage is worth elaborating, e.g. with more electron-releasing effects. Steric effects also need to be explored.

Finally, studies using a dansyl-propyl trisulfide probe revealed localisation in the endoplasmic reticulum, in keeping with the organelle responsible for S-S biochemistry processing in which an unfolded protein response may well be operative as with ajoene. These findings have pointed towards future studies needing to study the interplay of UPR and H_2S signally in apoptosis promotion.

CHAPTER 6: Experimental

6.1 Synthesis Methods

Commercially sourced precursor chemicals from Sigma Aldrich and Merck were used without additional purification. Reaction solvents underwent distillation under a nitrogen atmosphere. Tetrahydrofuran (THF) was dried over sodium wire benzophenone, acetonitrile (ACN) was distilled from calcium hydride (CaH_2), and dichloromethane (DCM) was distilled over phosphorus pentoxide. Other reagents were purified using established standard procedures.

Temperature conditions for reactions are given, covering room temperature (RT) and a spectrum of low-temperature reactions ranging from an ice-water slurry (0 °C) to the use of acetone/liquid nitrogen (-78 °C). Temperature-regulated oil baths were used for high temperature reactions.

Thin-layer chromatography (TLC) as performed using Merck aluminium-backed silica 60 F254 plates, with visualization provided by short-wave (254 nm) or long-wave (365 nm) UV-light or by using the following stains with subsequent heating: anisaldehyde stain as a 2.5% solution of anisaldehyde in sulfuric acid and ethanol (1:10 v/v); ninhydrin stain as a 0.3% solution of ninhydrin in absolute ethanol and glacial acetic acid (97:3 v/v); $KMnO_4$ stain prepared by dissolving 1.5 g of $KMnO_4$, 10 g K_2CO_3, and 1.25 mL 10% NaOH in 200 mL water. Purification by column chromatography was carried out using flash silica gel from Sigma Aldrich, with the mobile phase comprising mixtures of ethyl acetate (EtOAc) and hexane. Purity data was afforded by high-performance liquid chromatography (HPLC) with a UV detector, using an Agilent 1220 unit equipped with an Agilent ZORBAX Eclipse Plus C-18 column.

^1H NMR and ^{13}C NMR spectra were recorded on Varian 300 MHz, Varian 400 MHz Unity INOVA and Varian 600 MHz Unity INOVA NMR instruments. All NMR spectra were recorded at 25 °C. Chemical shifts (δ) are reported in ppm relevant to the deuterated solvent peaks (chloroform: δ 7.26 in ^1H NMR and δ 77.16 in ^{13}C NMR; dimethylsulfoxide: δ 2.50 in ^1H NMR and δ 39.52 in ^{13}C NMR). *J*-coupling (*J*) is given in Hz. High-resolution mass spectrometry was performed at the Central Analytical Facilities, School of Chemistry, University of Stellenbosch on a Waters Synapt G2 machine in ESI mode.

6.2 General Method for sodium 4-methylbenzenesulfonothioate salt[141]

$TolSO_2Na$ (105.71 g, 600 mmol, 1eq.) and S_8 (19.24 g, 75 mmol, 1 eq.) were dissolved in pyridine (500 mL) to give a yellow solution.[141] The reaction was stirred under N_2 at 50 ºC for 1 h to give a white suspension. After another 2 h, the reaction was filtered and washed with anhydrous diethyl ether. The residue was recrystallized from anhydrous ethanol to afford $TolSO_2SNa$ (106.01 g, 89%) as a white crystalline solid.

6.3 General Procedure for Synthesis of Thiotosylates 1a-u.

6.3.1 Synthesis of Aliphatic and Benzylic Thiotosylates (Procedure 1)

Aliphatic thiotosylates were synthesized using one of two established methods.[141] In Procedure 1, a solution of sodium 4-methylbenzenesulfonothioate (1 mmol) in dry acetonitrile (4 mL) was prepared and maintained under a nitrogen atmosphere. To this, RX (1.2 mmol) was added. The mixture was stirred at room temperature until TLC indicated the complete consumption of the limiting reagent. The acetonitrile was then removed under vacuum. The resulting residue was extracted with ethyl acetate (3 x 20 mL) from water (10 mL). The organic layers were combined, washed with brine (10 mL), and dried over anhydrous magnesium sulfate ($MgSO_4$). After removing the solvent under reduced pressure, the residue was purified by column chromatography using a mixture of ethyl acetate and hexane, yielding the desired aliphatic thiotosylates **1a-1p**.

6.3.1.1 Library 1 via Procedure 1

S-Allyl 4-methyl-benzene-sulfonothioate (**1a**)[494]

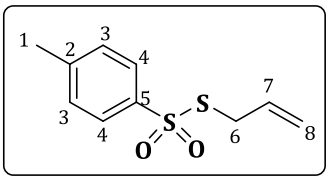

Sodium 4-methylbenzenesulfonothioate (1.00 g, 4.76 mmol, 1 eq.) and allyl bromide (690.5 mg mL, 5.71 mmol, 1.2 eq.) were reacted to afford sulfonothioate **1a** as colourless oil (800.0 mg, 74%). ^{1}H NMR (300 MHz, $CDCl_3$) δ 7.80 (d, *J* = 8.3, 2H, H-4), 7.33 (d, *J* = 8.4, 2H, H-3), 5.86 – 5.57 (m, 1H, H-7), 5.30 – 5.03 (m, 2H, H-8), 3.67 (m, *J* = 7.0, 2H, H-6), 2.45 (s, 3H, H-1).

S-(3-Hydroxypropyl) 4-methylbenzenesulfonothioate (**1b**)[495]

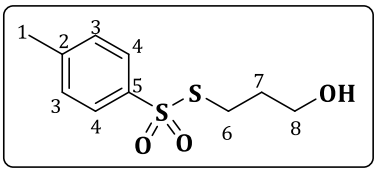

Sodium 4-methylbenzenesulfonothioate (500.0 mg, 2.38 mmol, 1 eq), 3-bromopropanol (336.7 mg, 2.85 mmol, 1.2 eq) were reacted to afford sulfonothioate **1b** as a white solid (400.0 mg, 68%). ^{1}H NMR (300 MHz, $CDCl_3$) δ 7.85 (d, *J* = 8.3, 2H, H-4), 7.37 (d, *J* = 8.3, 2H, H-3), 3.73 (t, *J* = 5.8, 2H, H-8), 3.14 (t, *J* = 7.0, 2H, H-6), 2.48 (s, 3H, H-1), 1.93 (m, *J* = 6.0, 2H, H-7).

S-Dodecyl- [4-methylbenzene] sulfonothioate (**1c**)[496]

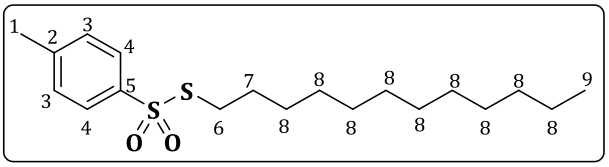

Sodium 4-methylbenzenesulfonothioate (1.00 g, 4.76 mmol, 1 eq.) and 1-bromododecane (1.42 g, 5.71 mmol, 1.2 eq.) were reacted to afford sulfonothioate **1c** as a white solid (821.0 mg, 48%). ^{1}H NMR (300 MHz, $CDCl_3$) δ 7.81 (d, *J* = 8.4 Hz, 2H, H-4), 7.31 (d, *J* = 8.4, 2H, H-3), 2.98 (t, *J* = 7.4 Hz, 2H, H-6), 2.45 (s, 3H, H-1), 1.6-1.54 (m, 2H, H-7), 1.26-1.20 (m, 18H, H-8), 0.88 (t, *J* = 6.7, 3H, H-9).

S-Hexyl-[4-methylbenzene] sulfonothioate (**1d**) [494]

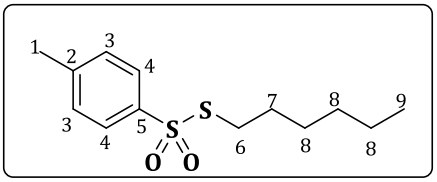

Following Procedure 1, sodium 4-methylbenzenesulfonothioate (1.10 g, 5.23 mmol, 1 eq.) and hexyl bromide (1.04 g, 6.28 mmol, 1.2 eq.) were reacted to afford **1d** as a yellowish solid (1.21 g, 84%). ^{1}H NMR (300 MHz, $CDCl_3$) δ 7.48 (d, 2H, H-4), 7.14 (d, *J* = 8.4 Hz, 2H, H-3), 2.78 (t, 2H, H-6), 2.34 (s, 3H, H-1), 1.73 – 1.59 (m, 2H, H-7), 1.38 – 1.22 (m, 6H, H-7), 0.89 (t, *J* = 6.9 Hz, 3H, H-8).

S-Benzyl 4-methylbenzenesulfonothioate (**1e**)[453]

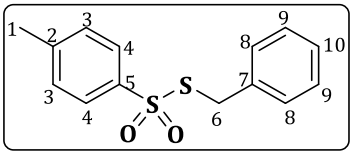

Sodium 4-methylbenzene sulfonothioate (2.00 g, 9.52 mmol, 1 eq.) and benzyl bromide (1.95 g, 11.42 mmol, 1.2 eq.) were reacted to afford **1e** as a white

solid (2.50 g, 94%). ^{1}H NMR (400 MHz, $CDCl_3$) δ 7.73 (d, 2H, H-4), 7.29 – 7.25 (m, 2H, H-3), 7.24 – 7.09 (m, 5H, H-8/H-9/H-10,), 4.25 (s, 2H, H-6), 2.43 (s, 3H, H-1).

S-Propyl 4-methylbenzenesulfonothioate (**1f**)[497]

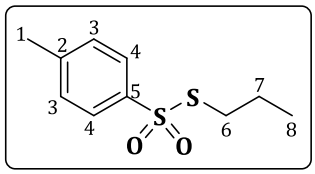

Following Procedure 1, sodium 4-methylbenzenesulfonothioate (500.0 mg, 2.30 mmol, 1 eq) and propyl iodide (336.0 mg, 2.70 mmol, 1.2 eq) were reacted to afford **1f** as a colourless oil (492.08 mg, 92.5% yield). ^{1}H NMR (300 MHz, $CDCl_3$) δ 7.81 (d, 2H, H-3), 7.34 (d, *J* = 8.0 Hz, 2H, H-4), 2.97 (t, 2H, H-6), 2.45 (s, 3H, H-1), 1.71 – 1.57 (m, 2H, H-7), 0.93 (t, 3H, H-8).

S-(Prop-2-yn-1-yl) 4-methylbenzenesulfonothioate (**1g**)[497]

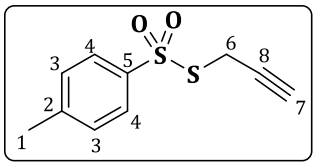

Following Procedure 1, sodium 4-methylbenzenesulfonothioate (500.0 mg, 2.30 mmol, 1 eq.) and propargyl bromide (336.0 mg, 2.70 mmol, 1.2 eq.) were reacted to afford **1g** as a yellowish solid (400.0 mg, 92%). ^{1}H NMR (300 MHz, $CDCl_3$) δ 7.80 (d, *J* = 8.1 Hz, 2H, H-4), 7.39 (d, *J* = 8.7 Hz, 2H, H-3), 3.86 (d, *J* = 2.4 Hz, 2H, H-6), 2.48 (s, 3H, H-1), 2.10 (t, *J* = 2.7 Hz, 1H, H-7).

S-(Tert-butyl) 4-methylbenzenesulfonothioate (**1h**)[498]

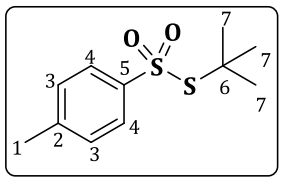

Following Procedure 1, sodium 4-methylbenzenesulfonothioate (400.0 mg, 1.90 mmol, 1 eq.) and *t*-Butyl bromide (312.0 mg, 2.28 mmol, 1.2 eq.) were reacted to afford **1h** as a white solid (390.0 mg, 83%). ^{1}H NMR (300 MHz, $CDCl_3$) δ 7.83 (d, *J* = 8.4, 2H, H-4), 7.32 (d, *J* = 8.6, 2H, H-3), 2.44 (s, 3H, H-1), 1.44 (s, 9H, H-7).

S-(((2S,3S,4S,5S,6S)-3,4,5-Tris(benzyloxy)-6-methoxytetrahydro-2H-pyran-2-yl) methyl) 4-methylbenzenesulfonothioate (**1i**). The synthesis was carried out in six steps.[499]

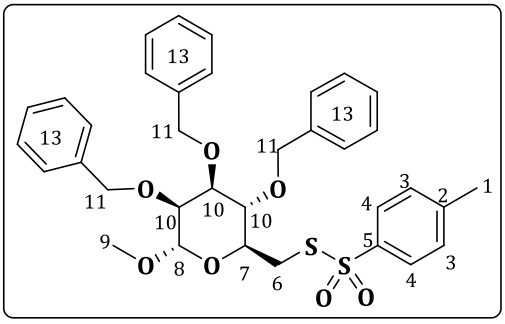

Step 1: Selective Protection of the Primary Hydroxy Group with TIPSCl

Methyl-α-D-mannopyranoside (500.0 mg, 2.58 mmol, 1 eq.) was dissolved in anhydrous THF (20 mL) in a dry reaction flask. Imidazole (530.0 mg, 7.74 mmol, 3 eq.) was added to the flask and stirred until it dissolved completely. TIPSCl (1.63 g, 7.74 mmol, 3 eq.) was added dropwise to the reaction mixture while stirring at room temperature. The reaction was allowed to proceed overnight (approximately 16 hours) at room temperature with continuous stirring. After completion, the reaction was quenched with water (20 mL), the organic material was extracted with DCM. The organic layer was separated and washed with water and brine. The organic layer was dried over anhydrous $MgSO_4$, filtered, and concentrated under reduced pressure to obtain the crude TIPS-protected methyl-α-mannopyranoside to proceed to the next step.

Step 2: Benzylation of 3,4,5 Hydroxyl groups

The TIPS-protected methyl-α-D-mannopyranoside obtained from step 1 (600.0 mg, 1.71 mmol, 1 eq.) was dissolved in anhydrous THF (15 mL) in a dry reaction flask. Sodium hydride (51.3 mg, 60% in oil, 2.14 mmol, 1.25 eq.) was added to the reaction flask under a fume hood while stirring. The mixture was stirred for 30 minutes. Benzyl chloride (1.17g, 6.85 mmol, 4 eq.) was added dropwise to the reaction mixture while stirring. The reaction mixture was stirred at room temperature overnight, and progress was monitored using TLC. After completion, the reaction was quenched by slowly adding methanol (5 mL). The organic compounds were extracted with DCM and the organic layers were combined, washed with water and brine, and dried over anhydrous $MgSO_4$. The organic layer was filtered, and the solvent was removed under reduced pressure to obtain the crude product.

Step* 3: *Deprotection of TIPS Group

The crude TIPS-protected methyl 2,3,4-tri-O-benzyl-α-D-mannopyranoside obtained from step 2 (450.0 mg, 0.724 mol, 1 eq.) was dissolved in THF (15 mL) in a dry reaction flask. TBAF (263.6 mg, 1.090 mmol, 1.5 eq.) was added to the reaction mixture and stirred at room temperature for 1-2 hours. The progress of the reaction was monitored using TLC. After completion, the reaction was quenched with water, and the product was extracted with DCM. The organic layer was dried over anhydrous $MgSO_4$, filtered, and concentrated under reduced pressure. The crude product was purified by column chromatography using ethyl acetate/hexane as the eluent, yielding 2,3,4-tri-O-benzyl-α-D-mannopyranoside (120.0 mg, 35% yield over three steps)

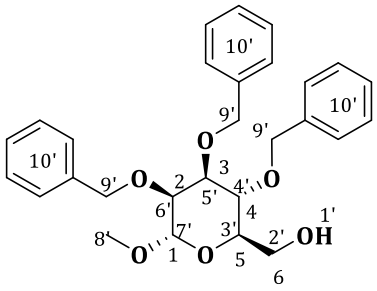

Methyl 2,3,4-tri-O-benzyl-a-D-mannopyranoside

^{1}H NMR (300 MHz, $CDCl_3$) δ 7.40 – 7.28 (m, 15H, ArH), 4.96 (d, *J* = 11.0, 1H, H-5), 4.06 – 3.71 (m, 3H, H-4'/H-5'/H-6'), 3.71 – 3.57 (m, 1H, H-7'), 3.32 (s, 3H, H-8'), 2.11 (d, *J* = 36.0, 1H, H-3').

Step* 4: *Mesylation

To a solution of 2,3,4-tri-O-benzyl-α-D-mannopyranoside (100.0 mg, 0.215 mmol, 1 eq) in anhydrous DCM (5 mL), triethylamine (65.2 mg, 0.645 mmol, 3 eq.), and DMAP (3.59 mg, 0.0212 mmol, 11 mol%) were added. The mixture was stirred at 0 °C while methanesulfonyl chloride (36.9 mg, 0.322 mmol, 1.5 equiv.) was added. After removing the ice-water bath, the reaction continued at room temperature overnight. The solution was then diluted with DCM (20 mL) and washed sequentially with saturated aqueous $NaHCO_3$, and brine. The organic phase was dried over $MgSO_4$, filtered, evaporated, and dried under high vacuum to obtain the mesylate intermediate as a crude pale-yellow gum (60.0 mg).

Step* 5: *Iodination

The intermediate mesylate (60.0 mg, 0.103 mmol, 1 eq.) was used without further purification. To it, potassium iodide (342.2 mg, 2.06 mmol, 20 eq.) and DMF (5 mL) were added. The reaction mixture was stirred and heated to reflux for 3 hours. After reaction completion, the mixture was filtered to remove potassium mesylate, and DMF was evaporated nearly to dryness. Ethanol was added to the residue, and the mixture was stirred at a cold temperature to induce crystallization. The resulting solid was filtered to yield 3,4,5-tribenzyl-2-(iodomethyl)-6-methoxytetrahydro-2H-pyran, assume near-quantitative yield as a crude (37.0 mg).

Step* 6: *Thiotosylation

Finally, crude iodo derivative (37.0 mg, 0.064 mmol, 1 eq.) and sodium 4-methylbenzenesulfonothioate (16.2 mg, 0.077 mmol, 1.2 equiv.) were reacted in acetonitrile (3 mL) overnight to produce **1i**. The product was isolated to obtain **1i** as a white solid (30.0 mg, 73% yield: $[\alpha]_D^{20}$ = +66.3 (*c* = 1.0, $CHCl_3$); IR (ν_{max}/cm^{-1}) 1138, 698; ^1H NMR (300 MHz, $CDCl_3$) δ 7.73 (d, *J* = 8.3 Hz, 2H, H-4), 7.41–7.27 (m, 15H, H-13), 7.18 (d, *J* = 8.3 Hz, 2H, H-3), 4.94 (d, *J* = 11.1 Hz, 1H, H-7), 4.75–4.50 (m, 6H, H-11), 3.85–3.64 (m, 4H, H-10), 3.49–3.40 (m, 1H, H-8), 3.21 (s, 3H, H-9), 3.15–3.05 (m, 1H, H-6), 2.39 (s, 3H, H-1); ^{13}C NMR (101 MHz, $CDCl_3$) δ 144.6, 142.1, 138.4, 138.4, 138.3, 129.8, 128.5, 128.5, 128.5, 128.5, 128.2, 128.0, 127.9, 127.8, 127.8, 127.4, 99.1, 80.2, 77.6, 75.2, 74.8, 73.1, 72.3, 70.5, 55.0, 38.3, 21.7; HRMS (ESI^+) *m/z* $[M + H]^+$ calcd for $C_{35}H_{39}O_7S_2$ 635.2137, found 635.2130.

<u>*S*-(3-((5-(Dimethylamino) naphthalene)-1-sulfonamido) propyl) 4 methylbenzene sulfonothioate (**1j**).</u>[484] The synthesis was carried out in four steps.

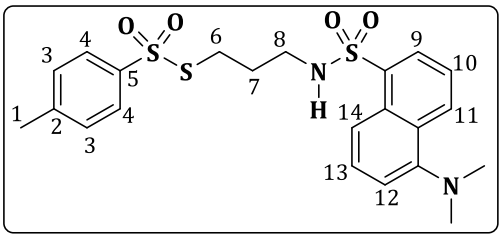

A solution of 3-aminopropan-1-ol (167.0 mg, 2.22 mmol, 1.5 eq) was added dropwise to a mixture of dansyl chloride (400.0 mg, 1.48 mmol, 1 eq) and triethylamine (300.1 mg, 2.97 mmol, 2 eq) in 7 mL of DCM at 0°C under a nitrogen atmosphere. The reaction mixture was then allowed to warm to room temperature. TLC indicated complete conversion of the starting dansyl chloride to a less polar, fluorescent product. The mixture was diluted with 30 mL of DCM, washed with 15

mL of saturated sodium bicarbonate solution, and dried over magnesium sulfate. After removing the solvent under reduced pressure, the residue was purified by column chromatography on silica gel using ethyl acetate as the eluent to afford the product (i) as a solid (434.0 mg, 95% yield).

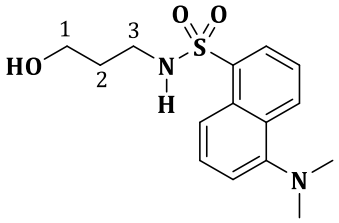

5-(dimethylamino)-*N*-(3-hydroxypropyl)naphthalene-1-sulfonamide

^{1}H NMR (300 MHz, $CDCl_3$) δ 8.50 (d, *J* = 8.6 Hz, 1H, Ar-H), 8.24 (, d, *J* = 8.6 Hz, 1H, Ar-H), 8.23 (d, *J* = 7.3 Hz, 1H, Ar-H), 7.53 - 7.45 (m, 2H, Ar-H), 7.12 (d, *J* = 7.3 Hz, 1H, Ar-H), 5.31 (t, 1H, NH), 3.62 (t, *J* = 5.4 Hz, 2H, H-1), 3.07 (q, *J* = 6.0 Hz, 2H, H-3), 2.85 (s, 6H, NMe_2), 1.60 (pent, *J* = 6.3 Hz, 2H, H-2).

Step* 2: *Mesylation

Compound (**i**) (420.0 mg, 1.36 mmol, 1 eq) and triethylamine (275.6 mg, 2.72 mmol, 2 eq) were dissolved in 8 mL of dry DCM under a nitrogen atmosphere and cooled to 0°C. Mesyl chloride (141 mg, 1.22 mmol, 1 eq) in 1 mL of DCM was then added dropwise. The reaction mixture was allowed to warm to room temperature, and after 20 minutes, thin-layer chromatography (TLC) (ethyl acetate: petroleum ether = 1:1) showed complete conversion of the starting material. Saturated sodium bicarbonate solution (10 mL) was added, and the organic phase was extracted with DCM (3 × 20 mL). The combined organic layers were dried over magnesium sulfate, and the solvent was evaporated. The resulting residue was purified by column chromatography using ethyl acetate as the eluent, yielding compound (**ii**) as a luminous green oil (475.0 mg, 90% yield).

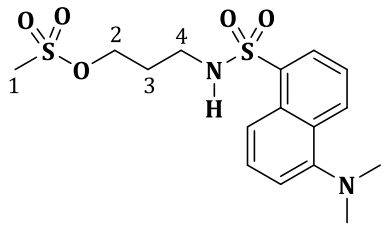

^{1}H NMR (300 MHz, $CDCl_3$) δ 8.46 (d, *J* = 7.91 Hz, 1H, ArH), 8.15 (d, *J* = 8.6 Hz, 1H, ArH), 8.10 (d, *J* = 7.1 Hz, 1H, ArH), 7.49 – 7.57 (m, 2H, ArH), 7.23 (d, *J* = 7.4 Hz, 1H, ArH), 5.22 (t, 1H, NH), 4.21 (t, *J* = 5.8 Hz, 2H, H-2), 3.02 (q, *J* = 6.4 Hz, 2H, H-3), 2.78 (s, 6H, NMe_2), 2.14 (s, 3H, H-1), 1.85 (m, *J* = 6.6 Hz, 2H, H-2).

Step* 3: *Iodination

Compound **(ii)** (460.0 mg, 1.10 mmol, 1eq) was dissolved in 25 mL of acetonitrile containing sodium iodide (NaI, 3.75 g, 23.8 mmol, 20 eq) under nitrogen. The reaction mixture was stirred at 60°C for 18 hours. TLC confirmed the complete conversion of the mesylate to the less polar iodide. After removing the solvent under reduced pressure, 30 mL of saturated aqueous sodium sulfite (Na_2SO_3) was added. The organic phase was extracted with diethyl ether (3 × 20 mL), followed by washing with brine (3 × 10 mL). The combined organic extracts were dried over magnesium sulfate, and the solvent was evaporated under vacuum. The residue was purified via silica-gel column chromatography (EtOAc: hexane = 1:3), yielding (**iii**) as a luminous green wax (425.0 mg, 85% yield).

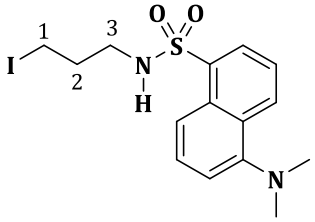

5-(dimethylamino)-*N*-(3-iodopropyl)naphthalene-1-sulfonamide

^{1}H NMR (300 MHz, $CDCl_3$) δ 8.39 (d, *J* = 8.6 Hz, 1H, ArH), 8.21 (d, *J* = 8.4 Hz, 1H, ArH), 8.27 (d, *J* = 7.1 Hz, 1H, ArH), 7.55 – 7.49 (m, 2H, ArH), 7.19 (d, 1H, ArH), 4.97(t, 1H, NH), 2.97 (q, *J* = 5.9 Hz, 2H, H-3), 2.91 (t, *J* = 5.3 Hz, 2H, H-1), 2.87 (s, 6H, NMe_2), 1.83 (m, *J* = 6.0 Hz, 2H, H-2).

Step* 4: *Thiotosylation

Iodide (**iii**) (400.0 mg, 0.956 mmol, 1 eq) and sodium thiosulfonate (241.3 mg, 115 mmol, 1.2 eq) were dissolved in 30 mL of acetonitrile and stirred at room temperature overnight under nitrogen. Thin-layer chromatography (TLC) indicated the formation of the thiotosylate product, which appeared lower than the iodide on the TLC plate. Despite the excess of potassium thiosulfonate, the reaction did not reach completion. The solvent was removed under reduced pressure, and the organic phase was extracted with 20 mL of ethyl acetate, followed by washing with water (3 × 20 mL) and brine (1 × 20 mL). The organic layer was dried over magnesium sulfate, and the solvent was evaporated under vacuum. Column chromatography was not performed as the resulting yellow oil was unstable and prone to decomposition. The crude product was directly used in the synthesis of trisulfide **93**, yielding 336.0 mg (73%).

6.3.2 General Procedure of the Synthesis of Aromatic Thiotosylates (Procedure 2) and cysteine thiotosylate

The said thiotosylates were synthesized following a published procedure protocol.[444,445] RSSR (1 mmol), sodium 4-methylbenzenesulfinate (2.5 mmol), and I_2 (1.9 mmol) were dissolved in 6 mL of dichloromethane (DCM) and stirred at room temperature overnight. Upon confirmation of complete product conversion by TLC, the reaction was quenched with 3 mmol of saturated magnesium thiosulfate (10 ml). The organic products were extracted with DCM (3 x 15 mL) from 10 mL of water. The organic phase was dried over $MgSO_4$, filtered, and the solvent was removed under vacuum. Purification via silica gel chromatography (EtOAc: hexane) yielded the desired thiotosylate.

6.3.2.1 Library 1 (Via Procedure 2)

(*R*)-Ethyl 2-((tert-butoxycarbonyl) amino)-3-(tosylthio) propanoate (**1k**)[444,500]

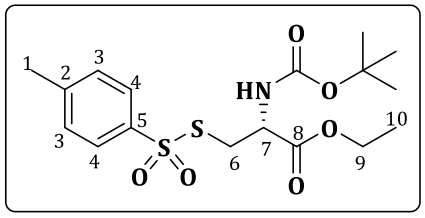

L-Cysteine ethyl ester hydrochloride (1.00 g, 5.39 mmol, 1 eq) was suspended in DCM (20 mL). To this solution was added $NaHCO_3$ (1.36 g, 16.17 mmol, 3 eq). The reaction was cooled to -5 °C in an ice bath and stirred for 10 minutes. Then, di-*tert*-butyl dicarbonate (1.18 g, 5.39 mmol, 1 eq) was subsequently added and the reaction mixture was allowed to stir for 12 hours with slow warming to room temperature. TLC confirmed the completion of the reaction, and the product was extracted from the aqueous layer into DCM (3 x 30 mL) after first adjusting the pH to 7. The combined organic layers were dried over $MgSO_4$, filtered, and concentrated under reduced pressure. The crude product was purified by column chromatography using a mixture of ethyl acetate and hexane as the eluent, yielding ethyl *N*-(*tert*-butoxycarbonyl)-L-cysteinate as a white solid (1.25 g, 88%).

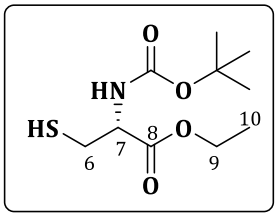

^{1}H NMR (300 MHz, $CDCl_3$) δ 5.43 (d, *J* = 7.8 Hz, 1H, NH), 4.60–4.55 (m, 1H, H-7), 4.27–4.19 (m, 2H, H-9), 3.00–2.95 (m, 2H, H-6), 1.45 (s, 9H, ^{t}Bu), 1.29 (t, *J* = 7.1 Hz, 3H, H-10). The spectral data of the product matched the literature values.[500]

Thereafter, ethyl *N*-(tert-butoxycarbonyl)-*L*-cysteinate (1.07 g, 3.09 mmol, 1 eq) was dissolved in ethyl acetate (15 mL). Sodium iodide, (4.60 mg, 0.031 mmol, 0.01 eq) and hydrogen peroxide (0.35 mL, 8.8 M, 3.09 mmol, 1 eq) were added to the solution at 0 °C. The mixture was stirred for 30 minutes, and the reaction was monitored by TLC, which showed the formation of a less polar spot corresponding to the cystine disulfide. The reaction was quenched with saturated sodium thiosulfate solution and extracted with ethyl acetate (3 x 30 mL). The combined organic layers were dried over $MgSO_4$, filtered, and concentrated under reduced pressure. The resulting residue, identified as crude disulfide, was used in the next step without further purification.

Following Procedure 2 for the final step, disulfide bond cleavage was carried out. The crude disulfide (1.20 g, 2.42 mmol, 1 eq) was dissolved in DCM (20 mL) and treated with sodium 4-methylbenzenesulfinate (1.38 g, 7.73 mmol, 3.2 eq) and iodine (1.23 g, 4.83 mmol, 2 eq.). The mixture was purified by flash column chromatography using 30% ethyl acetate in hexane as the eluent, yielding **1k** as a white crystalline solid (860.0 mg, 88%): mp 52–54 °C; $[\alpha]_D^{20}$ = -2.5 (*c* = 1.0, $CHCl_3$); IR (ν_{max}/cm^{-1}) 3363, 1735, 1695; ^{1}H NMR (300 MHz, $CDCl_3$) δ 7.83 (d, *J* = 8.4, 2H, H-4), 7.37 (d, *J* = 8.1, 2H, H-3), 4.54 (s, 1H, H-1), 4.21 (q, *J* = 7.1, 2H, H-9), 3.61 – 3.33 (dd, 1H, H-6), 2.48 (s, 3H, H-1), 1.46 (s, 9H, *t*-Bu), 1.30 (t, *J* = 7.1, 3H, H-10). ^{13}C NMR (101 MHz, $CDCl_3$) δ 169.8, 155.1, 145.2, 141.9, 130.1, 127.3, 80.6, 62.3, 53.1, 37.9, 28.4, 21.8, 14.2; HRMS (ESI$^+$) *m/z* $[M + H]^+$ calcd for $C_{17}H_{26}NO_6S_2$ 404.1202, found 404.1207.

6.3.2.2 Aromatic Thiotosylate

S-Phenyl 4-methylbenzenesulfonothioate (**1l**)[107]

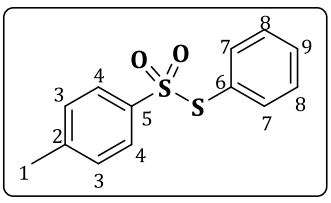

Sodium 4-methylbenzenesulfinate (2.05 g, 11.32 mmol, 2.5 eq.), diphenyl disulfide (1.00 g, 4.58 mmol, 1 eq.), and iodine (2.17 g, 8.57 mmol, 1.9 eq.) were reacted to afford sulfonothioate **1l** as a colourless solid (950.0 mg, 80%). ^{1}H NMR (300

MHz, $CDCl_3$) δ 7.50–7.46 (m, 1H, H-9), 7.43 (d, *J* = 8.3 Hz, 2H, H-4), 7.39–7.26 (m, 4H, H-7/H-8), 7.20 (d, *J* = 8.3 Hz, 2H, H-3), 2.42 (s, 3H, H-1).

S-(4-Fluorophenyl) 4-methylbenzenesulfonothioate (**1m**)[501]

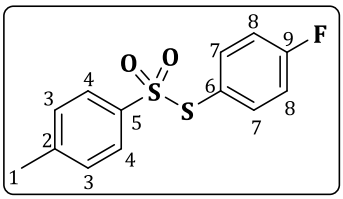

Sodium 4-methylbenzenesulfinate (2.20 g, 12.8 mmol, 2.5 eq), 1,2-bis(4-fluorophenyl) disulfane (1.21 g, 5.13 mmol, 1 eq) and I_2 (2.47 g, 9.74 mmol, 1.9 eq) were reacted to afford sulfonothioate **1m** as white solid (1.21 g, 86%). ^{1}H NMR (400 MHz, $CDCl_3$) δ 7.43 – 7.56 (m, 2H, H-8), 7.23 (dd, *J* = 8.0, 2H, H-7), 7.20 (d, *J* = 8.9, 2H, H-4), 6.93 – 6.86 (d, 2H, H-3), 2.46 (s, 3H, H-1).

S-(4-Methoxyphenyl) 4-methylbenzenesulfonothioate (**1n**)[501]

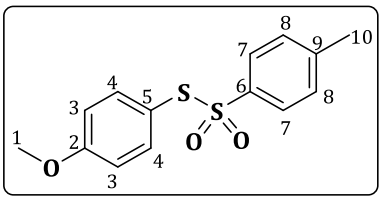

Sodium 4-methylbenzenesulfinate (800.0 mg, 4.49 mmol, 2.5 eq), 1,2-bis(4-methoxyphenyl) disulfane (500.0 mg, 1.81 mmol, 1 eq.) and I_2 (866.0 mg, 3.41 mmol, 1.9 eq.) were reacted to afford sulfonothioate **1n** as white solid (480.0 mg, 90%). ^{1}H NMR (300 MHz, $CDCl_3$) δ 7.88 (d, *J* = 7.2, 2H, H-7), 7.35 (d, 2H, H-4), 7.14 (d, *J* = 8.5, 2H, H-8), 6.21 (d, *J* = 7.4, 1H, H-3), 3.76 (s, 3H, H-1), 2.42 (s, 3H, H-10).

S-(Pyridin-4-yl) 4-methylbenzenesulfonothioate (**1o**)[501]

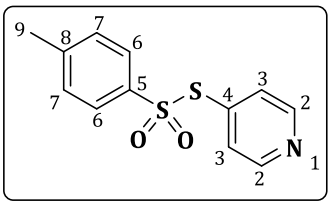

Sodium 4-methylbenzenesulfinate (1.40 g, 7.90 mmol, 2.5 eq), 1,2-di(pyridin-4-yl) disulfane (700.0 mg, 3.1 mmol, 1 eq.) and I_2 (1.51 g, 6.04 mmol, 1.9 eq.) were reacted to afford sulfonothioate **1o** as white solid (570.0 mg, 67%). ^{1}H NMR (300 MHz, $CDCl_3$) δ 8.52 (d, *J* = 3.9, 2H, H-2), 7.81 – 7.68 (m, 2H, H-6), 7.58 (d, *J* = 8.5, 2H, H-3), 7.25 (d, *J* = 8.0, 2H), 2.42 (s, 3H, H-9).

S-(4-Tolyl) 4-methylbenzenesulfonothioate (**1p**)[501]

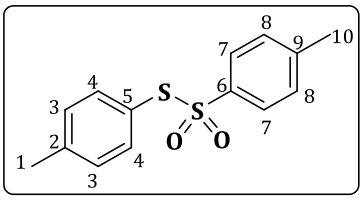

Sodium 4-methylbenzenesulfinate (1.360 g, 7.61 mmol, 2.5 eq), 1,2-bis(4-tolyl) disulfane (750.0 mg, 3.04 mmol, 1 eq.) and I_2 (1.470 g, 5.78 mmol, 1.9 eq.) were reacted to afford sulfonothioate **1p** as white solid (625.0 mg, 73%). ^{1}H NMR (300 MHz, $CDCl_3$) δ 7.41 (d, *J* = 8.2, 2H, H-7), 7.30 (d, 2H, H-4), 7.25 (d, 2H, H-8), 7.19 (d, *J* = 7.4, H-3), 2.43 (s, 3H, H-10), 2.36 (s, 3H, H-1).

6.3.2.3 Library 2 and 3 (Procedure 1 only)

S-(4-Fluorobenzyl) 4-methylbenzenesulfonothioate (**1q**)[502]

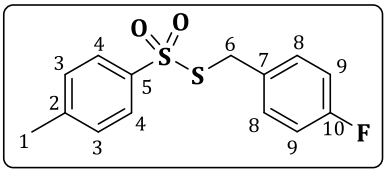

Sodium 4-methylbenzenesulfonothioate (1.00 g, 4.76 mmol, 1 eq) and 1-(chloromethyl)-4-fluorobenzene (825.0 mg, 5.71 mmol, 1.2 eq) were reacted to afford **1q** as a white solid (930.0 mg, 66% yield). ^{1}H NMR (400 MHz, $CDCl_3$) δ 7.72 – 7.67 (m, 2H, H-9), 7.26 (d, *J* = 8.0, 2H, H-4), 7.14 (m, *J* = 5.3, 8.9, 2H, H-8), 6.93 – 6.85 (m, 2H, H-3), 4.21 (s, 2H, H-6), 2.42 (s, 3H, H-1).

S-(4-Chlorobenzyl) 4-methylbenzenesulfonothioate (**1r**)[502]

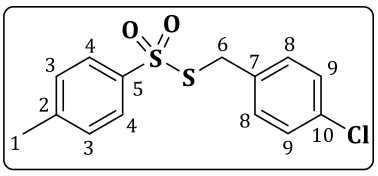

Sodium 4-methylbenzenesulfonothioate (1.00 g, 4.76 mmol, 1 eq) and 1-chloro-4-(chloromethyl) benzene (919.1 mg, 5.71 mmol, 1.2 eq) were reacted to afford **1r**as a white solid (1.11 g, 75% yield). ^{1}H NMR (400 MHz, $CDCl_3$) δ 7.69 – 7.64 (dt, 2H, H-9), 7.25 (d, *J* = 7.2, 2H, H-4), 7.19 – 7.14 (m, 2H, H-8), 7.13 – 7.06 (m, 2H, H-3), 4.21 (s, 2H, H-6), 2.43 (s, 3H, H-1).

S-(4-Bromobenzyl) 4-methylbenzenesulfonothioate (**1s**)[502]

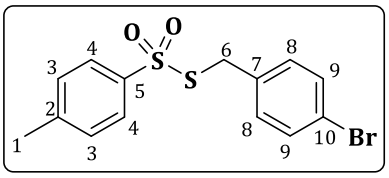

Sodium 4-methylbenzenesulfonothioate (1.50 g, 7.13 mmol, 1 eq) and 1-bromo-4-(chloromethyl) benzene (1.76 g, 8.56 mmol, 1.2 eq) were reacted to afford **1s** as a white solid (1.80 g, 71% yield). ^{1}H NMR (400 MHz, $CDCl_3$) δ 7.63 (d, *J* = 8.5, 2H, H-9), 7.31 – 7.25 (d, 2H, H-4), 7.22 (d, *J* = 7.9, 2, H-8), 7.01 (d, *J* = 8.7, 2H, H3), 4.17 (s, 2H, H-6), 2.41 (s, 3H, H-1).

S-(4-Methylbenzyl) 4-methylbenzenesulfonothioate (**1t**)[502]

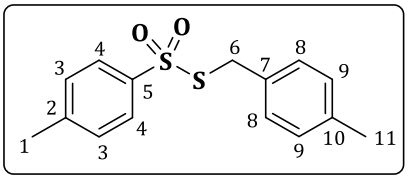

Sodium 4-methylbenzenesulfonothioate (2.00 g, 9.51 mmol, 1 eq) and 1-(chloromethyl)-4-methylbenzene (1.61 g, 11.42 mmol, 1.2 eq) were reacted to afford **1t** as a white solid (1.91 g, 69% yield). ^{1}H NMR (400 MHz, $CDCl_3$) δ 7.74 (d, *J* = 8.5, 2H, H-4), 7.28 (d, *J* = 8.0, 2H, H-3), 7.09 – 7.01 (m, 4H, H-3/H-9), 4.21 (s, 1H, H-6), 2.44 (s, 2H, H-1), 2.30 (s, 2H, H-11).

S-(4-Methoxybenzyl) 4-methylbenzenesulfonothioate (**1u**)[502]

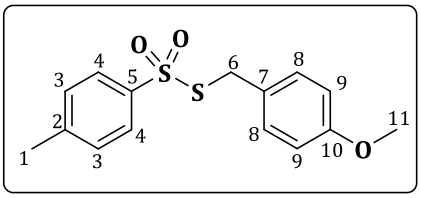

Sodium 4-methylbenzenesulfonothioate (2.00 g, 9.51 mmol, 1 eq) and 1-(chloromethyl)-4-methoxybenzene (1.80 g, 11.4 mmol, 1.2 eq) were reacted to afford **1u** as a white solid (2.50 g, 85% yield). ^{1}H NMR (300 MHz, $CDCl_3$) δ 7.74 (d, *J* = 8.5, 2H, H-4), 7.27 (d, 2H, H-8), 7.10 (d, *J* = 8.9, 2H, H-3), 6.76 (d, *J* = 7.3, 2H, H-9), 4.21 (s, 2H, H-6), 3.77 (s, 3H, H-11), 2.44 (s, 3H, H-1).

S-(4-(Trifluoromethyl) benzyl) 4-methylbenzenesulfonothioate (**1v**)[502]

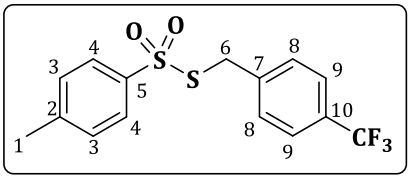

Sodium 4-methylbenzenesulfonothioate (1.00 g, 4.76 mmol, 1 eq) and 1-(bromomethyl)-4-(trifluoromethyl) benzene (1.36 g, 5.71 mmol, 1.2

eq) were reacted to afford **1v** as a white solid (1.21 g, 73% yield). ^{1}H NMR (400 MHz, $CDCl_3$) δ 7.63 – 7.58 (td, 1H, H-9), 7.43 (d, *J* = 8.0, 2H, H-8), 7.31 – 7.25 (m, 2H, H-4), 7.19 (d, *J* = 8.6, 1H, H-3), 4.30 (s, 1H, H-6), 2.40 (s, 1H, H-1).

6.4 General Procedure for Synthesis of Disulfanyl acetate (Procedure 3) 2a-2o

Disulfanyl acetates were all synthesized by reaction of the corresponding thiosulfonate (1 equiv.) with potassium thioacetate (1.3 equiv.) in DCM at rt for a few hours for aliphatic cases, and -40 °C for aromatic variants, the method modelled on a recent literature procedure. The reaction temperature of -40 °C was maintained using an acetone-liquid nitrogen bath. Here, the thiotosylate was always used as the limiting reagent and checked for total consumption (by TLC). While the aliphatic variants could be column chromatographed, the aromatic ones needed to be used as crude, in both cases following the filtration of salts and the evaporation of solvent.

6.4.1 Libraries 1 and 2

SS-Propyl ethane (dithioperoxoate) **2a**[497]

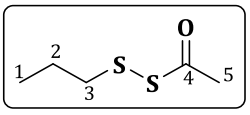

1f (450.0 mg, 1.68 mmol, 1 eq) and potassium thioacetate (402.5 mg, 2.184 mmol, 1.3 eq) were reacted in DCM to afford thioacetate **2a** as a yellowish clear oil (315.0 mg, 70% yield). ^{1}H NMR (300 MHz, $CDCl_3$) δ 2.81 (t, 2H, H-3), 2.49 (s, 2H, H-5), 1.68 (t, *J* = 7.3 Hz, 2H, H-2), 0.91 (t, *J* = 7.2 Hz, 3H, H-1).

S, S-Hexyl-ethane(dithioperoxoate) (**2b**)[441]

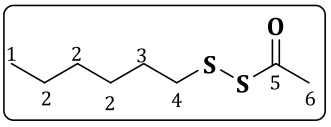

1d (1.30 g, 4.78 mmol, 1eq) and potassium thioacetate (708.0 mg, 6.13 mmol, 1.3 eq.) were reacted to afford thioacetate **2b** as a clear oil (1.31 g, 70%). ^{1}H NMR (300 MHz, $CDCl_3$) δ 2.72 (t, 2H, H-4), 2.44 (s, 3H, H-6), 1.63 (t, *J* = 7.5, 2H, H-3), 1.44 – 1.21 (m, 6H, H-2), 0.89 (t, *J* = 6.8, 3H, H-1).

S-(Prop-2-yn-1-yl) 4-methylbenzenesulfonothioate (**2c**)

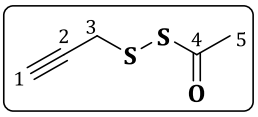

1g (250.0 mg, 1.1 mmol, 1 eq.) and potassium thioacetate (210.0 mg, 1.44 mmol, 1.3 eq.) were reacted to afford thioacetate **2c** as a colourless oil (131.0 mg, 81%). IR (ν_{max}/cm^{-1}) 3287, 1727; ^{1}H NMR (300 MHz, $CDCl_3$) δ 3.48 (d, *J* = 2.7 Hz, 2H, H-3), 2.49 (s, 3H, H-5), 2.30 (t, *J* = 2.7 Hz, 1H, H-1); ^{13}C NMR (101 MHz, $CDCl_3$) δ 194.2, 78.4, 73.1, 29.0, 26.8; HRMS (ASAP^{+}) *m/z* [M + H]$^{+}$ calcd for $C_5H_7OS_2$ 146.9938, found 146.9943.

SS-Allyl ethane(dithioperoxoate) (**2d**)[497]

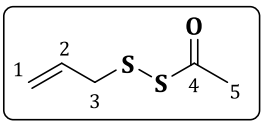

1a (1.30 g, 4.78 mmol, 1eq) and potassium thioacetate (708.0 mg, 6.13 mmol, 1.3 eq.) were reacted to afford thioacetate **2d** as a yellowish clear oil (1.31 g, 70.8%). ^{1}H NMR (300 MHz, $CDCl_3$) δ 5.95 – 5.62 (m, 1H, H-2), 5.32 – 4.98 (m, 2H, H-1), 3.34 (d, *J* = 7.4, 2H, H-3), 2.44 (s, 3H, H-5).

SS-Dodecyl ethane(dithioperoxoate) (**2e**)[139]

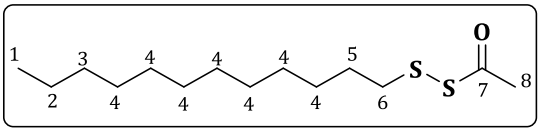

1c (650.0 mg, 2.39 mmol, 1eq) and potassium thioacetate (354.0 mg, 3 mmol, 1.3 eq.) were reacted to afford thioacetate **2e** as a yellowish clear oil (655.0 mg, 70%). ^{1}H NMR (300 MHz, $CDCl_3$) δ 3.05 (t, *J* = 7.5 Hz, 2H, H-6), 2.56 (s, 3H, H-8), 2.30 (t, *J* = 7.5 Hz, 2H, H-5), 1.50-1.20 (m, 22H, H-4), 0.88 (t, *J* = 6.8 Hz, 3H, H-1), 2.44 (s, 3H, H-5).

SS-(*Tert*-butyl) ethane(dithioperoxoate) (**2f**)[503]

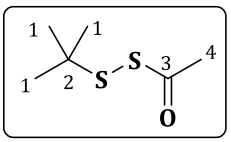

1h (350 mg, 1.43 mmol, 1eq) and potassium thioacetate (212.6 mg, 1.86 mmol, 1.3 eq.) were reacted to afford thioacetate **2f** as a yellowish clear oil (150.0 mg, 69%). ^{1}H NMR (300 MHz, $CDCl_3$) δ = 2.47 (s, 3H, H-4), 1.37 (s, 9H, H-1).

SS-(*p*-Tolyl) ethane(dithioperoxoate) (**2g**)

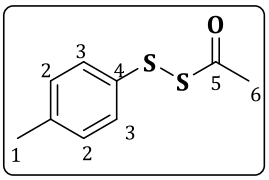

Following Procedure 3, **1p** (400.0 mg, 1.4 mmol, 1eq) and potassium thioacetate (213.0 mg, 1.8 mmol, 1.3 eq.) were reacted to afford thioacetate **2g** as a white solid (210.0 mg, 73%). The compound was used as a crude product as the sample degraded during purification on silica.

SS-(4-Methoxyphenyl) ethane(dithioperoxoate) (**2h**)

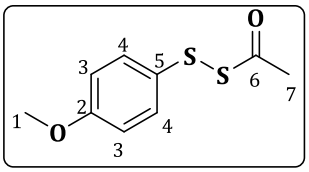

Following Procedure 3, **1m** (320.0 mg, 1 mmol, 1eq) and potassium thioacetate (161.0 mg, 1.4 mmol, 1.3 eq.) were reacted to afford thioacetate **2h** as a white solid (153.0 mg, 65%). The compound was used as a crude product as the sample degraded during purification on silica.

6.4.2 Library 3

SS-Benzyl ethane(dithioperoxoate) (**2i**)[504]

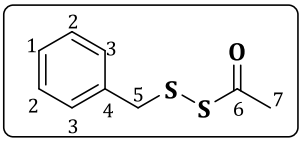

Following Procedure 3, **1e** (400.0 mg, 1.4 mmol, 1eq) and potassium thioacetate (213.0 mg, 1.8 mmol, 1.3 eq.) were reacted to afford thioacetate **2i** as a white solid (200.0 mg, 70%). ^{1}H NMR (400 MHz, $CDCl_3$) δ 7.38 – 7.24 (m, 5H, H-1/H-2/H-3), 3.93 (s, 2H, H-5), 2.34 (s, 3H, H-7).

SS-(4-Fluorobenzyl) ethane(dithioperoxoate) (**2j**)[504]

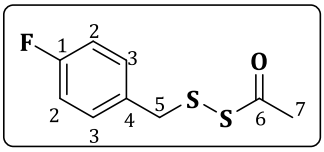

Following Procedure 3, **1q** (180.0 mg, 0.60 mmol, 1eq) and potassium thioacetate (90.0 mg, 0.79 mmol, 1.3 eq.) were reacted to afford thioacetate **2j** as white clear oil (71.0 mg, 54%). ^{1}H NMR (400 MHz, $CDCl_3$) δ 7.30 – 7.24 (m, 2H, H-2), 7.01 (t, *J* = 8.7, 2H, H-3), 3.90 (s, 2H, H-5), 2.37 (s, 3H, H-7).

SS-(4-Chlorobenzyl) ethane(dithioperoxoate) (**2k**)[504]

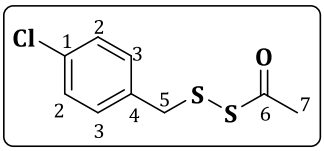

Following Procedure 3, **1r** (1.14 g, 3.64 mmol, 1 eq.) and potassium thioacetate (541.0 mg, 4.74 mmol, 1.3 eq.) were reacted to afford thioacetate **2k** as clear oil (611.0 mg, 72%). ^{1}H NMR (400 MHz, $CDCl_3$) δ 7.58 (d, *J* = 7.2, 1H, H-2), 7.41 (d, *J* = 9.4, 1H, H-3), 3.95 (s, 1H, H-5), 2.37 (s, 1H, H-7).

SS-(4-Bromobenzyl) ethane(dithioperoxoate) (**2l**)[141]

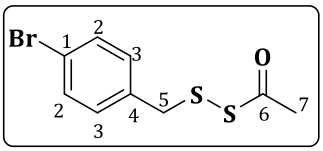

Following Procedure 3, **1s** (837.0 mg, 2.34 mmol, 1eq) and potassium thioacetate (347.0 mg, 3.05 mmol, 1.3 eq.) were reacted to afford thioacetate **2l** as a yellowish clear oil (545.0 mg, 84%). ^{1}H NMR (400 MHz, $CDCl_3$) δ 7.45 (d, *J* = 8.4, 2H, H-2), 7.18 (d, *J* = 8.5, 2H, H-3), 3.87 (s, 2H, H-5), 2.37 (s, 3H, H-7).

SS-(4-Methylbenzyl) ethane(dithioperoxoate) (**2m**)[504]

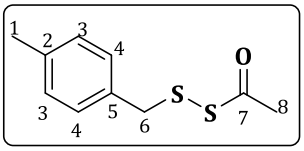

Following Procedure 3, **1t** (1.00 g, 3.42 mmol, 1eq) and potassium thioacetate (507.0 mg, 4.45 mmol, 1.3 eq.) were reacted to afford thioacetate **2m** as a white clear oil (610.0 mg, 84%). ^{1}H NMR (400 MHz, $CDCl_3$) δ 7.20 (d, *J* = 8.1, 2H, H-4), 7.13 (d, *J* = 7.7, 2H, H-3), 3.91 (s, 2H, H-6), 2.35 (s, 3H, H-1), 2.34 (s, 3H, H-7).

SS-(4-Methoxybenzyl) ethane(dithioperoxoate) (**2n**)[141,504]

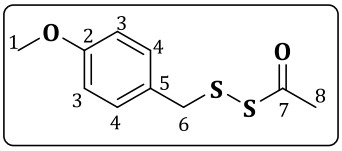

Following Procedure 3, **1u** (400.0 mg, 1.3 mmol, 1eq) and potassium thioacetate (193.0 mg, 1.7 mmol, 1.3 eq.) were reacted to afford thioacetate **2n** as clear oil (277.0 mg, 93%). ^{1}H NMR (400 MHz, $CDCl_3$) δ 7.22 (d, *J* = 8.8, 2H, H-4), 6.84 (d, *J* = 8.8, 2H, H-3), 3.89 (s, 2H, H-6), 3.78 (s, 3H, H-1), 2.34 (s, 3H, H-8).

SS-(4-(Trifluoromethyl) benzyl) ethane(dithioperoxoate) (**2o**)[141]

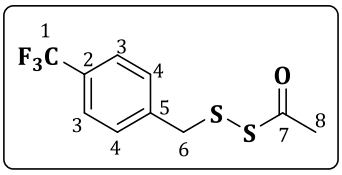

Following Procedure 3, **1v** (600.0 mg, 1.7 mmol, 1eq) and potassium thioacetate (257.0 mg, 2.2 mmol, 1.3 eq.) were reacted to afford thioacetate **2o** as a clear oil (375.0 mg, 81%). ^{1}H NMR (300 MHz, $CDCl_3$) δ 7.58 (d, *J* = 8.7, 2H, H-3), 7.41 (d, *J* = 8.7, 2H, H-4), 3.94 (s, 2H, H-6), 2.36 (s, 3H, H-8).

6.5 General Procedure for Synthesizing Trisulfide Libraries 1, 2 and 3

The thiosulfonate **1** (1.2 eq) and disulfanyl acetate (1.0 eq) were taken up in THF (0.1-0.2 M) under N_2 and cooled to -78 °C for 10 minutes. Sodium methoxide (1 M, 1.0 eq) was added slowly dropwise via syringe (10-20 sec) and the resultant solution stirred rapidly for 30 sec following the methoxide addition. The reaction was then quenched with saturated aqueous ammonium chloride (5 mL), and the product extracted into EtOAc (3 x 10 mL). After drying ($MgSO_4$) and solvent evaporation, the residue was purified by silica column chromatography using hexane as the eluent for organotrisulfides, with 5–10% EtOAc in hexane used in a few cases.

6.5.1 Library 1

1-Allyl-3-propyltrisulfane, (**45**)[53]

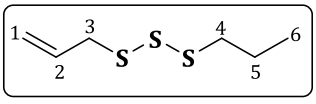

From thiotosylate **1a** (127.8 mg, 0.560 mmol) and **2a** (70.0 mg, 0.467 mmol) in THF (3 mL) and sodium methoxide (0.47 mL, 1M, 0.47 mmol) to afford trisulfide **45** (80.0 mg, 95 %) as an oil. IR (ν_{max}/cm^{-1}) 722, 476; ^{1}H NMR (300 MHz, $CDCl_3$) δ 5.93–5.83 (m, 1H, H-2), 5.26–5.18 (m, 2H, H-1), 3.51 (d, *J* = 7.2 Hz, 2H, H-3), 2.86 (t, *J* = 7.2 Hz, 2H, H-4), 1.85–1.72 (m, 2H, H-5), 1.02 (t, *J* = 7.2 Hz, 3H, H-6); ^{13}C NMR (101 MHz, $CDCl_3$) δ 133.0, 119.1, 41.7, 41.2, 22.3, 13.3; HRMS (ASAP$^+$) *m/z* $[M + H]^+$ calcd for $C_6H_{13}S_3$ 181.0179, found 181.0186.

3-(Hexyltrisulfanyl)propan-1-ol, (**63**)

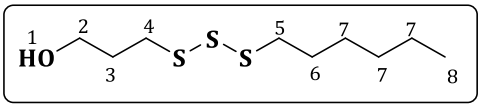

From thiotosylate **1b** (119.0 mg, 0.484 mmol) and disulfanyl acetate **2b** (77.0 mg, 0.400 mmol) in THF (3 mL) and sodium methoxide (0.4

mL, 1M, 0.40 mmol) to afford trisulfide **63** (86.0 mg, 90%) as a colourless oil. IR (ν_{max}/cm^{-1}) 3325, 788, 475; ^{1}H NMR (300 MHz, $CDCl_3$) δ 3.78 (t, *J* = 6.2 Hz, 2H, H-1, H-2), 3.00 (t, *J* = 7.1 Hz, 2H, H-4), 2.88 (t, *J* = 7.4 Hz, 2H, H-5), 2.07–1.96 (m, 2H, H-3), 1.78–1.68 (m, 2H, H-6), 1.54 (s, OH, 1H, H-1), 1.47–1.28 (m, 6H, H-7), 0.89 (t, *J* = 6.9 Hz, 3H, H-8); ^{13}C NMR (101 MHz, $CDCl_3$) δ 61.1, 39.1, 35.4, 31.6, 31.5, 28.9, 28.3, 22.6, 14.1; HRMS (ASAP^{+}) *m/z* [M]$^{+}$ calcd for $C_9H_{20}OS_3$ 240.0676, found 240.0677.

1-Benzyl-3-hexyltrisulfane (**64**).

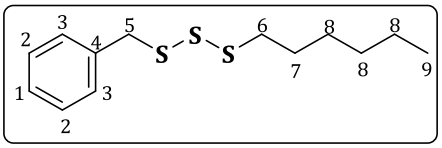

From thiosulfonate **1e** (86.8 mg, 0.312 mmol) and disulfanyl acetate **2b** (50.0 mg, 0.260 mmol) in THF (2 mL) and sodium methoxide (0.26 mL, 1M, 0.26 mmol) to afford trisulfide **64** (60.0 mg, 85%) as a colourless oil. IR (ν_{max}/cm^{-1}) 696, 468; ^{1}H NMR (300 MHz, $CDCl_3$) δ 7.38–7.25 (m, 5H, H-1/H-2/H-3), 4.11 (s, 2H, H-5), 2.83 (t, *J* = 7.2 Hz, 2H, H-6), 1.80–1.65 (m, 2H, H-7), 1.47–1.25 (m, 6H, H-8), 0.91 (t, *J* = 6.8 Hz, 3H, H-9); ^{13}C NMR (101 MHz, $CDCl_3$) δ 136.8, 129.6, 128.8, 127.7, 43.3, 39.2, 31.5, 29.0, 28.3, 22.7, 14.1; HRMS (ASAP^{+}) *m/z* [M + H]$^{+}$ calcd for $C_{13}H_{21}S_3$ 273.0805, found 273.0793.

1-Dodecyl-3-phenyltrisulfane (**65**).[139]

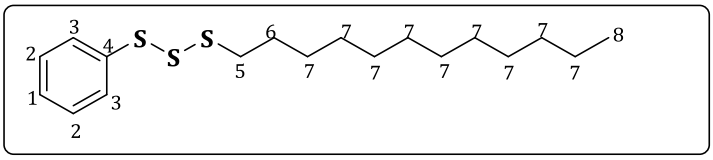

From thiosulfonate **1l** (184.0 mg, 0.697 mmol) and disulfanyl acetate **2e** (160.0 mg, 0.579 mmol) in THF (4 mL) and sodium methoxide (0.57 mL, 1M, 0.57 mmol) to afford trisulfide **65** (117.0 mg, 59%) as a yellow oil. IR (ν_{max}/cm^{-1}) 470; ^{1}H NMR (300 MHz, $CDCl_3$) δ 7.65–7.58 (m, 2H, H-3), 7.39–7.28 (m, 3H, H-1/H-2), 2.82 (t, *J* = 7.4 Hz, 2H, H-5), 1.73–1.61 (m, 2H, H-6), 1.39–1.22 (s, 18H, H-7), 0.89 (t, *J* = 6.8 Hz, 3H, H-8); ^{13}C NMR (101 MHz, $CDCl_3$) δ 137.4, 130.4, 129.2, 128.3, 39.2, 32.1, 29.8, 29.8, 29.7, 29.6, 29.5, 29.3, 29.1, 28.7, 22.8, 14.2.

1-(4-Fluorophenyl)-3-propyltrisulfane (**66**).

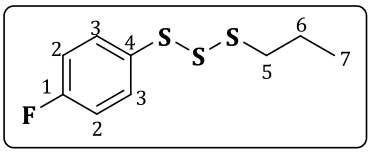

From thiosulfonate **1m** (135.4 mg, 0.480 mmol) and disulfanyl acetate **2a** (60.0 mg, 0.400 mmol) in THF (3 mL) and sodium methoxide (0.40 mL, 1M, 0.40 mmol) to afford trisulfide **66** (57.0 mg, 61%) as a yellow oil. IR (ν_{max}/cm^{-1}) 473; ^{1}H NMR (300 MHz, $CDCl_3$) δ 7.64–7.57 (m, 2H, H-2), 7.10–7.02 (m, 2H, H-3), 2.81 (t, *J* = 7.4 Hz, 2H, H-5), 1.80–1.65 (m, 2H, H-6), 0.98 (t, *J* = 7.4 Hz, 3H, H-7); ^{13}C NMR (101 MHz, $CDCl_3$) δ 163.3 (d, J_{CF} = 248.5 Hz), 133.3 (d, J_{CF} = 8.0 Hz), 132.7, 116.4, (d, J_{CF} = 22.1 Hz), 41.4, 22.4, 13.2; HRMS (ASAP^{+}) *m/z* [M]$^{+}$ calcd for $C_9H_{11}FS_3$ 234.0007, found 234.0010.

2-(*Tert*-butyltrisulfanyl) pyridine (**67**)

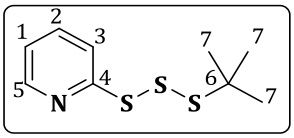

From thiosulfonate **1o** (77.6 mg, 0.293 mmol) and disulfanyl acetate **2f** (40.0 mg, 0.244 mmol) in THF (2 mL) and sodium methoxide (0.24 mL, 1M, 0.24 mmol) to afford trisulfide **67** (38.0 mg, 67%) as an orange oily liquid. IR (νmax/cm−1) 476; ^{1}H NMR (300 MHz, $CDCl_3$) δ 8.49 (m, 1H), 7.84-7.78 (m, *J* = 8.1 Hz, 1H), 7.68 (td, *J* = 7.8, 1.8 Hz, 1H), 7.17 – 7.10 (m, 1H), 1.41 (s, 9H); 13C NMR (101 MHz, CDCl3) δ 160.0, 159.3, 149.8, 137.3, 121.3, 49.6, 31.0, 30.3, 30.0. HRMS was not obtained.

(*R*)-Ethyl 3-(allyltrisulfanyl)-2-((*tert*-butoxycarbonyl) amino) propanoate (**73**)

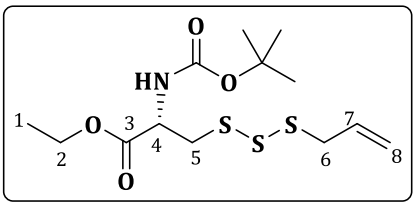

From thiosulfonate **1k** (98.0 mg, 0.243 mmol) and disulfanyl acetate **2d** (30.0 mg, 0.203 mmol) in THF (2 mL) and sodium methoxide (0.20 mL, 1M, 0.20 mmol, 1 eq) to afford trisulfide **73** (69.0 mg, 96%) as a colourless oil. $[\alpha]_D^{20}$ = +98.3 (*c* = 1.0, $CHCl_3$); IR (ν_{max}/cm^{-1}) 635, 477; ^{1}H NMR (300 MHz, $CDCl_3$) δ 5.96–5.80 (m, 1H, H-7), 5.38 (br s, 1H, NH), 5.29–5.18 (m, 2H, H-2), 4.64 (m, 1H, H-4), 4.22 (q, *J* = 7.1 Hz, 2H, H-2), 3.50 (d, *J* = 7.2 Hz, 2H, H-6), 3.42–3.25 (m, 2H, h-8), 1.45 (s, 9H, *t*-Bu), 1.30 (t, *J* = 7.1 Hz, 3H, H-1); ^{13}C NMR (101 MHz, $CDCl_3$) δ 170.6, 155.2, 132.7, 119.5, 80.4, 62.0,

53.2, 41.7, 41.5, 28.5, 14.3; HRMS (ESI$^+$) *m/z* [M + H]$^+$ calcd for $C_{13}H_{24}NO_4S_3$ 354.0867, found 354.0869.

(2*S*, 3*S*, 4*S*, 5*S*, 6*S*)-2-((Allyltrisulfanyl)methyl)-3,4,5-tris(benzyloxy)-6 methoxytetrahydro-2H-pyran (**74**).

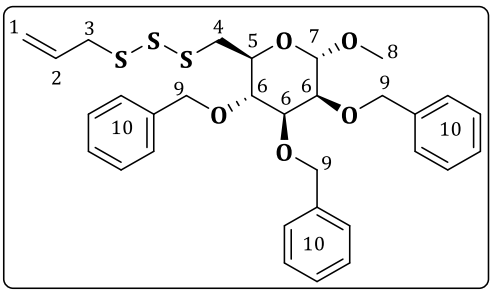

From thiosulfonate **1i** (130.0 mg, 0.205 mmol) and disulfanyl acetate **2d** (25.0 mg, 0.169 mmol) in THF (4 mL) and sodium methoxide (0.17 mL, 1M, 0.17 mmol) to afford trisulfide **74** (65.0 mg, 66%) as a colourless thick oily liquid. $[\alpha]_D^{20}$ = +138.9 (*c* = 1.0, $CHCl_3$); IR (ν_{max}/cm^{-1}) 477; ^{1}H NMR (300 MHz, $CDCl_3$) δ 7.40–7.27 (m, 15H, H-10), 5.94–5.78 (m, 1H, H-2), 5.25–5.14 (m, 2H, H-1), 4.97 (d, *J* = 10.8 Hz, 1H, H-5), 4.75–4.60 (m, 6H, H-9), 3.94–3.75 (m, 4H, H-4), 3.49 (d, *J* = 7.2 Hz, 2H, H-3), 3.42 (dd, *J* =13.4 , 2.1 Hz, 1H, H-7), 3.34 (s, 3H, H-8), 3.07 (dd, *J* = 9.0 Hz, 1H, H-5); ^{13}C NMR (101 MHz, $CDCl_3$) δ 138.6, 138.5, 138.4, 132.8, 128.6, 128.6, 128.5, 128.5, 128.1, 128.0, 127.9, 127.8, 127.8, 119.2, 99.2, 80.4, 77.9, 75.3, 75.0, 73.0, 72.4, 70.7, 55.1, 42.0, 41.7; HRMS (ESI$^+$) *m/z* [M + H]$^+$ calcd for $C_{31}H_{37}O_5S_3$ 585.1803, found 585.1813.

1-Dodecyl-3-(prop-2-yn-1-yl) trisulfane (**75**).

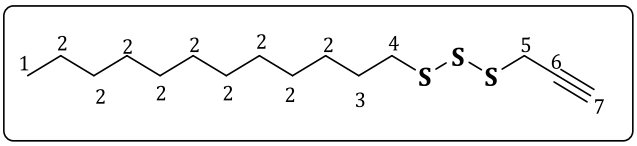

From thiotosylate **1c** (107.0 mg, 0.300 mmol) and disulfanyl acetate **2c** (37.0 mg, 0.253 mmol) in THF (2 mL) and sodium methoxide (0.25 mL, 1M, 0.25 mmol) to afford trisulfide **75** (40.0 mg, 52%) as a colourless oil. IR (ν_{max}/cm^{-1}) 635, 477; ^{1}H NMR (300 MHz, $CDCl_3$) δ 3.62 (d, *J* = 2.7 Hz, 2H, H-5), 2.91 (t, *J* = 7.4 Hz, 2H, H-4), 2.33 (d, *J* = 2.7 Hz, 1H, H-7), 1.80–1.68 (m, 2H, H-3), 1.45–1.23 (m, 18H, H-2), 0.88 (t, *J* = 6.8 Hz, 3H, H-1); ^{13}C NMR (101 MHz, $CDCl_3$) δ 79.1, 72.8, 39.5, 32.1, 29.8, 29.8, 29.7, 29.6, 29.5, 29.3, 29.0, 28.7, 26.8, 22.8, 14.2; HRMS (ASAP$^+$) *m/z* [M + H]$^+$ calcd for $C_{15}H_{29}S_3$ 305.1431, found 305.1429.

1- Allyl-3-(4-methoxyphenyl) trisulfane (**77**).

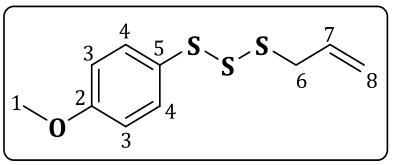

From thiosulfonate **1n** (262.0 mg, 0.891 mmol) and disulfanyl acetate **2d** (110.0 mg, 0.743 mmol) in THF (5 mL) and sodium methoxide (0.74 mL, 1M, 0.74 mmol) to afford trisulfide **77** (116.0 mg, 64%) as a yellow oil. IR (ν_{max}/cm^{-1}) 467; ^{1}H NMR (300 MHz, $CDCl_3$) δ 7.57 (d, *J* = 8.9 Hz, 2H, H-3), 6.89 (d, *J* = 8.9 Hz, 2H, H-4), 5.91–5.72 (m, 1H, H-7), 5.19–5.02 (m, 2H, H-8), 3.82 (s, 3H, H-1), 3.42 (d, *J* = 7.2 Hz, 2H, H-6); ^{13}C NMR (101 MHz, $CDCl_3$) δ 160.8, 134.2, 132.7, 128.0, 119.2, 114.9, 55.5, 41.8; HRMS (ASAP$^+$) *m/z* [M + H]$^+$ calcd for $C_{10}H_{13}OS_3$ 245.0129, found 245.0129.

Ethyl *N*-(tert-butoxycarbonyl)-*S*-(*p*-tolyldisulfaneyl)-*L*-cysteinate (**89**).

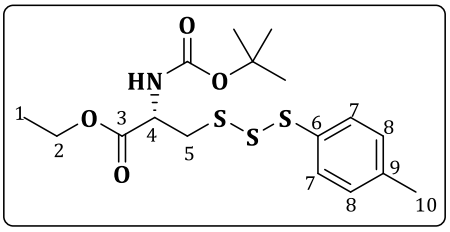

From thiosulfonate **1k** (146.0 mg, 0.362 mmol) and disulfanyl acetate **2g** (60.0 mg, 0.303 mmol) in THF (2 mL) and sodium methoxide (0.30 mL, 1M, 0.30 mmol) to afford trisulfide **89** (86.0 mg, 70%) as a colourless solid. mp 80-82 °C; $[\alpha]_D^{20}$ = +115.0 (*c* = 1.0, $CHCl_3$); IR (ν_{max}/cm^{-1}) 3369, 1735, 481; ^{1}H NMR (300 MHz, $CDCl_3$) δ 7.50 (d, *J* = 8.1 Hz, 2H, H-7), 7.17 (d, *J* = 8.1 Hz, 2H, H-8, H-8), 5.36 (br s, 1H, NH), 4.59 (m, 1H, H-4), 4.22 (q, *J* = 7.2 Hz, 2H, H-2), 3.42–3.21 (m, 2H, H-5), 2.36 (s, 3H, H-10), 1.46 (s, 9H, *t*-Bu), 1.29 (t, *J* = 7.2 Hz, 3H, H-1); ^{13}C NMR (101 MHz, $CDCl_3$) δ 170.6, 155.1, 139.2, 133.0, 131.5, 130.1, 80.3, 62.0, 53.1, 41.4, 28.5, 21.3, 14.3; HRMS (ESI$^+$) *m/z* [M + H]$^+$ calcd for $C_{17}H_{26}NO_4S_3$ 404.1024, found 404.1018.

1-(4-Methoxyphenyl)-3-phenyltrisulfane (**90**).

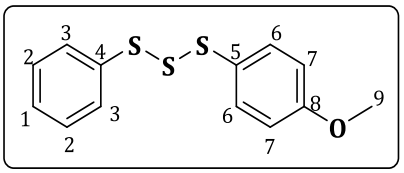

From thiosulfonate **1l** (148.0 mg, 0.561 mmol) and disulfanyl acetate **2h** (100.0 mg, 0.467 mmol) in THF (3 mL) and sodium methoxide (0.47 mL, 1M, 0.47 mmol) to afford trisulfide **90** (84.0 mg, 64%) as a green oil. IR (ν_{max}/cm^{-1}) 469; ^{1}H NMR (300 MHz, $CDCl_3$) δ 7.53–7.45 (m, 4H, H-6/H-3), 7.32–7.23 (m, 3H, H-1/H-2), 6.85–6.78 (m, 2H, H-7), 3.81 (s, 3H, H-9); ^{13}C NMR (101 MHz, $CDCl_3$) δ 160.8, 136.8,

134.4, 130.0, 129.2, 128.1, 127.4, 114.9, 55.6; HRMS (ASAP$^+$) *m/z* [M]$^+$ calcd for $C_{13}H_{12}OS_3$ 280.0050, found 280.0053.

1-(4-Fluorophenyl)-3-(4-methoxyphenyl) trisulfane (**91**).

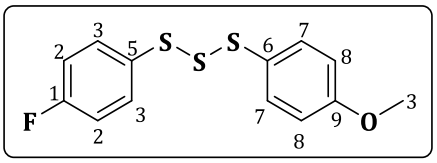

From thiosulfonate **1m** (63.0 mg, 0.223 mmol) and disulfanyl acetate **2h** (40.0 mg, 0.187 mmol) in THF (2 mL) and sodium methoxide (0.18 mL, 1M, 0.18 mmol) to afford trisulfide **91** (45.0 mg, 81%) as a green to yellow oil. IR (ν_{max}/cm^{-1}) 463; ^{1}H NMR (300 MHz, $CDCl_3$) δ 7.52–7.44 (m, 4H, H-3/H-7), 7.00–6.93 (m, 2H, H-2), 6.83–6.78 (m, 2H, H-8), 3.81 (s, 3H, H-3); ^{13}C NMR (101 MHz, $CDCl_3$) δ 163.0 (d, *J* = 165.0 Hz), 160.8, 134.3, 132.9 (d, *J* = 5.0 Hz), 132.0, 127.1, 116.3 (d, *J* = 15.1 Hz), 114.9, 55.6; HRMS (ASAP$^+$) *m/z* [M]$^+$ calcd for $C_{13}H_{11}FOS_3$ 297.9956, found 297.9957.

1-(4-Fluorophenyl)-3-(*p*-tolyl) trisulfane (**92**).

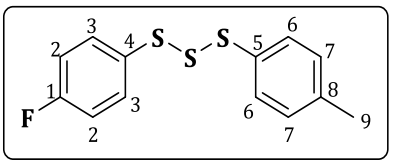

From thiosulfonate **1m** (51.0 mg, 0.181 mmol) and disulfanyl acetate **2g** (30.0 mg, 0.151 mmol) in THF (1 mL) and sodium methoxide (0.15 mL, 1M, 0.15 mmol) to afford trisulfide **92** (38.0 mg, 89%) as a yellow to green oil. IR (ν_{max}/cm^{-1}) 502; ^{1}H NMR (300 MHz, $CDCl_3$) δ 7.53–7.46 (m, 2H, H-2), 7.43–7.39 (m, 2H, H-3), 7.12–7.07 (m, 2H, H-7), 7.00–6.93 (m, 2H, H-6), 2.35 (s, 3H); ^{13}C NMR (101 MHz, $CDCl_3$) δ 163.3 (d, *J* = 249.5 Hz), 139.1, 133.4, (d, *J* = 9.1 Hz), 133.0, 132.0, 131.3, 130.0, 116.3 (d, *J* = 22.1 Hz), 21.3; HRMS (ASAP$^+$) *m/z* [M]$^+$ calcd for $C_{13}H_{11}FS_3$ 282.0007, found 282.0011.

5-(Dimethylamino)-N-(3-(propyltrisulfaneyl) propyl) naphthalene-1-sulfonamide (**96**)

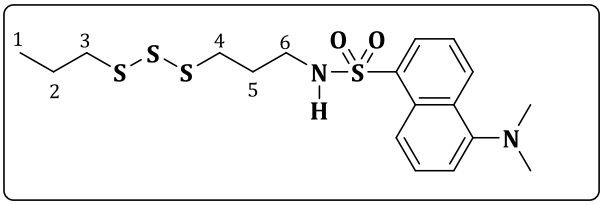

From thiosulfonate **1j** (646.0 mg, 1.35 mmol) and disulfanyl acetate **2a** (169.0 mg, 1.12 mmol) in THF (5 mL) and sodium methoxide (1.1 mL, 1M, 1.1 mmol) to afford trisulfide **96** (340.0 mg, 70%) as a luminous-

green oil. IR (ν_{max}/cm^{-1}) 1143, 478; ^{1}H NMR (400 MHz, $CDCl_3$) δ 8.58 – 8.53 (m, 1H, Ar-H), 8.31 – 8.24 (m, 2H, Ar-H), 7.60 – 7.49 (m, 2H, Ar-H), 7.19 (d, *J* = 8.5 Hz, 1H, Ar-H), 4.97 – 4.79 (m, 1H, NH), 3.04 (d, *J* = 6.4 Hz, 2H, H-6), 2.89 (s, 6H, NMe_2), 2.82 – 2.65 (m, 4H, H-3/H-4), 1.90 – 1.80 (m, 2H, H-5), 1.76 – 1.61 (m, 2H, H-2), 0.97 (t, *J* = 7.3 Hz, 3H, H-1); ^{13}C NMR (101 MHz, $CDCl_3$) δ 133.4, 129.6, 128.7, 122.1, 117.4, 114.2, 44.3, 42.4, 40.5, 39.6, 34.2, 31.9, 27.3, 21.0, 12.0; HRMS (ASAP$^+$) *m/z* [M]$^+$ calcd for $C_{18}H_{26}N_2O_2S_4$ 430.0877, found 431.0980.

6.5.2 Library 2

1-Allyl-3-benzyltrisulfane (**76**)

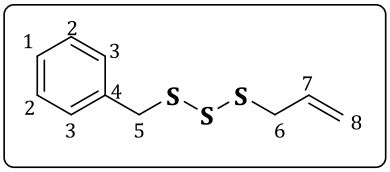

From thiosulfonate **1e** (225.0 mg, 0.809 mmol) and disulfanyl acetate **2d** (100.0 mg, 0.674 mmol) in THF (4 mL) and sodium methoxide (0.67 mL, 1M, 0.67 mmol) to afford trisulfide **76** (102.0 mg, 66%) as colourless oil. IR (ν_{max}/cm^{-1}) 761, 474; ^{1}H NMR (400 MHz, $CDCl_3$) δ 7.37 – 7.27 (m, *J* = 4.5 Hz, 5H, H-1/H-2, H-3), 5.93 – 5.80 (m, *J* = 7.3 Hz, 1H, H-7), 5.25 – 5.15 (m, 2H, H-8), 4.10 (s, 2H, H-5), 3.48 – 3.39 (d, 2H, H-6); ^{13}C NMR (101 MHz, $CDCl_3$) δ 136.6, 132.8, 129.5, 128.7, 127.7, 119.2, 43.4, 41.7; HRMS (ASAP$^+$) *m/z* [M]$^+$ calcd for $C_{10}H_{12}S_3$ 228.0109, found 228.0114.

1-Allyl-3-(4-fluorobenzyl) trisulfane (**97**)

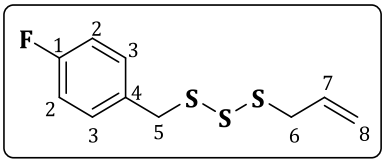

From thiosulfonate **1q** (479.0 mg, 1.62 mmol) and disulfanyl acetate **2d** (200.0 mg, 1.35 mmol) in THF (4 mL) and sodium methoxide (1.35 mL, 1M, 1.35 mmol) to afford trisulfide **97** (170.0 mg, 51%) as colourless oil. IR (ν_{max}/cm^{-1}) 754, 474; ^{1}H NMR (600 MHz, $CDCl_3$) δ 7.33 – 7.27 (m, *J* = 8.6, 5.4 Hz, 2H, H-1/H-2), 7.03 (t, *J* = 8.7 Hz, 2H, H-3), 5.92 - 5.84 (m, 1H, H-7), 5.26 – 5.17 (m, 2H, H-8), 4.07 (s, 3H, H-5), 3.47 (d, *J* = 7.3 Hz, 2H, H-6); ^{13}C NMR (151 MHz, $CDCl_3$) δ 163.1 (d, *J* = 240.5 Hz), 161.5, 132.7, 132.4, 131.0, 131.1 (*J* = 7.0 Hz), 119.2, 115.6, 115.5, 42.4, 41.6; HRMS (ASAP$^+$) *m/z* [M]$^+$ calcd for $C_{10}H_{11}FS_3$ 246.0800, found 246.0080.

1-Allyl-3-(4-chlorobenzyl) trisulfane (**98**)

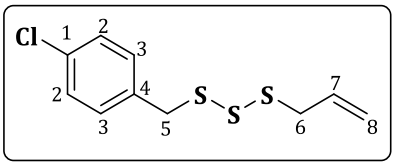

From thiosulfonate **1r** (253.0 mg, 0.809 mmol) and disulfanyl acetate **2d** (100.0 mg, 0.674 mmol) in THF (3 mL) and sodium methoxide (0.67 mL, 1M, 0.674 mmol) to afford trisulfide **98** (166.0 mg, 93%) as colourless oil. IR (ν_{max}/cm^{-1}) 720, 477; ^{1}H NMR (300 MHz, $CDCl_3$) δ 7.49 – 7.09 (m, 4H, H-1/H-2/H-3), 5.97 – 5.78 (m, 1H, H-7), 5.29 – 5.14 (m, 2H, H-8), 4.06 (s, 2H, H-5), 3.48 (d, *J* = 9.3 Hz, 2H, H-6); ^{13}C NMR (75 MHz, $CDCl_3$) δ 135.2, 133.6, 132.7, 130.8, 128.9, 119.3, 42.4, 41.6, 29.8; HRMS (ASAP$^+$) *m/z* [M]$^+$ calcd for $C_{10}H_{11}ClS_3$ 261.9700, found 261.9731.

1-Allyl-3-(4-bromobenzyl) trisulfane (**99**)

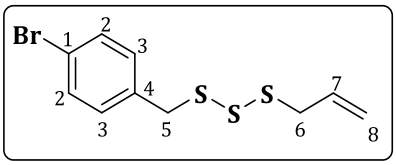

From thiosulfonate **1s** (483.0 mg, 1.35 mmol) and disulfanyl acetate **2d** (167.0 mg, 1.13 mmol) in THF (4 mL) and sodium methoxide (1.1 mL, 1M, 1.13 mmol) to afford **99** (200.0 mg, 57%) as colourless oil. IR (ν_{max}/cm^{-1}) 718, 476; ^{1}H NMR (300 MHz, $CDCl_3$) δ 7.52 – 7.37 (d, 2H, H-2), 7.23 – 7.15 (d, 2H, H-3), 5.96 – 5.75 (m, 1H. H-7), 5.28 – 5.13 (m, 2H, H-8), 4.02 (s, 2H, H-5), 3.46 (d, *J* = 9.1 Hz, 2H, H-6); ^{13}C NMR (101 MHz, $CDCl_3$) δ 135.6, 132.6, 131.7, 131.0, 121.6, 119.2, 77.3, 76.7, 41.5; HRMS (ASAP$^+$) *m/z* [M]$^+$ calcd for $C_{10}H_{11}BrS_3$ 305.9150, found 305.9189.

1-Allyl-3-(4-methylbenzyl) trisulfane (**100**)

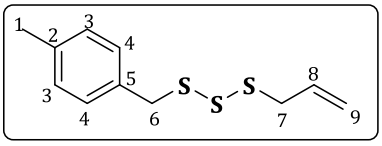

From thiosulfonate **1t** (307.0 mg, 1.05 mmol) and disulfanyl acetate **2d** (130.0 mg, 0.876 mmol) in THF (3 mL) and sodium methoxide (0.87 mL, 1M, 0.87 mmol) to afford **100** (160.0 mg, 75.2%) as colourless oil. IR (ν_{max}/cm^{-1}) 460; ^{1}H NMR (300 MHz, $CDCl_3$) δ 7.24 - 7.22 (d, *J* = 8.1, 2H, H-4), 7.16 – 7.13 (d, *J* = 9.2, 2H, H-3), 5.94 – 5.78 (m, 1H, H-8), 5.26 – 5.17 (m, 2H, H-9), 4.08 (s, 2H, H-6), 3.47 (d, *J* = 7.3, 2H, H-7), 2.35 (s, 3H, H-1); ^{13}C NMR (75 MHz, $CDCl_3$) δ 137.4, 133.5, 132.8, 129.4, 119.1, 43.1, 41.8, 41.6, 21.3; HRMS (ASAP$^+$) *m/z* [M]$^+$ calcd for $C_{11}H_{14}S_3$ 242.0570, found 242.1097.

1-Allyl-3-(4-methoxybenzyl) trisulfane (**101**)

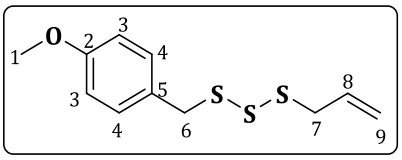

From thiosulfonate **1u** (499.0 mg, 1.62 mmol) and disulfanyl acetate **2d** (200.0 mg, 1.35 mmol) in THF (4 mL) and sodium methoxide (1.3 mL, 1M, 1.3 mmol) to afford trisulfide **101** (250.0 mg, 71%) as colourless oil. IR (ν_{max}/cm^{-1}) 747, 544; ^{1}H NMR (300 MHz, $CDCl_3$) δ 7.34 – 7.22 (d, 2H, H-4), 6.94 – 6.83 (d, 2H, H-3), 5.91 (m, *J* = 9.9, 7.3 Hz, 1H, H-8), 5.29 – 5.17 (m, 2H, H-9), 4.10 (s, 2H, H-6), 3.83 (s, 3H, H-1), 3.50 (d, *J* = 7.2 Hz, 2H, H-7); ^{13}C NMR (101 MHz, $CDCl_3$) δ 158.5, 132.1, 130.0, 127.8, 118.4, 113.4, 42.2, 40.9; HRMS (ASAP$^+$) *m/z* [M+H]$^+$ calcd for $C_{11}H_{14}OS_3$ 259.0250, found 259.0294.

1-Allyl-3-(4-(trifluoromethyl) benzyl) trisulfane (**102**)

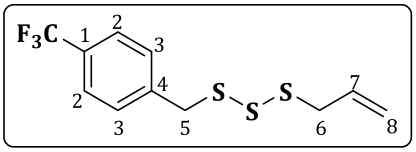

From thiosulfonate **1v** (280.0 mg, 0.809 mmol) and disulfanyl acetate **2d** (100.0 mg, 0.674 mmol) in THF (3 mL) and sodium methoxide (0.6 mL, 1M, 0.6 mmol) to afford **102** (153.0 mg, 76%) as a colourless oil. IR (ν_{max}/cm^{-1}) 754, 619; ^{1}H NMR (400 MHz, $CDCl_3$) δ 7.63 – 7.54 (d, 2H, H-2), 7.45 (d, *J* = 8.1 Hz, 2H, H-3), 5.86 (m, 1H, H-7), 5.27 – 5.15 (m, 2H, H-8), 4.11 (s, 2H, H-5), 3.46 (dt, *J* = 7.3, 1.0 Hz, 2H, H-6); ^{13}C NMR (101 MHz, $CDCl_3$) δ 140.9, 132.7, 129.8, 125.5-125.7 (q, J = 270.0 Hz), 42.5, 41.6; HRMS (ASAP$^+$) *m/z* [M] + calcd. for $C_{11}H_{11}F_3S_3$ 295.9975, found 295.9970.

6.5.3 Library 3

1,3-Dibenzyltrisulfane (**54**)[93]

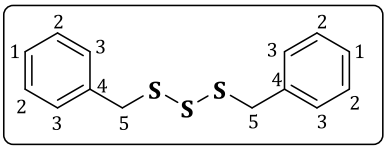

From thiosulfonate **1e** (505.0 mg, 1.82 mmol) and disulfanyl acetate **2i** (300.0 mg 1.51 mmol) in THF (5 mL) and sodium methoxide (1.5 mL, 1M, 1.5 mmol) to afford **54** (375.0 mg, 89%) as white crystals. ^{1}H NMR (600 MHz, $CDCl_3$) δ 7.38 – 7.21 (m, 10H, H-1/H-2/H-3), 4.02 (s, 4H, H-5).

1,3-Bis(4-fluorobenzyl) trisulfane (**103**)[93]

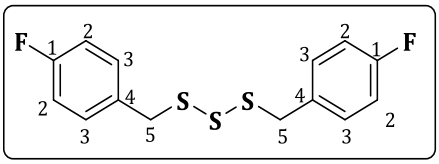

From thiosulfonate **1q** (131.0 mg, 0.443 mmol) and disulfanyl acetate **2j** (80.0 mg, 0.369 mmol) in THF (3 mL) and sodium methoxide (0.36 mL, 1M, 0.36 mmol) to afford **103** (90.0 mg, 77%) as white crystals. ^{1}H NMR (600 MHz, $CDCl_3$) δ 7.25 (m, *J* = 8.6, 5.4 Hz, 2H, H-2), 6.99 (t, *J* = 8.7 Hz, 3H, H-3), 3.98 (s, 4H, H-5).

1,3-Bis(4-chlorobenzyl) trisulfane (**104**)[93]

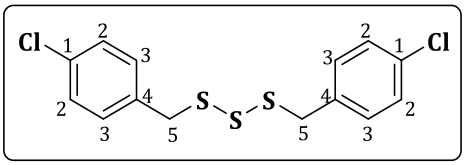

From thiosulfonate **1r** (112.0 mg, 0.360 mmol) and disulfanyl acetate **2k** (70.0 mg, 0.300 mmol) in THF (3 mL) and sodium methoxide (0.30 mL, 1M, 0.30 mmol) to afford **104** (70.0 mg, 67%) as white crystals. ^{1}H NMR (400 MHz, $CDCl_3$) δ 7.30 (d, *J* = 8.5 Hz, 4H, H-2), 7.23 (d, *J* = 8.7 Hz, 4H, H-3), 3.98 (s, 4H, H-5).

1,3-Bis(4-bromobenzyl) trisulfane(**105**)[93]

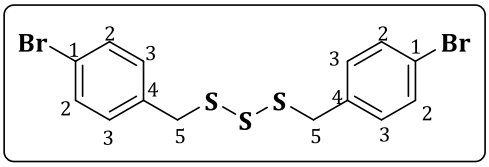

From thiosulfonate **1s** (361.0 mg, 1.01 mmol) and disulfanyl acetate **2l** (234.0 mg, 0.844 mmol) in THF (4 mL) and sodium methoxide (0.8 mL, 1M, 0.80 mmol) to afford **105** (250.0 mg, 67%) as white crystals. ^{1}H NMR (400 MHz, $CDCl_3$) δ 7.46 (d, *J* = 8.6 Hz, 2H, H-2), 7.19 (d, *J* = 8.7, 2H, H-3), 3.97 (s, 4H, H-5).

1,3-Bis(4-methylbenzyl) trisulfane (**106**)[93]

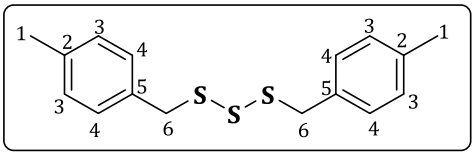

From thiosulfonate **1t** (436.0 mg, 1.49 mmol) and disulfanyl acetate **2m** (264.0 mg, 1.24 mmol) in THF (4 mL) and sodium methoxide (1.2 mL, 1M, 1.2 mmol) to afford **106** (355.0 mg, 93%) as a white powder. ^{1}H NMR (400 MHz, $CDCl_3$) δ 7.23 (d, *J* = 8.0 Hz, 4H, H-3), 7.16 (d, *J* = 7.9 Hz, 4H, H-4), 4.04 (s, 4H, H-6), 2.36 (s, 6H, H-1).

1,3-Bis(4-methoxybenzyl) trisulfane (**107**)

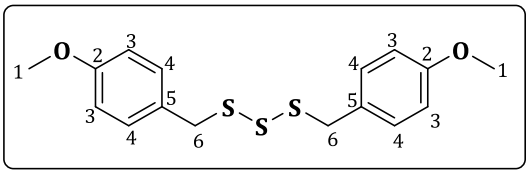

From thiosulfonate **1u** (227.0 mg, 0.735 mmol) and disulfanyl acetate **2n** (140.0 mg, 0.613 mmol) in THF (3 mL) and sodium methoxide (0.18 mL, 1M, 0.18 mmol) to afford **107** (163.0 mg, 78%) as white solid crystals. ^{1}H NMR (600 MHz, $CDCl_3$) δ 7.24 (d, *J* = 8.7 Hz, 2H, H-3), 6.86 (d, *J* = 8.7 Hz, 2H, H-4), 4.02 (s, 4H, H-6), 3.80 (s, 6H, H-1); ^{13}C NMR (151 MHz, $CDCl_3$) δ 159.3, 130.7, 128.6, 114.2, 55.4, 42.8; HRMS (ASAP^{+}) *m/z* [M]$^{+}$ calcd. for $C_{16}H_{18}O_2S_3$ 338.0460, found 257.2480 as $C_8H_9OS_3$ due to the loss of one methoxybenzyl group C_8H_9O.

1,3-Bis(4-(trifluoromethyl) benzyl) trisulfane (**108**)[93]

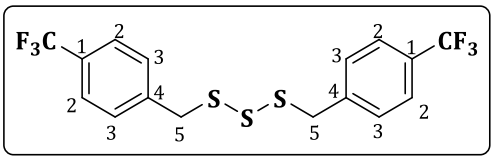

From thiosulfonate **1v** (292.0 mg, 0.842 mmol) and disulfanyl acetate **2o** (187.0 mg, 0.702 mmol) in THF (4 mL) and sodium methoxide (0.7 mL, 1M, 0.7 mmol) to afford **108** (190.0 mg, 65%) as a white solid. ^{1}H NMR (400 MHz, $CDCl_3$) δ 7.59 (d, *J* = 8.1 Hz, 4H, H-2), 7.41 (d, *J* = 8.0 Hz, 4H, H-3), 4.05 (s, 4H).

6.6 Synthesis of the Azide Probe, 112, via 2 steps

Step 1: Synthesis of (4-bromo-N-butyl-1,8-naphthalimide)[483]

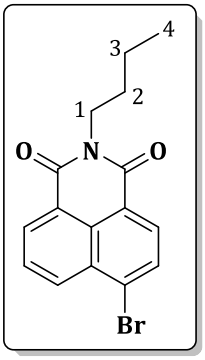

6-bromo-2-butyl-1*H*-benzo[*de*]isoquinoline-1,3(2*H*)-dione

Compound **116** was synthesized following the procedure outlined by Song et al.[483] A mixture of 4-bromo-1,8-naphthalic anhydride (800 mg, 2.89 mmol, 1 eq.) and *n*-butylamine (1.90 g, 25.99 mmol, 9 eq.) was dissolved in acetic acid (15 mL) and heated to reflux under nitrogen for 6 hours. After completion of the reaction, the solution was poured into distilled water, resulting in the formation of a precipitate. This precipitate was filtered, washed with water, and the resulting yellow powder was collected.

Recrystallization from ethanol afforded compound **116** as white crystals (810.0 mg, 84 %). ^{1}H NMR (400 MHz, $CDCl_3$) δ 8.56 (d, *J* = 6.2 Hz, 1 H, ArH), 8.47 (d, *J* = 8.1 Hz, 1 H, ArH), 8.10 (d, *J* = 7.9 Hz, 1 H, ArH), 7.99 (d, *J* = 7.4 Hz, 1 H, ArH), 7.80 (t, *J* = 7.0 Hz, *J* = 8.5 Hz, 1 H, ArH), 4.16 (t, *J* = 7.5 Hz, 2 H, H-1), 1.69-1.74 (m, 2 H, H-2), 1.41-1.48 (m, 2 H, H-3), 0.98 (t, *J* = 7.5 Hz, 3 H, H-4).

Step 2: Synthesis of 2 (4-azido-N-butyl-1,8-naphthalimide) (**112**).[483]

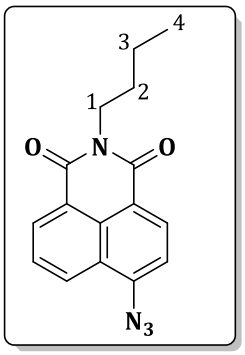

6-azido-2-butyl-1*H*-benzo[*de*]isoquinoline-1,3(2*H*)-dione

A solution of compound **116** (700 mg, 2.11 mmol, 1 eq.) and sodium azide (1.37 g, 21.07 mmol, 10 eq.) in DMF (13 mL) was stirred at 40 °C for 4 hours. Upon completion, the reaction mixture was poured into water, forming a precipitate which was subsequently filtered and rinsed with water. The resulting yellow powder was collected and recrystalised from ethanol (450 mg, 72%). ^{1}H NMR (300 MHz, $CDCl_3$) δ 8.64 (d, *J* = 7.3 Hz, 1H, ArH), 8.54 (d, *J* = 7.3 Hz, 1H, ArH), 8.40 (d, 1H, ArH), 8.00 (t, 1H, ArH), 7.80 (d, 1H, ArH), 4.22 – 4.11 (t, J = 8.0 Hz, 2H, H-1), 1.77 – 1.64 (m, 2H, H-2), 1.45 (m, *J* = 8.5, 2H, H-3), 0.98 (t, *J* = 7.3 Hz, 3H, H-4).

6.7 Biological Procedures

All biological work was carried out in a biosafety-certified laboratory with regulated temperature, airflow, and filtration. Strict protocols for handling, storage, and disposal were adhered to. Cell culture solutions were sterilized by autoclaving before use.

6.7.1 Cell Culture

Origin and Maintenance of Cell Lines

The human epithelial breast cancer cell line MDA-MB-231 was purchased from ATCC. The oesophageal cancer cell line WHCO1 was derived from a South African patient with oesophageal squamous cell carcinoma, derived from moderately differentiated tumour resections with metastatic disease.[456] Both cell lines were cultured in Dulbecco's Modified Eagle Medium (DMEM, Gibco®) supplemented with 10% fetal bovine serum (FBS, Gibco®) and 1% penicillin-streptomycin (Pen Strep, Gibco®). Complete media refers to FBS and penicillin-streptomycin supplemented media. MTT solutions were prepared by dissolving MTT (Sigma-Aldrich, RSA) in phosphate-buffered saline (PBS, pH 7.4, Gibco®). A 10% (w/v) sodium dodecyl sulfate (SDS) solution was made by dissolving the SDS powder in a 0.01 M HCl solution.

Cell Growth Conditions

Cells were grown in 100 mm sterile tissue culture dishes (Nest®, non-pyrogenic) in 8 mL of complete media and maintained in a humidified incubator (37°C, 5% CO_2, 91% humidity). All procedures were conducted in a UV-sterilised laminar flow hood and all equipment was sanitised with 70% ethanol. Cells were cultures until reaching 75-80% confluence, and then split using the protocol below. All experiments were performed on logarithmically growing cells.

Cell Splitting

The media was removed by suction, and then 0.25% Trypsin-EDTA (Gibco®) (2 mL) was added. After 5 minutes, detached cells were collected in a sterile 15 mL centrifuge tubes (NEST®, non-pyrogenic) and the trypsin was neutralised with complete media (2 mL). The mixture was centrifuged at 5000 rpm for 5 minutes to pellet the cells. Thereafter the supernatant was removed, and the pellet was re-suspended in complete media (2 mL). To maintain the cell line, the pellet suspension (300 µL) was added to a new dish with complete media (8 mL) and cultured again until 75% confluency.

Thawing and Freezing Cells

Cells from cryostorage were rapidly thawed at 37 °C, and the thawed cell solution (1 mL) was then added to a dish containing complete media (7 mL). The media was refreshed the following day, and the date and passage numbers were documented. For long-term storage, one 70-80% confluent dish of cells were trypsinised, and collected as described before. The pellet was resuspended in 1 mL of freeze-down media containing 10% DMSO, 20% FBS, and 1% Penicillin-streptomycin in DMEM. The samples were transferred to a 2 mL cryotube and frozen at -80 °C for a few days before transfer to liquid nitrogen for long term cryopreservation.

Determining Cell Concentration

Cell concentrations were determined by mixing a cell suspension (10 µL) with 0.1% trypan blue solution (10 µL) (Invitrogen®, Thermo Fischer Scientific). A 10 µL sample of this mixture was placed on a cell counting chamber slide (Invitrogen®) and analysed using an automated cell counter (Invitrogen®, Countess 3 FL) to quantify number of live and dead cells per millilitre.

6.7.2 Cell Viability Assay (MTT)

The cells were assessed for cytotoxicity using MTT cell viability assay. The WHCO1 cells were cultured to 70-80% confluency and collected and counted as described above. They were then seeded in 96-well plates (NEST®) at a density of 2.5–3.0 x 10^3 cells/well in complete media (90 µL). The cells were then allowed to settle overnight in the culture incubator as described above and then treated with the compounds at eight different concentrations each at 2-fold dilution. The concentration range selected depended on the compound under investigation but could fall within the broader range of 50 nM – 200 µM in 0.1% DMSO. Control cells were treated with 0.1% DMSO alone.

Each drug concentration was added to the cells in triplicate. The drug concentrations were prepared by first preparing stock solutions of the compounds in DMSO at a concentration of 100 mM. From this, eight 2-fold dilutions of the stock solutions in DMSO were prepared from 0.781 – 100 mM. These solutions were then diluted 100-fold into complete media to give 7.81 – 1000 µM solutions and 1% DMSO. These solutions were then added to the cells by transferring 10 µL of the media-compound solution to 90 µL of

cells to give a final concentration of compound in cells of 0.781 – 100 µM. Control wells received 0.1% DMSO alone as the vehicle.

Thereafter, the compounds were incubated with the cells for 48 hours. At the conclusion of the incubation period, MTT solution (10 µL, 5mg/mL in PBS) was added to each well and incubated for an additional 4 hours to allow for the formazan crystals to form. Thereafter, SDS solution (100 µL, 10% w/v in 0.01 M HCl) (was added to each well and incubated for 24 hours at 37°C. The absorbance of each well was measured at 595 nm using a Multiskan FC multi-well reader (Thermo Scientific®). The background absorbance of the media, test compound, and MTT reagent alone (i.e. without cells) was subtracted from each reading. The data was then analysed using GraphPad Prism 7 or 9, applying non-linear regression analysis fitted to a sigmoidal dose-response curve at 595 nm versus log (concentration) to obtain the IC_{50} value. Each compound was tested independently at least three times. The overall procedure is summarized in **Table 6.1**.

Table 6.1: Summary of MTT procedure

Step	Description	Details
1	**Seeding Cells**	2.5 – 3.0 x 10^3 cells/well in 90 µL complete media
2	**Compound Treatment**	In the broad range 200 µM to 50 nM depending on the compound and 0.1% DMSO in media as the vehicle
3	**Incubation**	48 hours
4	**MTT Solution Addition**	10 µL of 5mg/mL MTT in PBS, 4 hours incubation
5	**Formazan Solubilization**	100 µL of 10% SDS in 0.01 M HCl, 24 hours incubation
6	**Absorbance Measurement**	595 nm using Multiskan GO FC plate reader
7	**Data Analysis**	GraphPad Prism 8.01, sigmoidal dose-response curve fitting

6.8 Perthiol Stability Study (Ellman's Assay)

Calibration Curve of DTNB with NAC

The NAC stock solution of 1.5 mM was prepared in reaction buffer (24.5 mg in 100 mL PBS). From this stock solution, six dilutions were prepared as shown in **Table 6.2**. These dilutions were further diluted in reaction buffer to obtain final NAC concentrations of 150, 125, 100, 75, 50, and 25 µM used for the reactions.

Table 6.2: Standard solutions preparations of NAC

Standard	Volume Reaction ACN/Buffer	Volume of NAC	Final Concentration (mM)
A	100	24.5 mg in 100 mL	1.50
B	5	25	1.25
C	10	20	1.00
D	15	15	0.750
E	20	10	0.500
F	25	5	0.250
G	30	0	0

To prepare the Ellman's reagent, a 10 mM stock solution was made by dissolving 4 mg of Ellman's reagent in 1 mL of reaction buffer. For the calibration curve, 50 µL of this Ellman's reagent solution was added to 2.5 mL of reaction buffer in a glass vial. Next, 250 µL of each diluted NAC solution was added. The final concentrations of NAC after dilution are: 150 µM initial -> 13.4 µM final, 125 µM initial -> 11.2 µM final, 100 µM initial -> 8.9 µM final, 75 µM initial -> 6.7 µM final, 50 µM initial -> 4.5 µM final, and 25 µM initial -> 2.2 µM final.

Stability Assay using DTNB

The compounds *p*-OMe-BnSSH; **110**, and *p*-Br-BnSSH; **111** was synthesised by acid deprotection method.[351] Here, *p*-Br-BnSSAc; **2l**, (7 mg, 0.025 mmol) and *p*-MeO-BnSSAc; **2n**, (5.8 mg, 0.025 mmol) were dissolved in a mixture of 0.1 mL AcCl in 1.9 mL methanol. The reaction progress was monitored using TLC (hexane: EtOAc). After completion, the reaction mixture was evaporated under reduced pressure using a rotary evaporator to yield the crude perthiol product which was dissolved immediately in 16.6 mL of a 50:50 acetonitrile: PBS buffer solution to prepare a stock solution at a concentration of 1.5 mM. From this, a 1 mM dilution also in 50:50 ACN: PBS was prepared for use in subsequent reactions.

Ellman's Reagent was prepared by dissolving 4 mg of DTNB in 1 mL of reaction buffer to create a 10 mM solution. In the mixing step, 50 µL of the Ellman's Reagent solution was combined with 2.5 mL of reaction buffer in a series of vials. To each vial, 250 µL of the 1

mM perthiol stock solution was added at different timepoints, as 0, 10, 20, 30, 40, 50, 60, 70 minutes, which resulted in a final perthiol concentration of 0.089 mM. The mixtures were incubated at room temperature for 15 minutes, after which the absorbance at 412 nm was measured for each sample using a spectrophotometer.

6.9 Quantification of Sulfhydryl Groups in WHCO1 Cancer Cells

WHCO1 cells were seeded in 24-well plates at a density of 50,000 cells per well and allowed to attach overnight. The trisulfides under investigation in this experiment were (*p*-H; **54**, *p*-Br; **105**, *p*-OMe; **107**), as well as the disulfide BnSSBn, each prepared at a molarity of 1 mM by dissolving (3 mg, 0.0103 mmol), (4.5 mg, 0.0103 mmol), (3.5 mg, 0.0103 mmol), (3.1 mg, 0.0103 mmol), respectively, in the appropriate volume of DMSO. DTNB was prepared as a 10 mM solution in PBS (see **Table 6.3**). All compounds were diluted to a working concentration of 0.1 mM in DMEM before use. The cells were treated with the three trisulfide derivatives (*p*-H; **54**, *p*-Br; **105**, *p*-OMe; **107**) and a disulfide (BnSSBn), by adding 0.1 mL of the compound solution to 0.9 mL of cells, to give a final concentration 100 µM compound and 0.1 % DMSO.

Table 6.3: Sample Data on Concentrations, Masses, and Volumes Used

Substrate	Mass / mg	Moles / mmol	Volume of DMSO / mL	Molarity / mM	Dilution to 0.1 mM in DMEM
54 (*p*-H)	3.0	0.0103	10.3	1	0.1 mL in 0.9 mL cells in DMEM
105 (*p*-Br)	4.5	0.0103	10.3	1	0.1 mL in 0.9 mL cells in DMEM
107 (*p*-OMe)	3.5	0.0103	10.3	1	0.1 mL in 0.9 mL cells in DMEM
BnSSBn	3.1	0.0103	10.3	1	0.1 mL in 0.9 mL cells in DMEM
DTNB	4.0	0.0103	1 (in PBS)	10	Dilute to 1 mM in buffer

Cells treated with 0.1% DMSO alone were used as controls, and all treatments were conducted in triplicate. After incubation for 3 hours with the compounds, the media was collected and centrifuged to obtain the supernatant. A 1 mM DTNB solution was prepared in PBS, and 100 µL of this solution was mixed with 100 µL of the supernatant in a 2 mL microcentrifuge tube (final concentration is now 500 µM). The mixture was incubated for 30 minutes. Following incubation, this mixture was then diluted 10-fold by taking 200uL

and adding to 1.8 mL PBS to give a total volume of 2 mL. The absorbance was measured at 412 nm using a UV spectrophotometer.

6.10 H_2S Evaluation in WHCO1 Cancer Cells

Timeline Study

WHCO1 cells were seeded in 24-well plates at 50 000 cells per well and cultured for a few days until they reached approximately 80% confluence. A 10 mM stock solution of each compound was made in DMSO. A stock solution of 1 mM was made for the probe, **110**, in acetonitrile. The compounds were then diluted to 10 μM in DMEM and 0.1% DMSO and added to the cells (by adding 0.1 mL diluted stock solutions into 0.9 mL cells). The compounds used were the homo trisulfides series (*p*-H; **54,** *p*-F; **103**, *p*-Cl; **104**, *p*-Br; **105**, p-CH_3; **106**, *p*-OMe; **107,** *p*-CF_3, **108**). These compounds were incubated with the cells for the indicated times as 10 minutes, 1h or 3h. Thereafter, the media was removed, and the probe, **112**, was added at 10 μM in 0.5 mL for 10-minutes.

Control cells were treated with either the drug alone, probe alone, or Na_2S (10 μM) with the probe. The preparations of concentrations illustrated in **Table 6.4**.

Table 6.4: Sample Data on Concentrations, Masses, and Volumes

Substrate	54	103	104	105	106	107	108	BnS_2Bn	NAP, 112
Mass/mg	2.9	3.2	3.6	4.5	3.2	3.5	4.3	2.5	3.0
No of mmoles	0.0101								0.0101
Volume of DMSO / mL	1								10 mL (ACN)
Molarity / mM	10								1
Dilution to 10 μM in DMEM	4.8 μL in 5 mL								50 μL in 5 mL

Fluorescent Imaging

Fluorescent images were obtained using the Nikon fluorimeter, with a FITC filter at an emission wavelength of 509 nm. Each experimental condition was conducted in triplicate, and each experiment was performed independently three times. The fluorescent images were analysed using ImageJ software. The analysis involved the following steps:

1. **Image Import and Preprocessing:**

   The images were imported into ImageJ.
2. **Quantification of Fluorescence:**

   For each well determination, three regions of interest (ROIs) around the well

were selected and the mean fluorescence intensity for each ROI was measured. This for each experiment 9 data points were obtained per compound, and this was repeated in triplicate to give a total of 27 data points which were averaged to give the mean and standard deviation for each compound.

Statistical Analysis:

Statistical significance was determined using two-way ANOVA, followed by post hoc tests where appropriate. A p-value of less than 0.05 was considered significant.

6.11 Live Cell Confocal Imaging

MDA-MB-231 cells were plated at a density of 2 x 10^4 cells per well in 8-well chambered cover glass plates (Lab-Tek II, 1.5 borosilicate, Australia) in 200 µL supplemented DMEM media. The cells were allowed to settle overnight in a humidified incubator.

The following day, stock solution (100 mM) of DPTS in DMSO was diluted into media to make 2mL of a 50 µM DPTS solution and 0.05% DMSO. The media was then removed from the cells and replaced with this 50 µM DPTS solution or media with 0.05% DMSOP alone for control cells. After 30 minutes, the trackers were added to the cells at the following concentrations: Lysotracker (50 nM), Mitotracker (25 nM) and ER tracker (1 µM). The trackers were firstly diluted into media and then added to the cells. Control cells received either media alone or trackers alone.

Imaging and Analysis

Thirty minutes after compound and label addition, live cell imaging was performed using a Zeiss LSM 880 Confocal Fast AiryScan microscope. Imaging sessions lasted approximately 3 hours, during which cells were maintained in an incubation chamber at 37 °C under 5% CO_2. Data analysis was conducted and analysed using the Zen 3.4 Blue Edition and Black® software.

6.12 Computational Procedure

Calculations involved for pKa values

The pK_a values were determined using a computational DFT procedure for AH and A-(as described above) to obtain thermodynamic data and methods outlined in the literature and below for H^+ in particular.[505,506] The pK_a for a perthiol was calculated using the solution phase Gibb's free energy of the deprotonation reaction, $AH \rightleftharpoons A^- + H^+$, where $pK_a = \Delta G_{aq}^* / 2.303RT$ and $\Delta G_{aq}^* = G_{aq}^*(A^-) + G_{aq}^*(H^+) - \Delta G_{aq}^*(AH)$. Note, the aqueous phase

proton (H^+) free energy is calculated using $\Delta G_{aq^*}(H^+) = Gg°(H^+) + \Delta G_{aq,solv}(H^+) + \Delta G^{1atm \rightarrow 1M}$. $\Delta G_{aq,\ solv}(H^+)$ = -265.9 kcal/mol was taken from the literature,[506] and $Gg°(H^+)$ was calculated using $Gg°(H^+) = Hg° - TSg°$, where E_{0K}=0, $Hg°$=5/2RT= 1.48 kcal/mol, and $Sg°$ = 26.05 cal/(mol ·K).[506] $\Delta G^{1atm \rightarrow\ 1M}$= 1.89 k_{cal}/mol, corresponding to the free energy change due to changing the standard state from 1 atm to 1 M. The Gibbs free energy of a proton was empirically scaled by -14.542 kcal/mol from the generally accepted -265.9 kcal/mol for all pK_a calculations such that the calculated pK_a value for a known compound (an unsubstituted benzyl trisulfide) fit the literature value of 6.2 ± 0.1 more closely.[506,507] This empirical scaling does not change the linear correlations (gradients remain the same) shown in Figures 5.19-5.20, only the y-axis intercepts change.

References

(1) Xiao, X.; Xue, J.; Jiang, X. *Nat. comm.* **2018**, *9*, 2191.
(2) Rattanachaikunsopon, P.; Phumkhachorn, P. *Biosci Biotechnol Biochem.* **2008**, *72*, 2987.
(3) Tsai, C. Y.; Wang, C. C.; Lai, T. Y.; Tsu, H. N.; Wang, C. H.; Liang, H. Y.; Kuo, W. W. *Int J Cardiol.* **2013**, *168*, 1286.
(4) Ariga, T.; Seki, T. *BioFactors.* **2006**, *26*, 93.
(5) Lei, Y. P.; Liu, C. T.; Sheen, L. Y.; Chen, H. W.; Lii, C. K. *Mol Nutr Food Res.* **2010**, *54 Suppl 1*, S42.
(6) Jiang, X.; Zhu, X.; Liu, N.; Xu, H.; Zhao, Z.; Li, S.; Li, S.; Cai, J.; Cao, J. *Int.j.bio. sci.* **2017**, *13*, 167.
(7) Hosono, T.; Fukao, T.; Ogihara, J.; Ito, Y.; Shiba, H.; Seki, T.; Ariga, T. *J. Bio. Chem.* **2005**, *280*, 41487.
(8) Seki, T.; Hosono, T.; Hosono-Fukao, T.; Inada, K.; Tanaka, R.; Ogihara, J.; Ariga, T. *Asia Pac. J.Clin. Nut.* **2008**, *17 Suppl 1*, 249.
(9) DeVault, R.; Rosenbrook, W. *J.anti.* **1973**, *26*, 532.
(10) Waring, P.; Eichner, R.; Tiwari-Palni, U.; Mullbacher, A. *Aust. J. Chem.* **1987**, *40*, 991.
(11) Nozawa, K.; Udagawa, S.-I.; Nakajima, S.; Kawai, K.-I. *Chem. Pharm. Bull.* **1987**, *35*, 3460.
(12) Kawahara, N.; Nozawa, K.; Yamazaki, M.; Nakajima, S.; Kawai, K.-i. *Chem. Pharm. Bull.***1990**, *38*, 73.
(13) Mitrovic, P.; Orc ic , D. Z.; Sakac , Z.; Marjanovic -Jeromela, A.; Grahovac, N. L.; Milos evic , D.; Marisavljevic , D. *J. Serb. Chem. Soci.* **2012**, *77*, 1363.
(14) Kajula, M.; Ward, J. M.; Turpeinen, A.; Tejesvi, M. V.; Hokkanen, J.; Tolonen, A.; Hkkanen, H.; Picart, P.; Ihalainen, J.; Sahl, H.-G.; Pirttila, A. M.; Mattila, S. *J. Nat. Pro.* **2016**, *79*, 685.
(15) Hodges, R.; Shannon, J. *Aust. J. Chem.* **1966**, *19*, 1059.
(16) Takahashi, C.; Numata, A.; Ito, Y.; Matsumura, E.; Araki, H.; Iwaki, H.; Kushida, K. *J. Chem.Soc, Perkin Transactions 1.* **1994**, 1859.
(17) Feng, Y.; Blunt, J. W.; Cole, A. L. J.; Munro, M. H. G. *J. Nat. Prod.* **2004**, *67*, 2090.
(18) Dong, J.-Y.; He, H.-P.; Shen, Y.-M.; Zhang, K.-Q. *J. Nat. Prod.* **2005**, *68*, 1510.
(19) Carr, G.; Tay, W.; Bottriell, H.; Andersen, S. K.; Mauk, A. G.; Andersen, R. J. *Org. Lett.* **2009**, *11*, 2996.
(20) Adams, T. C.; Payette, J. N.; Cheah, J. H.; Movassaghi, M. *Org. Lett.* **2015**, *17*, 4268.
(21) Saito, T.; Suzuki, Y.; Koyama, K.; Natori, S.; Iitaka, Y.; Kinosita, T. *Chem. Pharm. Bull.* **1988**, *36*, 1942.
(22) Takahashi, C.; Minoura, K.; Yamada, T.; Numata, A.; Kushida, K.; Shingu, T.; Hagishita, S.; Nakai, H.; Sato, T.; Harada, H. *Tetrahedron* **1995**, *51*, 3483.
(23) Fujimoto, H.; Sumino, M.; Okuyama, E.; Ishibashi, M. *J. Nat. Prod.* **2004**, *67*, 98.
(24) Li, L.; Li, D.; Luan, Y.; Gu, Q.; Zhu, T. *J.Nat. Prod.* **2012**, *75*, 920.
(25) Makarieva, T. N.; Stonik, V. A.; Dmitrenok, A. S.; Grebnev, B. B.; Isakov, V. V.; Rebachyk, N. M.; Rashkes, Y. W. *J.nat. prod.***1995**, *58*, 254.
(26) Litaudon, M.; Guyot, M. *Tetrahedron. Lett.***1991**, *32*, 911.
(27) Liu, H.; Fujiwara, T.; Nishikawa, T.; Mishima, Y.; Nagai, H.; Shida, T.; Tachibana, K.; Kobayashi, H.; Mangindaan, R. E. P.; Namikoshi, M. *Tetrahedron* **2005**, *61*, 8611.
(28) Morita, K.; Kobayashi, S. *Tetrahedron Lett.* **1966**, *7*, 573.

(29) Morita, K.; Kobayashi, S. *Chem. Pharm. Bull.* **1967**, *15*, 988.
(30) Chen, C. C.; Ho, C. T. *J. Agri. Food Chem.***1986**, *34*, 830.
(31) Pluth, M. D.; Bailey, T. S.; Hammers, M. D.; Hartle, M. D.; Henthorn, H. A.; Steiger, A. K. *Synlett* **2015**, *26*, 2633.
(32) Miyazawa, M.; Osman, F. *Nat. prod. lett.***2001**, *15*, 171.
(33) Rezanka, T.; Dembitsky, Valery M. *Euro. J.Org. Chem.***2002**, *2002*, 2400.
(34) Hausen, B. M.; Wolf, C. *Ameri. J. Cont. Derm.***1996**, *7*, 41.
(35) Anthoni, U. *Phytochem.* **1980**, *19*, 1228.
(36) Copp, B. R.; Blunt, J. W.; Munro, M. H.; Pannell, L. K. *Tetrahedron Lett.***1989**, *30*, 3703.
(37) Pearce, A. N.; Babcock, R. C.; Battershill, C. N.; Lambert, G.; Copp, B. R. *J.org. chem.* **2001**, *66*, 8257.
(38) Hausen, B. M.; Wolf, C. *Amer. J. Contact Derm.***1996**, *7*, 41.
(39) Ichimaru, M.; Kato, A.; Hashimoto, Y. *J.nat. prod.***2000**, *63*, 1675.
(40) Konishi, M.; Ohkuma, H.; Saitoh, K.-I.; Kawaguchi, H.; Golik, J.; Dubay, G.; Groenewold, G.; Krishnan, B.; Doyle, T. W. *J.anti.* **1985**, *38*, 1605.
(41) Lam, K. S.; Veitch, J. A.; Golik, J.; Krishnan, B.; Klohr, S. E.; Volk, K. J.; Forenza, S.; Doyle, T. W. *J. Am. Chem. Soc.***1993**, *115*, 12340.
(42) Golik, J.; Dubay, G.; Groenewold, G.; Kawaguchi, H.; Konishi, M.; Krishnan, B.; Ohkuma, H.; Saitoh, K.; Doyle, T. W. *J.Am.Chem. Soc.* **1987**, *109*, 3462.
(43) Lee, M. D.; Dunne, T. S.; Siegel, M. M.; Chang, C. C.; Morton, G. O.; Borders, D. B. *J. Am. Chem. Soc.* **1987**, *109*, 3464.
(44) Nicolaou, K. C.; Clark, D. *Angew. Chem. Int. Ed. Engl.* **1992,** *31*, 855.
(45) Nicolaou, K. C.; Hummel, C. W.; Nakada, M.; Shibayama, K.; Pitsinos, E. N.; Saimoto, H.; Mizuno, Y.; Baldenius, K. U.; Smith, A. L. *J. Am. Chem. Soc.* **1993**, *115*, 7625.
(46) Lee, M. D.; Ellestad, G. A.; Borders, D. B. *Acc.Chem.Res.* **1991**, *24*, 235.
(47) McDonald, L. A.; Capson, T. L.; Krishnamurthy, G.; Ding, W.-D.; Ellestad, G. A.; Bernan, V. S.; Maiese, W. M.; Lassota, P.; Kramer, R. A.; Ireland, C. M. *J. Am. Chem. Soc.* **1996**, *118*, 10898.
(48) Oku, N.; Matsunaga, S.; Fusetani, N. *J.Am.Chem. Soc.* **2003**, *125*, 2044.
(49) Nicolaou, K. C.; Li, R.; Lu, Z.; Pitsinos, E. N.; Alemany, L. B. *J. Am. Chem. Soc***. 2018**, *140*, 8091.
(50) Nicolaou, K. C.; Lu, Z.; Li, R.; Woods, J. R.; Sohn, T.-i. *J. Am. Chem. Soc.* **2015**, *137*, 8716.
(51) Nicolaou, K. C.; Li, R.; Lu, Z.; Pitsinos, E. N.; Alemany, L. B.; Aujay, M.; Lee, C.; Sandoval, J.; Gavrilyuk, J. *J. Am. Chem. Soc.* **2018**, *140*, 12120.
(52) Cao, M.; Yang, D.; Adhikari, A.; Ye, F.; Zheng, C.; Yan, W.; Meng, S.; Su, P.; Shen, B. *Org. Lett.* **2023**, *25*, 961.
(53) Boelens, M.; De Valois, P. J.; Wobben, H. J.; Van der Gen, A. *J. Agri. Food Chem.* **1971**, *19*, 984.
(54) Knudsen, J. T.; Tolllsten, L. *Bot.J.Linn. Soc.***2008**, *119*, 45.
(55) Rajanikanth, B.; Ravindranath, B.; Shankaranarayana, M. L. *Phytochem.* **1984**, *23*, 899.
(56) Kouokam, J. C.; Jahns, T.; Becker, H. *Planta Med* **2002**, *68*, 1082.
(57) Pino, J. A.; Quijano-Celí s, C. E.; Fuentes, V. *J. Essent. Oil Bear. Plants.* **2008,** *11*, 203.
(58) von Szczepanski, C.; Zgorzelak, P.; Hoyer, G. A. *Arzneimittelforschung* **1972**, *22*, 1975.
(59) De Sousa, J. R.; Demuner, A. J.; Pinheiro, J. A.; Breitmaier, E.; Cassels, B. K. *Phytochemistry* **1990**, *29*, 3653.
(60) Benavides, P.; Young, M.; Giesbrecht, A. *L. Phytochemistry Rev.* **2001**, *57*, 743.

(61) Silva, J.; do Nascimento, S.; Okabe, D.; Pinto, A.; de Oliveira, F.; da Paixa o, T.; Siqueira, M.; Baetas, A.; de Andrade, M. *Pharmacognosy Rev.* **2018**, *12*.
(62) Kohama, Y.; Iida, K.; Semba, T.; Mimura, T.; Inada, A.; Tanaka, K.; Nakanishi, T. *Chem. pharm. bull.***1992**, *40*, 2210.
(63) Park, Y.; Liu, Y.; Hong, J.; Lee, C.-O.; Cho, H.; Kim, D.-K.; Im, K. S.; Jung, J. H. *J.nat. prod.* **2003**, *66*, 1495.
(64) Benevides, P. J.; Young, M. C.; Giesbrecht, A. M.; Roque, N. F.; Bolzani, V. S. *Phytochemistry* **2001**, *57*, 743.
(65) De Xifra, E. W.; Sandy, J.; Davies, R.; Neuberger, A.; Moore, M. *Philos. Trans. R. Soc. Lond. Ser. B* **1976**, *273*, 79.
(66) Ali, D.; Amer, Y.; Petersen, W. F.; Kaschula, C. H.; Hunter, R. *SynOpen* **2021**, *05*, 49.
(67) Clennan, E. L.; Stensaas, K. L. *Org. Prep. Proced. Int.* **1998,** *30*, 551**.**
(68) Steudel, R. *Chem. Rev.* **2002**, *102*, 3905.
(69) Switzer, C. H.; Guttzeit, S.; Eykyn, T. R.; Eaton, P. *Redox Biol.* **2021**, *47*, 102155.
(70) Cerda, M. M.; Hammers, M. D.; Earp, M. S.; Zakharov, L. N.; Pluth, M. D. *Org. Lett.* **2017**, *19*, 2314.
(71) Khongorzul, P.; Ling, C. J.; Khan, F. U.; Ihsan, A. U.; Zhang, J. Mol. Cancer Res: *MCR .***2020***, 18, 3.*
(72) Wang, D.-Y.; Guo, W.; Fu, Y. *Acc. Chem. Res.* **2019**, 52, 2290.
(73) Strecker, W. *Ber. Dtsch. Chem. Ges.* **1908,** *41*, 1105.
(74) Fuson, R. C.; Price, C. C.; Burness, D. M.; Foster, R. E.; Hatchard, W. R.; Lipscomb, R. D. *J. Org. Chem.* **1946,** *11*, 487.
(75) Feher, F.; Krause, G.; Vogelbruch, K. *Chem. Ber.* **1957**, *90*, 1570.
(76) Labuk, P.; Duda, A.; Penczek, S. *Phosphorus, Sulfur, Silicon Relat. Elem.* **1989,** *42*, 107.
(77) Baker, A.; Graz, M.; Saunders, R.; Evans, G. J. S.; Kaul, S.; Wirth, T. *J. Flow Chem. .***2013**, *3*, 118.
(78) Riding, R. W.; Thomas, J. S. *J. Chem. Soc. Trans.* **1923**, *123*, 3271.
(79) Dannley, R. L.; Zazaris, D. A. *Can. J. Chem.* **1965**, *43*, 2610.
(80) Fuson, R. C.; Burness, D. M.; Foster, R. E.; Lipscomb, R. D. *J. Org. Chem.* **1946**, *11*, 499.
(81) Salivon, N.; Filinchuk, Y.; Olijnyk, V. Z. Anorg. Allg. Chem. **2006,** *632*, 1610.
(82) Bogdándi, V.; Ida, T.; Sutton, T. R.; Bianco, C.; Ditrói, T.; Koster, G.; Henthorn, H. A.; Minnion, M.; Toscano, J. P.; van der Vliet, A.; Pluth, M. D.; Feelisch, M.; Fukuto, J. M.; Akaike, T.; Nagy, P. *Brit. J. of Pharm.* **2019**, *176*, 646.
(83) Deryagina, E.; Kozlov, I.; Vershal, V.; Babkin, V. *Russ. J. Gen. Chem.* **1996,** *66*, 1240.
(84) Sinha, P.; Kundu, A.; Roy, S.; Prabhakar, S.; Vairamani, M.; Sankar, A. R.; Kunwar, A. *Organometallics.* **2001**, *20*, 157.
(85) Steudel, R. *Chem. Rev.* **2002**, *102*, 3905.
(86) Milligan, B.; Saville, B.; Swan, J. M. *J. Chem. Soc* .**1961**, 4850.
(87) Milligan, B.; Saville, B.; Swan, J. M. *J. Chem. Soc* .**1963**, 3608.
(88) Pitombo, L. R. M. *Chem. Ber.* **1962**, *95*, 2960**.**
(89) Buckman, J. D.; Field, L. *J. Org. Chem.* **1967**, *32*, 454.
(90) Bowman, G. T.; Field, L. *J. Org. Chem.* **1982**, *47*, 222.
(91) Chandra, R.; Field, L. *J. Org. Chem.***1986**, *51*, 1844.
(92) Capozzi, G.; Capperucci, A.; Degl'Innocenti, A.; Del Duce, R.; Menichetti, S. *Tetrahedron Lett.* **1989**, *30*, 2991.

(93) Bhattacherjee, D.; Sufian, A.; Mahato, S. K.; Begum, S.; Banerjee, K.; De, S.; Srivastava, H. K.; Bhabak, K. P. *Chem. Commun.* **2019**, *55*, 13534.
(94) Viglianisi, C.; Bonardi, C.; Ermini, E.; Capperucci, A.; Menichetti, S.; Tanini, D. *Synthesis* **2019**, *51*, 1819.
(95) Schorlemmer, C. *J. Chem. Soc.* **1869,** *22*, 254.
(96) Qiao, Z.; Jiang, X. *Org. Biomol. Chem..***2017,** 15, 1942.
(97) Milligan, B.; Swan, J. *J. Chem. Soc.* **1965,** 2901.
(98) Liang, S.; Ma, L.; Guo, Z.; Liu, F.; Lin, Z.; Yi, W. *Angew. Chem. Int. Ed.* **2024**, *63*, e202404139.
(99) Bloch, I.; Bergmann, M. *Ber. Dtsch. Chem. Ges. (A and B Series).* **1920**, 53, 961.
(100) Twiss, D. *J. Am. Chem. Soc.* **1927,** 49, 491.
(101) Feher, F.; Weber, H. *Chem. Ber.* **1958,** 91, 642.
(102) Wardell, J. L.; Clarke, P. L. *J. Organomet. Chem.* **1971**, *26*, 345.
(103) Mott, A. W.; Barany, G. *J. Chem. Soc., Perkin Trans.* **1984,** 2615.
(104) Knoth, W.; Gattow, G. *Z. Anorg. Allg. Chem.* **1987,** *552*, 181.
(105) Munavalli, S.; Muller, A. J.; Rossman, D. I.; Rohrbaugh, D. K.; Ferguson, C. P. *J. Fluorine Chem.***1994,** *67*, 37.
(106) Derbesy, G.; Harpp, D. N. *Tetrahedron Lett.* **1994**, *35*, 5381.
(107) Zysman-Colman, E.; Harpp, D. N. *J. Org. Chem.* **2003**, *68*, 2487.
(108) Clayton, J.; Etzler, D. *J. Am. Chem. Soc.* **1947,** *69*, 974.
(109) Nakabayashi, T.; Tsurugi, J.; Yabuta, T. *J. Org. Chem*. 1964, *29*, 1236.
(110) Kresze, G.; Patzschke, H.-P. *Chem. Ber.* **1960**, *93*, 380.
(111) Vineyard, B. D. *J. Org. Chem.* 1966, *31*, 601.
(112) Vineyard, B. D. *J. Org. Chem.***1967,** *32*, 3833.
(113) Harpp, D. N.; Steliou, K.; Chan, T. H. *J. Am. Chem. Soc.* **1978,** *100*, 1222.
(114) Banerji, A.; Kalena, G. P. *Tetrahedron Lett.***1980**, *21*, 3003.
(115) Mott, A. W.; Barany, G. *Synthesis (Stuttgart)* **1984**, 657.
(116) Barany, G.; Mott, A. W. *J. Org. Chem*.**1984**, *49*, 1043.
(117) An, H.; Zhu, J.; Wang, X.; Xu, X. *Bioorg. Med. Chem. Lett.* **2006**, *16*, 4826.
(118) An, H.; Mo, X.; Google Patents: 2010.
(119) Nicolaou, K.; Li, R.; Lu, Z.; Pitsinos, E. N.; Alemany, L. B.; Aujay, M.; Lee, C.; Sandoval, J.; Gavrilyuk, J. *J. Am. Chem. Soc.* **2018**, *140*, 12120.
(120) Bohme, H.; Zinner, G. *Justus Liebigs Ann. Chem.***1954**, *585*, 142.
(121) Bohme, H.; Ham, G. V. *Justus Liebigs Ann. Chem.***1958,** *617*, 62.
(122) Bohme, H.; Clement, M. *Justus Liebigs Ann. Chem.***1952**, *576*, 61.
(123) Williams, C. R.; Britten, J. F.; Harpp, D. N. *J. Org. Chem.***1994,** *59*, 806.
(124) Abu-Yousef, I. A.; Rys, A. Z.; Harpp, D. N. *J. Sulfur Chem.* **2006,** *27*, 15.
(125) Williams, C. R.; Britten, J. F.; Harpp, D. N. *J. Org. Chem.***1994,** *59*, 806.
(126) Feher, F.; Kruse, W. *Chem. Ber.* **1958**, *91*, 2528.
(127) Nakabayashi, T.; Tsurugi, J. *J. Org. Chem*. **1961**, 26, 2482.
(128) Harpp, D.; Ash, D. *Int J Sul Chem.* **1971**, *1*, 211.
(129) Rys, A. Z.; Harpp, D. N. *Tetrahedron Lett.* **2000**, *41*, 7169.
(130) Hou, Y.; Abu-Yousef, I. A.; Harpp, D. N. *Tetrahedron Lett.* **2000**, *41*, 7809.
(131) Hou, Y.; Abu-Yousef, I. A.; Doung, Y.; Harpp, D. N. *Tetrahedron Lett.* **2001**, *42*, 8607.
(132) Abu-Yousef, I. A.; Rys, A. Z.; Harpp, D. N. *J. Sulfur Chem.* **2007**, *28*, 251.
(133) Kim, J.; Movassaghi, M. *J. Am. Chem. Soc.* **2010**, *132*, 14376.

(134) Lach, S.; Sliwka-Kaszynska, M.; Witt, D. *Synlett.* **2010**, *210*, 2857.
(135) Wang, W.; Lin, Y.; Ma, Y.; Tung, C.-H.; Xu, Z. *Organic Lett.* **2018**, *20*, 3829.
(136) Xue, J.; Jiang, X. *Nature Commun.* **2020**, *11*, 4170.
(137) Xue, J.; Jiang, X. *Organic Lett.* **2020**, *22*, 8044.
(138) Harpp, D. N.; Friedlander, B. T.; Larsen, C.; Steliou, K.; Stockton, A. *J. Org. Chem.* **1978**, *43*, 3481.
(139) Lach, S.; Witt, D. *Synlett* **2013**, *24*, 1927.
(140) Harpp, D. N.; Ash, D. K.; Smith, R. A. *J. Org. Chem.***1979**, *44*, 4135.
(141) Xiao, X.; Feng, M.; Jiang, X. *Angew. Chem. Int. Ed.* **2016**, *55*, 14121.
(142) Kagami, H.; Motoki, S. *J. Org. Chem.***1977,** *42*, 4139**.**
(143) Harpp, D. N.; Ash, D. K.; Back, T. G.; Gleason, J. G.; Orwig, B. A.; VanHorn, W. F.; Snyder, J. P. *Tetrahedron Lett.***1970**, *11*, 3551.
(144) Gaensslen, M.; Minkwitz, R.; Molzbeck, W.; Oberhammer, H. *Inorg. Chem.* **1992,** *31*, 4147.
(145) Xu, S.; Wang, Y.; Radford, M. N.; Ferrell, A. J.; Xian, M. *Organic Lett.***2018**, *20*, 465.
(146) Ali, D.; Hunter, R.; Kaschula, C. H.; De Doncker, S.; Rees-Jones, S. C. M. *J. Org. Chem.* **2019**, *84*, 2862.
(147) Kang, J.; Ferrell, A. J.; Chen, W.; Wang, D.; Xian, M. *Organic lett.* **2018**, *20*, 852.
(148) Tsurugi, J.; Kawamura, S.; Horii, T. *J. Org. Chem.***1971**, *36*, 3677.
(149) Kharasch, N.; Potempa, S. J.; Wehrmeister, H. L. *Chemical Rev.***1946**, *39*, 269.
(150) Lach, S.; Witt, D. *Heteroatom Chem.* **2014**, *25*, 10.
(151) Harpp, D. N.; Granata, A. *Tetrahedron Lett.* **1976**, *17*, 3001.
(152) Bailey, T. S.; Zakharov, L. N.; Pluth, M. D. *J. Am. Chem. Soc.* **2014**, *136*, 10573.
(153) Bolton, S. G.; Cerda, M. M.; Gilbert, A. K.; Pluth, M. D. *Free Radic. Biol. Med.* **2019**, *131*, 393.
(154) Topçul, M.; Çetin, I . **2015**, p 1.
(155) Guan, X. *Acta Pharm. Sin. B.* **2015,** 5**.**
(156) Patel, A. *JAMA Oncology.* **2020**, *6*, 1488.
(157) Sung, H.; Ferlay, J.; Siegel, R. L.; Laversanne, M.; Soerjomataram, I.; Jemal, A.; Bray, F. *CA Cancer J. Clin.* **2021**, *71*, 209.
(158) World Health, A.; World Health Organization: Geneva, **2017**.
(159) Wang, H.-C.; Hsieh, S.-C.; Yang, J.-H.; Lin, S.-Y.; Sheen, L.-Y. *Nutr. Cancer.* **2012**, *64*, 770.
(160) Kumar, V.; Abbas, A. K.; Aster, J. C.; Robbins, S. L. *Robbins basic pathology*; 9th ed. ed.; Elsevier/Saunders: Philadelphia, PA, **2013**.
(161) Kontomanolis, E. N.; Koutras, A.; Syllaios, A.; Schizas, D.; Mastoraki, A.; Garmpis, N.; Diakosavvas, M.; Angelou, K.; Tsatsaris, G.; Pagkalos, A.; Ntounis, T.; Fasoulakis, Z. *Anticancer Res.* **2020**, *40*, 6009.
(162) Pitot, H. C. *Jpn. J. Cancer Res: Gann* **1989**, *80*, 599.
(163) W Troll, a.; Wiesner, R. *Annu. Rev. Pharmacol. Toxicol.***1985**, *25*, 509.
(164) Pitot, H. C. *Cancer* **1993**, *72*, 962.
(165) Hanahan, D.; Weinberg, R. A. *Cell.* **2000**, *100*, 57.
(166) Hanahan, D.; Weinberg, R. A. *Cell.* **2011**, *144*, 646.
(167) Hanahan, D. *Cancer Discov.* **2022**, *12*, 31.
(168) Jones, R. G.; Thompson, C. B. *Genes Dev* **2009**, *23*, 537.
(169) Nicastro, H. L.; Ross, S. A.; Milner, J. A. *Cancer Prev Res (Phila)* **2015**, *8*, 181.

(170) Semenza, G. L. *Nat. Rev. Cancer.* **2003,** *3*, 721.
(171) Yilmaz, M.; Christofori, G.; Lehembre, F. *Trends Mol Med.* **2007**, *13*, 535.
(172) Gkretsi, V.; Stylianopoulos, T. *Front Oncol* **2018**, *8*, 145.
(173) Nicholson, L. B. *Essays Biochem.* **2016**, *60*, 275.
(174) Janssen, L. M. E.; Ramsay, E. E.; Logsdon, C. D.; Overwijk, W. W. *J Immunother. Cancer* **2017**, *5*, 79.
(175) Annema, N.; Heyworth, J. S.; McNaughton, S. A.; Iacopetta, B.; Fritschi, L. *J. Am. Diet. Assoc.* **2011**, *111*, 1479.
(176) Blasco, M. A. *Nat Rev Genet* **2005**, *6*, 611.
(177) Chakravarti, D.; LaBella, K. A.; DePinho, R. A. *Cell* **2021**, *184*, 306.
(178) Yuan, S.; Norgard, R. J.; Stanger, B. Z. *Cancer discovery* **2019**, *9*, 837.
(179) Amin, A. R.; Kucuk, O.; Khuri, F. R.; Shin, D. M. *J. Clin. Oncol.* **2009**, *27*, 2712.
(180) Zhang, Y.; Liu, X.; Ruan, J.; Zhuang, X.; Zhang, X.; Li, Z. *Biomed Pharmacother* **2020**, *123*, 109730.
(181) Rana, S. V.; Pal, R.; Vaiphei, K.; Sharma, S. K.; Ola, R. P. *Nutr. Res. Rev.* **2011**, *24*, 60.
(182) Bayan, L.; Koulivand, P. H.; Gorji, A. *Avicenna J. Phytomed.* **2014**, *4*, 1.
(183) Katare, C.; Sonali, S. *Int. J. Pharm. Bio. Sci.* **2014**, *5*, 112.
(184) Arijit, M.; Sabyasachi, B.; Sankhadip, B.; Sujayita, M.; Rebecca, A. H.; Mohammad Hosein, F.; Anupam, B.; Anupam, B. *Pharmacol. Res.* **2021.**
(185) Rivlin, R. S. *J. Nutr.* **2001,** *131*, 951S.
(186) El-Bayoumy, K.; Sinha, R.; Pinto, J. T.; Rivlin, R. S. *J. Nutr.* **2006**, *136*, 864S.
(187) Weisberger, A. S.; Pensky, J. *Cancer. Res.* **1958**, *18*, 1301.
(188) Weisberger, A. S.; Pensky, J. *Cancer. Res.* **1958**, *18*, 1301.
(189) You, W.-C.; Blot, W. J.; Chang, Y.-S.; Ershow, A.; Yang, Z. T.; An, Q.; Henderson, B. E.; Fraumeni, J. F., Jr; Wang, T.-G. *JNCI:* J. Natl. Cancer Inst. **1989**, *81*, 162.
(190) Buiatti, E.; Palli, D.; Decarli, A.; Amadori, D.; Avellini, C.; Bianchi, S.; Biserni, R.; Cipriani, F.; Cocco, P.; Giacosa, A.; Marubini, E.; Puntoni, R.; Vindigni, C.; Fraumeni Jr., J.; Blot, W. *Int. J. Cancer.* **1989**, *44*, 611.
(191) Iscovich, J. M.; L'Abbe , K. A.; Castelleto, R.; Calzona, A.; Bernedo, A.; Chopita, N. A.; Jmelnitzsky, A. C.; Kaldor, J. *Int. J. Cancer.* **1992**, *51*, 851.
(192) Hansson, L. E.; Nyre n, O.; Bergstro m, R.; Wolk, A.; Lindgren, A.; Baron, J.; Adami, H. O. *Int. J. Cancer.* **1993**, *55*, 181.
(193) Steinmetz, K. A.; Kushi, L. H.; Bostick, R. M.; Folsom, A. R.; Potter, J. D. *Am J Epidemiol* **1994**, *139*, 1.
(194) Witte, J. S.; Longnecker, M. P.; Bird, C. L.; Lee, E. R.; Frankl, H. D.; Haile, R. W. *Am J Epidemiol* **1996**, *144*, 1015.
(195) Dorant, E.; van den Brandt, P. A.; Goldbohm, R. A.; Sturmans, F. *Gastroenterology* **1996**, *110*, 12.
(196) Franceschi, S.; Parpinel, M.; La Vecchia, C.; Favero, A.; Talamini, R.; Negri, E. *Epidemiology* **1998**, *9*, 338.
(197) Gao, C. M.; Takezaki, T.; Ding, J. H.; Li, M. S.; Tajima, K. *Jpn J Cancer Res* **1999**, *90*, 614.
(198) Levi, F.; Pasche, C.; La Vecchia, C.; Lucchini, F.; Franceschi, S. *Br J Cancer* **1999**, *79*, 1283.
(199) Fleischauer, A. T.; Poole, C.; Arab, L. *Am J. Clin. Nutr.* **2000**, *72*, 1047.
(200) Fleischauer, A. T.; Arab, L. *J. Nutr.* **2001**, *131*, 1032s.

(201) Takezaki, T.; Gao, C. M.; Wu, J. Z.; Ding, J. H.; Liu, Y. T.; Zhang, Y.; Li, S. P.; Su, P.; Liu, T. K.; Tajima, K. *Jpn J. Cancer. Res.* **2001**, *92*, 1157.
(202) Mun oz, N.; Plummer, M.; Vivas, J.; Moreno, V.; De Sanjose, S.; Lopez, G.; Oliver, W. *Int. J. Cancer.* **2001**, *93*, 417.
(203) De Stefani, E.; Correa, P.; Boffetta, P.; Ronco, A.; Brennan, P.; Deneo-Pellegrini, H.; Mendilaharsu, M. *Eur. J. Cancer. Prev.* **2001**, *10*, 357.
(204) Setiawan, V. W.; Yu, G. P.; Lu, Q. Y.; Lu, M. L.; Yu, S. Z.; Mu, L.; Zhang, J. G.; Kurtz, R. C.; Cai, L.; Hsieh, C. C.; Zhang, Z. F. *Asian. Pac. J. Cancer. Prev.* **2005**, *6*, 387.
(205) Galeone, C.; Pelucchi, C.; Levi, F.; Negri, E.; Franceschi, S.; Talamini, R.; Giacosa, A.; La Vecchia, C. *Am. J. Clin. Nutr.* **2006**, *84*, 1027.
(206) Ngo, S. N.; Williams, D. B.; Cobiac, L.; Head, R. J. *J Nutr* **2007**, *137*, 2264.
(207) Shukla, Y.; Kalra, N. *Cancer Lett.* **2007**, *247*, 167.
(208) Pourfarzi, F.; Whelan, A.; Kaldor, J.; Malekzadeh, R. *Int.J.Cancer.* **2009**, *125*, 1953. (207)
(209) Zhou, Y.; Zhuang, W.; Hu, W.; Liu, G. J.; Wu, T. X.; Wu, X. T. *Gastroenterology* **2011**, *141*, 80.
(210) Zhu, B.; Zou, L.; Qi, L.; Zhong, R.; Miao, X. *Clin. Gastroenterol. Hepatol.* **2014**, *12*, 1991.
(211) Turati, F.; Rossi, M.; Pelucchi, C.; Levi, F.; La Vecchia, C. *Br. J. Nutr.* **2015**, *113 Suppl 2*, S102.
(212) Wang, W.; Dong, Z.; Zhang, X.; Li, W.; Li, P.; Chen, X. *Iran J. Public Health.* **2018**, 47, 1327.
(213) Kim, H.; Keum, N.; Giovannucci, E. L.; Fuchs, C. S.; Bao, Y. *Int J Cancer* **2018**, *143*, 1047.
(214) Li, W.-Q.; Zhang, J.-Y.; Ma, J.-L.; Li, Z.-X.; Zhang, L.; Zhang, Y.; Guo, Y.; Zhou, T.; Li, J.-Y.; Shen, L.; Liu, W.-D.; Han, Z.-X.; Blot, W. J.; Gail, M. H.; Pan, K.-F.; You, W.-C. *BMJ (Clinical research ed.)* **2019**, *366*, l5016.
(215) Wu, X.; Shi, J.; Fang, W. X.; Guo, X. Y.; Zhang, L. Y.; Liu, Y. P.; Li, Z. *Asia. Pac. J. Clin. Oncol.* **2019**, *15*, e132.
(216) Yuan, P.; Lin, L.; Zheng, K.; Wang, W.; Wu, S.; Huang, L.; Wu, B.; Chen, T.; Li, X.; Cai, L. *B.M.J. Open.* **2020**, *10*, e042341.
(217) Wang, Y.; Huang, P.; Wu, Y.; Liu, D.; Ji, M.; Li, H.; Wang, Y.; Wang, Y.; Huang, P.; Wu, Y.; Liu, D.; Ji, M.; Li, H.; Wang, Y. *Oncol. Lett.* **2022**, *23*, 125.
(218) Pickering, C. *Chronological History of Plants* **1979**, *2*, 450.
(219) Bozin, B.; Mimica-Dukic, N.; Samojlik, I.; Goran, A.; Igic, R. *Food.Chem.* **2008**, *111*, 925.
(220) Agarwal, K. C. *Med. Res. Rev.* **1996**, *16*, 111.
(221) Matsuura, H.; Ushiroguchi, T.; Itakura, Y.; Hayashi, N.; Fuwa, T. *Chem. Pharm. Bull.***1988**, *36*, 3659.
(222) Amagase, H.; Petesch, B. L.; Matsuura, H.; Kasuga, S.; Itakura, Y. *J. Nutr.* **2001**, *131*, 955S.
(223) Amagase, H. *J. Nutr.* **2006**, *136*, 716S.
(224) Yee, M. M. *Am. Sci. Res. J. Eng. Technol. Sci.* **2019**, *54*, 30.
(225) Shang, A.; Cao, S.-Y.; Xu, X.-Y.; Gan, R.-Y.; Tang, G.-Y.; Corke, H.; Mavumengwana, V.; Li, H.-B. *Foods* **2019**, *8*, 246.
(226) De Greef, D.; Barton, E. M.; Sandberg, E. N.; Croley, C. R.; Pumarol, J.; Wong, T. L.; Das, N.; Bishayee, A. *Semin Cancer Biol* **2021**, *73*, 219.
(227) Fukushima, S.; Takada, N.; Hori, T.; Min, W.; Wanibuchi, H.; Yamamoto, S. *J. Nutr.* **2001**, *131*, 1049S.
(228) Trio, P. Z.; You, S.; He, X.; He, J.; Sakao, K.; Hou, D.-X. *Food Funct.* **2014**, *5*, 833.
(229) Block, E. *Sci. Am.***1985**, *252*, 114.

(230) Yingngam, B.; Navabhatra, A.; Brantner, A. H.; Keatkwanbud, N.; Krongyut, T.; Nakonrat, P.; Triet, N. T. *Sustain. Chem. Pharm.* **2022**, *27*, 100655.
(231) Farhat, Z.; Hershberger, P. A.; Freudenheim, J. L.; Mammen, M. J.; Hageman Blair, R.; Aga, D. S.; Mu, L. *Eur. J. Nutr.* **2021**, *60*, 3585.
(232) Ichikawa, M.; Ide, N.; Yoshida, J.; Yamaguchi, H.; Ono, K. *J. Agric. Food Chem.* **2006**, *54*, 1535.
(233) Butt, M. S.; Sultan, M. T.; Butt, M. S.; Iqbal, J. *Crit. Rev. Food Sci. Nutr.* **2009**, *49*, 538.
(234) Zhang, Y.; Liu, X.; Ruan, J.; Zhuang, X.; Zhang, X.; Li, Z. *Biomed. Pharmacother.* **2020**, *123*, 109730.
(235) Schafer, G.; H Kaschula, C. *Anti-Cancer Agents Med Chem.* ***2014****, 14, 233.*
(236) Stoll, A.; Seebeck, E. *Helv Chim Acta.* **1948**, *31*, 189.
(237) Block, E.; Ahmad, S.; Catalfamo, J. L.; Jain, M. K.; Apitz-Castro, R. *J. Am. Chem. Soc.***1986,** *108*, 7045.
(238) Block, E.; Dethier, B.; Bechand, B.; Cotelesage, J. J. H.; George, G. N.; Goto, K.; Pickering, I. J.; Mendoza Rengifo, E.; Sheridan, R.; Sneeden, E. Y.; Vogt, L. *J. Agric. Food. Chem.* **2018**, 66, 10193.
(239) Munchberg, U.; Anwar, A.; Mecklenburg, S.; Jacob, C. *Org. Biomol. Chem.***2007**, *5*, 1505.
(240) Yagdi, E.; Cerella, C.; Dicato, M.; Diederich, M. *Food.Chem. Toxicol.***2016**, *95*, 219.
(241) Brodnitz, M. H.; Pascale, J. V.; Van Derslice, L. *J. Agric. Food. Chem.***1971**, *19*, 273.
(242) O'Gara, E. A.; Hill, D. J.; Maslin, D. J. *J. Appl. Environ. Microbiol.* **2000**, *66*, 2269.
(243) Wong, W. W.; Macdonald, S.; Langler, R. F.; Penn, L. Z. *Anticancer.Res.***2000**, *20*, 1367.
(244) Pinto, J. T.; Qiao, C.; Xing, J.; Rivlin, R. S.; Protomastro, M. L.; Weissler, M. L.; Tao, Y.; Thaler, H.; Heston, W. D. *Am. J. Clin. Nutr.* **1997**, *66*, 398.
(245) Munday, R.; Munday, J. S.; Munday, C. M. *Free. Radic. Biol. Med.* **2003**, *34*, 1200.
(246) Cerella, C.; Scherer, C.; Cristofanon, S.; Henry, E.; Anwar, A.; Busch, C.; Montenarh, M.; Dicato, M.; Jacob, C.; Diederich, M. *Apoptosis: an international journal on programmed cell death*. **2009**, *14*, 641.
(247) Ansary, J.; Forbes-Hernandez, T. Y.; Gil, E.; Cianciosi, D.; Zhang, J.; Elexpuru-Zabaleta, M.; Simal-Gandara, J.; Giampieri, F.; Battino, M. *Antioxidants (Basel, Switzerland)* **2020**, *9*, 619.
(248) Milner, J. A. *J. Nutr.* **2006**, *136*, 827S.
(249) Lawson, L. D.; Gardner, C. D. *J. Agric. Food. Chem.* **2005**, *53*, 6254.
(250) Lawson, L. D.; Ransom, D. K.; Hughes, B. G. *Thromb. Res.* **1992**, *65*, 141.
(251) Freeman, F.; Kodera, Y. *J. Agric. Food. Chem.***1995**, 43, 2332.
(252) Lawson, L. D.; Hunsaker, S. M. *Nutrients.***2018**, *10*, 812.
(253) Nagae, S.; Ushijima, M.; Hatono, S.; Imai, J.; Kasuga, S.; Matsuura, H.; Itakura, Y.; Higashi, Y. *Planta. Med.* **1994**, *60*, 214.
(254) Germain, E.; Auger, J.; Ginies, C.; Siess, M. H.; Teyssier, C. *Xenobiotica* **2002**, *32*, 1127.
(255) Gao, C.; Jiang, X.; Wang, H.; Zhao, Z.; Wang, W. *J. Drug. Metab.Toxicol.* **2013**, *4*, 1.
(256) Lawson, L. D.; Wang, Z. J. *Planta. Medica.* **1993**, *59*.
(257) Cerella, C.; Dicato, M.; Jacob, C.; Diederich, M. *Anti-Cancer. Agents. Med. Chem.* **2011**, *11*, 267.
(258) Tong, D.; Qu, H.; Meng, X.; Jiang, Y.; Liu, D.; Ye, S.; Chen, H.; Jin, Y.; Fu, S.; Geng, J. *Oncol.Rep.* **2014**, *32*, 1124.
(259) Yin, X.; Zhang, R.; Feng, C.; Zhang, J.; Liu, D.; Xu, K.; Wang, X.; Zhang, S.; Li, Z.; Liu, X.; Ma, H. *Onco.l Rep.* **2014**, *32*, 1748.

(260) Yin, X.; Zhang, J.; Li, X.; Liu, D.; Feng, C.; Liang, R.; Zhuang, K.; Cai, C.; Xue, X.; Jing, F.; Wang, X.; Wang, J.; Liu, X.; Ma, H. Int. J. Mol. Sci. **2014**, *15*, 12422.
(261) Xiao, D.; Zeng, Y.; Singh, S. V. *Mol. Carcinog.* **2009**, *48*, 1018.
(262) Parker, A. L.; Kavallaris, M.; McCarroll, J. A. *Front Oncol* **2014**, *4*, 153.
(263) Kelkel, M.; Cerella, C.; Mack, F.; Schneider, T.; Jacob, C.; Schumacher, M.; Dicato, M.; Diederich, M. *Carcinogenesis* **2012**, *33*, 2162.
(264) Hosono, T.; Fukao, T.; Ogihara, J.; Ito, Y.; Shiba, H.; Seki, T.; Ariga, T. *J. Biol. Chem.* **2005**, *280*, 41487.
(265) Cerella, C.; Scherer, C.; Cristofanon, S.; Henry, E.; Anwar, A.; Busch, C.; Montenarh, M.; Dicato, M.; Jacob, C.; Diederich, M. *Apoptosis* **2009**, *14*, 641.
(266) Wang, Y.-B.; Qin, J.; Zheng, X.-Y.; Bai, Y.; Yang, K.; Xie, L.-P. *Phytomedicine* **2010**, *17*, 363.
(267) Shin, D. Y.; Kim, G.-Y.; Lee, J. H.; Choi, B. T.; Yoo, Y. H.; Choi, Y. H. *Int. J. Mol. Sci.* **2012**, *13*, 14158.
(268) Xu, L.; Yu, J.; Zhai, D.; Zhang, D.; Shen, W.; Bai, L.; Cai, Z.; Yu, C. *Evid.Based Complement. Alternat. Med.* **2014**, *20*, 378684.
(269) Zhang, Y.; Li, H. Y.; Zhang, Z. H.; Bian, H. L.; Lin, G. *Oncol Lett.* **2014**, *8*, 2591.
(270) Shin, D. Y.; Kim, G.-Y.; Hwang, H. J.; Kim, W.-J.; Choi, Y. H. *Environ. Toxicol. Pharmacol.* **2014**, *37*, 74.
(271) Wang, Y.; Sun, Z.; Chen, S.; Jiao, Y.; Bai, C. *Tumor Biol.* **2016**, *37*, 3727.
(272) Kaschula, C. H.; Hunter, R.; Cotton, J.; Tuveri, R.; Ngarande, E.; Dzobo, K.; Scha fer, G.; Siyo, V.; Lang, D.; Kusza, D. A.; Davies, B.; Katz, A. A.; Parker, M. I. *Mol. Carcino.* **2016**, *55*, 1213.
(273) Puccinelli, M. T.; Stan, S. D. *Int. J. Mol. Sci.* **2017**, *18*.
(274) Elango, E. M.; Asita, H.; Nidhi, G.; Seema, P.; Banerji, A.; Kuriakose, M. A. *J. Appl. Genet.* **2004**, *45*, 469.
(275) Tao, Q.; Wu, C.; Xu, R.; Niu, L.; Qin, J.; Liu, N.; Zhang, P.; Wang, C. *Cell Tissue Res.* **2017**, *370*, 379.
(276) Li, Y.; Zhang, J.; Zhang, L.; Si, M.; Yin, H.; Li, J. *Carcino.* **2013**, *34*, 1601.
(277) Lai, K. C.; Hsu, S. C.; Kuo, C. L.; Yang, J. S.; Ma, C. Y.; Lu, H. F.; Tang, N. Y.; Hsia, T. C.; Ho, H. C.; Chung, J. G. *Environ. Toxicol.* **2013**, *28*, 479.
(278) Lai, K. C.; Hsu, S. C.; Yang, J. S.; Yu, C. C.; Lein, J. C.; Chung, J. G. *J.Cell. Mol. Med.* **2015**, *19*, 474.
(279) Nabekura, T.; Kamiyama, S.; Kitagawa, S. *Biochem. Biophys. Res. Commun.* **2005, 327, 866.**
(280) Xia, Q.; Wang, Z.-Y.; Li, H.-Q.; Diao, Y.-T.; Li, X.-L.; Cui, J.; Chen, X.-L.; Li, H. *Evid. Based Complement. Alternat. Med.* **2012**, 719805.
(281) Wang, Z.; Xia, Q.; Cui, J.; Diao, Y.; Li, J. *Oncol. Rep.* **2014**, *31*, 2720.
(282) Pan, Y.; Lin, S.; Xing, R.; Zhu, M.; Lin, B.; Cui, J.; Li, W.; Gao, J.; Shen, L.; Zhao, Y.; Guo, M.; Wang, J. M.; Huang, J.; Lu, Y. *Antioxid. Redox. Signal.* **2016**, *24*, 839.
(283) Wu, C. C.; Sheen, L. Y.; Chen, H. W.; Kuo, W. W.; Tsai, S. J.; Lii, C. K. *J Agric. Food Chem.* **2002**, *50*, 378.
(284) Fukao, T.; Hosono, T.; Misawa, S.; Seki, T.; Ariga, T. *Food.Chem. Toxicol.* **2004**, *42*, 743.
(285) Tsai, C.-W.; Chen, H.-W.; Yang, J.-J.; Sheen, L.-Y.; Lii, C.-K. *J. Agric. Food. Chem.* **2007**, *55*, 1019.
(286) Tsai, C.-W.; Yang, J.-J.; Chen, H.-W.; Sheen, L.-Y.; Lii, C.-K. *J. Nutr.* **2005**, *135*, 2560.

(287) Hosono, T.; Fukao, T.; Ogihara, J.; Ito, Y.; Shiba, H.; Seki, T.; Ariga, T. *J. Biol. Chem.* **2005**, *280*, 41487.
(288) Sakamoto, K.; Lawson, L. D.; Milner, J. A. *Nutr. Cancer.* **1997**, *29*, 152.
(289) Li, W.; Tian, H.; Li, L.; Li, S.; Yue, W.; Chen, Z.; Qi, L.; Hu, W.; Zhu, Y.; Hao, B.; Gao, C.; Si, L.; Gao, F. *Acta. Biochim. Biophys. Sin. (Shanghai)* **2012**, *44*, 577.
(290) Xiao, D.; Choi, S.; Johnson, D. E.; Vogel, V. G.; Johnson, C. S.; Trump, D. L.; Lee, Y. J.; Singh, S. V. *Oncogene* **2004**, *23*, 5594.
(291) Xiao, D.; Singh, S. V. *Carcinogenesis.***2005**, *27*, 533.
(292) Kim, Y.-A.; Xiao, D.; Xiao, H.; Powolny, A. A.; Lew, K. L.; Reilly, M. L.; Zeng, Y.; Wang, Z.; Singh, S. V. *Molecular Cancer Therapeutics* **2007**, *6*, 1599.
(293) Shankar, S.; Chen, Q.; Ganapathy, S.; Singh, K. P.; Srivastava, R. K. *Mol. Cancer Ther.* **2008**, *7*, 2328.
(294) Li, N.; Guo, R.; Li, W.; Shao, J.; Li, S.; Zhao, K.; Chen, X.; Xu, N.; Liu, S.; Lu, Y. *Carcinogenesis*. **2005**, *27*, 1222.
(295) Wang, Z.; Xia, Q.; Cui, J.; Diao, Y.; Li, J. *Oncol. Rep.***2014**, *31*, 2720.
(296) Wang, H.; Sun, N.; Li, X.; Li, K.; Tian, J.; Li, J. *Oncol.Rep.* **2016**, *35*, 3648.
(297) Zhang, Y.; Xie, W.-P.; Zhang, Y.-K.; Chen, Y.-Q.; Wang, D.-L.; Li, G.; Guan, D.-H. *Onco. Targets. Ther.* **2018**, *11*, 271.
(298) Xiao, D.; Singh, S. In *Proc. Am. Assoc. Cancer Res.* **2003**, *44*, p 197.
(299) Herman-Antosiewicz, A.; Singh, S. V. *J. Biol. Chem.* **2005**, *280*, 28519.
(300) Ha, M. W.; Ma, R.; Shun, L. P.; Gong, Y. H.; Yuan, Y. *World J. Gastroenterol.* **2005**, *11*, 5433.
(301) Hosono, T.; Fukao, T.; Ogihara, J.; Ito, Y.; Shiba, H.; Seki, T.; Ariga, T. *J.Biol.Chem* **2005**, *280*, 41487.
(302) Wu, C. C.; Chung, J. G.; Tsai, S. J.; Yang, J. H.; Sheen, L. Y. *Food.Chem.Toxicol.* **2004**, *42*, 1937.
(303) Shin, S. S.; Song, J. H.; Hwang, B.; Park, S. L.; Kim, W. T.; Park, S. S.; Kim, W. J.; Moon, S. K. *Food. Nutr. Res* **2017**, *61*, 1338918.
(304) Zheng, J.; Cheng, X.; Xu, S.; Zhang, L.; Pan, J.; Yu, H.; Bao, J.; Lu, R. *Food Funct* **2019**, *10*, 7253.
(305) Clarke, N.; Irvine, W. A. *Chemistryopen*. **2022**.
(306) Williams, L.; Rosner, H.; Levy, H.; Barton, E. *West. Indian. Med. J.* **2007**, *56*, 17.
(307) Wooten, J.; Mavingire, N.; Arau jo, C. A.; Aja, J.; Wauchope, S.; Delgoda, R.; Brantley, E. *Fitoterapia* **2022**, *160*, 105203.
(308) Lowe, H. I. C.; Facey, C. O. B.; Toyang, N. J.; Bryant, J. L. *Anticancer. Res.* **2014**, *34*, 1637.
(309) Silva, J. P.; Nascimento, S.; Okabe, D.; Pinto, A.; Oliveira, F.; Paixa o, T.; Siqueira, M.; Baetas, A.; Andrade, M. *Pharmacognosy.Rev.* **2018**, *12*, 85.
(310) Gojon, G.; Morales, G. A. *Antioxid.Redox.Signal*. **2020**, *33*, 1010.
(311) Xu, W.; Xi, B.; Wu, J.; An, H.; Zhu, J.; Abassi, Y.; Feinstein, S. C.; Gaylord, M.; Geng, B.; Yan, H.; Fan, W.; Sui, M.; Wang, X.; Xu, X. *Mol. Cancer Ther.* **2009, 8, 3318.**
(312) Block, E.; Ahmad, S.; Jain, M. K.; Crecely, R. W.; Apitz-Castro, R.; Cruz, M. R. *J. Am. Chem. Soc.***1984**, 106, 8295.
(313) Xiao, D.; Herman-Antosiewicz, A.; Antosiewicz, J.; Xiao, H.; Brisson, M.; Lazo, J. S.; Singh, S. V. *Oncogene* **2005**, *24*, 6256.
(314) Anwar, A.; Gould, E.; Tinson, R.; Iqbal, J.; Hamilton, C. *Curr. Pharmacol. Rep.* **2018**, *4*, 397.

(315) Nepravishta, R.; Sabelli, R.; Iorio, E.; Micheli, L.; Paci, M.; Melino, S. *The FEBS j.* **2012**, *279*, 154.
(316) Cavallito, C. J.; Bailey, J. H. *J. Am. Chem. Soc.***1944**, *66*, 1950.
(317) Kaschula, C. H.; Hunter, R.; Stellenboom, N.; Caira, M. R.; Winks, S.; Ogunleye, T.; Richards, P.; Cotton, J.; Zilbeyaz, K.; Wang, Y. *Eur. J. Med. Chem.* **2012**, *50*, 236.
(318) Jacob, C. *Nat. Prod. Rep.* **2006**, *23*, 851.
(319) Sparnins, V. L.; Barany, G.; Wattenberg, L. W. *Carcinogenesis* **1988**, *9*, 131.
(320) Pinto, J. T.; Krasnikov, B. F.; Cooper, A. J. *J Nutr*. **2006**, *136*, 835s.
(321) Seki, T.; Hosono, T.; Hosono-Fukao, T.; Inada, K.; Tanaka, R.; Ogihara, J.; Ariga, T. *Asia Pac. J. Clin. Nutr.* **2008**, *17 Suppl 1*, 249.
(322) Myers, A. G.; Cohen, S. B.; Kwon, B. M. *J. Am. Chem. Soc.***1994**, *116*, 1255.
(323) Zhang, G.; Li, B.; Lee, C.-H.; Parkin, K. L. *J. Agric. Food Chem.* 2010, 58, 1564.
(324) Herman-antosiewicz, A.; Powolny, A. A.; Singh, S. V. *Acta Pharmacol. Sin.***2007**, *28*, 1355.
(325) Nagy, P. *Antioxid Redox Signal* **2013**, *18*, 1623.
(326) Bianco, C. L.; Akaike, T.; Ida, T.; Nagy, P.; Bogdandi, V.; Toscano, J. P.; Kumagai, Y.; Henderson, C. F.; Goddu, R. N.; Lin, J.; Fukuto, J. M. *Br J Pharmacol* **2019**, *176*, 671.
(327) Liang, D.; Wu, H.; Wong, M. W.; Huang, D. *Org. Lett.***2015**, *17*, 4196.
(328) Cai, Y.-R.; Hu, C.-H. *J. Phys. Chem.* **2017**, 121, 6359.
(329) Whitesides, G. M.; Lilburn, J. E.; Szajewski, R. P. *J. Org. Chem.* **1977**, *42*, 332.
(330) Beaupre, D. M.; Weiss, R. G. *Molecules.* **2021**, *26*, 3332.
(331) Hiskey, R. G.; Carroll, F. *J. Am. Chem. Soc.***1961**, *83*, 4644.
(332) Cuevasanta, E.; Lange, M.; Bonanata, J.; Coitin o, E. L.; Ferrer-Sueta, G.; Filipovic, M. R.; Alvarez, B. *J. Biol. Chem.* **2015**, *290*, 26866.
(333) Liang, D.; Wu, H.; Wong, M. W.; Huang, D. *Org. Lett.* **2015**, *17*, 4196.
(334) Benavides, G. A.; Squadrito, G. L.; Mills, R. W.; Patel, H. D.; Isbell, T. S.; Patel, R. P.; Darley-Usmar, V. M.; Doeller, J. E.; Kraus, D. W. *Proc Natl Acad Sci U S A* **2007**, *104*, 17977.
(335) Park, C.-M.; Weerasinghe, L.; Day, J. J.; Fukuto, J. M.; Xian, M. *Mol. BioSyst.* **2015**, *11*, 1775.
(336) Jacob, C.; Anwar, A.; Burkholz, T. *Planta medic.* **2008**, *74*, 1580.
(337) Cuevasanta, E.; Mo ller, M. N.; Alvarez, B. *Arch. Biochem. Biophys.***2017**, *617*, 9.
(338) Wood, J. L. *Methods Enzymol* **1987**, *143*, 25.
(339) Benchoam, D.; Semelak, J. A.; Cuevasanta, E.; Mastrogiovanni, M.; Grassano, J. S.; Ferrer-Sueta, G.; Zeida, A.; Trujillo, M.; Mo ller, M. N.; Estrin, D. A.; Alvarez, B. *J. Biol. Chem.***2020**, *295*, 15466.
(340) Ono, K.; Akaike, T.; Sawa, T.; Kumagai, Y.; Wink, D. A.; Tantillo, D. J.; Hobbs, A. J.; Nagy, P.; Xian, M.; Lin, J.; Fukuto, J. M. *Free Radic. Biol. Med.* **2014**, *77*, 82.
(341) Fosnacht, K. G.; Sharma, J.; Champagne, P. A.; Pluth, M. D. *J. Am. Chem. Soc.* **2024**, *146*, 18689.
(342) Yadav, P. K.; Martinov, M.; Vitvitsky, V.; Seravalli, J.; Wedmann, R.; Filipovic, M. R.; Banerjee, R. *J. Am. Chem. Soc.* **2016**, *138*, 289.
(343) Kawamura, S.; Kitao, T.; Nakabayashi, T.; Horii, T.; Tsurugi, J. *J. Org. Chem.* **1968**, *33*, 1179.
(344) Everett, S. A.; Wardman, P. *Methods Enzymol.***1995**, *251*, 55.
(345) Francoleon, N. E.; Carrington, S. J.; Fukuto, J. M. *Arch Biochem. Biophys.* **2011**, *516*, 146.

(346) DeNicola, G. M.; Karreth, F. A.; Humpton, T. J.; Gopinathan, A.; Wei, C.; Frese, K.; Mangal, D.; Yu, K. H.; Yeo, C. J.; Calhoun, E. S.; Scrimieri, F.; Winter, J. M.; Hruban, R. H.; Iacobuzio-Donahue, C.; Kern, S. E.; Blair, I. A.; Tuveson, D. A. *Nature* **2011**, *475*, 106.
(347) Montenarh, M.; Saidu, N. E. *Nat. Prod. Commun.* **2012**, *7*, 401.
(348) Iciek, M.; Kwiecien, I.; Włodek, L. *Environ. Mol. Mutagen.***2009**, 50, 247.
(349) Filomeni, G.; Rotilio, G.; Ciriolo, M. *J. Nutr.* **2008**, *138*, 2053.
(350) Everett, S. A.; Wardman, P. *Methods Enzymol* **1995**, *251*, 55.
(351) Chatterji, T.; Keerthi, K.; Gates, K. S. *Bioorg. Med. Chem. Lett.***2005**, *15*, 3921.
(352) Ida, T.; Sawa, T.; Ihara, H.; Tsuchiya, Y.; Watanabe, Y.; Kumagai, Y.; Suematsu, M.; Motohashi, H.; Fujii, S.; Matsunaga, T.; Yamamoto, M.; Ono, K.; Devarie-Baez, N. O.; Xian, M.; Fukuto, J. M.; Akaike, T. *Proc. Natl. Acad. Sci. U. S. A* **2014**, *111*, 7606.
(353) Pharoah, B. M.; Khodade, V. S.; Eremiev, A.; Bao, E.; Liu, T.; O'Rourke, B.; Paolocci, N.; Toscano, J. P. *Antioxidants* **2022**, *11*, 1010.
(354) Ngowi, E. E.; Afzal, A.; Sarfraz, M.; Khattak, S.; Zaman, S. U.; Khan, N. H.; Li, T.; Jiang, Q. Y.; Zhang, X.; Duan, S. F.; Ji, X. Y.; Wu, D. D. *Int.J. Biol.Sci.* **2021**, *17*, 73.
(355) Khattak, S.; Rauf, M. A.; Khan, N. H.; Zhang, Q.-Q.; Chen, H.-J.; Muhammad, P.; Ansari, M. A.; Alomary, M. N.; Jahangir, M.; Zhang, C.-Y.; Ji, X.-Y.; Wu, D.-D. *Molecules.* **2022**, *27*, 3389.
(356) Filipovic, M. R.; Zivanovic, J.; Alvarez, B.; Banerjee, R. *Chemical Rev.* **2018**, *118*, 1253.
(357) Ercole, F.; Li, Y.; Whittaker, M. R.; Davis, T. P.; Quinn, J. F. *J. Mater. Chem. B.* **2020**, *8*, 3896.
(358) Zhao, Y.; Biggs, T. D.; Xian, M. *Chem.Comm.***2014**, *50*, 11788.
(359) Beauchamp, R. O.; Bus, J. S.; Popp, J. A.; Boreiko, C. J.; Andjelkovich, D. A.; Leber, P. *CRC Crit. Rev. Toxicol.***1984**, *13*, 25.
(360) Rickard, D.; Luther, G. W. *Chem. Rev.* **2007**, *107*, 514.
(361) Riahi, S.; Rowley, C. N. *J. Phys. Chem. B.* **2014**, *118*, 1373.
(362) Ou, H.-W.; Chou, M.-S.; Chang, H.-Y. *Aerosol Air Qual. Res.***2020.**
(363) Zheng, Y.; Ji, X.; Ji, K.; Wang, B. *Acta Pharm. Sin. B.* **2015**, *5*, 367.
(364) Hughes, M. N.; Centelles, M. N.; Moore, K. P. *Free Radic. Biol. Med.* **2009**, *47*, 1346.
(365) Koppenol, W. H.; Bounds, P. L. *Arch. Biochem. Biophys.* **2017**, *617*, 3.
(366) Mustafa, A. K.; Gadalla, M. M.; Sen, N.; Kim, S.; Mu, W.; Gazi, S. K.; Barrow, R. K.; Yang, G.; Wang, R.; Snyder, S. H. *Sci. Signal.* **2009**, *2*, ra72.
(367) Hoffmann, M. R.; Lim, B. C. *Environ. Sci. Technol.***1979**, *13*, 1406.
(368) Kotronarou, A.; Hoffmann, M. R. *Environ. Sci. Technol.***1991**, *25*, 1153.
(369) Das, T. N.; Huie, R. E.; Neta, P.; Padmaja, S. *J. Phys. Chem.***1999**, *103*, 5221.
(370) May, P. M.; Batka, D.; Hefter, G.; Königsberger, E.; Rowland, D. *Chem. Comm.* **2018**, *54*, 1980.
(371) Shackelford, R. E.; Mohammad, I. Z.; Meram, A. T.; Kim, D.; Alotaibi, F.; Patel, S.; Ghali, G. E.; Kevil, C. G. *Pathophysiology.* **2021**, *28*, 437.
(372) Mo dis, K.; Coletta, C.; Erde lyi, K.; Papapetropoulos, A.; Szabo, C. *FASEB J.* **2013**, *27*, 601.
(373) Fu, M.; Zhang, W.; Wu, L.; Yang, G.; Li, H.; Wang, R. *Proc. Natl. Acad. Sci. U. S. A.* **2012**, *109*, 2943.
(374) Łowicka, E.; Bełtowski, J. *Pharmacol. Rep.* **2007**, *59*, 4.
(375) Rajendran, S.; Shen, X.; Glawe, J.; Kolluru, G. K.; Kevil, C. G. *Compr. Physiol.***2019**, *9*, 1213.
(376) Ding, H.; Chang, J.; He, F.; Gai, S.; Yang, P. *Adv. Healthc. Mater.* **2022**, *11*, 2101984.
(377) Blachier, F.; Beaumont, M.; Kim, E. *Curr. Opin. Clin. Nutr. Metab. Care.* **2019**, *22*, 68.

(378) Shen, X.; Carlstro m, M.; Borniquel, S.; Ja dert, C.; Kevil, C. G.; Lundberg, J. O. *Free Radic. Biol. Med.* **2013**, *60*, 195.
(379) De Preter, G.; Deriemaeker, C.; Danhier, P.; Brisson, L.; Cao Pham, T. T.; Gre goire, V.; Jordan, B. F.; Sonveaux, P.; Gallez, B. *Mol. Cancer Ther.* **2016**, *15*, 154.
(380) Li, H.; Xu, F.; Gao, G.; Gao, X.; Wu, B.; Zheng, C.; Wang, P.; Li, Z.; Hua, H.; Li, D. *Redox Biol.* **2020**, *34*, 101564.
(381) Khan, N. H.; Ngowi, E. E.; Li, Y.; Khattak, S.; Zhao, Y.; Shahid, M.; Zafar, U.; Waheed, I.; Khan, F.; Virk, R.; Hussain, I.; Cao, J.; Liu, H.; Liu, Z.; Wu, D.-D.; Ji, X.-Y. *GPD* **2022**, *2*.
(382) Szabo, C.; Papapetropoulos, A. *Pharmacol. Rev.* **2017**, *69*, 497.
(383) Chuah, S. C.; Moore, P. K.; Zhu, Y. Z. *Am. J. Physiol.-Heart Circ. Physiol.* **2007**, *293*, H2693.
(384) Predmore, B. L.; Kondo, K.; Bhushan, S.; Zlatopolsky, M. A.; King, A. L.; Aragon, J. P.; Grinsfelder, D. B.; Condit, M. E.; Lefer, D. J. *Am. J. Physiol.-Heart Circ. Physiol.* **2012**, *302*, H2410.
(385) Zhang, F.; Jin, H.; Wu, L.; Shao, J.; Zhu, X.; Chen, A.; Zheng, S. *Oxid. Med. Cell. Longev.***2017**, *2017*, 1406726.
(386) Panza, E.; De Cicco, P.; Armogida, C.; Scognamiglio, G.; Gigantino, V.; Botti, G.; Germano, D.; Napolitano, M.; Papapetropoulos, A.; Bucci, M.; Cirino, G.; Ianaro, A. *Pigment Cell Melanoma Res.* **2015**, *28*, 61.
(387) Iciek, M.; Bilska-Wilkosz, A.; Go rny, M.; Sokołowska-Jez ewicz, M.; Kowalczyk-Pachel, D. *Antioxidants* **2016**, *5*, 46.
(388) Chen, Y.; Qiang, J.; Dong, C. *Intermetallics.* **2016**, *68*, 23.
(389) Tsai, C.-Y.; Wen, S.-Y.; Shibu, M. A.; Yang, Y.-C.; Peng, H.; Wang, B.; Wei, Y.-M.; Chang, H.-Y.; Lee, C.-Y.; Huang, C.-Y.; Kuo, W.-W. *Int. J. Cardiol.* **2015**, *195*, 300.
(390) Kashfi, K.; Olson, K. R. *Biochem. Pharmacol.***2013**, *85*, 689.
(391) Rose, P.; Moore, P. K.; Zhu, Y. Z. *Trends. Pharmacol. Sci.* **2018**, *39*, 624.
(392) Yagdi Efe, E.; Dicato, M.; Diederich, M. *Phytochem. Rev.* **2019**, *18*, 1167.
(393) Kimura, H. *Front. Physiol.* **2012**, *3*, 101.
(394) Hildebrandt, T. M.; Grieshaber, M. K. *Febs j* **2008**, *275*, 3352.
(395) Kolluru, G.; Shen, X.; Bir, S.; Kevil, C. *Nitric Oxide.* **2013**, *35*.
(396) Akbari, M.; Sogutdelen, E.; Juriasingani, S.; Sener, A. *Oxidative Medicine and Cellular Longevity.* **2019**, *2019*, 2360945.
(397) Vasas, A.; Do ka, E.; Fa bia n, I.; Nagy, P. *Nitric Oxide.* **2015**, *46*, 93.
(398) Sawahata, T.; Neal, R. *Mol.Pharmacol.***1982**, *21*, 464.
(399) Kim, S. J.; Kim, H. S.; Seo, Y. R. *Oxid. Med. Cell. Longev.* **2019**, *2019*, 5381692.
(400) Zhang, W.; Hu, X.; Shen, Q.; Xing, D. *Nat. Commun.* **2019**, *10*, 1704.
(401) Deavall, D. G.; Martin, E. A.; Horner, J. M.; Roberts, R. *J.Toxicol* **2012**, *2012*, 645460.
(402) Iciek, M.; Kwiecien, I.; Włodek, L. *Environ. Mol. Mutagen.* **2009**, *50*, 247.
(403) Antosiewicz, J.; Herman-Antosiewicz, A.; Marynowski, S. W.; Singh, S. V. *Cancer Res* **2006**, *66*, 5379.
(404) Wang, H. C.; Yang, J. H.; Hsieh, S. C.; Sheen, L. Y. *J Agric.Food.Chem*. **2010**, *58*, 7096.
(405) Na, H.-K.; Kim, E.-H.; Choi, M.-A.; Park, J.-M.; Kim, D.-H.; Surh, Y.-J. *Biochem. Pharmacol.* **2012**, *84*, 1241.
(406) Abe, K.; Kimura, H. *J. Neurosci.***1996**, *16*, 1066.
(407) Geng, B.; Yang, J.; Qi, Y.; Zhao, J.; Pang, Y.; Du, J.; Tang, C. *Biochem. Biophys. Res. Commun.***2004**, *313*, 362.
(408) Fu, Z.; Liu, X.; Geng, B.; Fang, L.; Tang, C. *Life Sci.* **2008**, *82*, 1196.

(409) Distrutti, E.; Sediari, L.; Mencarelli, A.; Renga, B.; Orlandi, S.; Antonelli, E.; Roviezzo, F.; Morelli, A.; Cirino, G.; Wallace, J. L.; Fiorucci, S. *J. Pharmacol. Exp. Ther.* **2006**, *316*, 325.
(410) Wang, Y.; Zhao, X.; Jin, H.; Wei, H.; Li, W.; Bu, D.; Tang, X.; Ren, Y.; Tang, C.; Du, *J. Arterioscler. Thromb. Vasc. Biol*.**2009**, *29*, 173.
(411) Desai, K. M.; Chang, T.; Untereiner, A.; Wu, L. *Expert. Rev. Clin. Pharmacol.* **2011**, *4*, 63.
(412) Panagaki, T.; Randi, E. B.; Augsburger, F.; Szabo, C. *Proc. Natl. Acad. Sci. U. S. A.* **2019**, *116*, 18769.
(413) Paul, B. D.; Snyder, S. H. *Biochem Pharmacol.* **2018**, *149*, 101.
(414) Wu, D.; Si, W.; Wang, M.; Lv, S.; Ji, A.; Li, Y. *Nitric Oxide* **2015**, *50*, 38.
(415) Meram, A. T.; Chen, J.; Patel, S.; Kim, D. D.; Shirley, B.; Covello, P.; Coppola, D.; Wei, E. X.; Ghali, G.; Kevil, C. G.; Shackelford, R. E. *Anticancer Res.* **2018**, *38*, 3843.
(416) Cuevasanta, E.; Denicola, A.; Alvarez, B.; Mo ller, M. N. *PLOS ONE* **2012**, *7*, e34562.
(417) Olson, K. R.; DeLeon, E. R.; Liu, F. *Nitric Oxide* **2014**, *41*, 11.
(418) Chen, H.-J.; Qian, L.; Li, K.; Qin, Y.-Z.; Zhou, J.-J.; Ji, X.-Y.; Wu, D.-D. **2022**.
(419) Blackstone, E.; Morrison, M.; Roth, M. B. *Science* **2005**, *308*, 518.
(420) Reiffenstein, R. J.; Hulbert, W. C.; Roth, S. H. *Annu Rev Pharmacol Toxicol* **1992**, *32*, 109.
(421) Nicholson, R. A.; Roth, S. H.; Zhang, A.; Zheng, J.; Brookes, J.; Skrajny, B.; Bennington, R. *J Toxicol Environ Health A* **1998**, *54*, 491.
(422) Warenycia, M. W.; Smith, K. A.; Blashko, C. S.; Kombian, S. B.; Reiffenstein, R. J. *Arch Toxicol* **1989**, *63*, 131.
(423) Hu, X.; Xiao, Y.; Sun, J.; Ji, B.; Luo, S.; Wu, B.; Zheng, C.; Wang, P.; Xu, F.; Cheng, K.; Hua, H.; Li, D. *Acta Pharmaceutica Sinica B* **2021**, *11*, 1148.
(424) Wang, R. H.; Chu, Y. H.; Lin, K. T. *Int J Mol Sci* **2021**, *22*.
(425) Cao, X.; Ding, L.; Xie, Z. Z.; Yang, Y.; Whiteman, M.; Moore, P. K.; Bian, J. S. *Antioxid Redox Signal* **2019**, *31*, 1.
(426) Szabo, C.; Coletta, C.; Chao, C.; Mo dis, K.; Szczesny, B.; Papapetropoulos, A.; Hellmich, M. R. *Proc Natl Acad Sci U S A.* **2013**, *110*, 12474.
(427) Bhattacharyya, S.; Saha, S.; Giri, K.; Lanza, I. R.; Nair, K. S.; Jennings, N. B.; Rodriguez-Aguayo, C.; Lopez-Berestein, G.; Basal, E.; Weaver, A. L.; Visscher, D. W.; Cliby, W.; Sood, A. K.; Bhattacharya, R.; Mukherjee, P. *PLoS One* **2013**, *8*, e79167.
(428) Szabo, C.; Papapetropoulos, A. *Br J Pharmacol.* **2011**, *164*, 853.
(429) Murphy, B.; Bhattacharya, R.; Mukherjee, P. *The FASEB Journal.* **2019**, *33*, 13098.
(430) Szczesny, B.; Marcatti, M.; Zatarain, J. R.; Druzhyna, N.; Wiktorowicz, J. E.; Nagy, P.; Hellmich, M. R.; Szabo, C. *Sci.Rep.* **2016**, *6*, 36125.
(431) Wang, S. S.; Chen, Y. H.; Chen, N.; Wang, L. J.; Chen, D. X.; Weng, H. L.; Dooley, S.; Ding, H. G. *Cell Death Dis.* **2017**, *8*, e2688.
(432) Wang, M. J.; Cai, W. J.; Zhu, Y. C. *Clin Exp. Pharmacol. Physiol.* **2010**, *37*, 764.
(433) Panza, E.; Bello, I.; Smimmo, M.; Brancaleone, V.; Mitidieri, E.; Bucci, M.; Cirino, G.; Sorrentino, R.; d'Emmanuele di Villa Bianca, R. *Biomed. Pharmacother.* **2022**, *151*, 113137.
(434) Wang, H.; Sun, N.; Li, X.; Li, K.; Tian, J.; Li, J. *Oncol Rep.* **2016**, *35*, 3648.
(435) Jiang, X.-y.; Zhu, X.-s.; Xu, H.-y.; Zhao, Z.-x.; Li, S.-y.; Li, S.-z.; Cai, J.-h.; Cao, J.-m. *Acta. Pharmacol. Sin.* **2017**, *38*, 1048.
(436) Kamat, P. K.; Kalani, A.; Tyagi, S. C.; Tyagi, N. *J Cell Physiol.* **2014**, *230*, 378.
(437) Hellmich, M. R.; Coletta, C.; Chao, C.; Szabo, C. *Antioxid Redox Signal.* **2015**, *22*, 424.
(438) Szabo, C. *Cells.* **2021**, *10*, 220.

(439) Park, C.-M.; Johnson, B. A.; Duan, J.; Park, J.-J.; Day, J. J.; Gang, D.; Qian, W.-J.; Xian, M. *Org. lett.* **2016**, *18*, 904.
(440) Hunter, R.; Caira, M.; Stellenboom, N. *J.Org.Chem.* **2006**, *71*, 8268.
(441) Xiao, X.; Feng, M.; Jiang, X. *Angew Chem Int Ed.* **2016**, *55*, 14121.
(442) Takano, S.; Hiroya, K.; Ogasawara, K. *Chem.Lett.* **1983**, *12*, 255.
(443) Scholz, D. *Chem. Inf.* **1984**, *15*, no.
(444) Fujiki, K.; Tanifuji, N.; Sasaki, Y.; Yokoyama, T. *Synthesis.* **2002**, *02*, 0343.
(445) Taniguchi, N. *J. Org. Chem.* **2015**, *80*, 1764.
(446) Hile, A. G.; Shan, Z.; Zhang, S.-Z.; Block, E. *J. Agric. Food Chem.* **2004**, *52*, 2192.
(447) Stensaas, K. L.; Brownell, A. S.; Ahuja, S.; Kaiser Harriss, J.; Herman, S. R. *J. Sulfur Chem.* **2008**, *29*, 433.
(448) Trofimov, B. A.; Sinegovskaya, L. M.; Gusarova, N. K. J. Sulfur Chem. **2009**, *30*, 518.
(449) Liang, L.; Vincent, S. *Tetrahedron Lett.* **2017**, *58*.
(450) Liu, L.; Li, C.; Cochran, S.; Feder, D.; Guddat, L. W.; Ferro, V. *Bioorg. Med. Chem. Lett.* **2012**, *22*, 6190.
(451) Ali, D.; Hunter, R.; Kaschula, C.; Doncker, S.; Rees-Jones, S. *J. Org. Chem***. 2019**, *84*.
(452) Hye, K. **2017**.
(453) Kaschula, C. H.; Hunter, R.; Stellenboom, N.; Caira, M. R.; Winks, S.; Ogunleye, T.; Richards, P.; Cotton, J.; Zilbeyaz, K.; Wang, Y.; Siyo, V.; Ngarande, E.; Parker, M. I. *Eur J Med Chem.* **2012**, *50*, 236.
(454) Hunter, R.; Kaschula, C. H.; Parker, I. M.; Caira, M. R.; Richards, P.; Travis, S.; Taute, F.; Qwebani, T. *Bioorganic & Medicinal Chemistry Letters* **2008**, *18*, 5277.
(455) Kusza, D. A.; Venter, G. A.; Mabunda, M.; Biwi, J.; Samanta, S. K.; Klinck, J. D.; Singh, S. V.; Hunter, R.; Kaschula, C. H. *ChemMedChem* **2024**, e202400087.
(456) Veale, R.; Thornley, A. *S. Afr. J. Sci.***1989**, *85*, 357.
(457) Xu, W.; Shi, D.; Chen, K.; Palmer, J.; Popovich, D. G. *J. Microbiol. Methods.* **2023**, *214*, 106830.
(458) Rooprai, H. K.; Lawrence, P. V.; Keshavarz, S.; Yashod, P.; Gullan, R.; Selway, R.; Davies, D. *Anticancer Res.* **2020**.
(459) Jankech, T.; Pindjakova, D.; Kos, J.; Hutta, M.; Jampí lek, J. **2020**.
(460) Hopkins, A. L.; Keseru, G. M.; Leeson, P. D.; Rees, D. C.; Reynolds, C. H. *Nat. Rev. Cancer.* **2014**, *13*, 105.
(461) Gong, X.; Su, X.; Liu, H. *Molecules.* **2021**, *26*, 7186.
(462) Bailey, T. S.; Pluth, M. D. *Free Radic Biol Med.* **2015**, *89*, 662.
(463) Schmidt, R.; Logan, M. G.; Patty, S.; Ferracane, J. L.; Pfeifer, C. S.; Kendall, A. J. *ACS Omega* **2023**, *8*, 9356.
(464) Pan, J.; Carroll, K. S. *ACS chem. biol.***2013**, *8*, 1110.
(465) Santos, J. S.; Santos, J. C. C. In *H_2S in Plants*; Modolo, L. V., Da-Silva, C. J., Singh, V. P., Tripathi, D. K., Fotopoulos, V., Eds.; *Academic Press*. **2024**, 47.
(466) Chan, K.-Y.; Wasserman, B. P. *Cereal Chemistry* **1993**, *70*, 22.
(467) Goerigk, L.; Grimme, S. *Phys. Chem. Chem. Phys.* **2011**, *13*, 6670.
(468) Grimme, S.; Ehrlich, S.; Goerigk, L. *J. Comput. Chem.* **2011**, *32*, 1456.
(469) Weigend, F. *Phys. Chem. Chem. Phys.***2006**, *8*, 1057.
(470) Weigend, F.; Ahlrichs, R. *Phys. Chem. Chem. Phys.***2005**, *7*, 3297.
(471) Marenich, A. V.; Cramer, C. J.; Truhlar, D. G. *J. Phys. Chem* .**2009**, *113*, 6378.

(472) Benchoam, D.; Semelak, J. A.; Cuevasanta, E.; Mastrogiovanni, M.; Grassano, J. S.; Ferrer-Sueta, G.; Zeida, A.; Trujillo, M.; Mo ller, M. N.; Estrin, D. A.; Alvarez, B. *J.Biol. Chem.* **2020**, *295*, 15466.
(473) Lin, J.; Akiyama, M.; Bica, I.; Long, F. T.; Henderson, C. F.; Goddu, R. N.; Suarez, V.; Baker, B.; Ida, T.; Shinkai, Y.; Nagy, P.; Akaike, T.; Fukuto, J. M.; Kumagai, Y. *Chem. Res. Toxicol.* **2019**, *32*, 447.
(474) Benavides, G. A.; Squadrito, G. L.; Mills, R. W.; Patel, H. D.; Isbell, T. S.; Patel, R. P.; Darley-Usmar, V. M.; Doeller, J. E.; Kraus, D. W. *Proc Natl Acad Sci.* **2007**, *104*, 17977.
(475) Ercole, F.; Whittaker, M. R.; Halls, M. L.; Boyd, B. J.; Davis, T. P.; Quinn, J. F. *Chem. Commun.* **2017**, *53*, 8030.
(476) Ballou, B.; Ernst, L. A.; Waggoner, A. S. *Curr. Med. Chem.* **2005**, *12*, 795.
(477) Zhang, L.; Li, S.; Hong, M.; Xu, Y.; Wang, S.; Liu, Y.; Qian, Y.; Zhao, J. *Org Biomol Chem.***2014**, *12*, 5115.
(478) Gilbert, A. K.; Pluth, M. D. *J. Am. Chem. Soc.***2022**, *144*, 17651.
(479) Bu, F.; Zhao, B.; Kan, W.; Ding, L.; Liu, T.; Wang, L.; Song, B.; Wang, W.; Deng, Q. *J Photochem.Photobiol A: Chem.***2020**, *387*, 112165.
(480) Powell, C. R.; Dillon, K. M.; Matson, J. B. *Biochem. Pharmacol*. **2018**, *149*, 110.
(481) Zhou, Y.; Mazur, F.; Liang, K.; Chandrawati, R. *Chem – Asian J.* **2022**, *17*, e202101399.
(482) Henthorn, H. A.; Pluth, M. D. *J Am Chem Soc.* **2015**, *137*, 15330.
(483) Song, L.; Yang, Y.; Zhang, Q.; Tian, H.; Zhu, W. *J Phys Chem B.* **2011**, *115*, 14648.
(484) Kaschula, C. H.; Hunter, R.; Cotton, J.; Tuveri, R.; Ngarande, E.; Dzobo, K.; Scha fer, G.; Siyo, V.; Lang, D.; Kusza, D. A.; Davies, B.; Katz, A. A.; Parker, M. I. *Mol Carcinog.* **2016**, *55*, 1213.
(485) Foldes-Papp, Z.; Demel, U.; Tilz, G. P. *Int.Immunopharmacol.* **2003**, *3*, 1715.
(486) Aaron, J. S.; Taylor, A. B.; Chew, T.-L. *J Cell Sci.* **2018**, 131.
(487) Dunn, K. W.; Kamocka, M. M.; McDonald, J. H. *Am J Physiol Cell Physiol.* **2011**, *300*, C723.
(488) Lakowicz, J. **2006**.
(489) Page, P. M.; McCarty, T. A.; Baker, G. A.; Baker, S. N.; Bright, F. V. *Langmuir* **2006**.
(490) Srinivasan, S.; Guha, M.; Kashina, A.; Avadhani, N. G. *Biochim Biophys Acta (BBA)-Bioenergetics.* **2017**, *1858*, 602.
(491) Everett, M. *Carl Zeiss MicroImaging: https://www. How-to-merge-coloc-correlation-coefficient-Manders-or-Pearson-from-multiple-single-images/together/attachment /download/zen-aim_colocalization.pdf.*
(492) Ferguson, S. M. *Curr Opin Neurobiol* **2018**, *51*, 45.
(493) Bravo-Sagua, R.; E Rodriguez, A.; Kuzmicic, J.; Gutierrez, T.; Lopez-Crisosto, C.; Quiroga, C.; Dí az-Elizondo, J.; Chiong, M.; G Gillette, T.; A Rothermel, B. *Curr Mol Med.* **2013**, *13*, 317.
(494) Silva, F.; Khokhar, S. S.; Williams, D. M.; Saunders, R.; Evans, G. J. S.; Graz, M.; Wirth, T. *Angew. Chem. Int. Ed. Engl.* **2018**, *57*, 12290.
(495) Su, Z.; Long, Z.; Huang, Z.; Yang, S.; Google Patents: **2017**.
(496) Carrigan, C. N.; Imperiali, B. *Anal. Biochem.* **2005**, *341*, 290.
(497) Field, L.; Hanley, W. S.; McVeigh, I. *J. Org. Chem.* **1971**, *36*, 2735.
(498) Wang, F.; Liu, B.-X.; Rao, W.; Wang, S. Y. *Org. lett.* **2020**.
(499) Liang, L.; Vincent, S. P. *Tetrahedron Lett.* **2017**, *58*, 3631.
(500) Song, L.-C.; Ge, J.-H.; Yan, J.; Wang, H.-T.; Luo, X.; Hu, Q.-M. *Eur J Inorg Chem.* **2008**, 64.
(501) Zhang, G.-Y.; Lv, S.-S.; Shoberu, A.; Zou, J.-P. *J. Org. Chem.* **2017**, *82*, 9801.
(502) Zilbeyaz, K.; Oztekin, A.; Kutluana, E. G. *Bioorg. Med. Chem.* **2021**, *40*, 116194.

(503) Wang, F.; Liu, B.-X.; Rao, W.; Wang, S.-Y. *Organic Lett.* **2020**, *22*, 6600.
(504) Ayodele, E.; Olajire, A.; Amuda, O.; Oladoye, S. *Bull Chem Soc Ethiop.* **2003**, 17.
(505) Dutra, F. R.; Silva, C. d. S.; Custodio, R. *J Phys Chem A.* **2020**, *125*, 65.
(506) Thapa, B.; Schlegel, H. B. *J Phys Chem A.* ***2*016**, *120*, 5726.
(507) Everett, S.; Folkes, L.; Wardman, P.; Asmus, K.-D. *Free Radic Res.* **1994**, *20*, 387.